



Swansea University
Prifysgol Abertawe



Swansea University E-Theses

Dye sensitised solar cells and time resolved photoacoustic calorimetry on thin films.

Schabauer, Johann Josef Anton

How to cite:

Schabauer, Johann Josef Anton (2008) *Dye sensitised solar cells and time resolved photoacoustic calorimetry on thin films..* thesis, Swansea University.

<http://cronfa.swan.ac.uk/Record/cronfa42365>

Use policy:

This item is brought to you by Swansea University. Any person downloading material is agreeing to abide by the terms of the repository licence: copies of full text items may be used or reproduced in any format or medium, without prior permission for personal research or study, educational or non-commercial purposes only. The copyright for any work remains with the original author unless otherwise specified. The full-text must not be sold in any format or medium without the formal permission of the copyright holder. Permission for multiple reproductions should be obtained from the original author.

Authors are personally responsible for adhering to copyright and publisher restrictions when uploading content to the repository.

Please link to the metadata record in the Swansea University repository, Cronfa (link given in the citation reference above.)

<http://www.swansea.ac.uk/library/researchsupport/ris-support/>

DYE SENSITISED SOLAR CELLS AND TIME RESOLVED PHOTOACOUSTIC CALORIMETRY ON THIN FILMS

Johann Josef Anton Schabauer

Swansea University

September 2008

A thesis submitted to the University of Wales, in fulfilment of the requirements for the degree
of Doctor of Philosophy

ProQuest Number: 10798073

All rights reserved

INFORMATION TO ALL USERS

The quality of this reproduction is dependent upon the quality of the copy submitted.

In the unlikely event that the author did not send a complete manuscript and there are missing pages, these will be noted. Also, if material had to be removed, a note will indicate the deletion.



ProQuest 10798073

Published by ProQuest LLC (2018). Copyright of the Dissertation is held by the Author.

All rights reserved.

This work is protected against unauthorized copying under Title 17, United States Code
Microform Edition © ProQuest LLC.

ProQuest LLC.
789 East Eisenhower Parkway
P.O. Box 1346
Ann Arbor, MI 48106 – 1346



The author hereby declares, that this work has not previously been accepted in substance for any degree and is not being concurrently submitted in candidature for any degree.

Signed (Johann Schabauer)

Date28/09/2008.....

This thesis is the result of my own investigations, except where otherwise stated. Where correction services have been used, the extent and nature of the correction is clearly marked in footnotes.

Other sources are acknowledged by footnotes giving explicit references. A bibliography is appended.

Signed (Johann Schabauer)

Date28/09/2008.....

I hereby give consent for my thesis, if accepted, to be available for photocopying and for inter-library loan, and for the title and summary to be made available to outside organisations.

Signed (Johann Schabauer)

Date28/09/2008.....

THESIS SUMMARY

Candidate's Surname:.....SCHABAUER

Candidate's Forenames:Johann Josef Anton

Candidate for the Degree of PhD

Full title of thesis:.....

“Dye sensitised solar cells and time resolved photoacoustic calorimetry on thin films” ...

.....

Summary:

This work is primarily a study of the photoelectrochemical characterisation of dye sensitised solar cells. The specific parts of the cell and their role towards overall cell efficiency are considered in detail. A large number of cells have been characterised in which the nature of: the TiO₂ semiconductor, the absorbing dye, electrolyte, and the nature of the conducting electrodes, were varied. The photoelectric properties of the cells were measured using a Xe-arc sun simulator mimicking the incident solar radiation at ground level. Cell voltage and current were measured while operating under different temperatures and irradiation intensities. It was found, that a thick layer of Pt at the counter electrode did not improve the performance of the cell. Plastic cells are smaller and lighter, but lack in efficiency when compared to glass cells which is down to the lower series resistance of the transparent conducting oxide used. Higher concentrated electrolytes can lead to better results. At higher illumination intensities, back irradiation of the cell becomes favourable down to charge transfer limitations, especially in gel and solid electrolytes.

Another significant part of the research documented in this thesis was the development of thin film and interfacial time resolved photoacoustic calorimetry as a novel method for the time resolved measurement of non-radiative processes of dyes adsorbed at interfaces or as thin solid films. In our case, the dyes were either adsorbed on the mesoporous TiO₂ semiconductor film used in dye sensitised solar cells, or incorporated in a polymer matrix. Using this approach, we were able to directly measure triplet state lifetimes and quantum yields of charge injection into the semiconductor. Possible further applications for this method are discussed.

Acknowledgements

At this point I would like to take the opportunity to highlight a few of the many people who helped me to get to this stage.

First and foremost I want to thank my parents who, I like to think, always believed in me and supported me up to this point. Followed by my brother, my grandparents and the whole family clan, who always seemed to have arranged a long sequence of parties and feasts, whenever I came back home during my five year stay in sunny Wales.

A very warm thank you goes to the two supervisors and advisors I had throughout my stay at Swansea University, Peter Douglas, Chris Morley. It was a great honour and pleasure to work with you and the day trips, barbecues and especially a tour in a big van around Belgium will forever stay in my mind. As well as nights out with the whole group.

I also want to thank everyone at the Kodak European Research Center, Cambridge especially Chris Winscom, Nick Dartnell and Julie Baker. I had a very good time working with you.

A thank you goes to Hugh Burrows, Luis Arnaut and Carlos Serpa, who became a great friend through our work together, for their hospitality at their department at the Universidade de Coimbra. It was a very fruitful cooperation and I had a great time and met lots of memorable people in Coimbra.

A special thank you goes out to the boys (Big C, Chris W., Dave, Des, Lee, Paul, who were patient enough to teach me the important skills of pool and rugby. The Friday afternoon rugby sessions were the best. Andy and Brendan, it was always good have someone for that one pint!

John Tregembo needs to be mentioned, since he was the one who built all the hardware I needed for my rig and was always there to help as were John Lewis and Stan Szajda.

I want to thank the Erasmus programme, which made it possible for me to go to Portugal.

Finally, everyone, who was in our group or connected to our group throughout the years and helped making this such a great journey.

Table of Contents

	Page
<i>Chapter 1</i>	
Introduction	1
<i>Chapter 2</i>	
Experimental	35
<i>Chapter 3</i>	
Influence of variation of components on the performance of dye sensitised solar cells	87
<i>Chapter 4</i>	
Changes in cell performance with temperature; for cells made using the N3 dye; novel squaraine dyes; and different binders	134
<i>Chapter 5</i>	
Changes in cell performance with light intensity	166
<i>Chapter 6</i>	
Time resolved photoacoustic studies of dyes adsorbed to TiO ₂ films, and in thin polymer films	174
<i>Chapter 7</i>	
Future work and conclusions	203

Glossary

α	thermal expansion coefficient
A	cross sectional area, in diffusion, area over which diffusion occurs
A	absorption or optical density
c, c_1	concentration [$M L^{-1}$]
C_R	charge recombination rate
C_p	heat capacity at constant pressure
CS	charge separated
C_T	charge transfer rate
ΔS_{es}	electrostriction entropy of the solvent
ΔS_t	translational entropy of the electron
ΔV_{es}	volume changes associated with electrostriction
D	diffusion coefficient
DSSC	dye sensitised solar cell
ϵ	molar absorption coefficient (extinction coefficient)
E_{CB}	energy of the edge of the conduction band
EL	electrolyte (1,2,3)
E_{hv}	energy of the laser pulse
$E^{0\circ}$	redox potential of the ground state of the sensitiser F Solar flux $1367 \pm 7 \text{ Wm}^{-2}$ (Irradiance produced by the extraterrestrial sun radiation on a surface perpendicular to the sun's ray at a mean sun-earth distance) (World Meteorological Organisation, WMO)
eV	electron volt (energy of 1 mole electrons = $1.602 \times 10^{-19} \text{ J}$)
ff	fill factor (Chapter 2, Figure 25)
f_R	probability factor of charge recombination within the semiconductor layer

FTO	fluorine doped tin oxide
Γ	number of moles of sensitizer per cm^{-2} of projected electrode surface
h	Planck constant (6.62619×10^{-34} J s)
HOMO	highest occupied molecular orbital
i	transmitted intensity
i_0	incident light intensity
i_{ph}	photocurrent density [mA cm^{-2}], equal I for 1 cm^2 cells
I_{ph}	photogenerated current within the cell [A]
I	current [A]
I_{max}	current drawn at maximum power point [A]
ITO	indium doped tin oxide
I_0	saturation current [A]
IPCE	incident photon to current conversion efficiency
i_s	irradiation intensity [W m^{-2}]
I_{sc}	short circuit current in [A]
j_1	flux per unit area
J_1	total one dimensional flux in diffusion
k	Boltzmann constant (1.38066×10^{-23} J K^{-1})
K_{VE}	conversion between molar volumes and energies
λ	wavelength [nm]
l	pathlength [cm]
LASER	light amplification by stimulated emission of radiation
LHE	light harvesting efficiency
LUMO	lowest unoccupied molecular orbital
m	mass

m_e	electron mass
MW	molecular weight
η	overall efficiency of the cell
η_c	efficiency of collecting the injected charge at the back contact
n	diode ideality factor
n_c	number of charge carriers
n_R	number of charge recombinations
Φ	quantum yield
Φ_{inj}	quantum yield of charge injection
P_{max}	maximum power of a cell in [W]
PAC	photo acoustic calorimetry
PEDOT	poly(3,4-ethylenedioxythiophene)
PEO	polyethylene oxide
PMMA	poly(methyl methacrylate); poly(methyl 2-methylpropenoate)
PV	photovoltaic
PVC	polyvinyl chloride
q	fundamental charge
ρ	solvent density
r_{ext}	equals the sum of the external load and the contact resistances
r_s	series resistance [Ω]
r_{sh}	shunt resistance [Ω]
R	gas constant $8.314 \text{ Jkg}^{-1}\text{K}^{-1}$
R_L	load resistance [Ω]
σ	molar absorption cross section [$\text{cm}^2 \text{ mol}^{-1}$]
S	entropy

S_1	pathlength from the counter electrode to the electrolyte TiO ₂ junction
S_2	pathlength from electrolyte TiO ₂ junction to TiO ₂ TCO junction
SQU	squaraine
θ_z	zenith angle of incident sunlight
t	time
T	temperature
T	temperature [K]
T	transmittance [%]
TCO	transparent conducting oxide
TR-PAC	time-resolved photo acoustic calorimetry
V	Potential [V]
V_s	bias voltage generated by DC-power supply [V]
V_{max}	voltage at maximum power point [V]
V_{OC}	open circuit potential in [V]
V_A	voltage measured channel A [V]
V_B	voltage measured channel B [V]
v_s	effective velocity of charge carrier in semiconductor
v_E	velocity of charge carrier in electrolyte matrix (gel, solvent)
z	distance

Equations and useful constants:

Maximum Power P_{\max}

$$P_{\max} = V_{\max} \cdot I_{\max} \qquad P_{\max} = I_{SC} \cdot V_{OC} \cdot ff$$

Fill Factor ff

$$ff = \frac{P_{\max}}{V_{OC} \cdot I_{SC}}$$

Overall Efficiency η

$$\eta = \frac{i_{ph} \cdot V_{OC} \cdot ff}{I_S}$$

Incident Photon to Current Conversion Efficiency **IPCE**

$$IPCE = \frac{1240 \cdot i_{ph} [mAcm^{-2}]}{\lambda[nm] \cdot I_{SC} [mWcm^{-2}]} \qquad IPCE(\lambda) = LHE(\lambda) \cdot \Phi_{inj} \cdot \eta_c$$

Light Harvesting Efficiency **LHE**

$$LHE(\lambda) = 1 - 10^{-\Gamma\sigma(\lambda)}$$

Energy Conversion wavelength [nm] – wavenumber [cm^{-1}] – electronvolt [eV]

$$eV = \frac{1240}{\lambda} \qquad cm^{-1} = eV \cdot 8.066 \cdot 10^3 \qquad \frac{10^7}{\lambda} = cm^{-1}$$

Ohm's Law

$$V = R \cdot I$$

Beer-Lambert's Law

$$A = c \cdot \varepsilon \cdot l \qquad A = \log \frac{i_0}{i} \qquad A = -\log T$$

Nernst Equation

$$E = E^\circ - \frac{R \cdot T}{n \cdot F} \ln \frac{[\text{educts}]}{[\text{products}]}$$

Fick's Law of Diffusion

$$J_1 = Aj_1 = -AD \frac{\partial c_1}{\partial z}$$

Temperature Dependency of a Non Doped Semiconductor

$$R = R_0 e^{-\alpha T}$$

CHAPTER 1

INTRODUCTION

Outline of the thesis

This thesis deals with dye sensitised solar cells. The principal of these photovoltaic devices has been around for seventeen years now and has attracted a lot of interest amongst chemists and physicists since the first paper was published [1]. Despite the enormous effort and range of investigations which have been made to develop and design a photovoltaic system which can compete with the common pure semiconductor devices, which are mainly silicon based, no real breakthrough has been made nor has there been any change to the principal elements and construction of the cell [2-11].

During the study presented here we have tried to define, characterise and ask questions of existing devices. By looking at the overall cell construction and photochemical process as being made up of separate parts and separate processes, we have tried to get to a better understanding of the processes within a cell and their interactions with each other, with the aim to define and improve the existing system [12].

The thesis gives a comparison of different ways to build a cell, and discusses the influence of temperature and light intensity on the working cell characteristics. Different types of semiconductor sols, dyes, supports, electrodes and electrolytes were used to build a number of different cells. The influence of cell size on performance is also discussed briefly.

In addition to these studies of cell design and performance a new method to measure non-radiative processes within thin solid films, based on time resolved photoacoustic calorimetry was developed [13].

Preliminary studies have also been made on the use of kinetic measurements to help understand electron transport processes within the cells .

1.1. Introduction:

Since the earth's resources of fossil fuels are running short it has become more and more important to look for alternatives which are both available in large quantities, and ecologically compatible. Possible renewable energy sources comprise wind, tidal energy, wood and of course sunlight. Since the sun is the most powerful power plant accessible to us, we should aim to use this very reliable and free source of energy.

Several attempts have been made to convert the light energy that is continuously irradiating our planet into useable forms of energy. The incident light can be used to heat, for example, water tanks on roofs of houses in some parts of the world. Solar-thermal systems can be used to heat water or to generate electricity through steam turbines, and heat pumps are used to harvest the thermal energy stored in the ground. An alternative idea is that of transforming the sun's energy into electrical energy by means of photovoltaic cells which are convenient to run many different kinds of consumer devices and machines, such as, pocket calculators, mobile phones, radios and televisions, domestic water heating; public installations in places of difficult access e.g. marine warning buoys, public telephones in the Australian desert; and even with larger scale installations, the potential to provide energy for transport. One major advantage of this photovoltaic technique is that it can operate without maintenance in remote rural areas, since it does not involve any mechanical parts and operation is ensured over a long period.

Over the last decade several different types of dye sensitised solar cells (DSSCs) have been reported with different results. The aim of those investigations was to find a solar cell design that can compete with the commercial crystalline and semi-amorphous pure semiconductor cells, which have good efficiencies and long term

stabilities, but which are expensive. To achieve this goal, photovoltaic devices which convert solar energy with a high efficiency in relation to their costs are required. It was first discovered by Alexandre-Edmond Becquerel in 1839 that some materials generated low levels of electric energy when exposed to sunlight [14]. It was however almost a century later, that the first method of transforming sunlight into electricity was patented. The idea behind this method is to excite a semiconductor and pump electrons from the semiconductor ground state into the conduction band. The market for such photovoltaic devices has been continuously growing since the first generation devices became available on the market. It is predicted that by 2020 photovoltaics will be a 100 Billion € market comprising first, second and third generation devices in mobile devices and electrical goods, as well as power supplies on and off the grid [15].

Photovoltaic devices are mainly based on two different kinds of solar cells depending on the type of semiconductor. First, there are pure semiconductor cells consisting of relatively small band-gap semiconductors. In this case the semiconductor itself is excited by the sunlight and electrons are transported from the valence band to the conduction band. Si, GaAs, CdS or CdTe semiconductors in single-crystalline, multi-crystalline and amorphous forms are mainly used for this kind of photovoltaic design. These devices have a relatively high efficiency in terms of overall light-to-current conversion, up to as much as 25%. The downsides of such elements are their high price and that the production requires very sophisticated procedures and high purity raw materials. Secondly, there are the dye-sensitised semiconductor solar cells. The first dye-sensitised cell was reported by O'Regan and Grätzel in 1991 [1]. They used TiO_2 as the semiconductor and showed that if they used TiO_2 particles in the nanometre range and spread them onto a conducting glass

substrate, they would end up with a 1000-fold increase in active surface area compared to the nominal area of the cell. This so-called nanoporous surface acts like a sponge and has a huge surface area for the dye molecules to link to it. TiO_2 is still the most commonly used semiconductor for this kind of photovoltaic element [16]. The substrate for such cells is often fluorine-doped SnO_2 coated glass with a sheet resistance of $7 - 15 \Omega \text{ cm}^{-2}$. The first cell, by O'Regan and Grätzel consisted of a redox couple in a liquid electrolyte, TiO_2 semiconductor, a Pt-counter electrode and conducting glass supports [1]. Since then, many different ideas for cell design have been applied and reported. Several wide gap semiconductors have been used, for example SnO_2 , NiO or ZnO, the latter of which has a similar bandgap to TiO_2 [17-21] (TiO_2 has a conduction band edge of -4.21 eV and ZnO of -4.19 eV with respect to the absolute vacuum scale (AVS) [22, 23]). Even hybrid cells consisting of a stacked dye sensitised cell together with a thin film semiconductor cell have been built and are reported to reach an overall efficiency of 15 % [24].

The principles of a dye sensitised solar cell

The idea behind these devices is to use a so-called sensitising dye to harvest visible light. The dye should possess a high enough excited state to inject electrons from there into the relatively high-lying conduction band of a wide band-gap semiconductor, often a semiconducting oxide [25, 26]. The dye may be seen as an energy pump from a low-lying energy state to a relatively high-lying energy state. Currently, the most commonly used dyes for this application are ruthenium complexes, in particular derivatives of carboxylated ter- and bipyridine ruthenium(II)

complexes. The dye used by O'Regan and Grätzel was a trimeric cationic ruthenium complex, $[\text{RuL}_2\{(\mu\text{-CN})\text{Ru}(\text{CN})\text{L}'_2\}_2]^{2+}$, where L is 2,2'-bipyridine-4,4'-dicarboxylic acid and L' is 2,2'-bipyridine. If we follow the path of the incident light, which hits the working electrode first, we find a series of interfaces: firstly a glass|TCO (transparent conducting oxide), then a TCO|TiO₂, a TiO₂|dye, a dye|electrolyte, an electrolyte|Pt, a Pt|TCO and finally a TCO|glass interface (see

Figure 1-2). A diagram of the energy levels of our reference system, the TiO₂ semiconductor, the N3 sensitiser dye and the iodide/iodine redox couple is shown in Figure 1-1. The energy levels are shown according to energy level diagrams given by Mosurkal *et al.* [27, 28]. The useful energy is determined by the potential difference between the I⁻/I₃⁻ redox potential and the conduction band edge of the semiconductor .

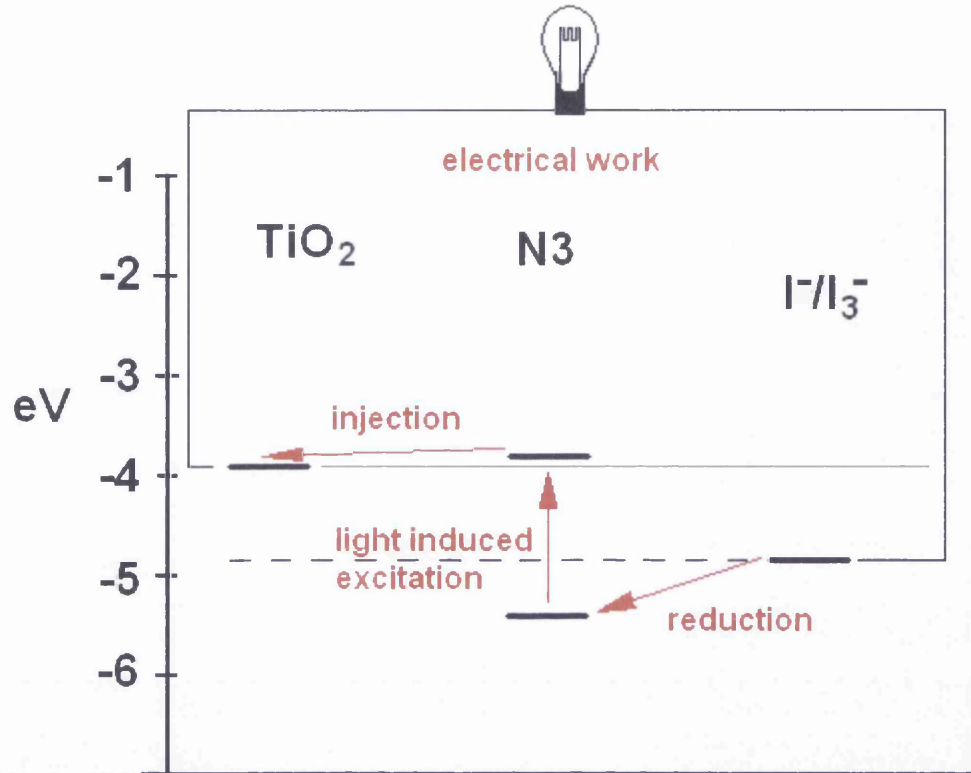


Figure 1-1 Energy level diagram of a DSSC, the potentials are in eV with respect to absolute vacuum scale

All these interfaces can be seen as parts of a dynamic system under light illumination and their electrical properties are liable to constant change. An idealised electrical circuit of the DSSC consists of a source, a series resistance, a shunt resistance, a diode and a load. Several parameters influence the overall series resistance as was shown by electron impedance spectroscopy (EIS) which is a useful tool to understand circuit-modelling of a DSSC [29]. The performance of a cell is often shown as a current voltage curve (such as shown in Chapter 2, Figure 2-25). Changes in the series resistance influence the slope of the vertical part of the voltage-

current curve, a theoretical series resistance of zero would lead to a vertical line starting from the open current voltage.

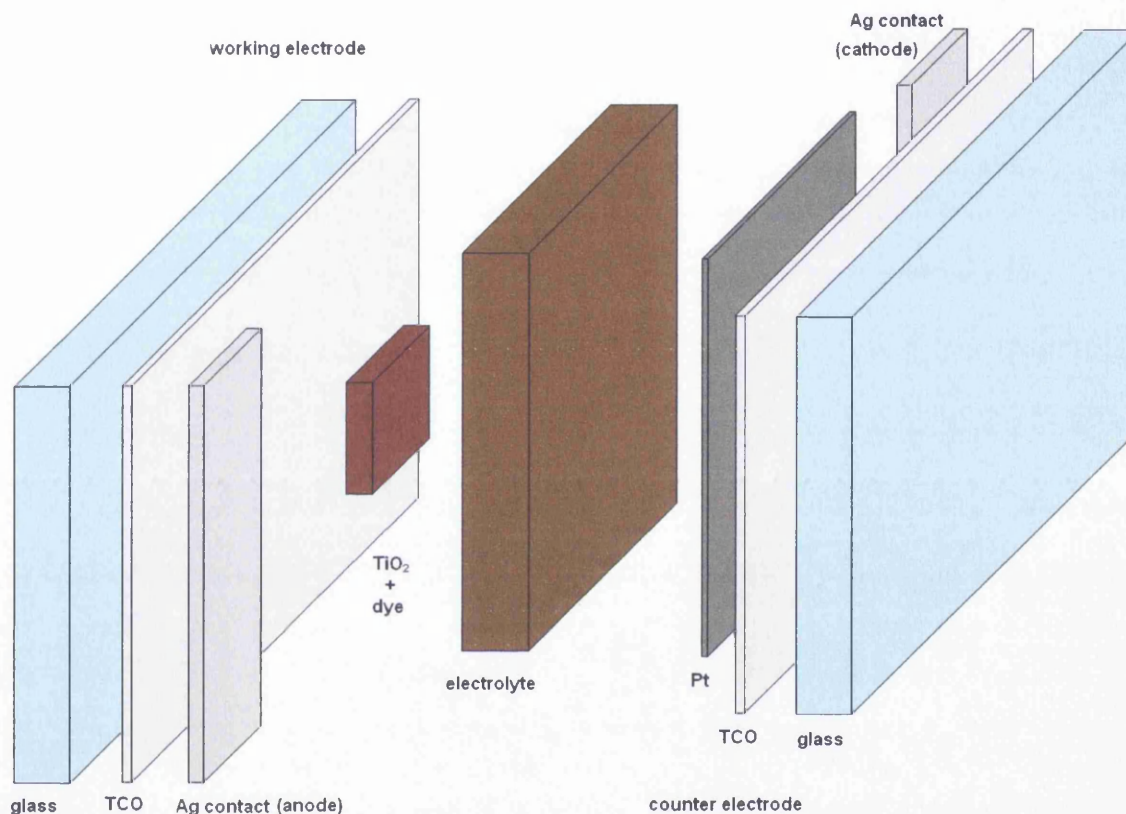


Figure 1-2 The build up of a dye sensitised solar cell of the sandwich “Grätzel” type. If the cell is operated in front irradiation mode, the incident light beam hits it from left to right, in back irradiation mode from right to left.

What we are therefore looking for is a very low series resistance. The shunt resistance influences the slope of the horizontal part of the curve; an infinite shunt resistance leads to a horizontal line and therefore no back reactions in the system. Several models try to explain the processes occurring within a working DSSC [30-

32]. Lower shunt resistance can occur due to small short circuit paths between the semiconductor and the counter electrode caused by irregularities during the cell assembly. There are however pathways for back reactions that can never be avoided, just lowered by good tuning of the energy levels of the individual cell parts. A direct contact of the electrolyte with the TCO surface should be avoided in order to minimise charge recombination. Another possible leakage pathway is recombination of electrons within the TiO_2 with the oxidised form of the electrolyte.

It is the function of the dye to make sure the sunlight is harvested with high efficiency, and to provide a sufficiently energetic excited state from which the electrons can be injected into the conduction band of the semiconductor at a rapid rate. Furthermore, it must be possible to reduce the dye, which is in its oxidised state after electron injection, by a redox couple in the electrolyte solution of the solar cell. Triiodide/iodide in acetonitrile is the redox couple of choice for most solar cell applications. Although the behaviour of different electrolytes of solid and liquid type has been investigated [33, 34], this is still the most favoured one. Its high redox exchange rates result from the relatively easily accessible energy levels in its oxidised (I_3^-) as well as in its reduced (I^-) state [35]. The range of electrolytes used include: redox couples dissolved in organic solvent or embedded in a gel matrix [36], ionic liquids [37, 38] or even conducting polymers [39]. In general, they can be categorised as liquid, gel and solid electrolytes.

Another approach is the use of solid or quasi-solid electrolytes where the electron-transporting species is embedded in a stable, immobile matrix of either relatively large cations or polymers [39, 40]. These systems currently have efficiencies which are lower than those of the liquid electrolyte dye-sensitised solar cells, and are in the region of 6 – 7% at best.

Gibbs Free Energy

Gibbs Free Energy is a thermodynamic potential, and the change in this energy associated with a chemical reaction is an indicator of whether the reaction will proceed spontaneously. The change in free energy is equal to the maximum useful work that can be accomplished by the reaction

$$\Delta G = w_{\max} \qquad \text{(Equation 1-1)}$$

Therefore a negative value of ΔG associated with a reaction indicates it will occur spontaneously. Whether a reaction is spontaneous or not can be assessed under standard conditions by looking at the thermodynamic quantities for the reactants and products. The change in the Gibbs free energy of a system is therefore equal to the change in the enthalpy of the system minus the change in the temperature of the product times the entropy of the system.

$$\Delta G = \Delta H - T\Delta S \qquad \text{(Equation 1-2)}$$

Excited-state energy levels

A molecule or atom provides several states (orbitals) which are different in energy and can be occupied by electrons. If a molecule or atom is excited by an energy source (heat, light, chemical reaction) the electrons in the HOMO can be elevated to higher states of energy. From there they can release this energy non-radiatively in which it is degraded to heat or radiatively in which they can perform a jump to a different lower lying energy state, or they can undergo reaction which may involve electron transfer to a different atom, ion or molecule. The release of energy from excited states can be spin allowed or spin forbidden and the probabilities of the different types of energy release (decay of excited states) are influenced by parameters such as spin coupling and energy level differences between orbitals. The Jablonski diagram (Figure 1-3) shows the different ways of decays from and between different energy states. Excited states can be triplet (total angular momentum of 1) or singlet (total angular momentum of 0). Changes between states of different spin are spin forbidden and are less favoured than jumps between states of the same spin, which do not have to overcome this probability barrier.

Jablonski diagram

The Jablonski diagram is a way to graphically present the different energy levels and electronic states of an atom or molecule. It can be used just to show the states of a molecule and can be of good use in order to show the different possibilities for deactivation of excited-states (see Figure 1-3).

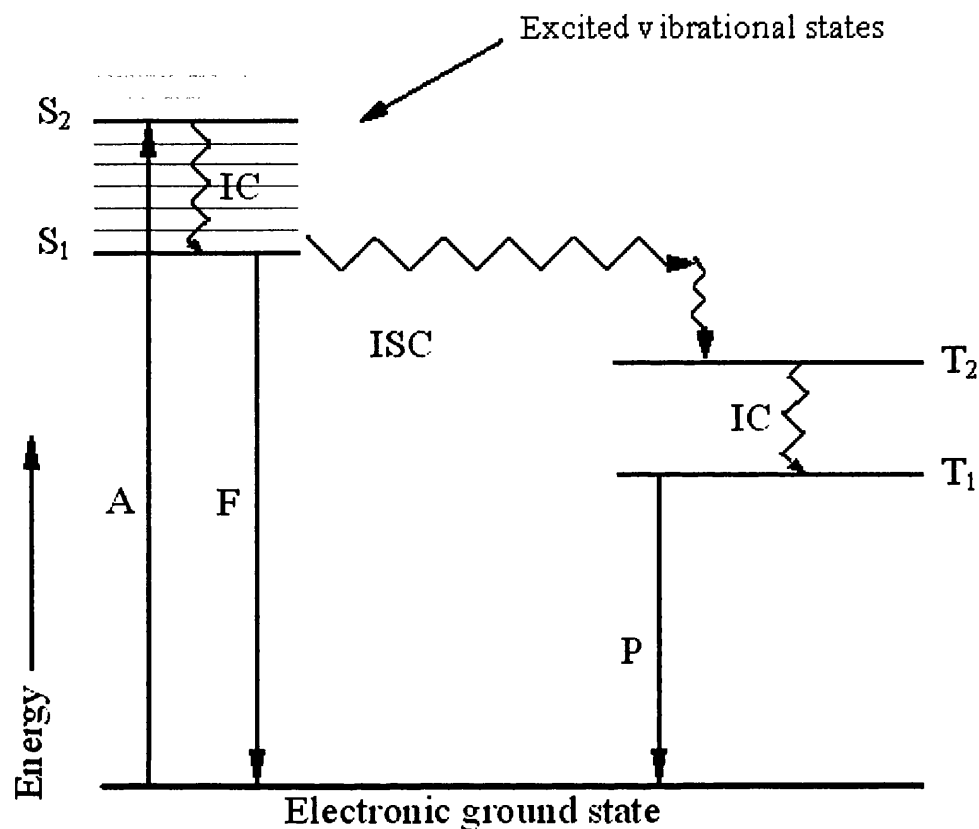


Figure 1-3 Jablonski diagram

S ₁ – S _n	Singlet states	P	Phosphorescence
T ₁ – T ₂	Triplet states	IC	Internal energy conversion
A	Absorption	ISC	Inter system crossing
F	Fluorescence		

Radiative emission between singlet states, usually to the ground state is called fluorescence. Fluorescence is a very fast emission process (i.e. fs-ns). Phosphorescence, on the other hand is a radiative emission from a triplet state to a

singlet state. It is a slower process, typically in the μs - ms range. Non-radiative transitions between states of the same spin are called internal conversion (IC), whereas non-radiative transitions between states of different spin are called inter-system crossing (ISC). The probability for inter-system crossing is often lower than for internal conversion since it is spin forbidden. Orbitals or energy levels are usually filled following the Pauli principle with electron pairs of anti-parallel spin. In the triplet state, the two electrons have the same spin which means if they are to be transformed from the triplet to the singlet state they have to change their spin.

Frank-Condon principle

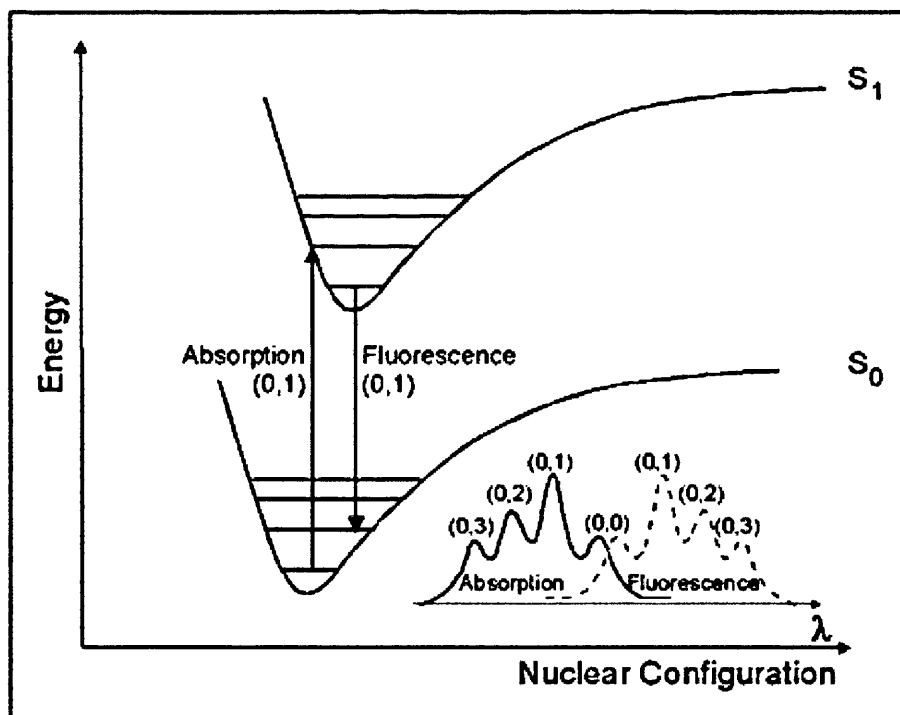


Figure 1-4 Frank-Condon principle energy diagram

The approximation that an electronic transition is most likely to occur without changes in the positions of the nuclei in the molecular entity and its environment, was formulated by J. Franck and R. Condon. The Franck Condon Principle states that electronic transfers occur at a much faster rate than nuclei can respond. The resulting state is known as the Franck Condon state and the transition involved is a “vertical” one on a potential energy diagram.

Electron Transfer

An electron transfer reaction is a reaction between two quantum states of the same (self-exchange reaction) or different species. There are no bonds formed or broken during a normal electron transfer reaction. The rates of electron transfer are usually very high compared to the rates of other chemical reactions. This is due to the fast electron jumps compared to the rearrangement of larger atoms, ions or molecules. (The size of the particles involved is often a rate determining parameter for chemical reactions or physical phenomena.)

Electron injection

Electron injection is one of the determining steps in DSSCs. The injection rate has to be close to unity in order to achieve high overall efficiencies. The competing reaction in a photovoltaic cell is the charge recombination reaction where electrons are lost from the conduction band of the semiconductor. The channels for such back reactions include reduction of the oxidised form of the electrolyte directly if it is in contact with the semiconductor, or back electron transfer to the oxidised form of the sensitiser.

$$k_{inj} = \left(\frac{4\pi^2}{h} \right) |V|^2 \rho(E) \quad \text{(Equation 1-3) [41]}$$

k_{inj} rate of electron injection

V coupling between the excited molecule and the semiconductor

$\rho(E)$ density of states of the conduction band

The sun as a light source

The spectrum of the sun resembles that of a black body at 5800 K, which is the approximate surface temperature of the sun. The sun's flux irradiating the earth's atmosphere is around 1370 Wm^{-2} and changes by about 6 – 7 percent over the span of a year. These changes are mostly down to changes in the earth-sun distance (average earth-sun distance 149,597,890 km).

The terrestrial sun irradiation is influenced by the atmosphere and is a sum of the extraterrestrial irradiation minus absorption in the atmosphere (direct radiation), scattering caused by molecules in the atmosphere (diffuse reflection), and ground reflection which is dependent on the local topography. The sun's irradiation is also influenced by weather conditions since water drops in the air and clouds can reflect some of this radiation straight back into space.

The sun is also not a very constant light source. Significant diurnal changes occur with the light intensity reaching its maximum around noon on a sunny day. There are seasonal variations as the Earth tilts upon its axis, and smaller changes throughout the year mostly corresponding to the change in earth-sun distance. The ground irradiation

is also influenced by the weather with clouds acting as the major contribution to changes in the light intensity. The average annual and daily irradiation values can be derived from local meteorological institutes.

Spectra of the sun, simulation of sunlight

When simulating solar radiation it is important to have a light source which provides a close match to the radiation emitted by a black body of 5800 K, then the earth's atmospheric conditions have to be mimicked. Solar simulators range from conventional tungsten lamps to high energy arc lamps. Tungsten lamps emit the spectrum of a 3200 K hot body so cannot represent the solar spectrum over the whole wavelength range. With the use of the right filters, however, they can provide a match for most of the visible range (500 – 750 nm). Such an apparatus can be useful to gain preliminary results when testing solar cells, although a considerable amount of the spectrum is lost in the UV. Solar simulators using mercury arc lamps are sometimes used but do not provide close enough matches for most applications. The best simulation of the solar spectrum can be achieved using xenon arc lamps which resemble the emission of a 5,800 K black body and provide the best artificial spectral match.

To simulate the terrestrial spectrum, filters are used to fulfil the role of the atmospheric layer. Depending on the angle of the incident sunlight to be modelled different filters are used. The one most widely used for testing photovoltaic devices is the AM 1.5 filter. It represents the absorbance of the atmosphere at an angle of the incident sunlight of 48.2°.

Filter type	Zenith angle θ_z
AM 0	0° (extraterrestrial)
AM 1	0° (terrestrial)
AM 1.5	48.2°
AM 2.0	60.1°

Table 1-1 The different types of air mass filters with the zenith angle they represent (Oriol Light Sources catalogue, 2004).

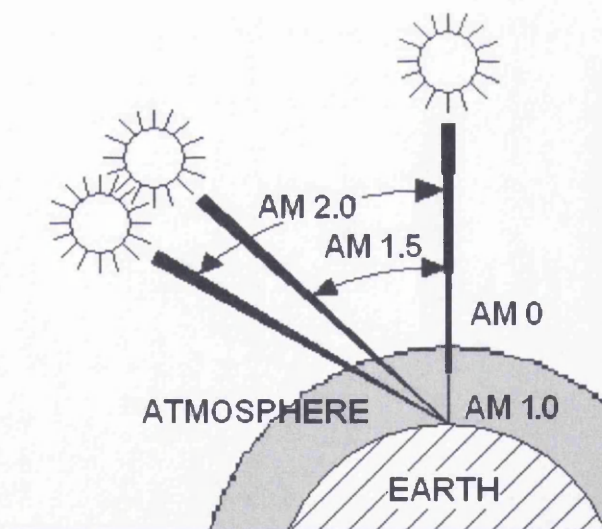


Figure 1-5 Illustration of the different zenith angles for different air mass filters. [42]

The different air mass filters represent the path length ratio the incident sun beam has to pass in relation to the path length if the sun is directly overhead (AM 1.0).

The dyes used for DSSCs

The range of dyes used to sensitise wide band-gap semiconductors for solar cells include organic, inorganic and organometallic compounds. Almost any kind of compound can be used for the dye providing it consists of a light harvesting (conjugated) system, an anchor group to link to the porous semiconductor surface and that it provides a channel for electron injection, and a high enough excited state level in order to inject charge into the semiconductor conduction band. The position and tuning of the redox potentials are essential for maximum energy generation. The perfect sensitiser dye would have an excited state which is slightly higher than the lowest level of the conduction band and a ground state low enough to be re-reduced by a redox species after the charge has passed through the load, thus ensuring a maximum energy gap between the conduction band and the reduced state of the redox species. If this is achieved, the next important characteristics of the sensitisers are their structure, extinction coefficient and absorption range. The goal is to harvest as much of the incoming sunlight as possible by the use of a monolayer of dye. Dye coagulation and multilayers should be prevented since they lead to inefficient injection and electron transfer processes which then lead to higher rates of back reactions (such as recombination reactions, and reduction of the redox species). Stacking of the molecules on the semiconductor surface is very important and the molecules should have a controllable geometry and stack well on the surface, in order to achieve a monolayer of dye with a maximum number of molecules of high extinction coefficient.

Since a considerable proportion of the sunlight is in the near and far infrared, the absorption of dye molecules should be extended to the red as much as possible but still maintain maximum light to current conversion in the visible region. One

approach to that could be the use of dye mixtures with organised stacking and layering of different dyes or the development and synthesis of compounds with different light absorbing systems connected by channels for electron transfer towards the semiconductor[5]. Electron donating functional groups can be used in order to generate this driving force towards highly efficient electron injection rates. The anchoring groups are mostly acidic groups like carboxylic, phosphonic or sulfonic acid groups with carboxylic acid groups reported to be the most efficient. They link the dye chromophore to the semiconductor by a range of different bindings from uni- and bidentate to bridging, and chelating mechanisms[43]. Several modes of linkages for N3 molecules have been suggested, including 1 – 3 of the possible four carboxylic anchoring groups for the dye. It is believed that the dye adsorption follows a two step mechanism. At low dye concentrations on the surface it is necessary to have small clusters of at least two dye molecules close to another in order to ensure the two electron oxidation of I⁻ [44].

Table of some sensitisers used on TiO₂

Class	Name	Formula	Ref.	Efficiency	Syn
Inorganic					
	cis-dicyanato bis(4,4-dicarboxy-2,2-bipyridine)iron(II)		[45]		
	Tripyridene-thiolato (4,4', 4'' – tricarboxy-2,2':6',2''-terpyridene)ruthenium(II)		[46]		No
	Diimine(diketonato)ruthenium(II)		[47]		Yes

	Bis(4,4'-dicarboxy-2,2'-bipyridene)di(thiocyanato-N)ruthenium(II) (N3 dye)	{(dcbp)Ru(NCS) ₂ } {(dcbp)Ru(Cl) ₂ } {(dcbp)Ru(H ₂ O) ₂ } ²⁻	[1, 48]	10.4%	Yes
	B-diketonato-bis(dicarboxybipyridene)ruthenium(II)	{(dcbp) ₂ Ru(L)}Cl L= acetylacetonate, 3-methyl-2,4-pentanedionate, 1,3-diphenyl-1,3-propandionate	[49]	5.7%	Yes
	Monocarboxyl or dicarboxyl pyridylquinoline ruthenium(II)	Cis-[Ru(4-carboxy-2-(2'-pyridil)quinoline) ₂ (NCS) ₂] Cis-[Ru(4-carboxy-2-(2'-(4'-carboxypyridil))quinoline) ₂ (NCS) ₂]	[50]	4.6%	Yes
	tris(isothiocyanato)-[N-(2,2':6,2''-terpyridine-4'-(4-carboxylic acid)phenyl)]ruthenium(II)		[51]	2.9%	Yes
		[Ru(4,4'-dicarboxy-2,2'-bipyridine)Cl(cymene)]NO ₃	[52]		yes
		[Ru(4,4'-dicarboxy-2,2'-bipyridine)(4,4'-dimethyl-2,2'-bipyridine)(NCS) ₂]	[52]	6.3%	Yes
		[Ru(4,4'-dicarboxy-2,2'-bipyridine)(4,4'-dihexyl-2,2'-bipyridine)(NCS) ₂]	[52]	6.7%	Yes
		[Ru(4,4'-dicarboxy-2,2'-bipyridine)(4,4'-dinonyl-2,2'-bipyridine)(NCS) ₂]	[52]	8.4%	yes
		[Ru(4,4'-dicarboxy-2,2'-bipyridine)(4,4'-tridecyl-2,2'-bipyridine)(NCS) ₂]	[52]	8.6%	Yes
	trithiocyanato 4,4',4''-tricarboxy-2,2'-6',2''-terpyridine ruthenium(II) (black dye)		[53, 54]		Yes

	cis-bis(4,7-dicarboxy-1,10-phenanthroline)dithiocyanato ruthenium(II)	(Ru(dcphen) ₂ (NCS) ₂)	[41]	6.1%	Yes
	cis-bis(4-monocarboxy-1,10-phenanthroline)dithiocyanato ruthenium(II)	(Ru(mcphen) ₂ (NCS) ₂)	[41]		Yes
	cis (4,7-dicarboxy-1,10-phenanthroline)(1,10-phenanthroline)dithiocyanato ruthenium(II)	(Ru(dcphen)(phen)(NCS) ₂)	[41]		Yes
	cis(4-monocarboxy-1,10-phenanthroline)(1,10-phenanthroline)dithiocyanato ruthenium(II)	(Ru(mcphen)(phen)(NCS) ₂)	[41]		Yes
	cisdicyanato bis(4,7-dicarboxy-1,10-phenanthroline)ruthenium(II) complex		[55]		
	cis-L bis(4,4'-dicarboxy-2,2'-bipyridine)ruthenium(II) complexes (L = diethyldithiocarbamate, dibenzylthiocarbamate, and pyrrolidinedithiocarbamate)		[56]		
	ruthenium phthalocyanines		[57]		
		4-(trans-2'-(2''-(5'',10'',15'',20''-tetraphenylporphyrinato zinc(II)-yl)ethen-1'-yl)-1-benzoic acid	[58]	4.11 %	
		4-(trans-2'-2''-(5'',10'',15'',20''-tetraxylylporphyrinato zinc(II)-yl)ethen-1'-yl)-1-benzoic acid	[58]	4.80 %	
		4-(trans-2'-(2''-(5'',10'',15'',20''-tetraphenylporphyrinato copper(II)-yl)ethen-1'-yl)-1-benzoic acid	[58]	0.45 %	

		4-(trans-2'-(2''-(5'',10'',15'',20''-tetraphenylporphyrinato zinc(II)yl(ethen-1'-yl))-1-phenylphosphonic acid	[58]	0.89 %	
		4-(trans-2'-(2''-(5'',10'',15'',20''-tetraphenylporphyrinato copper(II)yl(ethen-1'-yl))-1-phenylphosphonic acid	[58]	0.41 %	
Organic	porphyrin derivatives		[59-61]	Up to 3.5%	Yes
	coumarin derivatives		[62, 63]	Up to 6 %	
	eosinY		[64]	1.3%	
	polythiophenes		[65]	~ 2.4%	
	poly(3-thiophenemalonic acid)		[66]	1.6%	
	anthraquinone derivatives		[67]		
Natural	chlorophyll derivatives		[59, 60]		
	tannins		[68]		

Table 1-2 Gives a few representative examples of dyes already applied on DSSCs.

Photodegradation

Photodegradation is the decay of molecules induced by light. The incident energy is either too high and leads to a breaking of bonds or light could trigger a photochemical reaction (e.g. photooxidation) which leads to the destruction of the chemical nature of the substance.

Which semiconductors?

For DSSCs, several wide band gap semiconductors have been used. Besides TiO₂ [69], the most widely used and reported ones are NiO, ZnO [18, 70-72], CdO [73], ZnS [74] and SnO₂ [19, 75]. It is important to be able to tune the energy interactions between the molecule which is harvesting the incident light energy and the conduction band level of the semiconductor. Most groups apply the semiconductor as a sol and spread it over the surface. The semiconductor precursors for those are either ground from commercially available material [76, 77], precipitated [16, 69, 78] or even formed by microwave processing [79]. Other methods used are electrodeposition [18], chemical bath deposition or growth of the semiconductor surface on the substrate (successive ionic layer adsorption and reaction) [80, 81]. It has also been possible to grow nanotubes on the substrate [82]. After the substrate surface is covered with semiconductor, an annealing step follows. This helps to create better mechanical as well as electrical connections between semiconductor and substrate and fuses the semiconductor layer together (see sintering, page 25).

Crystal structure – particle size

TiO₂ occurs in three crystal structures. The rutile, anatase and brookite structures. Anatase TiO₂ is preferred for photovoltaic applications. Rutile and anatase are the most commonly observed ones. Brookite is the third and crystallises in an orthorhombic structure. A comparison of rutile and anatase structured TiO₂ cells was done by Park *et al.* [83]. It was also suggested, that not the crystal structure differences but the differences in dye adsorption (anatase could adsorb more dye molecules per unit area than rutile, probably down to differences in particle size), was responsible for the different efficiencies.

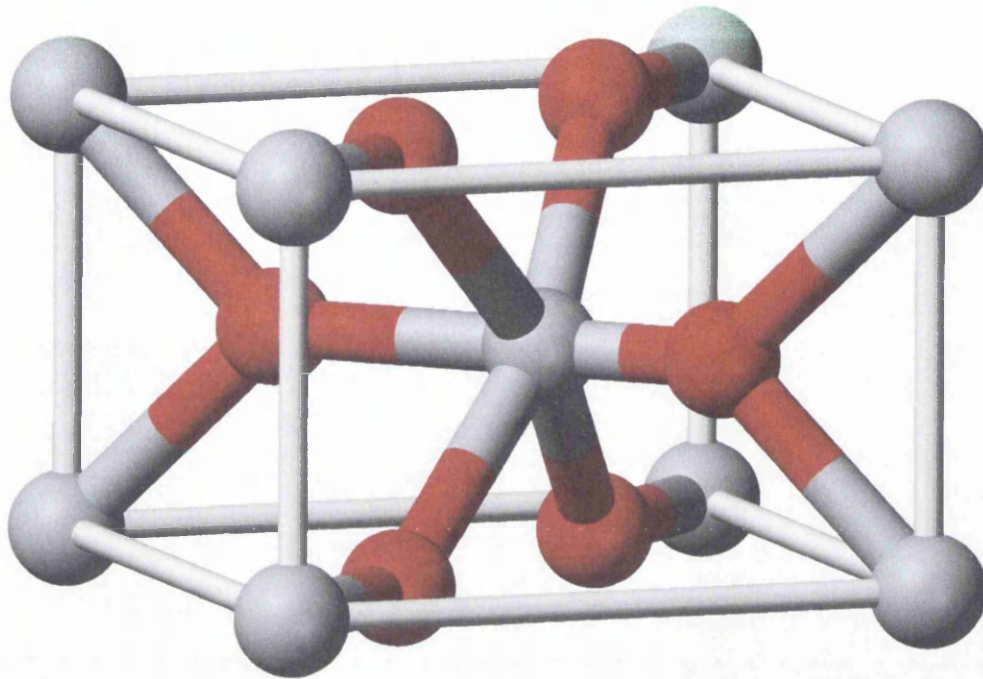


Figure 1-6 The rutile unit cell; the grey atoms represent Ti and the red ones O

(<http://en.wikipedia.org/wiki/Anatase>, accessed March 11,2006)

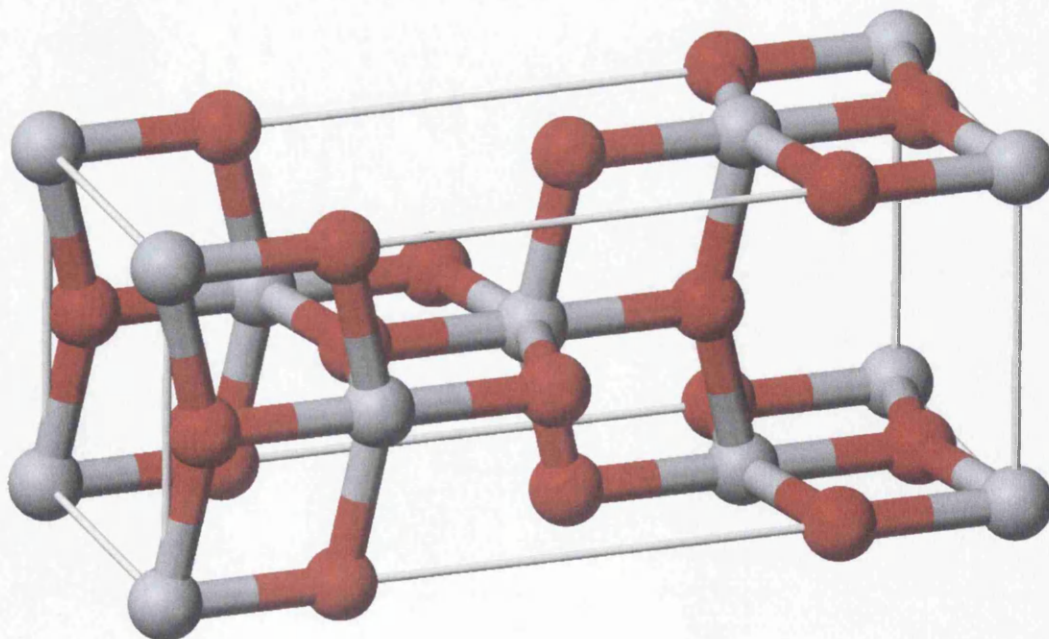


Figure 1-7 The anatase unit cell; the grey atoms represent Ti and the red ones O

(<http://en.wikipedia.org/wiki/Rutile>, accessed March 11,2006))

Sintering

Sintering is a process widely used in materials science and inorganic chemistry. Particles and crystals of one or several materials are fused together in a furnace to create a material of desired strength or morphology without a chemical reaction. The temperature often leads to a relaxation of tensions within the material and helps to create channels between the different particles. This may either lead to a better coverage of a substrate, a more uniform layer or even better electric conductivity, all of which are generally desirable characteristics for DSSCs. Temperature, film thickness, humidity, particle size together with particle pre-treatment and annealing time are parameters which influence the outcome of the sintering process.

Transparent conducting oxide (TCO)

Transparent conducting oxides are transparent oxide coatings which are doped with a metal to create a controlled electric conductivity. In PV-cells ITO (indium doped tin oxide) or FTO (fluorine doped tin oxide) are mainly used. During this project, both of the materials were used as a substrate for the PV-cells.

Electrolytes

There are three major categories of electrolytes: solid, gel and liquid. The solids are mostly conducting or doped polymers whereas the gel electrolytes consist of a gellified matrix which contains the charge carriers very much like in solution. Liquid electrolytes are mostly solvent based (acetonitrile) or ionic liquids.

Examples of solid electrolytes are polyethylene oxide-based polymers [84], pentacene based with iodine [85], and polysiloxanes with quaternary ammonium side groups which were reported to achieve overall conversion efficiencies of 2.67 % at 1000 Wm^{-2} [39]. Elastomeric electrolytes like poly(epichlorohydrin-co-ethylene oxide) filled with Na/I_2 as hole conductors [40] are amongst those reported, as well as thin layers of p-type NiO coated onto the TiO_2 layer [86]. An important characteristic of the electrolyte is also to inhibit charge recombination as much as possible. Layers of PEDOT (poly(3,4-ethylenedioxythiophene) have been involved in successful trials and were reported to enhance the photovoltaic characteristics of the PV-cell [87, 88]. Thin layers of PEDOT coated onto the semiconductor surface help to reduce the proportion of recombination reactions within the cell [89]. Hole conducting polymers such as poly(3-octylthiophene) or copolymers like thiophene-isothianaphthene have also been employed [90]. Detergent based electrolytes were introduced and claim neither to be solid nor liquid based [91]. Gel electrolytes offer the possibility of flexible PV-cells [92]. Different materials have been tried to serve as gel electrolytes such as polyacrylonitrile-based materials [84]. Polymer electrolytes in gel were also reported by Nogueira *et al.* and in this very informative paper Epichlomer-16, poly(epichlorohydrin-co-ethylene oxide, was used [36]. Polymer based gel or quasi-solid electrolytes containing imidazolium ionic liquids of different carbon chain length as charge carriers have also been reported [93, 94]. In general, heterocyclic, nitrogen containing rings and nitrogen containing compounds often improve the characteristics of the electrolyte. Gel electrolytes are reported which contain iodine doped ionic liquids and it seems that there is a trade off between the diffusion coefficient of the molecules and the lifetime of the electron during transport (the bulkier the cation, the longer the lifetime but the lower the diffusion coefficient) [95].

It was also shown that one can influence the photoelectrical characteristics by changing the chain length of the gelator since doing so influences the diffusion coefficient of the ionic liquid [38]. The performance of ionic liquid cells is also reported to be enhanced by addition of water, with an overall conversion efficiency of 4.2 % (at 1000 Wm^{-2}) [37]. A supposedly environmentally friendly, LiI/ethanol and 1 M 4-tert-butylpyridine containing electrolyte which achieved around 6 % overall energy conversion efficiency is also worth mentioning [96].

In the case of solvent based electrolytes used in DSSCs, most of the investigations focused on the use of additives which are mainly nitrogen containing compounds, in different concentrations and mixtures. Hara worked on the influence of the electrolyte on the overall performance of DSSCs using different derivatives of imidazolium iodides and achieved up to 9.2 % overall conversion efficiency using a “black dye” [53], a ruthenium (II) terpyridyl complex [97]. There are many other reports of the effects of different nitrogen containing compounds in the electrolyte on cell performance [33, 98-102].

Even polysaccharides were used as additives in the electrolytes, and these reported to give efficiencies of about 6 % ,when sensitised with N3 dye, with slight differences attributed to the saccharide concentration [34]. The effects of the redox species within the electrolyte was investigated by Liu Yao. In his paper, the influence of water and cations onto the energetic of the cell and the diffusion and mass transport properties of the charge carriers are discussed. A correlation was found between the diffusion coefficient of the redox species and the photocurrent of the cell [103].

Choice of sensitiser

Any body absorbs radiation of different wavelengths. Normally through this input of energy a body gets hotter. We observe in our everyday life many coloured objects. If an object has a certain colour it means that it reflects this single colour or a mixture of wavelengths which make up this colour. It also means that at the same time it absorbs the complementary part of the visible range.

There are two things that can be driven by this incoming energy. Either a body gets hotter or the energy is sufficient to excite the substance of which the body is made of and raise the energy levels of HOMO (highest occupied molecular orbital). The body is then said to be in an excited state.

Materials which are very good at absorbing light through the whole visible spectra are called dyes or pigments. They have absorption bands throughout the visible wavelength range and most of the incident light is transformed into excited state energy. Most successful in doing so are organic and inorganic systems made up from a variety of conjugated systems with different absorption bands.

Worlds energy generation now and 2020

Since the beginnings of the industrial revolution, the world's energy consumption increased and energy was mostly generated from conventional sources like coal, oil and wood. Around mid 20th century nuclear power started to become a considerable source of energy and by the end of the last century, alternative energy sources, like wind, hydro- and solar power became more interesting. It is predicted, that in the coming years the oil and coal consumption will decline and the focus will turn further towards those alternative sources of energy [104]. They are not only abundant in

excess, but their use has much less impact to our environment than the use of energy has nowadays. If only a very small fraction of the incident sunlight was used, all the oil and coal and nuclear energy sources could be replaced by solar energy. In 2007, grid-connected photovoltaic electricity was already the fastest growing energy source with solar cell production growing by 50 % [105].

References

1. O'Regan, B. and M. Gratzel, *Letters to Nature*, 1991. **353**: p. 737-740.
2. Argazzi, R., N.Y. Murakami Iha, H. Zabri, F. Odobel, C.A. Bignozzi, 2004. **248**(13-14): p. 1299.
3. Gratzel, M., *Comptes Rendus Chimie*, 2006. **9**(5-6): p. 578-583.
4. Gratzel, M., *Journal Of Photochemistry And Photobiology C-Photochemistry Reviews*, 2003. **4**(2): p. 145-153.
5. Gratzel, M., *Journal Of Photochemistry And Photobiology A-Chemistry*, 2004. **164**(1-3): p. 3-14.
6. Gratzel, M., 2004. **168**(3): p. 235.
7. Green, M.A., *Solar Energy*, 2004. **76**(1-3): p. 3-8.
8. Pandey, R.N., K.S.C. Babu, O.N. Srivastava, *Progress in Surface Science*, 1996. **52**(3): p. 125-192.
9. Peng, B., G. Jungmann, C. Jager, D. Haarer, H.-W. Schmidt, M. Thelakkat, *Coordination Chemistry Reviews*, 2004. **248**(13-14): p. 1479.
10. Saito, Y., T. Azechi, T. Kitamura, Y. Hasegawa, Y. Wada, S. Yanagida, *Coordination Chemistry Reviews*, 2004. **248**(13-14): p. 1469.
11. Spanggaard, H. and F.C. Krebs, 2004. **83**(2-3): p. 125.
12. Schabauer, J., C.P. Morley, J. Baker, N. Dartnell, P. Douglas, C. Winscom, *Synthesis and Reactivity in Inorganic Metal-Organic and Nano-Metal Chemistry*, 2007. **37**(5): p. 347-351.
13. Serpa, C., J. Schabauer, A.P. Piedade, C.J.P. Monteiro, M.M. Pereira, P. Douglas, H.D. Burrows, L.G. Arnaut, *Journal of the American Chemical Society*, 2008. **130**(28): p. 8876-8877.
14. Becquerel, A.E., *Comptes Rendus Hebdomadaires*, 1838. **9**: p. 561-567.
15. Hoffmann, W., *Solar Energy Materials and Solar Cells*, 2006. **90**(18-19): p. 3285-3311.
16. Saito, Y., S. Kambe, T. Kitamura, Y. Wada, S. Yanagida, *Solar Energy Materials and Solar Cells*, 2004. **83**(1): p. 1-13.
17. Keis, K., C. Bauer, G. Boschloo, A. Hagfeldt, K. Westermark, H. Rensmo, H. Siegbahn, *Journal of Photochemistry and Photobiology A: Chemistry*, 2002. **148**(1-3): p. 57-64.
18. Chen, Z., Y. Tang, L. Zhang, L. Luo, *Electrochimica Acta*, 2006. **51**(26): p. 5870-5875.
19. Chappel, S. and A. Zaban, *Solar Energy Materials and Solar Cells*, 2002. **71**(2): p. 141-152.
20. Benko, G., P. Myllyperkiö, J. Pan, A.P. Yartsev, V. Sundstrom, *Journal Of The American Chemical Society*, 2003. **125**(5): p. 1118-1119.
21. Morandeira, A., G. Boschloo, A. Hagfeldt, L. Hammarstrom, *Journal of Physical Chemistry B*, 2005. **109**(41): p. 19403-19410.
22. Xu, Y. and M.A.A. Schoonen, *American Mineralogist*, 2000. **85**(3-4): p. 543-556.
23. Hagfeldt, A. and M. Gratzel, *Chemical Reviews*, 1995. **95**(1): p. 49-68.
24. Liska, P., K.R. Thampi, M. Gratzel, D. Bremaud, D. Rudmann, H.M. Upadhyaya, A.N. Tiwari, *Applied Physics Letters*, 2006. **88**(20): p. 203103-1-203103-3.
25. Kavan, L. and M. Gratzel, *Electrochimica Acta*, 1995. **40**(5): p. 643-652.
26. Diebold, U., *Surface Science Reports*, 2003. **48**(5-8): p. 53-229.

27. Mosurkal, R., J.-A. He, K. Yang, L.A. Samuelson, J. Kumar, *Journal of Photochemistry and Photobiology A: Chemistry*, 2004. **168**(3): p. 191-196.
28. Mosurkal, R., Y.G. Kim, J. Kumar, L.A. Li, J. Walker, L.A. Samuelson, *Journal Of Macromolecular Science-Pure And Applied Chemistry*, 2003. **A40**(12): p. 1317-1325.
29. Kern, R., R. Sastrawan, J. Ferber, R. Stangl, J. Luther, *Electrochimica Acta*, 2002. **47**(26): p. 4213-4225.
30. Ferber, J., R. Stangl, J. Luther, *Solar Energy Materials and Solar Cells*, 1998. **53**(1-2): p. 29-54.
31. Stangl, R., J. Ferber, J. Luther, *Solar Energy Materials and Solar Cells*, 1998. **54**(1-4): p. 255-264.
32. Han, L., N. Koide, Y. Chiba, A. Islam, T. Mitate, *Comptes Rendus Chimie*, 2006. **9**(5-6): p. 645-651.
33. Kusama, H., M. Kurashige, H. Arakawa, *Journal of Photochemistry and Photobiology A: Chemistry*, 2005. **169**(2): p. 169-176.
34. Kaneko, M., T. Hoshi, Y. Kaburagi, H. Ueno, *Journal of Electroanalytical Chemistry*, 2004. **572**(1): p. 21-27.
35. Schwarzburg, K., R. Ernstorfer, S. Felber, F. Willig, *Coordination Chemistry Reviews*, 2004. **248**(13-14): p. 1259-1270.
36. Nogueira, A.F., J.R. Durrant, M.A. De Paoli, *Advanced Materials*, 2001. **13**(11): p. 826-830.
37. Mikoshiba, S., S. Murai, H. Sumino, T. Kado, D. Kosugi, S. Hayase, *Current Applied Physics*, 2005. **5**(2): p. 152-158.
38. Murai, S., S. Mikoshiba, S. Hayase, *Solar Energy Materials and Solar Cells*, 2007. **91**(18): p. 1707-1712.
39. Li, W., J. Kang, X. Li, S. Fang, Y. Lin, G. Wang, X. Xiao, *Journal of Photochemistry and Photobiology A: Chemistry*, 2005. **170**(1): p. 1-6.
40. Nogueira, A.F. and M.A. De Paoli, *Solar Energy Materials And Solar Cells*, 2000. **61**: p. 135-141.
41. Hara, K., H. Sugihara, Y. Tachibana, A. Islam, M. Yanagida, K. Sayama, H. Arakawa, G. Fujihashi, T. Horiguchi, T. Kinoshita, *Langmuir*, 2001. **17**(19): p. 5992-5999.
42. *Newport Corporation*, 2004.
43. Nazeeruddin, M.K., R. Humphry-Baker, P. Liska, M. Gratzel, *Journal Of Physical Chemistry B*, 2003. **107**(34): p. 8981-8987.
44. Fillinger, A. and B.A. Parkinson, *Journal of The Electrochemical Society*, 1999. **146**(12): p. 4559-4564.
45. Ferrere, S. and B.A. Gregg, *Journal Of The American Chemical Society*, 1998. **120**(4): p. 843-844.
46. Aiga, F. and T. Tada, *Solar Energy Materials and Solar Cells* 2005. **85**(3): p. 437-446.
47. Sugihara, H., S. Sano, T. Yamaguchi, M. Yanagida, T. Sato, Y. Abe, Y. Nagao, H. Arakawa, *Journal of Photochemistry and Photobiology A: Chemistry*, 2004. **166**(1-3): p. 81-90.
48. Nazeeruddin, M.K., S.M. Zakeeruddin, R. Humphry-Baker, S.I. Gorelsky, A.B.P. Lever, M. Grätzel, *Coordination Chemistry Reviews*, 2000. **208**(1): p. 213-225.

49. Takahashi, Y., H. Arakawa, H. Sugihara, K. Hara, A. Islam, R. Katoh, Y. Tachibana, M. Yanagida, *Inorganica Chimica Acta*, 2000. **310**(2): p. 169-174.
50. Yanagida, M., T. Yamaguchi, M. Kurashige, G. Fujihashi, K. Hara, R. Katoh, H. Sugihara, H. Arakawa, *Inorganica Chimica Acta*, 2003. **351**: p. 283-290.
51. Wang, Z.S., C.H. Huang, Y.Y. Huang, B.W. Zhang, P.H. Xie, Y.J. Hou, K. Ibrahim, H.J. Qian, F.Q. Liu, *Solar Energy Materials And Solar Cells*, 2002. **71**(2): p. 261-271.
52. Nazeeruddin, M.K., S.M. Zakeeruddin, J.J. Lagref, P. Liska, P. Comte, C. Barolo, G. Viscardi, K. Schenk, M. Graetzel, *Coordination Chemistry Reviews*, 2004. **248**(13-14): p. 1317.
53. Nazeeruddin, M.K., P. Pechy, M. Gratzel, *Chemical Communications*, 1997(18): p. 1705-1706.
54. Aiga, F. and T. Tada, *Journal Of Molecular Structure*, 2003. **658**(1-2): p. 25-32.
55. Sugihara, H., L.P. Singh, K. Sayama, H. Arakawa, M.K. Nazeeruddin, M. Gratzel, *Chemistry Letters*, 1998(10): p. 1005-1006.
56. Argazzi, R., C.A. Bignozzi, G.M. Hasselmann, G.J. Meyer, *Inorganic Chemistry*, 1998. **37**(18): p. 4533-4537.
57. Nazeeruddin, M.K., R. Humphry-Baker, M. Gratzel, B.A. Murrer, *Chemical Communications*, 1998(6): p. 719-720.
58. Nazeeruddin, M.K., R. Humphry-Baker, D.L. Officer, W.M. Campbell, A.K. Burrell, M. Gratzel, *Langmuir*, 2004. **20**(15): p. 6514-6517.
59. Kay, A. and M. Gratzel, *Journal Of Physical Chemistry*, 1993. **97**(23): p. 6272-6277.
60. Kay, A., R. Humphrybaker, M. Gratzel, *Journal Of Physical Chemistry*, 1994. **98**(3): p. 952-959.
61. Ma, T.L., K. Inoue, K. Yao, H. Noma, T. Shuji, E. Abe, J.H. Yu, X.S. Wang, B.W. Zhang, *Journal Of Electroanalytical Chemistry*, 2002. **537**(1-2): p. 31-38.
62. Enea, O., J. Moser, M. Gratzel, *Journal of Electroanalytical Chemistry*, 1989. **259**(1-2): p. 59-65.
63. Hara, K., Y. Tachibana, Y. Ohga, A. Shinpo, S. Suga, K. Sayama, H. Sugihara, H. Arakawa, *Solar Energy Materials And Solar Cells*, 2003. **77**(1): p. 89-103.
64. Sayama, K., M. Sugino, H. Sugihara, Y. Abe, H. Arakawa, *Chemistry Letters*, 1998(8): p. 753-754.
65. Yanagida, S., G.K.R. Senadeera, K. Nakamura, T. Kitamura, Y. Wada, *Journal of Photochemistry and Photobiology A: Chemistry*, 2004. **166**(1-3): p. 75.
66. Senadeera, G.K.R., T. Kitamura, Y. Wada, S. Yanagida, *Solar Energy Materials and Solar Cells*, 2005. **88**(3): p. 315-322.
67. Mothilal, K.K., J. Johnson Inbaraj, R. Gandhidasan, R. Murugesan, *Journal of Photochemistry and Photobiology A: Chemistry*, 2004. **162**(1): p. 9-16.
68. Tennakone, K., G. Kumara, A.R. Kumarasinghe, P.M. Sirimanne, K.G.U. Wijayantha, *Journal Of Photochemistry And Photobiology A-Chemistry*, 1996. **94**(2-3): p. 217-220.
69. Sankapal, B.R., M.C. Lux-Steiner, A. Ennaoui, *Applied Surface Science*, 2005. **239**(2): p. 165-170.

70. Keis, K., L. Vayssieres, S.-E. Lindquist, A. Hagfeldt, 1999. **12**(1-4): p. 487.
71. Bauer, C., G. Boschloo, E. Mukhtar, A. Hagfeldt, *Journal of Physical Chemistry B*, 2001. **105**(24): p. 5585-5588.
72. Kakiuchi, K., E. Hosono, S. Fujihara, *Journal of Photochemistry and Photobiology a-Chemistry*, 2006. **179**(1-2): p. 81-86.
73. Mane, R.S., H.M. Pathan, C.D. Lokhande, S.H. Han, *Solar Energy Materials and Solar Cells*, 2006. **80**(2): p. 185-190.
74. Sartale, S.D., B.R. Sankapal, M. Lux-Steiner, A. Ennaoui, *Thin Solid Films*, 2005. **480**: p. 168-172.
75. Tai, W.-P., *Solar Energy Materials And Solar Cells*, 2003. **76**(1): p. 65.
76. Nazeeruddin, M.K., A. Kay, I. Rodicio, R. Humphrybaker, E. Muller, P. Liska, N. Vlachopoulos, M. Gratzel, *Journal Of The American Chemical Society*, 1993. **115**(14): p. 6382-6390.
77. Nguyen, T.-V., H.-C. Lee, O.B. Yang, *Solar Energy Materials and Solar Cells*, 2006. **90**(7-8): p. 967-981.
78. Barbe, C.J., F. Arendse, P. Comte, M. Jirousek, F. Lenzenmann, V. Shklover, M. Gratzel, *Journal of the American Ceramic Society*, 1997. **80**(12): p. 3157-3171.
79. Hart, J.N., R. Cervini, Y.B. Cheng, G.P. Simon, L. Spiccia, *Solar Energy Materials and Solar Cells*, 2004. **84**(1-4): p. 135-143.
80. Mane, R.S., O.S. Joo, S.K. Min, C.D. Lokhande, S.H. Han, *Applied Surface Science*, 2006. **253**(2): p. 581-585.
81. Mane, R.S., Y.H. Hwang, C.D. Lokhande, S.D. Sartale, S.-H. Han, *Applied Surface Science*, 2005. **246**(1-3): p. 271-278.
82. Mor, G.K., O.K. Varghese, M. Paulose, K. Shankar, C.A. Grimes, *Solar Energy Materials and Solar Cells*, 2006. **90**(14): p. 2011-2075.
83. Park, N.G., J. van de Lagemaat, A.J. Frank, *Journal Of Physical Chemistry B*, 2000. **104**(38): p. 8989-8994.
84. Ileperuma, O.A., M.A.K.L. Dissanayake, S. Somasunderam, L.R.A.K. Bandara, *Solar Energy Materials and Solar Cells*, 2004. **84**(1-4): p. 117-124.
85. Senadeera, G.K.R., P.V.V. Jayaweera, V.P.S. Perera, K. Tennakone, *Solar Energy Materials and Solar Cells*, 2002. **73**(1): p. 103-108.
86. Bandara, J. and H. Weerasinghe, *Solar Energy Materials and Solar Cells*, 2005. **85**(3): p. 385-390.
87. Yeon Song, M., K.-J. Kim, D.Y. Kim, *Solar Energy Materials and Solar Cells*, 2005. **85**(1): p. 31-39.
88. Kim, Y., Y.-E. Sung, J.-B. Xia, M. Lira-Cantu, N. Masaki, S. Yanagida, *Journal of Photochemistry and Photobiology A: Chemistry*, 2008. **193**(2-3): p. 77-80.
89. Biancardo, M. and F.C. Krebs, *Solar Energy Materials and Solar Cells*, 2007. **91**: p. 1755-1762.
90. Gebeyehu, D., C.J. Brabec, N.S. Sariciftci, D. Vangeneugden, R. Kiebooms, D. Vanderzande, F. Kienberger, H. Schindler, *Synthetic Metals*, 2001. **125**(3): p. 279-287.
91. Maruthamuthu, P., S. Fiechter, H. Tributsch, *Comptes Rendus Chimie*, 2006. **9**(5-6): p. 684-690.
92. Haque, S.A., E. Palomares, H.M. Upadhyaya, L. Otley, R.J. Potter, A.B. Holmes, J.R. Durrant, *Chemical Communications*, 2003(24): p. 3008-3009.

93. Suryanarayanan, V., K.-M. Lee, W.-H. Ho, H.-C. Chen, K.-C. Ho, *Solar Energy Materials and Solar Cells*, 2007. **91**(15-16): p. 1467-1471.
94. Wang, P., S.M. Zakeeruddin, M. Grätzel, *Journal of Fluorine Chemistry*, 2004. **125**(8): p. 1241-1245.
95. Paulsson, H., L. Kloo, A. Hagfeldt, G. Boschloo, *Journal of Electroanalytical Chemistry*, 2006. **586**(1): p. 56-61.
96. An, H., B.F. Xue, D. Li, H. Li, Q.B. Meng, L. Guo, L. Chen, *Electrochemistry Communications*, 2006. **8**: p. 170-172.
97. Hara, K., T. Nishikawa, M. Kurashige, H. Kawauchi, T. Kashima, K. Sayama, K. Aika, H. Arakawa, *Solar Energy Materials And Solar Cells*, 2005. **85**: p. 21-30.
98. Kusama, H. and H. Arakawa, *Journal of Photochemistry and Photobiology A: Chemistry* 2004. **164**(1-3): p. 103-110.
99. Kusama, H. and H. Arakawa, *Solar Energy Materials and Solar Cells* 2004. **82**(3): p. 457-465.
100. Kusama, H. and H. Arakawa, *Solar Energy Materials and Solar Cells*, 2005. **85**(3): p. 333-344.
101. Kusama, H., H. Arakawa, H. Sugihara, *Journal of Photochemistry and Photobiology A: Chemistry* 2005. **171**(2): p. 197-204.
102. Kusama, H. and H. Sugihara, *Journal of Photochemistry and Photobiology A: Chemistry*, 2006. **181**(2-3): p. 268-273.
103. Liu, Y., A. Hagfeldt, X.R. Xiao, S.E. Lindquist, *Solar Energy Materials And Solar Cells*, 1998. **55**(3): p. 267-281.
104. Hubbert, M.K., *American Scientist*, 1984. **72**(3): p. 293-293.
105. www.wikipedia.com, accessed 20 July 2008.

CHAPTER 2

EXPERIMENTAL

2. Experimental

2.1. Solar cell preparation

The conducting fluorine-doped SnO₂ coated glass (8 Ω cm⁻² sheet resistance) is available in 100 mm x 100 mm sheets and was cut to smaller pieces of 20 mm x 25 mm. After cutting, the glass was rinsed with plenty of water and with ethanol to clean the conducting surface. Afterwards, the glass was dried with a hair dryer. The Solaronix TiO₂ HT–Paste (highly transparent, particle size 9 nm) was then stirred thoroughly with a glass pipette before being “squeegee” printed onto the SnO₂ coated side of the glass substrate. The squeegee printing method is used by several research groups [1-5]. In this method one or more layers of Scotch Magic® tape are affixed onto two opposite edges of the glass. The TiO₂ paste is then spread onto the conducting glass between the tape layers with the help of a microscope slide with a round, polished edge. The TiO₂ electrode substrates were then left to dry in air for about one to two hours. Afterwards, the tape was carefully removed and the glass with the TiO₂ layer was put into an oven at 430 °C for 30 min.

After this annealing step, the glass pieces were taken out of the oven and left to cool. Depending on whether they were used immediately or kept for later use they were either cooled down to about 80 °C and immediately immersed into the dye ethanol solution for adsorption, or kept in a dark, dry and dust-free place. Stock slides prepared this way can be used at any time by just putting them again into the oven for 30 min before being immersed in the dye ethanol solution as described above.

Adsorption of the sensitising dye was achieved by immersing the glass substrates in a 3 X 10⁻⁴ M solution of dye for 20 – 24 h. Although a swifter dye uptake technique with higher concentrations and a much shorter adsorption time of only a few hours

has been reported for the N719 dye (see section 2.1.8. for dye structures) we preferred to use longer immersion times since we intended to examine other dyes as well [6].

The counter electrode was made by a similar method using the same conducting glass substrate, but instead of the TiO₂ paste a Pt – catalyst paste (Solaronix SA) was squeegee printed onto the conducting side. The two tapes were removed shortly after the application of the Pt – paste and the counter electrodes were put into the oven at 100 °C for 10 min to dry and then left for 30 min at 400 – 430 °C. After removal and cooling the counter electrode was rinsed with absolute ethanol and dried with a hair dryer. The assembly of the sandwich cell was as follows. The polymer sealing material purchased from Solaronix was cut into 1.5 – 2 mm wide stripes and used to make a frame on the active side of the working electrode. Two slits of less than 1 mm width were left at the two top corners for filling the cell with electrolyte later on and the counter electrode was carefully put onto the working electrode with the Pt coated face pointing towards the working electrode.

The sandwich cell was then put onto a heating plate and low pressure was applied from the top until the sealing material had melted and the two electrodes were glued together. Using a micropipette or a syringe, the sandwich cell was then filled *via* one of the two holes taking advantage of the capillary effect. It was necessary to ensure that one air hole was always open and that the electrolyte solution was not sucked along the sealant to this air hole otherwise it blocked it. It is worth noting that small bubbles left in the electrolyte do not influence the efficiency of the PV cell much. A very good and educational paper which helps to understand the basic cell making process was written by Smestad [7].

The final sealing step can be something of a problem. It is achieved by sealing the two holes used for filling using small, square pieces of the sealing polymer which are

gently melted with a soldering iron by keeping a microscope slide between the iron and the sealing polymer. However, over time there is always a loss of electrolyte. This problem was partially overcome by use of a second sealing layer consisting of a two component glue (Araldite) which was coated around the sealant gap. This substantially improved the lifetime of the cell. The volatility of the acetonitrile based electrolyte is a problem which is also encountered by the manufacturers of liquid electrolyte solar cells [8, 9].

Most cells were prepared as described above, without the two extra “finishing steps” which have been reported in the literature [1]. But for some cells these “finishing steps” were included, and a description of these steps is as follows. It is believed that hydrolysis of ultrapure, and ultrasmall anatase particles onto the already sintered TiO_2 layer can increase the active surface area for dye adsorption. It also seems to increase the electron conducting efficiency of the semiconductor substrate, probably by lowering the series resistance arising at the dye-semiconductor contacts. It is believed that the electron transfer from anchored dye to semiconductor is controlled by electron tunneling and therefore one should be aiming to achieve the best coverage of the conducting oxide surface with the purest anatase crystals [10]. This is achieved by preparing an aqueous 2 M TiCl_4 solution, freshly diluting it in the ratio 1:10 and applying onto the 1 x 1 cm^2 TiO_2 electrode and leaving it overnight. This was done in a closed petri-dish ensuring that the atmosphere within it was humid enough in order to prevent drying out of the electrode overnight. Following this treatment the solution was rinsed off with water and the glass slides sintered again for 30 min at 430 °C and then used for cell preparation in the normal way.

Another method to increase cell efficiency, this time by generating an increase in the open circuit voltage and also the short circuit current of the cell, is to dip the

electrodes into tetra-butylpyridine after dye adsorption [1]. In our case this was achieved by adding tetra-butylpyridine to one of the electrolytes (EL3, see section 2.1.5 for electrolyte composition).

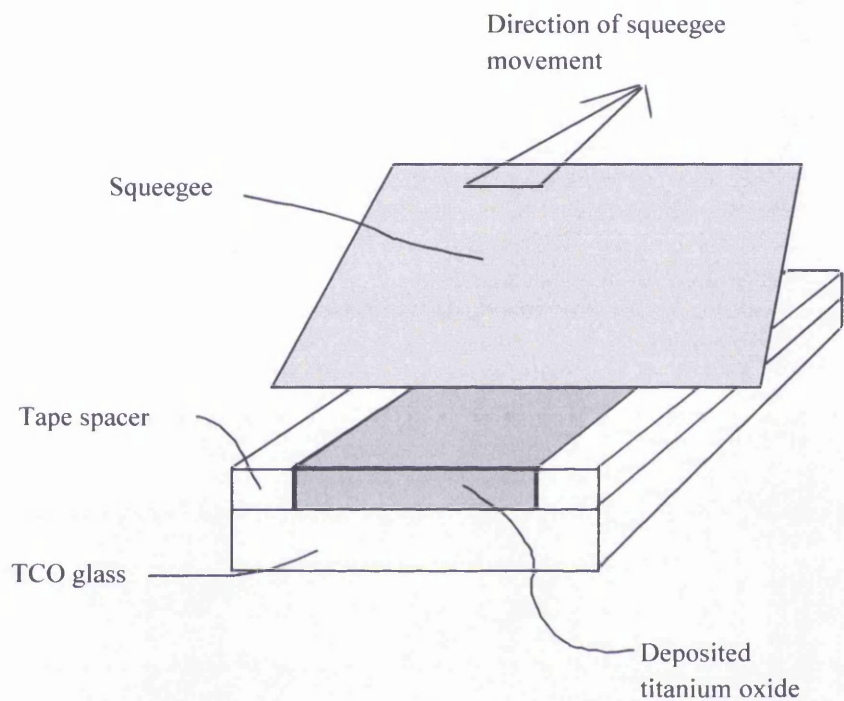


Figure 2-1 Squeegee printing process (www.solaronix.com) [11]

2.1.1.1. Stepwise assembly of a dye-sensitized solar cell:

(This method follows the procedure given on the www.solaronix.com homepage) [11]

1. never touch the glass with bare fingers; after you have done so, clean with ethanol and dry with hair dryer

2. the conducting side is the sticky one when touched gently with the fingernail
3. stir the nanopaste well before use, do not shake it
4. apply adhesive tape to conducting side of cell (two layers)
5. spread out approximately $10 \mu\text{L cm}^{-2}$ of titanium oxide paste with a squeegee (microscope slide with polished edges)
6. let electrode dry, till solvent is removed (Ti-Nanoxide HT paste turns transparent)
7. check for air bubbles
8. remove the adhesive tape without touching the prepared TiO_2 surface
9. heat the electrode to *ca.* $450 \text{ }^\circ\text{C}$ for 30 min
10. let it cool down to $60\text{-}80 \text{ }^\circ\text{C}$
11. prepare sensitizer solution in pure ethanol ($3 \times 10^{-4} \text{ M}$)
12. put the sintered electrode at $70 \text{ }^\circ\text{C}$ into the dye solution at room temperature
13. let the electrode impregnate in the stirred solution overnight (a properly impregnated electrode shows no white areas at all)
14. no water should contact the impregnated electrode
15. squeegee print the platinum catalyst onto the conducting side of the counter electrode
16. dry the counter electrode at $100 \text{ }^\circ\text{C}$ for 10 min prior to firing it at $400 \text{ }^\circ\text{C}$ for 30 min
17. assemble the cell as soon as the electrodes are prepared
18. build a frame with the sealing material on top of the glass electrodes

19. apply heat and press the two electrodes together till the sealant melts at 100–120°C
20. leave two holes in the sealing rim and put a droplet of electrolyte onto one hole and let it soak in; replenish the droplet from time to time to avoid bubble formation
21. seal the holes by using small squares of sealant and melt them with a soldering iron
22. prior to testing put silver paint onto the contacts

The preparation of DSSCs in pictures:

After the electrodes were brushed and rinsed with ethanol, they were dried with hot air and with the conducting side facing upwards placed on a paper which was masked with the outlines of the cell and working electrode size. Scotch magic tape[®] was used as a template for the working electrode thickness, with either one or two layers of tape being used, and the working electrode area of 1 x 1 cm was left out.

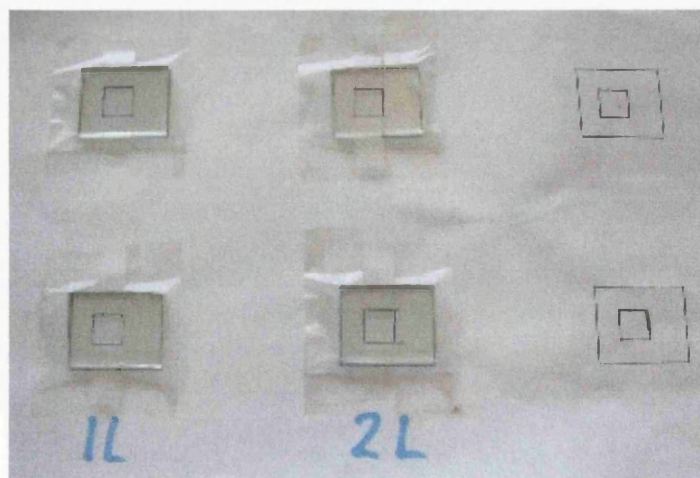


Figure 2-2 Cleaned conducting glass slides with masked working electrode area

Using a glass rod or a microscope slide with a rounded edge, the titania sol was spread over the slides and left to dry in air for 1½ to 2 h.

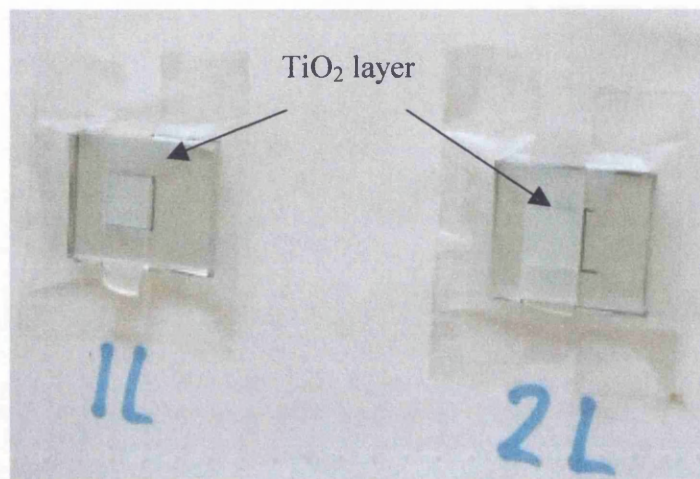


Figure 2-3 Working electrodes with fresh, squeegee printed titania sol; left, one layer of tape; right, two layers of tape

In this case where Solaronix HT nanopaste had been used, the working electrode was almost transparent after it had dried (Figure 2-4). In Figure 2-4 we see an electrode with one layer of template thickness on the left and two layers of the Scotch magic tape[®] on the right. The right working electrode is slightly more opaque than the left one. Next, the tape was removed and the electrodes were placed in a furnace at 430 °C for half an hour.

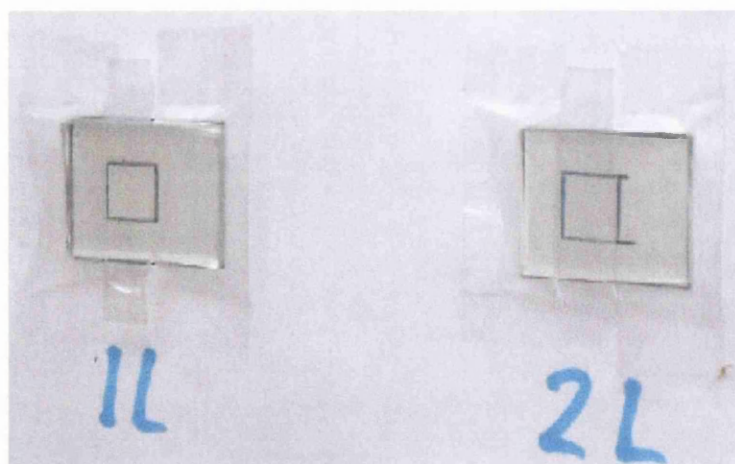


Figure 2-4 Working electrodes with the air dried semiconductor layer, ready for sintering; left, one layer of tape; right, two layers of tape

After the cells had cooled down to room temperature freshly prepared 0.2 M aqueous TiCl_4 solution was applied onto the working electrode (about $50 \mu\text{L}$ per cm^2). Distilled water was dropped into the petri-dish to ensure that the electrodes surfaces would not dry out overnight, and the dish closed and covered with aluminium foil.

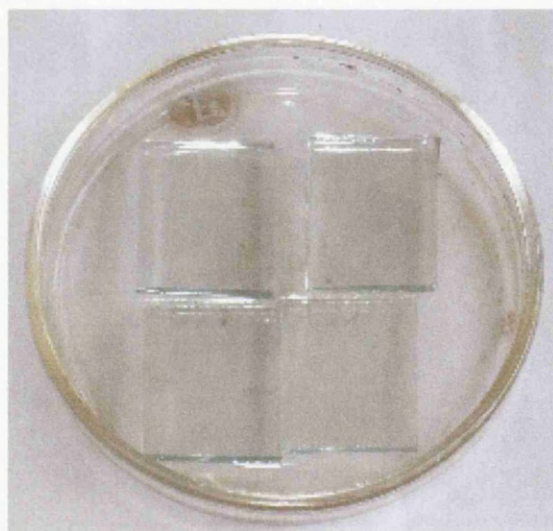


Figure 2-5 Already sintered electrodes kept in ethanol



Figure 2-6 Working electrodes in dye solution (SQU 1); the dye concentration was about 3×10^{-4} M

On the following day the glass slides were fired again at $430\text{ }^{\circ}\text{C}$ for another 30 min and after they had cooled down to about $80\text{ }^{\circ}\text{C}$ placed in an ethanolic dye solution. Under continuous stirring the slides were left for dye adsorption overnight. The hydrolysis of small and pure crystals from TiCl_4 solution on top of the semiconductor film originating from the sol was considered a finishing step which has not been done for all the cells. It was not believed to be of importance for relative comparison of cell performance within our series of experiments. But it was done to link the cell characteristics obtained in the work presented here to cell performances given in the literature and to gain the best possible cell output.

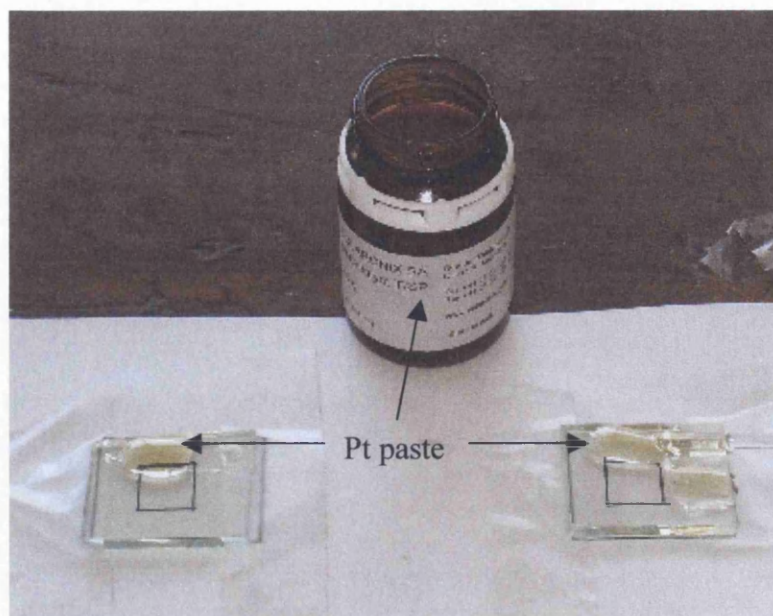


Figure 2-7 The Pt-paste ready to be spread over the counter electrode, small drops were already placed on the conducting glass surface

The counter electrodes were always prepared freshly on the day of cell assembly. Again, the conducting glass was cleaned with ethanol then two stripes of tape were used on each side of the glass slide and the Pt-paste was applied using a glass rod and spread evenly across the free conducting surface. Then the tape was removed and the slides heated for 10 min at 100 °C before firing them for half an hour at 430 °C.



Figure 2-8 the counter electrodes before firing after the tape was removed

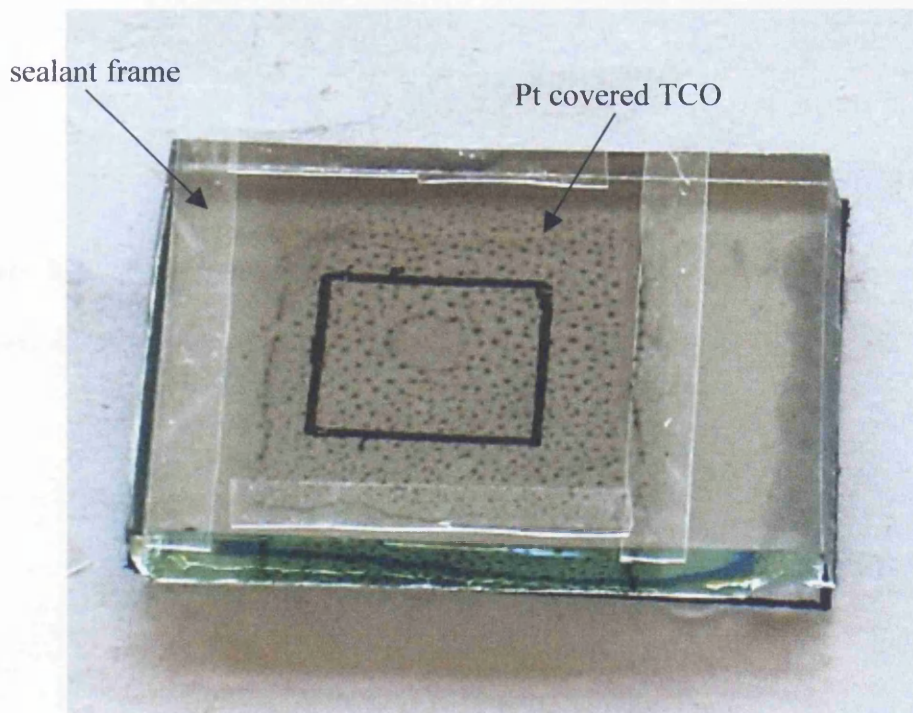


Figure 2-9 counter electrode with sealant frame

After the counter electrodes had cooled down to about 80 °C they were placed on a sheet of paper and the sealant frame was built around the edges of the cell, leaving two slits diagonally opposite which were later used to fill the cells with electrolyte.

The surface of the counter electrode shows grey clusters of Pt which, as will be discussed later in the thesis (see Chapter 3), act primarily to catalyse the electron transport between electrolyte and conducting oxide in the working solar cell.

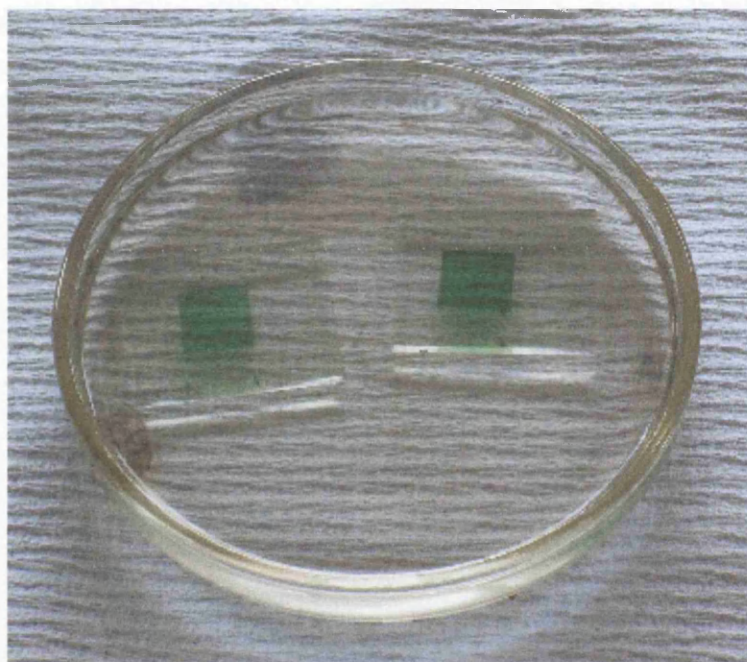


Figure 2-10 The dye adsorbed working electrodes were rinsed with ethanol and kept in fresh ethanol before cell assembly in order to prevent exposure to air moisture.

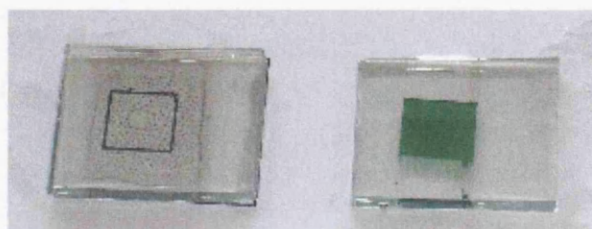


Figure 2-11 A counter and working electrode ready for assembly and sealing.

The working electrode was carefully put on top of the platinised counter electrode with the two conducting sides facing each other. Before heating the position of the sealant frame should be checked.

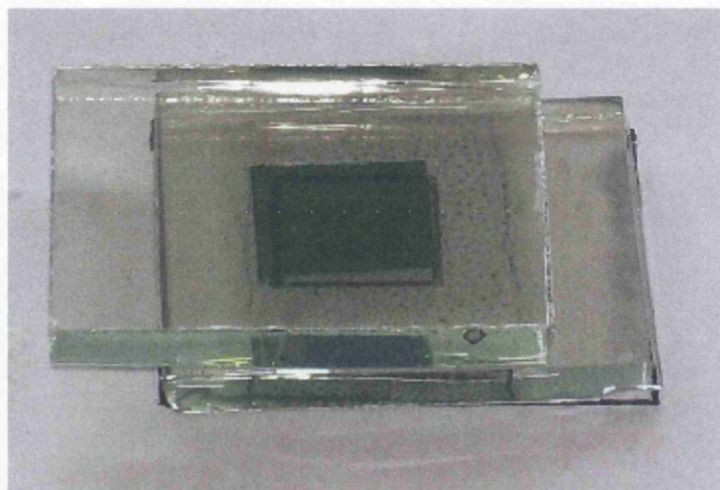


Figure 2-12 working and counter electrode put together with the hot-melt sealant frame already in place but not yet melted

Keeping the two glass slides tightly pressed together they were transferred onto an hotplate. The melting temperature of the sealant is 120 °C. A microscope slide was placed on top of the cell and gentle pressure was applied for about 2 minutes using a cork ring. The cell frame is sealed, when the hotmelt sealant becomes clear. It was important that the filling holes did not melt together. The cell was left to cool down and immediately afterwards filled with the electrolyte using a micro syringe. With improved technique, it was possible to fill the cell without leaving any trapped air bubbles between the two electrodes. Short stripes of the sealant material were cut, and using these and the soldering iron, the two filling holes were closed.



Figure 2-13 pressing the sandwich cell whilst sealing the cell

filling holes

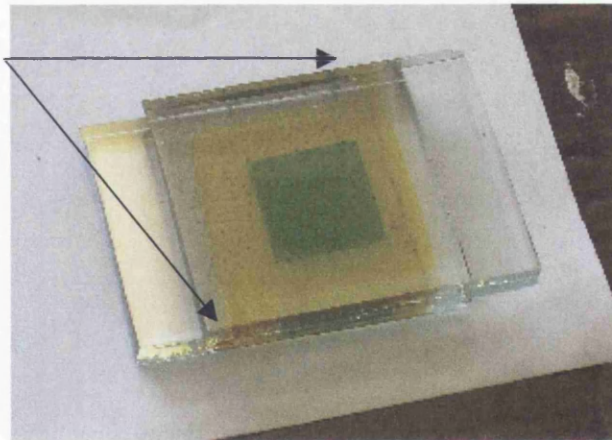


Figure 2-14 the sealed sandwich cell already filled with electrolyte

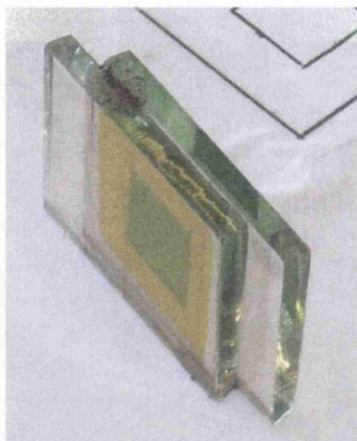


Figure 2-15 the filling holes are already closed with hot-melt

Araldite two component glue was mixed and spread over the filling holes and alongside the length of the cell for an extra sealing effect. Finally, conductive silver paint was applied to the two about 5 mm wide contact areas of each electrode. After the conductive paint and the Araldite had dried, the cell was ready for testing.



Figure 2-16 sealed cell standing

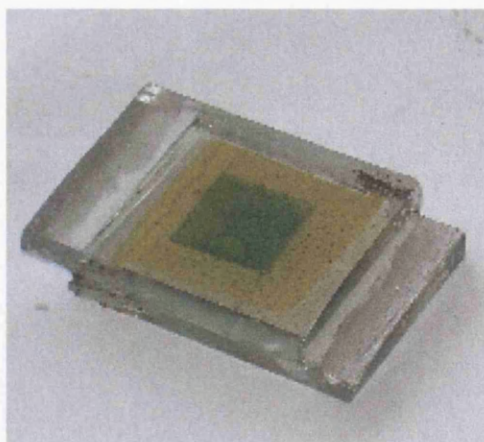


Figure 2-17 sealed cell

Figure 2-16 (left) and 2-17 (right) The last two steps of the cell making process. First, the filling holes which had been closed with hot-melt were sealed with Araldite and then conductive silver paint was applied to the two contact sites on the counter and the working electrode respectively.

2.1.2. Preparation of different types of Grätzel Cells

The Grätzel cells described above are sandwich type cells where the semiconductor film is applied onto a transparent support and electrically connected to the counter electrode by the means of an electrolyte. As part of this work, described in Chapter 3, cells have been made using different glass and plastic supports, TiO₂ sols, and gel and liquid electrolytes.

All of these cells were built with an active area of 1 cm x 1 cm of TiO₂ onto which the dye was adsorbed. The cells were generally built using the methods described in the literature [1]. All cells were made in triplicate. The following variations in cell design were made.

2.1.3. Transparent conducting oxide support.

As TCO support, we used either plastic or glass. Both ITO (indium doped tin oxide) (SPI, US) and FTO (fluorine doped tin oxide) (Solaronix, SA) glasses were used but only ITO was used with the plastic support. The FTO glass had a sheet resistance of 8 Ω cm⁻² while that of the ITO glass of about 20 Ω cm⁻². The TiO₂ layer could not be heat sintered on plastic so pressure sintering was used instead. This meant covering the TiO₂ layer with a thin elastic plastic sheet and pressing it using a hydraulic press at about 3000 – 4000 kg cm⁻². The surface characteristics and porosity of the pressure sintered semiconductor film are not known. It has been reported that temperature sintering influences the particle size as well as the pore size of the TiO₂ films substantially [12].

2.1.4. Differents sols

Alongside the Solaronix TiO₂ HT–Paste a number of different custom made sols were also used. These TiO₂ sols were prepared using P25 from Degussa following the preparation method reported by Nazeeruddin *et al.* [1]. A variety of different binders for the sols were used i.e. polyethyleneoxide MW 600.000 and MW 300.000 from BDH chemicals, ethyl cellulose from Aldrich, and acid washed cellulose from spruce which was supplied by Fluka.

Table 2-1 shows the composition of the different sols made. It was hoped that these additives would act as a binder as well as a matrix to influence the morphology and porosity of the TiO₂ surface. In all cases 300 mg of additive were added to 6 g of P25 (~ 5 % w/w) and ground together in a self made stainless steel ball mill.

Sol name	Composition
P02	P25 Degussa without binder
P03	P02 plus 300 mg ethyl cellulose (pre-ground in mortar)
P04	P02 plus 300 mg PE-oxide MW 300.000
P05	P02 plus 300 mg PE-oxide MW 600.000
P06	P02 plus 300 mg acid washed cellulose from spruce

Table 2-1 Titania sols used

In all cases these TiO₂ sols were squeegee printed using one layer of Scotch Magic tape. They were then air dried for about one hour before they were either heat sintered at 430 °C or put into an oven at 95 °C for an hour before pressure sintering. Care had to be taken not to keep the plastic substrates at high temperature for too long, since this destroyed the conducting layer.

The pressure-sintering step took place in a hydraulic press, applying about 3000–5000 kg per cm². After the sintering steps, the TiO₂ coated electrodes were put into a dye bath overnight. In all cases, the same dye, cis-di(thiocyanato)bis(2,2'-bipyridyl-4,4'-dicarboxylate)ruthenium(II) (N3 dye) was used. Optical density measurements of the films after dye adsorption were made to gain an idea of the amount of dye adsorbed onto the semiconductor layer, as well as their homogeneity and the reproducibility of the dye adsorption and TiO₂ coating.

2.1.5. Different electrolytes

Five different electrolytes were used although the redox couple for all of them was iodide/tri-iodide (I^-/I_3^-). Four of them were acetonitrile based liquid electrolytes with different concentrations [13, 14] of the redox couple components and one was a gel electrolyte.

Electrolyte	Manufacturer	Composition
Iodolite AN-50	Solaronix, SA, CH	50 mM of triiodide in acetonitrile, exact composition not known
EL1	N/A	0.3 M LiI/0.03 M I_2 in acetonitrile
EL2	N/A	0.5 M LiI/0.05 M I_2 in an 80:20 (v/v) mixture of 3-methyl-2-oxazolidinone (NMO)
EL3	N/A	1.0 M LiI/0.1 M I_2 in 60 % acetonitrile, 20 % 3-methyl-2-oxazolidinone and 20 % t-butyl-pyridine
EL4	Kodak European Research laboratory	(poly(epichlorohydrin-co-ethylene oxide) dissolved in acetone with about 30 mM triiodide in the gelified state

Table 2-2 Electrolytes used

The gel electrolyte was a polymer electrolyte (poly(epichlorohydrin-co-ethylene oxide) dissolved in acetone, which was prepared in the Kodak Laboratories in Cambridge, with a similar concentration of the redox couple in the gelified state to the concentration of the low concentration acetonitrile electrolyte, i.e. 30 mM triiodide.

2.1.6. Sealant

Liquid electrolyte cells were sealed with SX-1170 hot-melt from Solaronix SA and filled using capillary force as described above in section 2.1. The “hot-melt” melts at around 120 °C. A frame of 2 mm wide strips of hot-melt was built on top of the working electrode support just after it was taken out of the dye solution and dried with a hairdryer. Two filling holes of about 1 mm width were left open on two diagonal corners of the cell. Then the counter electrode which had just been platinized was placed on top of it. This “sandwich” was placed on a hotplate and gentle pressure was applied for about 1 to 2 minutes. After cooling down, the cells were filled with electrolyte from a micropipette using capillary action.

Gel electrolyte cells were sealed with a similar frame consisting of an adhesive polymer with no filling holes left open. A liquid solution of the polymer electrolyte in acetone was added ($400 \mu\text{L cm}^{-2}$) and the solvent evaporated off on a hotplate. After solvent evaporation the counter electrode was placed on top and both sides of the cell pressed together using gentle pressure for about 1–2 min.

2.1.7. Counter electrodes

For the counter electrodes, glass or plastic ITO or FTO substrates were used and a Pt-film was applied either by using a Pt-paste by Solaronix SA and squeegee printing it before heating it at 100 °C for 10 min followed by 430 °C for 30 min, or the Pt was sputtered onto the surface in a vacuum chamber (this latter process was carried out in Kodak European Research labs).

2.1.8. Sensitising dyes

The following list gives names, structure and sources for the sensitizing dyes used in this work.

1) cis-di(thiocyanato)bis(2,2'-bipyridyl-4,4'-dicarboxylate)ruthenium(II)-bis-tetrabutylammonium salt (N719 dye) purchased from by Johnson Matthey;

$M = 1187.7 \text{ g mol}^{-1}$

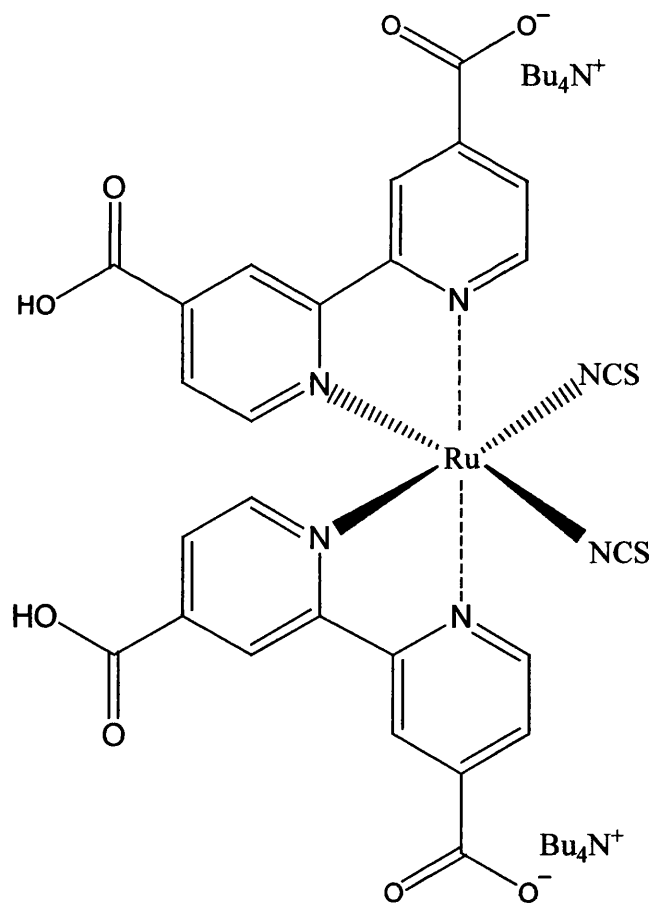


Figure 2-18 N719 dye

2) cis-di(thiocyanato)bis(2,2'-bipyridyl-4,4'-dicarboxylate)ruthenium(II)

(N3 dye) was purchased from Solaronix SA under the tradename Ruthenium 535.

M= 741.7 g mol⁻¹, including two molecules of water of crystallization.

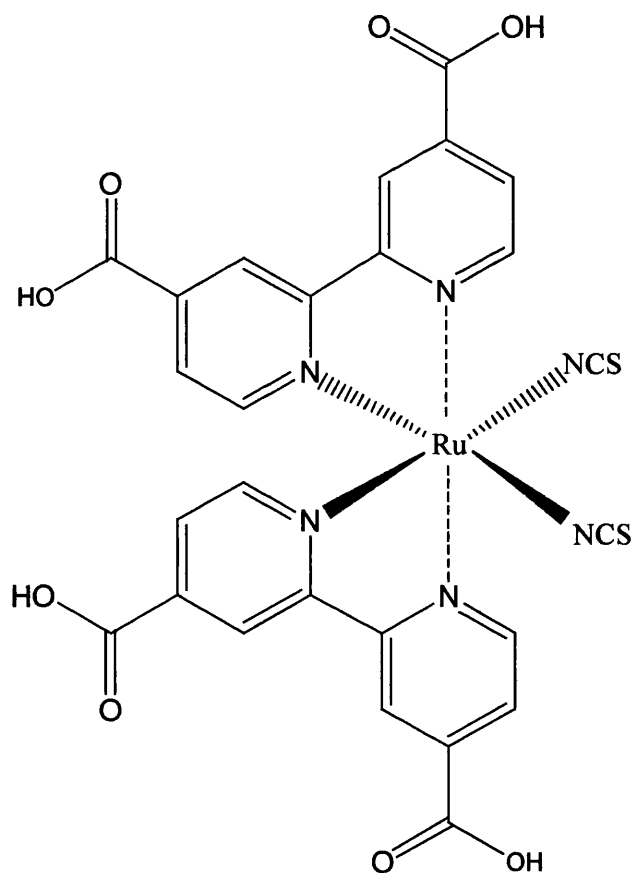


Figure 2-19 N3 dye

3) 5,10,15,20-tetrakis(4-sulphophenyl)porphyrinate manganese (III) chloride

MnTPPSO₃H

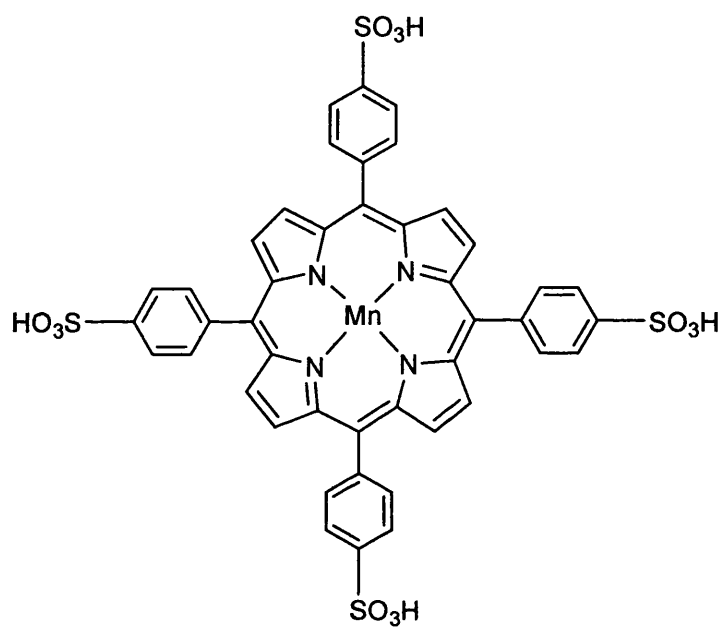


Figure 2-20 MnTPPS

Synthesised and supplied by Carlos Monteiro, Universidade de Coimbra, Portugal

[15].

4) 5,10,15,20-tetrakis(4-sulphophenyl)porphyrinate copper (II) CuTPPS

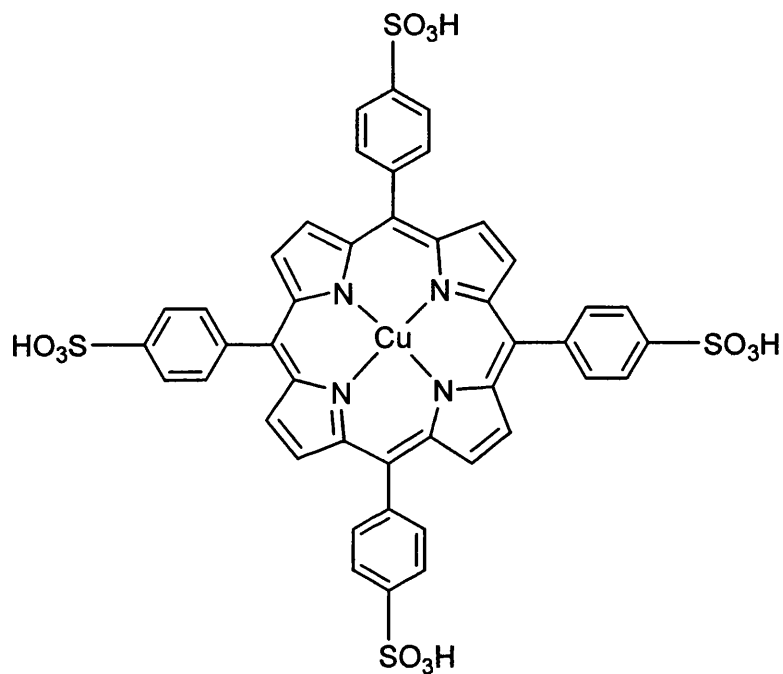


Figure 2-21 CuTPPS

Synthesised and supplied by Carlos Monteiro, Universidade de Coimbra, Portugal

[16].

5) (SQU1)

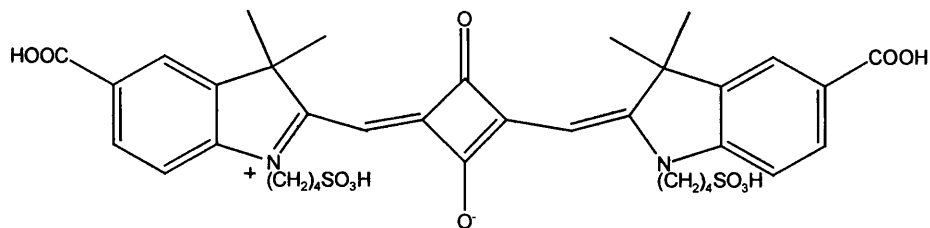


Figure 2-22 SQU1

Synthesised and supplied by Victoria Hughes, Swansea, whom I especially want to thank for supplying these dyes.

6) (SQU2)

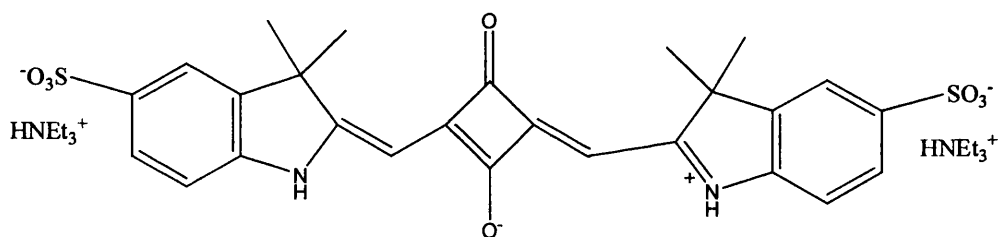


Figure 2-23 SQU2

Synthesised and supplied by Victoria Hughes, Swansea.

7) Polyaniline

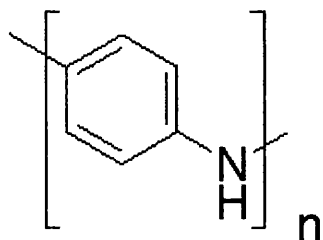


Figure 2-24 Polyaniline

This polymer was supplied by Dr. Hugh Burrows, Universidade de Coimbra, Portugal, but was originally synthesised at the University of Durham, UK. The polyaniline formed very long chains with a low degree of crosslinking, the exact molecular weight is not known [17, 18].

2.1.9. Photoelectrical Measurement

For the photoelectrical characterisation of the cells, two different set-ups were used depending on whether the cells were measured at the Kodak European Research Laboratory in Cambridge or at the laboratory at Swansea University. The set-up in Cambridge enabled us to measure I-V curves of cell over a range of solar irradiation intensities up to one Sun. This was carried out by biasing the cells with increasing voltage in equidistant steps and measuring the cell current. The instrumentation in Swansea made it possible to measure I-V curves over both a controlled light intensity and controlled temperature range. It was also possible to obtain the time resolved cell

response e.g. the build-up of electric potential and its decay over different light intensities and temperatures, with the equipment in Swansea.

For the comparison of the cell performances we have followed the approach of many other workers and used a “best cell” method of assessment, i.e. the photoelectrical characteristics of the best cell out of three were used for comparison. This is justified because of significant differences in short circuit current (I_{SC}) of cells of the same type because of unavoidable irreproducibilities in the process of cell assembly. There is always potential to create a channel for back reactions, thus lowering the shunt resistance of the cell which leads to a lower I_{SC} and fill factor (ff). All liquid electrolyte cells were irradiated from the front (i.e. the light is incident on the TiO_2 electrode first) whereas for some gel electrolyte cells it was possible to irradiate from either front or back when the counter electrode was transparent enough. Figure 2-25 shows a typical I-V curve of a solar cell and the parameters usually used to describe the cell's electrical characteristics. The figure also shows how the cell parameters, like short circuit and open circuit current, fill factor, maximum power point, can be determined graphically. This is a quick and easy method for a first estimation of cell efficiency and to compare different cells under changing conditions. The graphical method was used in this work to compare cell efficiency when cell modelling was not considered to give more meaningful data with respect to the time and effort it required.

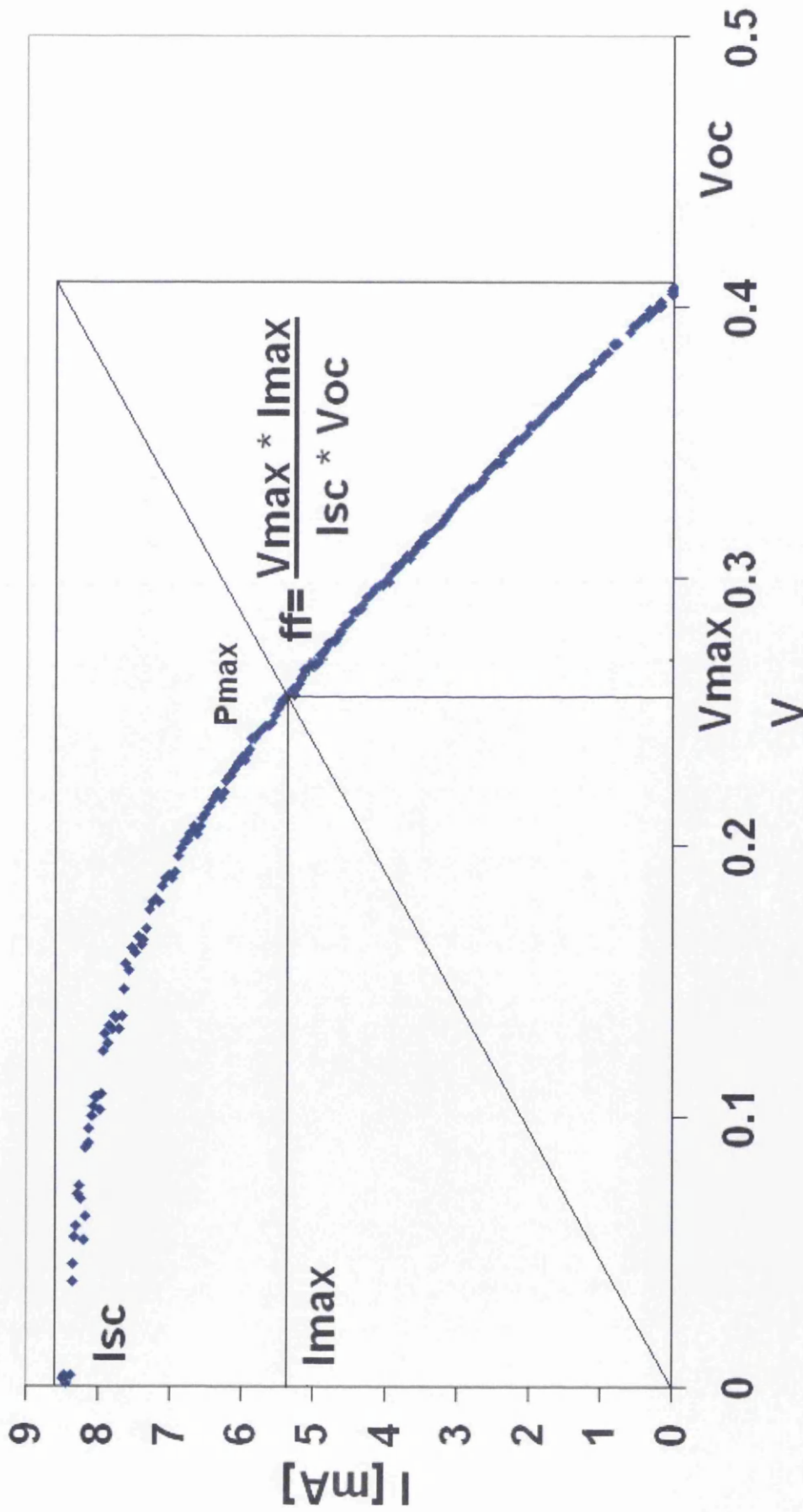


Figure 2-25 The current-voltage curve of a typical solar cell (SQ-P05 cell with 2 layers Scotch Magic tape at a temperature of 5 °C).

I_{sc} ... short circuit current

V_{oc} ... open circuit voltage

I_{max} ... current at max. power

V_{max} ... voltage at max. power

ff fill factor

P_{max} ... maximum power point

2.1.9.1. Cambridge facilities

The photoelectrical measurements took place using an arrangement of seven 50 W halogen lamps which were focused onto an area of uniform irradiation with a spectral distribution with a good match to the sun's spectrum in the visible region.

By changing the distance of the light source to the measured cell, an irradiation intensity up to one Sun could be used. The light intensity was evaluated using a Thales silicon photodiode Model IPL10050CW with an active area of 41.3 mm².

To create a voltage to current curve the cell current was scanned in 10 mV steps both up and down the potential of a cell in order to measure the hysteresis of the system and to adjust the measurement.

2.1.9.2. Swansea facilities

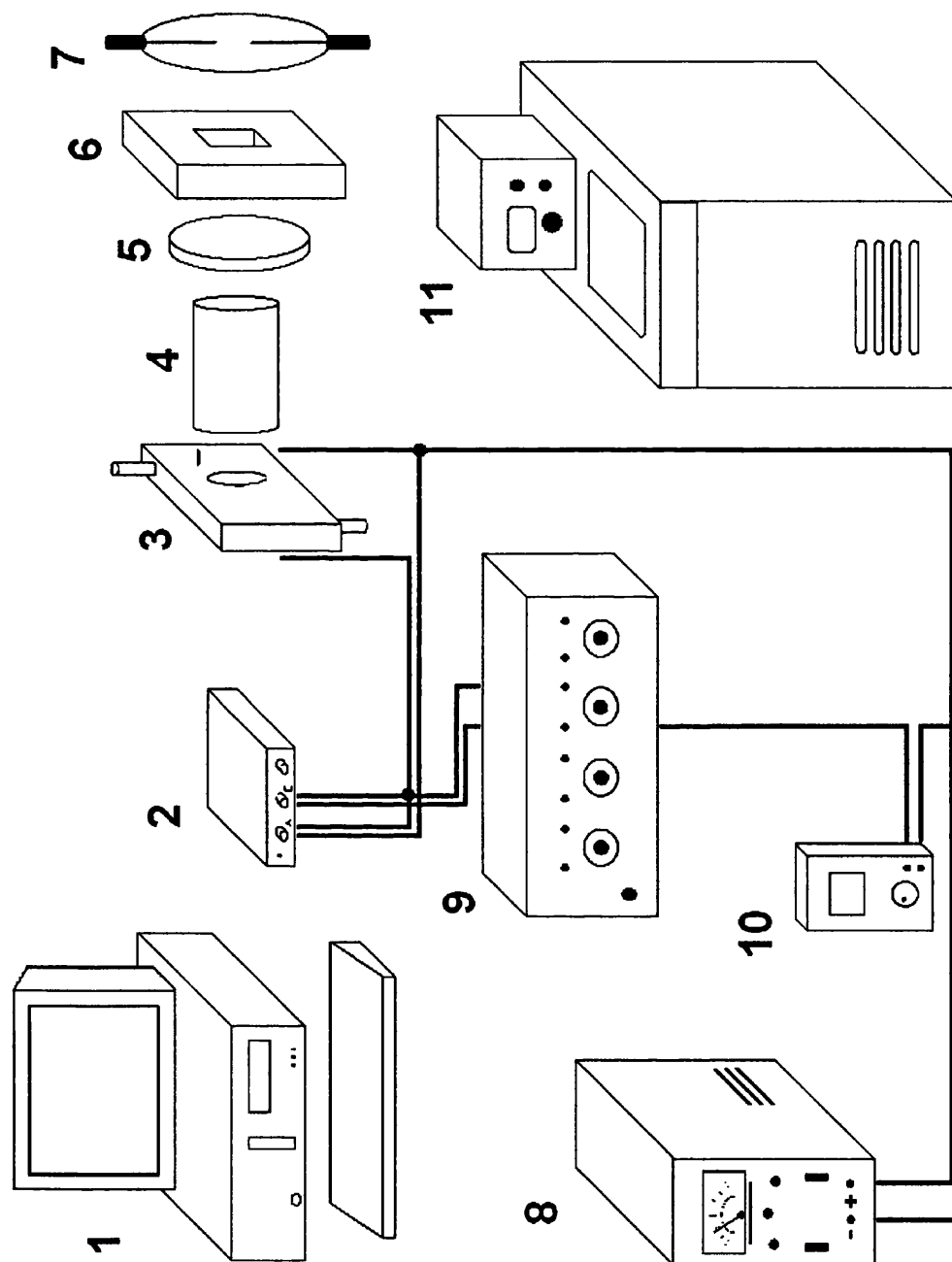
This irradiation system was designed to simulate the incident sunlight onto the earth's surface whilst ensuring the highest possible reproducibility of the individual experiments.

2.1.9.2.1. Overview of irradiation and measurement system

In order to characterise a photovoltaic cell a device simulating the sun's spectrum is needed. In order to match this spectrum a lamp has to be used which already possesses an emission spectrum close to the one of the sun at the earth's surface. In our case this was accomplished by using a 900 W Xenon arc lamp. The effect of atmospheric absorption was mimicked by a air mass filter. We used an AM 1.0 filter which corrects the xenon arc lamp emission to that of the sun when it is directly overhead. Variations in solar intensity were obtained using electrical control of the lamp current and/or neutral density filters of ~60% and ~20 % transmission across the

visible and near UV spectral range. The photoelectric measurements were obtained using an analog-digital converter, a PC, digital bench multimeters, a temperature control unit and a sample holder which can ensure controllable measurement conditions.

Figure 2-26 shown on the following page gives a scheme of the photoelectrical measurement setup used for the characterisation of the solar cells.



1	PC	2	PicoLog AD converter ADC-212	3	Sample holder
4	NaN ₂ UV cut-off filter	5	AM 1.0 filter	6	Shutter
7	900W Xenon arc lamp with transformer	8	DC source	9	Resistor decade for the changing load
10	Digital multimeter	11	Temperature control unit		

Figure 2-26 Set up of cell characterisation equipment

2.1.9.2.1.1. UV cut-off filter

When required, a five percent aqueous NaNO_2 solution was used as a UV cut-off filter. The aim was to exclude excitation of the TiO_2 semiconductor during the cell measurements. This was done for two reasons. First, it is believed that the semiconductor slowly decomposes during the irradiation process and thus UV irradiation could alter the performance of the cell throughout longer irradiation cycles [1]. And secondly, it allowed us to separate the electric signal caused by direct excitation of the TiO_2 from the one originating from excitation of the different sensitizer dyes. This makes it easier to understand those factors which influence cell performance.

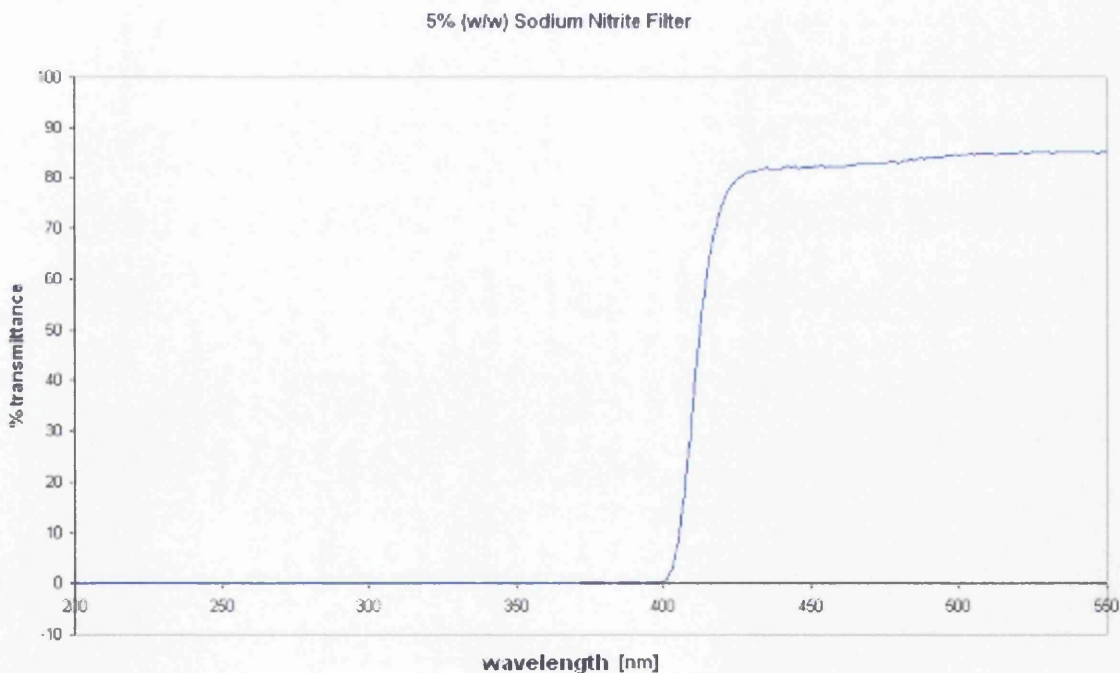


Figure 2-27 Transmission spectrum of UV filter (5% (w/w) aqueous solution of sodium nitrite); it provides a cut off filter up to 400 nm

2.1.9.2.1.2. Air mass filter

In our case an AM 1.0 filter, which, when combined with a Xe arc lamp, simulates the resulting solar irradiation from directly overhead at 0° zenith angle, perpendicular to the earth's surface. Many literature sources use an AM 1.5 filter which represents an absorption match to the earth's atmosphere if the sunlight hits the earth surface at 48.2° zenith angle.

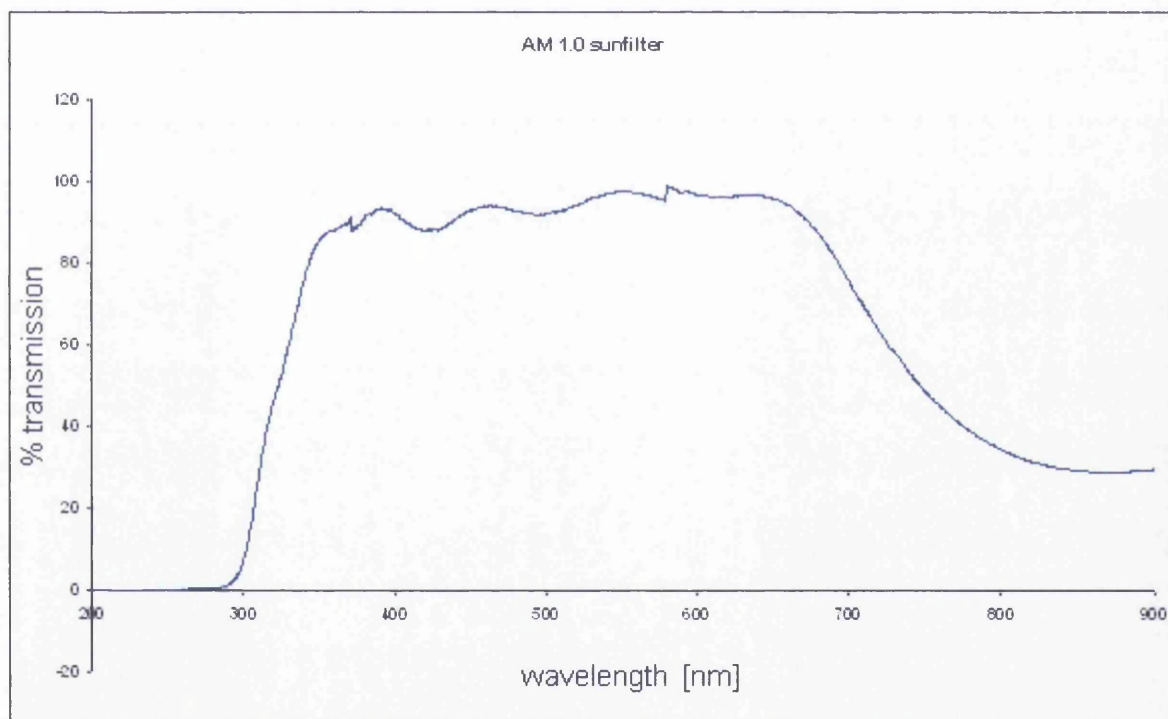


Figure 2-28 Transmission spectrum of AM 1.0 filter

2.1.9.2.1.3. Light source

The light source is a 900 W xenon arc lamp equipped with a shutter. The transformer has 12 different settings for light intensity. Two controls, one for high and low intensity, and one with settings from one to six. Those different illumination intensities are labeled L1 to L6 and H1 to H6 respectively. Before every experiment, the light intensities were measured at the exact position of the cell in order to compare results taken on different days. Also, in order to ensure a stable light source the lamp was usually turned on about two hours before the start of the experiment and before the calibration. There are however, always small changes in intensity, perhaps due to “arc wander” or unavoidable current fluctuations from the grid.

In Figure 2-29, two different calibration curves, using different detectors, are shown for the light intensity of the xenon arc lamp against the different transformer settings. The instruments used for this were a Scientech 365 photodiode and a handheld Littlemore Scientific light meter. The latter was used for all further light intensity measurements during the course of the project. The difference between the two measurements can be explained by the temperature dependence of the Scientech 365 photodiode. The Littlemore Scientific light meter has a temperature compensation mechanism, and thus gives a more accurate measurement of light intensity at higher illuminations.

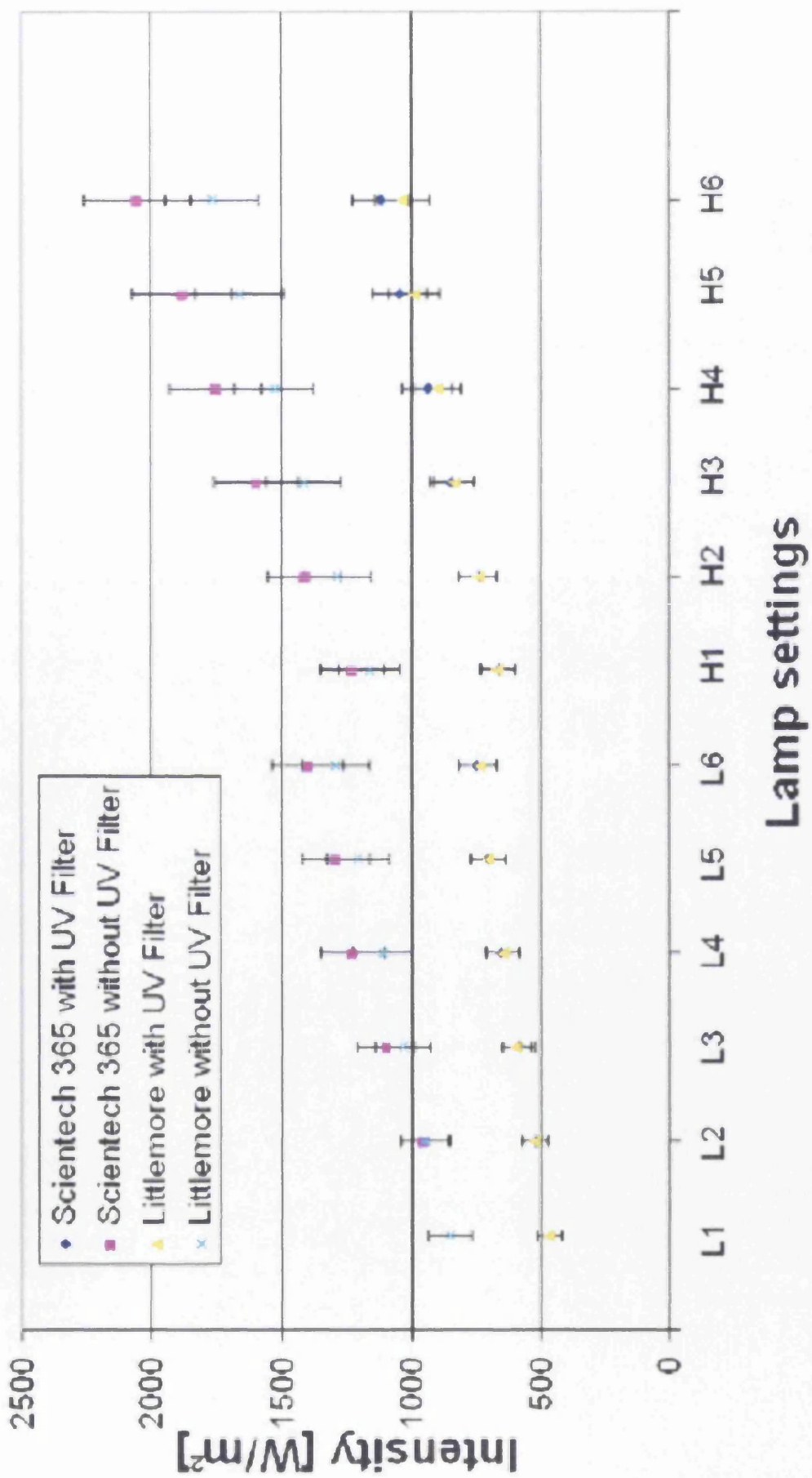


Figure 2-29 Lamp calibration: The light intensity output of the lamp was measured with and without the UV-cut-off filter using two different instruments for the intensity measurements (Scientech 365 photodiode and a Littlemore Scientific light meter).

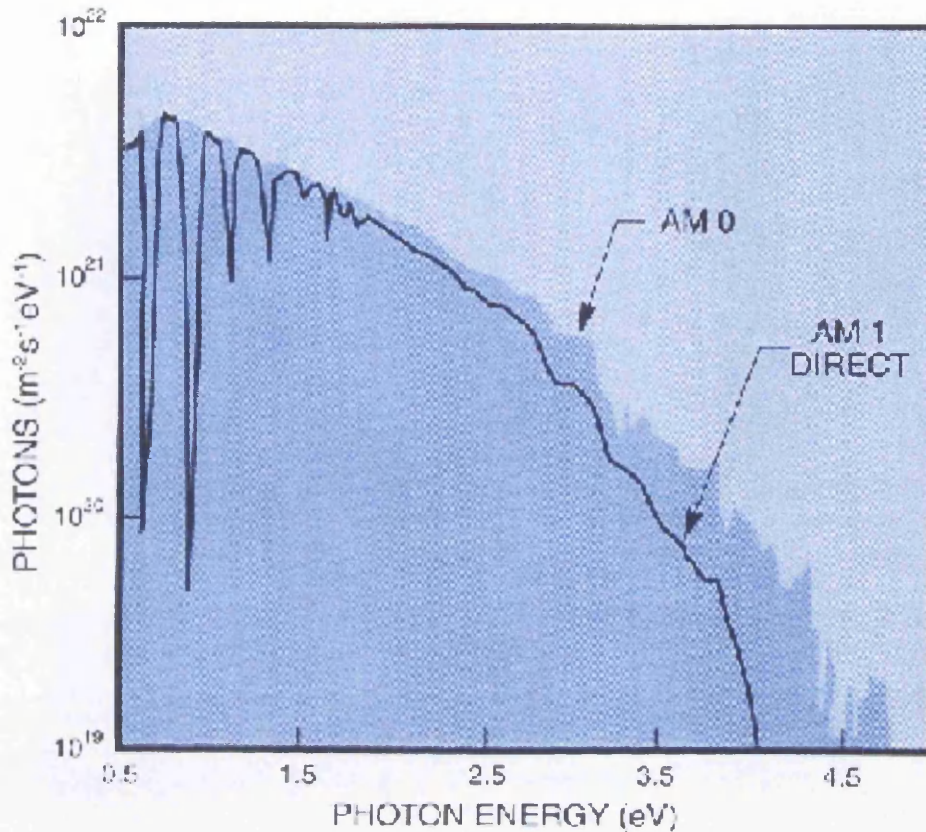


Figure 2-30 Sun spectrum of AM 1.0 filter and AM 0 for comparison (Oriental Light Sources).

2.1.9.2.1.4. Picolog ADC-212 analog-digital converter

The Picolog converter proved to be a powerful tool for all our data acquisition needs. It could either be used as a virtual two channel multimeter or as an oscilloscope. In order to use it the right software had to be downloaded from www.picotech.com. The version used was the r5_16_2. For the solar cell I-V curves one of the two channels of the picolog was used for the cell voltage and another one for the current (measuring voltage drop over a known load).

2.1.9.2.1.5. Keithley 617 source meter

This was used mainly for testing of measurement circuits and resistance measurements where no high current is needed since it could only supply a current of 2 mA at the maximum.

2.1.9.2.1.6. Keithley A195 bench multimeter

The bench multi meter was again used for testing of electric circuits and to double check the current readings obtained from the picolog.

2.1.9.2.1.7. Universal Light meter

The light meter was a handheld instrument purchased from Littlemore Scientific. It could measure the light intensity from the UV to the near infrared and give the results in Wm^{-2} , Lux, or Candela, furthermore it also provided a measurement of the temperature in degrees centigrade. When used for light intensity measurements the meter was mounted on a stand in the position of the sample holder. The photodiode would be at the exact position of the cell, just behind the sapphire window. The intensities given for the cell measurements are the intensities measured by this method. No corrections for the sapphire windows or the glass supports of the cells have been made.

2.1.9.2.1.8. The sample holder

This consists of two symmetrical brass parts with drilled channels for the cooling/heating water and connection to the temperature control unit.

Two holes are bored perpendicularly through the two plates and the thermal contact to the solar cell sandwiched between them is ensured by two transparent sapphire

windows (25 mm dia. and 1 mm width). Sapphire was chosen because it has very good thermal conductivity properties and is very robust. The space between the brass elements and around the sandwich cell was insulated with a Teflon ring. The remaining air gap on the outsides of the sapphire windows was further insulated with o-rings and glass plates on both sides.

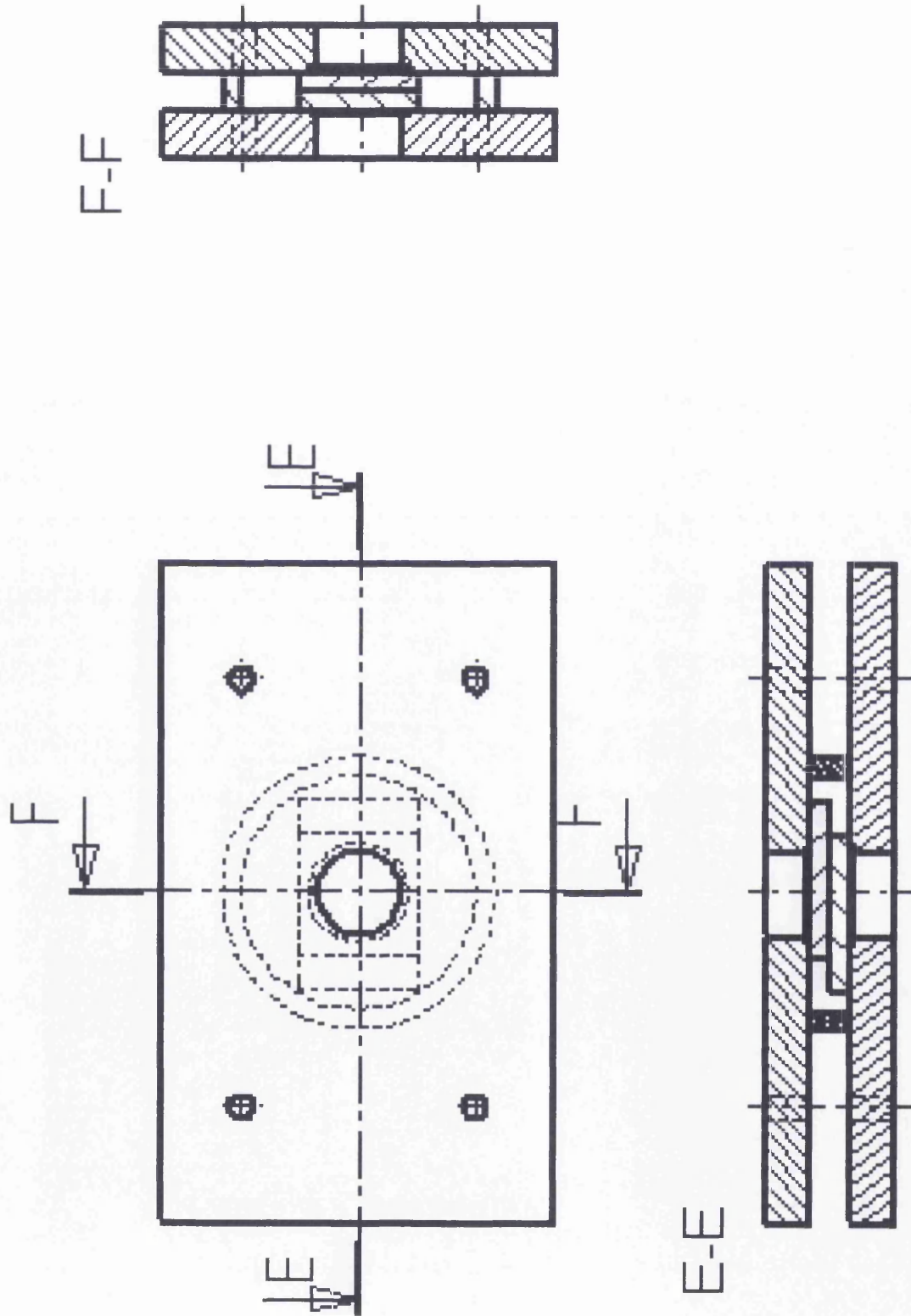


Figure 2-31 Sample holder: The two brass plates are shown with the DSSC sandwiched between them and a Teflon ring around it for insulation.

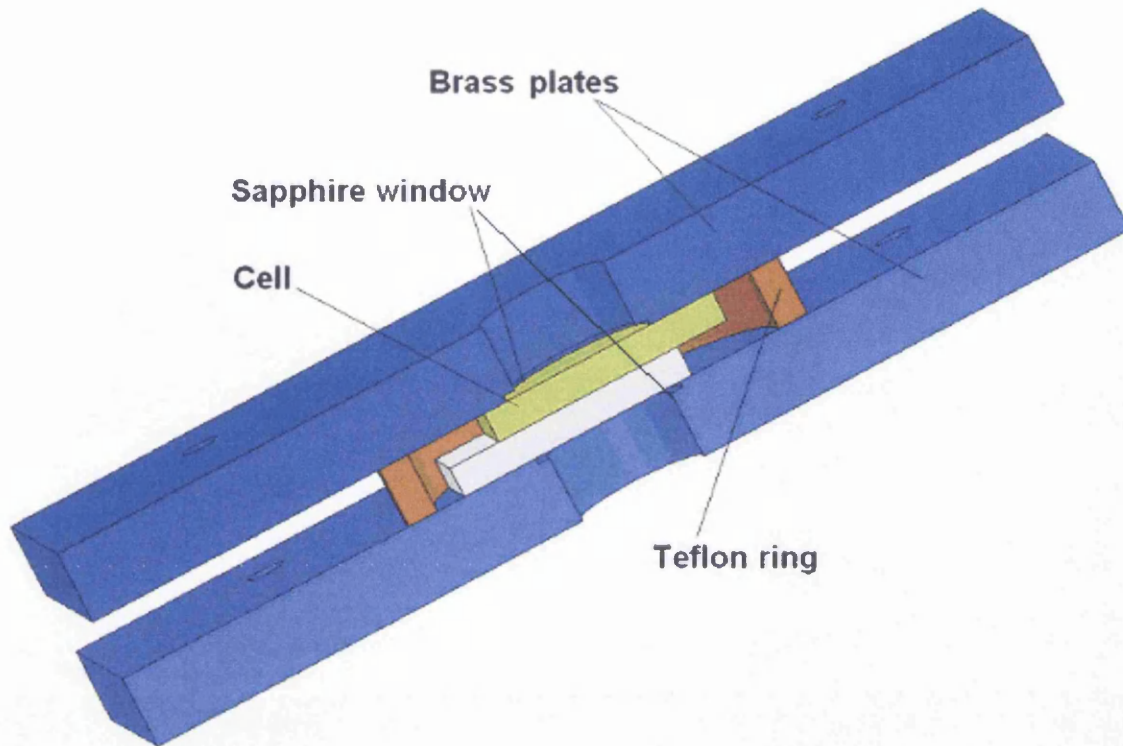


Figure 2-32 Cross section of the sample holder, including two sapphire windows, a glass cell and a Teflon distance ring.

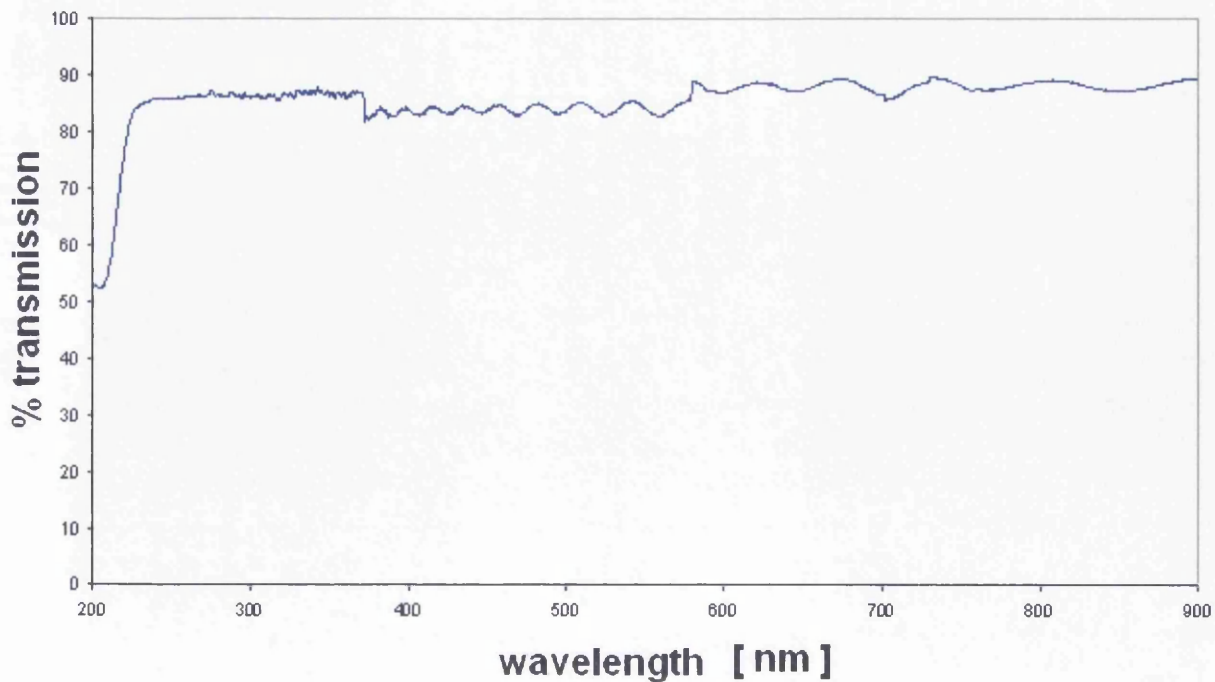


Figure 2-33 Transmission spectrum of one sapphire window (thickness 1 mm)

2.1.9.2.1.9. Temperature control unit

A temperature controlled unit was used for the cell measurements. It was possible both to either heat or cool the sample during cell testing. Using water the practical temperature range was *ca.* 1-70 °C. At higher temperatures, the electrolyte within the cell was lost very quickly and the cell ceased functioning.

2.1.9.2.1.10. Furnace

For the sintering of the semiconductor on the working electrode as well as for the platinisation of the counter electrode a furnace working at temperatures around 400 – 500 °C was necessary. The furnace used was a Gallenkamp bench furnace and the sintering temperature was 430 °C in almost all cases. For the preparation of the counter electrodes another oven set to 100 °C was also used.

2.9.2.1.11. Cyclic voltammetry

Cyclic voltammetry of the electrolytes and their components was carried out at Cardiff University and the author wants to especially thank Dr. Chris Morley from Cardiff University and Jeremie Pichereau from Swansea University for their help with the cyclic voltammetry measurements.

2.9.2.1.12. Optical microscopy

Optical Microscopy was done the using an Olympus BH-2 microscope and pictures were taken using a Nikon Coolpix L4 digital camera or a Hitachi VK-c150ed MOS colour video camera.

2.9.2.1.13. Scanning electron microscopy (SEM)

Electron microscopy was done at Swansea University using a JEOL JSM-35C scanning electron microscope and at the ICEMS-Mechanical Engineering Department at the University of Coimbra, Portugal (special thanks go to Peter Davies, School of Engineering, Swansea University and Ana P. Piedade, ICEMS-Mechanical Engineering Department, University of Coimbra).

2.1.9.2.2. Electric circuits for measurement of cell characteristics

2.1.9.2.2.1. Circuit for I-V measurement

For the I-V characterisation of the solar cells two voltages were measured, one over two cell contacts and one over the load. From the voltage measured across the known load the current (I) was derived by using Ohm's law. A digital multimeter was used as an ammeter in order to compare and double check the current drawn.

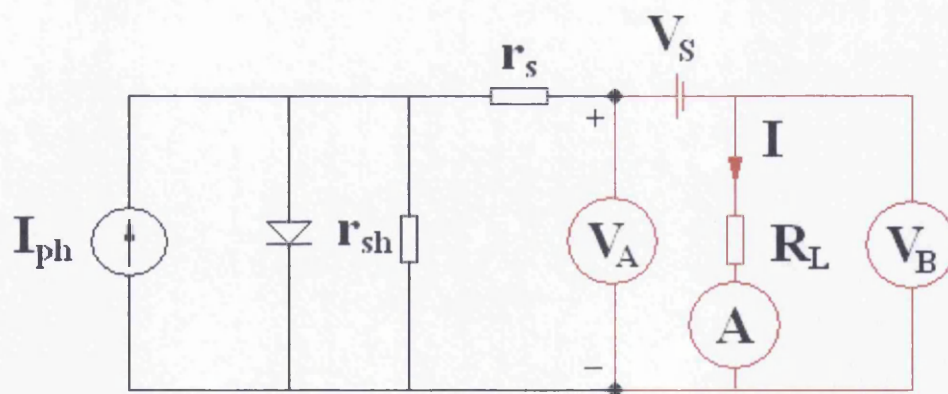


Figure 2-34 shows the equivalent circuit of a solar cell including the measurement set-up for measurement of I-V curves (coloured). V_A and V_B stand for the voltage measured at channel A and channel B of the picolog respectively. V_S represents the

bias voltage generated by the DC-power supply. A represents the digital-multimeter used to measure the current.

2.1.9.2.2.2. Circuit for resistance measurements

For overall resistance measurements and the time response of cells when exposed to light of different intensities and temperatures a slightly different measurement set-up was used. This involved the Keithley source meter itself as a bias source since it can source up to 2.5 mA which was sufficient for this purpose. No ammeter was used. Voltages V_A and V_B were taken and using Ohm's law and a known load resistance, the overall cell resistance was derived.

$$I = \frac{V_B}{R_L} = \frac{V_A}{r_C} \quad \rightarrow \quad r_C = \frac{V_A \cdot R_L}{V_B} \quad \text{(Equation 2-1)}$$

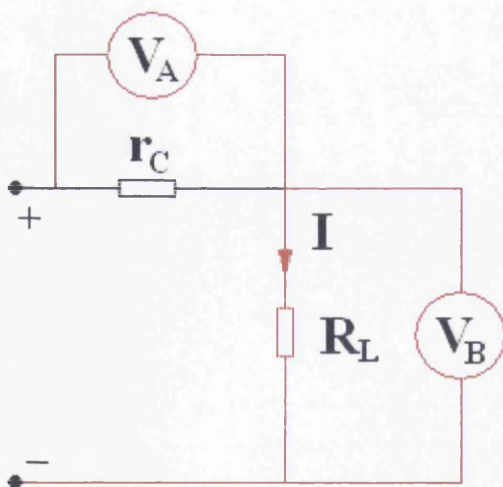


Figure 2-35 shows the measurement circuit for the resistance measurement of the cell. Voltages V_A and V_B represent the voltages measured with channel A and B of the picolog respectively. R_L and r_c are the load and the overall cell resistances.

2.1.9.2.3. UV-vis measurements

Absorption and transmission measurements of solutions, filters, cell parts and assembled cells were recorded using a Unicam UV300 (Swansea) or a Shimadzu UV-2100 (Coimbra) spectrophotometer.

2.1.10 Modeling of I-V curves

For the modeling of the measured curves software developed in the Netherlands by the Netherland Energy Research Foundation (ECN) was used [19, 20]. With the programs IVfit and IVgen we were able to fit the recorded I-V curves and also generate theoretical curves according to specified parameters. The calculations were based on mainly two different models the one-diode and the two-diode model which could be chosen in advance. In many cases, the results gained by the two different models are very similar, but one has to be aware of discrepancies in a few cases.

2.2. Photoacoustic calorimetry (PAC) measurements

2.2.1. TiO₂ film preparation

The TiO₂ films were prepared following the squeegee print method as described in the literature [1]. As a glass support, non-conducting microscope slides were cut to size (25 mm x 25 mm x 1 mm) and the Ti-Nanoxide HT sol (particle size 9 nm) purchased from Solaronix SA was spread on top of them using one layer of Scotch Magic tape as a template. This achieved a layer thickness of about 3-4 μm. The morphology of the films and the cross section are shown in the result section.

For these PAC experiments, the nanoporous titania layer was not simply saturated with dye as it would be for use in a photovoltaic cell. The intention was rather to create a uniform titania layer with a homogenous dye layer adsorbed onto it.

Furthermore an important requirement was the need to keep these films light-transmissive in order to match their absorbances with reference materials. The different dyes were adsorbed by immersing the slides into ethanoic solutions of the dye and matching their absorbances at the excitation wavelength (535 nm). The absorbances were in a range between 0.2 and 0.3 before deduction of the TiO₂ background signal. The dye adsorption time was between about 5 min for the lower optical densities using the N3 dye and a few hours for the high optical density MnTPPS reference samples. This gave us a sufficiently strong PAC signal and good signal to background ratio at relatively low laser intensity which gave the added advantage of minimizing general heating of the sample over time by the excitation pulse.

In general it was observed that the porphyrin dyes which carry sulfonic anchoring groups seemed to take longer to adsorb to the titania surface than the ruthenium dye which had a carboxylic acid anchoring group, although the reason for this was not known.

2.2.2. Materials for PAC

The porphyrins were synthesized in Coimbra by Carlos J. P. Monteiro. (The author wants to especially thank Carlos J. P. Monteiro and Mariette M. Pereira for providing the dyes.) Except PtOEP, which was purchased from Frontier Scientific, UK.

2.2.2.1. Dyes used for photoacoustic measurements

The following page shows a table giving the lumophores used besides N3 for PAC.

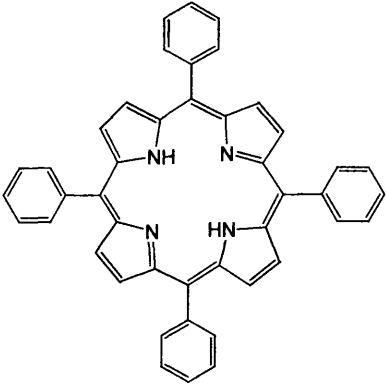
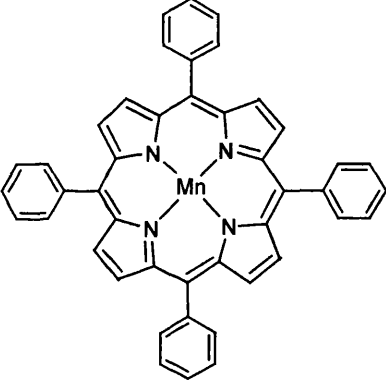
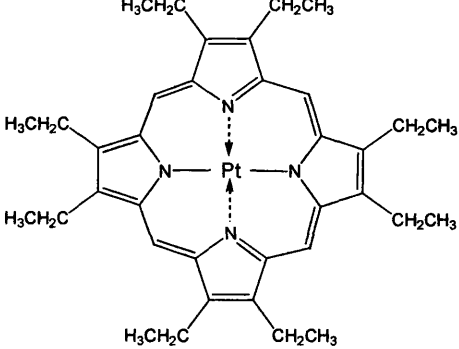
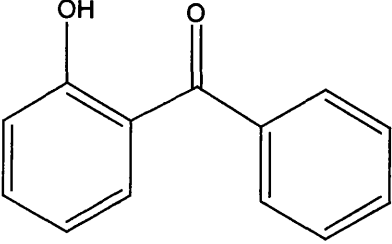
Name	Abbrev.	Structure
Tetraphenylporphyrin	TPP	
Manganese-tetraphenylporphyrin	MnTPP	
Platinum-octaethylporphyrin	PtOEP	
2-Hydroxybenzophenone	HBP	

Table 2-3 Lumophores used for PAC in polymers

2.2.2.2. Preparation of PVC, PMMA, cellulose acetate solutions:

Stock solutions with comparable viscosities were prepared using similar methods as described in [21]. Stirring the solutions over a period of several hours proved to be essential in order to gain good rheology for spin coating, with the best results obtained by slow addition of the polymer to the solvent.

Volume	Polymer	Solvent
25 mL	2 g PVC	THF
25 mL	2.5 g cellulose acetate	THF
25 mL	2.5 g PMMA	CHCl ₃

Table 2-4 polymer stock solutions

From these stock solutions, dye-polymer solutions were prepared. First, the dyes were dissolved in THF and the absorptions of the samples at the excitation wavelength (532 nm) were matched by appropriate dilution. 0.5 mL of this dye solution were mixed with 1.25 mL of the required polymer solution and continuously stirred. A blank without any dye was prepared alongside the dye loaded polymer films.

2.2.2.3. Film preparation (spin coating)

The polymer layers were applied onto the pre-cut glass slides (25 mm x 25 mm x 1 mm). Thin layers of dye incorporated in the polymer matrix were coated by applying 70 μ L of the polymer solution in a circle and spinning it using a Speedline Technologies Spincoater Model 6700.

In general it was found that cellulose acetate films were the most homogenous both in terms of lumophore distribution and thickness. Typically, cellulose acetate films were made by spin coating for 15 s at 1500 rpm, 15 s at 2000 rpm and 15 s at 2500 rpm. PMMA samples on the other hand were spun for 30 s at 600 rpm 10 s at 1600 rpm and 5 s at 4000 rpm; because of their lower viscosity it was necessary to spin at a slower initial speed in order to obtain a thick enough film for a good PAC signal.

2.2.3. Flash photolysis

Flash photolysis experiments were carried in Coimbra using an Applied Photophysics LKS.60 laser-flash-photolysis spectrometer, with a Spectra-Physics Quanta-Ray GCR-130 Nd:YAG laser (second harmonic, 532 nm) and a Hewlett-Packard Infinium Oscilloscope. Absorption and fluorescence emission spectra were recorded with Shimadzu UV-2100 and SPEX Fluoromax 3.22 spectrophotometers, respectively. An integrating sphere was used for the fluorescence measurements.

2.2.4. Solid state photoacoustic measurements (solid state PAC)

The equipment used for photoacoustic calorimetry measurements was custom built by the author and collaborators in the PAC group in Coimbra. The apparatus used is based on the front-face irradiation cell used for high sensitivity PAC measurements with liquid solutions and is described in detail later in the thesis [22]. The irradiation of the sample was made through a window onto the sample and then onto a dielectric mirror which prevents direct irradiation of the transducer. A sample holder was constructed to ensure that (from the bottom to the top) the transducer, the mirror, the sample and the window are always kept at the same relative position, and

also kept at the same position relative to the laser pulse at all times. Acoustic coupling through the two solid-solid sample interfaces (to the window and through the mirror) was accomplished with a transparent viscous liquid such as hexadecane or glycerol. A constant weight on top of the window was put on for constant pressure conditions. We used either a Spectra Physics Quanta Ray model laser (8 ns pulse width) or the EKSPLA PL 2143A model (30 ps) Nd:YAG laser for sample excitation. The second harmonic at $\lambda=532$ nm was used in both cases. The results obtained were the same with either laser. Pulses at frequencies ranging from 2 Hz to 10 Hz were used without any difference in the photoacoustic signals detected. A small fraction of the laser beam was reflected to a photodiode and used to trigger the transient recorder (Tektronix DSA 601, 1 Gs s^{-1}). The photoacoustic waves, detected with a 2.25 MHz Panametrics transducer (model 5676) and captured by the transient recorder, were transferred to a PC for data analysis. In a PAC experiment, 50 to 100 waves of the sample film and background (TiO_2 or silanised TiO_2 films) were recorded and averaged under the same experimental conditions. Four sets of averaged sample and background waves were used for the data analysis at a given laser intensity, and four laser intensities were employed in each experiment. The different laser intensities were obtained by interposing neutral density filters with transmissions between 25% and 100%, between the laser and the sample.

References:

1. Nazeeruddin, M.K., A. Kay, I. Rodicio, R. Humphrybaker, E. Muller, P. Liska, N. Vlachopoulos, M. Gratzel, *Journal Of The American Chemical Society*, 1993. **115**(14): p. 6382-6390.
2. Kallioinen, J., G. Benko, V. Sundstrom, J.E.I. Korppi-Tommola, A.P. Yartsev, *Journal Of Physical Chemistry B*, 2002. **106**(17): p. 4396-4404.
3. Yanagida, S., G.K.R. Senadeera, K. Nakamura, T. Kitamura, Y. Wada, *Journal of Photochemistry and Photobiology A: Chemistry*, 2004. **166**(1-3): p. 75.
4. Ferrere, S., *Inorganica Chimica Acta*, 2002. **329**: p. 79-92.
5. Liu, Y., A. Hagfeldt, X.R. Xiao, S.E. Lindquist, *Solar Energy Materials And Solar Cells*, 1998. **55**(3): p. 267-281.
6. Nazeeruddin, M.K., R. Splivallo, P. Liska, P. Comte, M. Gratzel, *Chemical Communications*, 2003(12): p. 1456-1457.
7. Smestad, G.P., *Solar Energy Materials And Solar Cells*, 1998. **55**(1-2): p. 157-178.
8. An, H., B.F. Xue, D. Li, H. Li, Q.B. Meng, L. Guo, L. Chen, *Electrochemistry Communications*, 2006. **8**: p. 170-172.
9. Ileperuma, O.A., M.A.K.L. Dissanayake, S. Somasunderam, L.R.A.K. Bandara, *Solar Energy Materials and Solar Cells*, 2004. **84**(1-4): p. 117-124.
10. Hannappel, T., B. Burfeindt, W. Storck, F. Willig, *Journal Of Physical Chemistry B*, 1997. **101**(35): p. 6799-6802.
11. <http://www.solaronix.com> (accessed May 23, 2005).
12. Huang, C.-Y., Y.-C. Hsu, J.-G. Chen, V. Suryanarayanan, K.-M. Lee, K.-C. Ho, *Solar Energy Materials and Solar Cells*, 2006. **90**(15): p. 2391-2397.
13. Hara, K., T. Nishikawa, M. Kurashige, H. Kawauchi, T. Kashima, K. Sayama, K. Aika, H. Arakawa, *Solar Energy Materials And Solar Cells*, 2005. **85**: p. 21-30.
14. Fukui, A., R. Komiya, R. Yamanaka, A. Islam, L. Han, *Solar Energy Materials And Solar Cells*, 2006. **90**: p. 649-658.
15. Gonsalves, A., R.A.W. Johnstone, M.M. Pereira, A.M.P. deSantAna, A.C. Serra, A. Sobral, P.A. Stocks, *Heterocycles*, 1996. **43**(4): p. 829-838.
16. Gonsalves, A., J. Varejao, M.M. Pereira, *Journal of Heterocyclic Chemistry*, 1991. **28**(3): p. 635-640.
17. Adams, P.N., P.J. Laughlin, A.P. Monkman, A.M. Kenwright, *Polymer*, 1996. **37**(15): p. 3411-3417.
18. Marques, A.P., C.M.A. Brett, H.D. Burrows, A.P. Monkman, B. Retimal, *Journal of Applied Polymer Science*, 2002. **86**(9): p. 2182-2188.
19. Burgers, A.R., J.A. Eikelboom, A. Schönecker, W.C. Sinke, *Netherlands Energy Research Foundation ECN-RX-96-022*, 1996.
20. Burgers, A.R., *Energy Research Center of the Netherlands ECN*, 2004.
21. Douglas, P. and K. Eaton, *Sensors and Actuators B* 2002. **82**: p. 200-208.
22. Arnaut, L.G., R.A. Caldwell, J.E. Elbert, G.E. Melton, *Rev. Sci. Instrum.*, 1992. **63**: p. 5381.

CHAPTER 3

INFLUENCE OF VARIATION OF COMPONENTS ON THE PERFORMANCE OF DYE SENSITISED SOLAR CELLS

3.1. Introduction

The main parts of a DSSC, and therefore those features which offer the possibility for variations in cell design are: the support for the TCO, the type of TCO doping (usually F or In doped SnO_2), the type, thickness and morphology of the semiconductor layer, the dye, the electrolyte, sealing method, cell size and layout.

A series of different dye sensitized solar cells (DSSCs) was built by changing the main components of a cell. Comparisons and differentiation measurements on the photoelectrical characteristics were made. Data for the variation in cell performance with cell design over a range of light intensities are given and reasons for good and bad performances are discussed. All cells were built with an active area of 1 cm x 1 cm of TiO_2 onto which selected dyes were adsorbed. The cells were generally built using the methods described in the literature [1]. All cells were made in triplicate. Table 3-1 gives a list of the cells made together with their performance characteristics for two different light intensities i.e. 0.1 Sun and 1.0 Sun which are at the low and the high end of our measurements. The values for the cell parameters result from a curve fit of the measured I-V curves (see section 2.1.10 in Chapter 2). Data for gel electrolyte cells is given for front illumination at 0.1 Sun and for back illumination (where possible due to cell transmittance) at 1.0 Sun. It is hoped that the results described in this chapter will lead to a better understanding of how the shape of the voltage to current curves is influenced by cell design over a wide range of light intensities.

Either conducting glass or conducting plastic was used as a support. The conducting surface consisted of a doped TCO (transparent conducting oxide) layer. The TCO was either ITO (indium tin oxide) or FTO (fluorine tin oxide). Glass is in general rigid, heavy and bulky whereas plastic offers the advantages of flexibility and

light weight. However the sheet resistance of the plastic substrates tends to be much higher and therefore the cell efficiency is generally reduced.

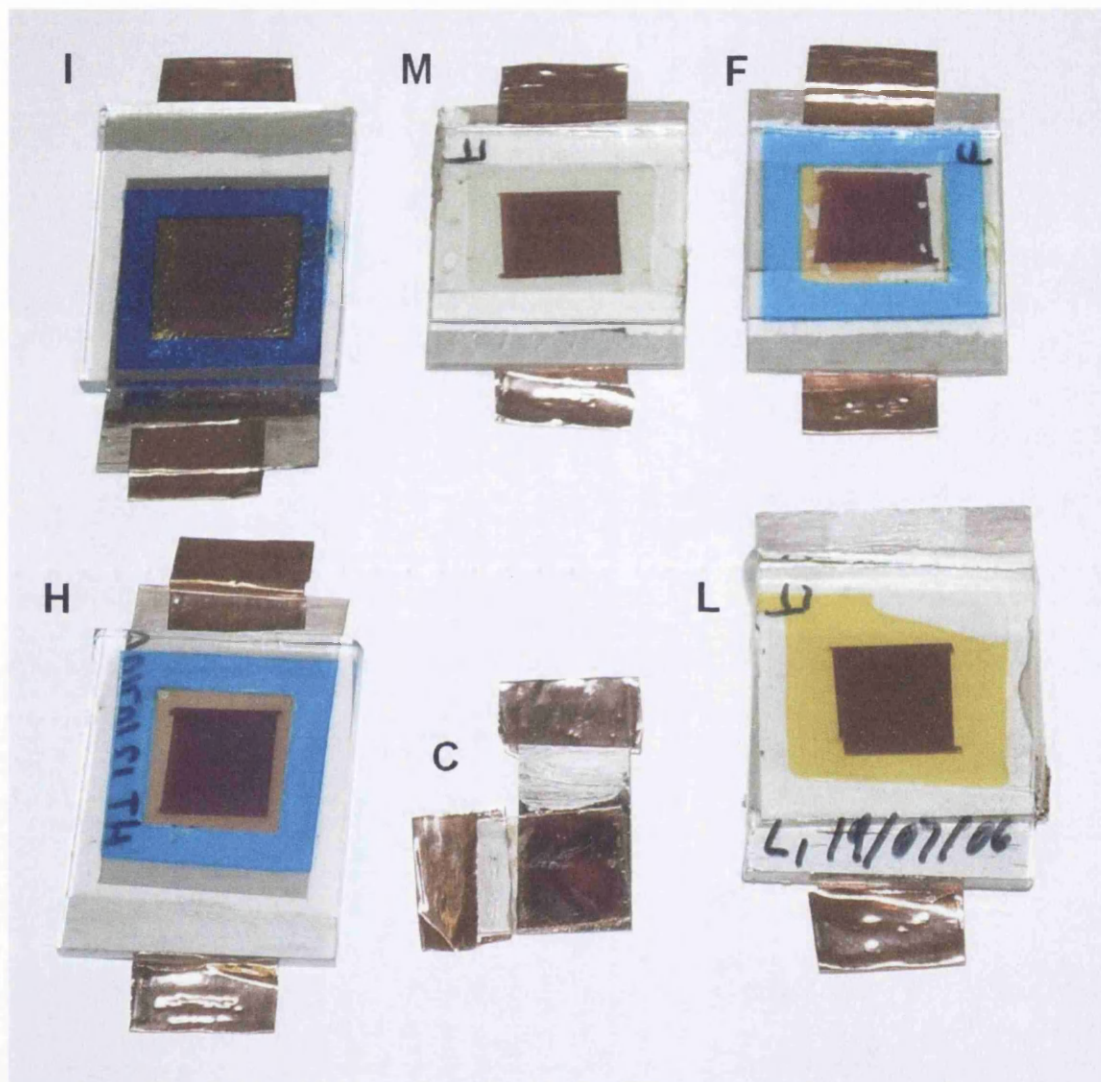


Figure 3-1 A selection of different cell types built in order to compare the function of the individual parts of the cell. The range of cell types includes: gel or solvent electrolytes with changing concentration of the redox couple, glass or plastic substrates with ITO or FTO as conducting oxide layer, different sols and binders, and transparent and non-transparent counter electrodes which were either sputtered onto the substrate or spread and then annealed. The active area was 1 x 1 cm for all the cells. The cells, as they are given in Table 3-1 were: from top left to right cells **I**, **M**, and **F**; bottom left to right cells **H**, **C**, and **L**.

Cell Type	A	B	C	D	F	G	H	I	J	K	L	M
TiO ₂												
P05	X	X	X		X					X	X	X
P06				X		X	X	X	X			
Electrolyte												
liquid 0.3 M LiI/0.03 M I ₂	X					X						
liquid 0.5 M LiI/0.05 M I ₂									X		X	X
gel		X	X	X	X		X	X		X		
Substrate												
FTO glass 8 Ohms	X	X		X		X	X	X	X	X	X	
plastic 50 Ohms			X									
ITO glass 15 - 30 Ohms					X							X
Sealant												
hot sealant+Araldite	X					X			X		X	X
adhesive sealant				X	X		X	X		X		
no sealant		X	X									
Counter electrode												
Pt - paste on glass	FTO	FTO		FTO	ITO	FTO			FTO	FTO	FTO	ITO
sputtered Pt on plastic			900 s				10 s	900 s				
VOC 0.1 Sun mV	326	525	587	611	609	310	628	617	399	623	411	376
ISC 0.1 Sun microA	863	648	66.8	966	808	520	902	960	801	894	1180	763
ff exp. 0.1 Sun	60.0	69.4	69.3	64.4	59.5	58.7	62.5	64.1	64.1	61.5	65.7	54.4
shunt resistance 0.1 Sun	3580	104000	81000	80000	34800	4560	64000	44300	8500	36000	8853	4648
STDEV Rsh	19.1	13476	3892	3945	864	35.3	2152	1281	102	826	76.6	58.0
series resistance 0.1 Sun	10.8	0.0022	0.059	67.4	129.1	5.6	88.9	70.5	11.3	100.6	17.1	54.9
STDEV Rse	0.9	7.0	87.5	2.6	3.1	2.1	3.1	2.9	2.0	2.6	0.9	1.7
efficiency 0.1 Sun %	1.7	2.3	0.3	3	2.9	0.9	3.5	3.8	2.1	3.4	3.1	1.5
VOC 1.0 Sun				665	657	389	681	675	499	672	520	
ISC 1.0 Sun microA				5278	4291	6724	4268	3662	10732	4785	12633	
ff mod. 1.0 Sun				49.2	33.2	51.0	47.0	65.6	47.4	45.1	41.1	
shunt resistance 1.0 Sun				2938.7	1.30E+21	599.6	1656	2612	785.5	1524	5.2E+19	
STDEV Rsh				184	3.70E+38	21.9	32.5	39.7	71.2	55.0	1.2E+17	
series resistance 1.0 Sun				24.7	85.9	12.5	53.8	14.2	14.4	35.7	16.3	
STDEV Rse				0.37	0.72	0.23	0.42	1.36	0.17	0.41	0.19	
efficiency 1.0 Sun %				1.8	0.9	1.3	1.4	1.6	2.6	1.5	2.8	

Table 3-1 Different cells built by interchanging the different build up elements. Their photoelectric characteristics are given for 0.1 and 1.0 Sun respectively. All cells were irradiated from the front but cells **D, F, H,** and **K** at 1.0 Sun.

3.2. The support

Physical characteristics:

The major advantage of plastic over glass is the much lower weight per area. A sheet of ITO plastic weighs about 0.025 g cm^{-2} at a thickness of about 0.2 mm. ITO glass weighs roughly 10 times as much at 0.250 g cm^{-2} for a thickness of 1 mm. Whereas the FTO glass substrate which is 3 mm thick weighs three times as much as the ITO at 0.740 g cm^{-2} . Plastic solar cells are more flexible than glass ones, but since the relatively thick layer of TiO_2 is not that well attached to the plastic surface this is not necessarily always an advantage because the TiO_2 may detach upon bending.

3.2.1. Glass

3.2.1.1. *FTO vs. ITO (cell F vs K)*

As Table 3-1 illustrates cells made using FTO are between 1.2 and 2 times better than comparable cells made using ITO. In terms of performance parameters this is due primarily to the lower sheet resistance of $8 \Omega \text{ cm}^{-2}$ for FTO compared to that of $15 - 30 \Omega \text{ cm}^{-2}$ for ITO. We expect that the cells should differ in performance only in a constant value, which is a function of their series resistance, and as such makes a contribution to the cell series resistance. Indeed, that is what can be observed. The open circuit voltage is the same for cells using either FTO or ITO glass. However, the short circuit current differed by about 12–15 %, with the lower series resistance having the higher current (Figure 3-2) and at 1 Sun the series resistance of the ITO cell is twice that of the FTO cell (86Ω and 36Ω respectively). This is in good concordance with Ohms law and means that at one Sun irradiation intensity the cell with the twice as high series resistance displays an overall efficiency half as big as the

cell with the lower series resistance. The difference in this one parameter influences the slope and with it the fill factor of the whole I-V curve of otherwise identical cells. It is noteworthy, that the V_{OC} and the I_{SC} of the two cells are not remarkably different. It is just the shape of the curve especially the slope of the vertical section between these two points which was influenced by the series resistance.

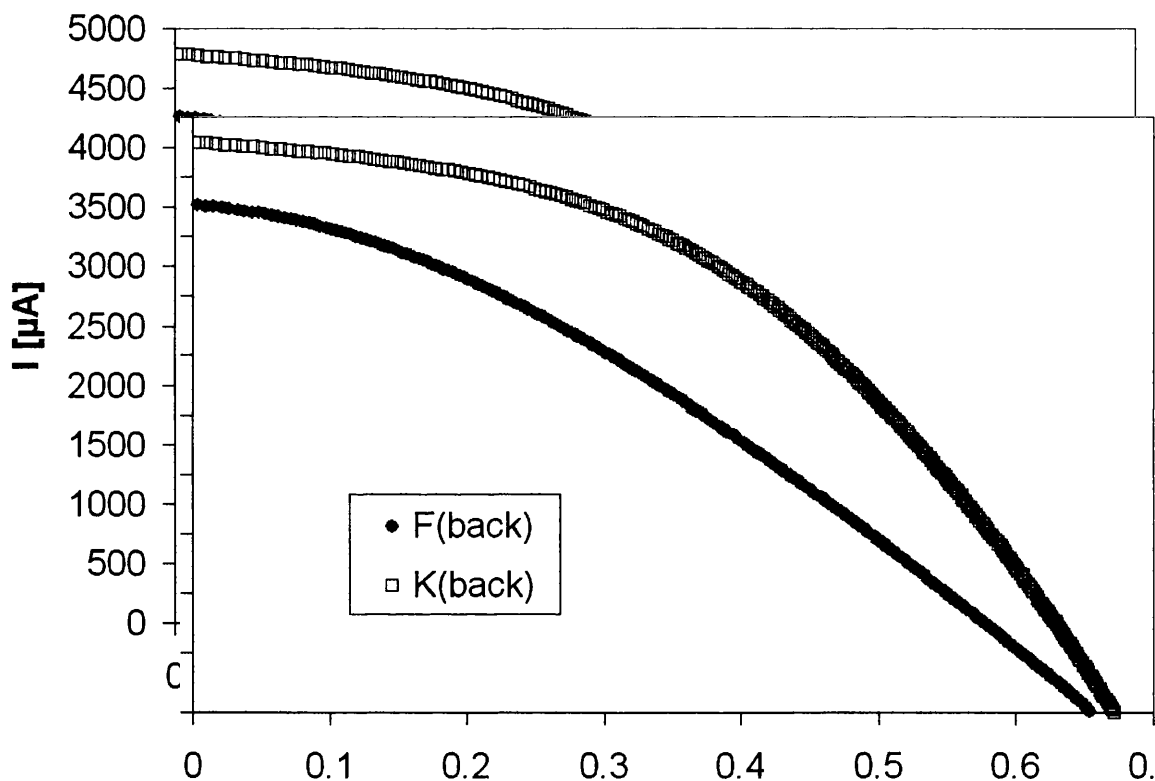


Figure 3-2, the I-V curves of the two cells F and K. Both are prepared with gel electrolyte and the curves shown result from back irradiation. Cell F has an ITO glass support and cell K FTO glass support. The difference in the slopes should be noted.

The most striking difference between these two cell designs is found when comparing the overall efficiency. Here the low resistance FTO glass displays

considerably better performance. Since the overall efficiency is a function of the fill factor which decreases with higher series resistance, this was expected. The experiment verifies that the series resistance influences the slope of the vertical contribution to the I-V curve, the fill factor and with it the efficiency of the cell linearly over the whole light intensity range from 0.1 to 1.0 Sun. Figure 3-4 shows that the plots of cell efficiency against light intensity are both linear and plots for the FTO and ITO cells run parallel to each other.

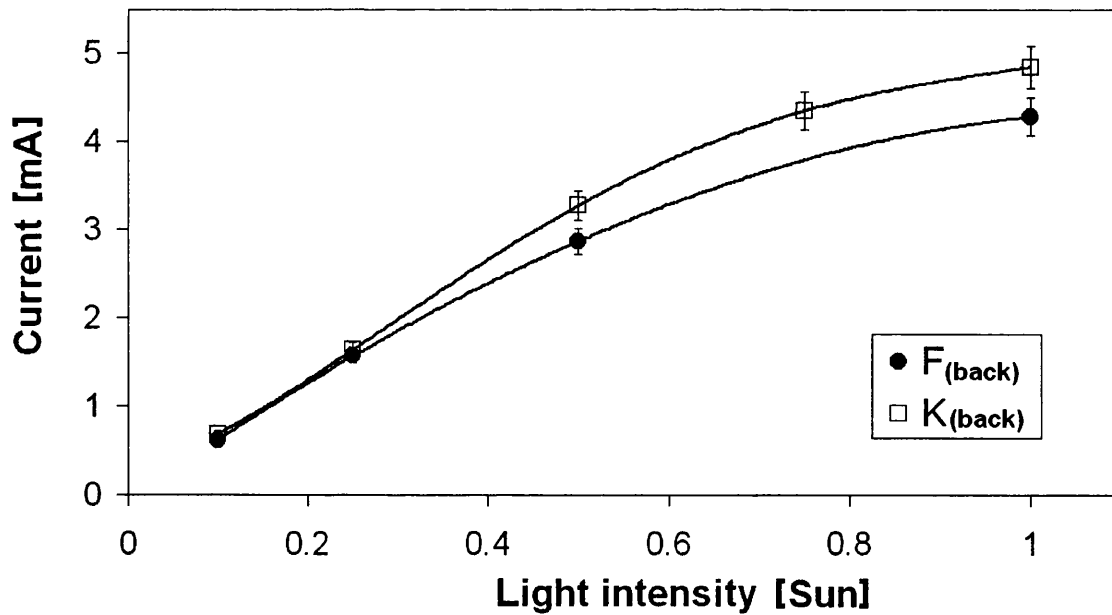


Figure 3-3 The short circuit current of cells built with either FTO (KB) or ITO (FB) glass support. The error bars represent an error of $\pm 5\%$.

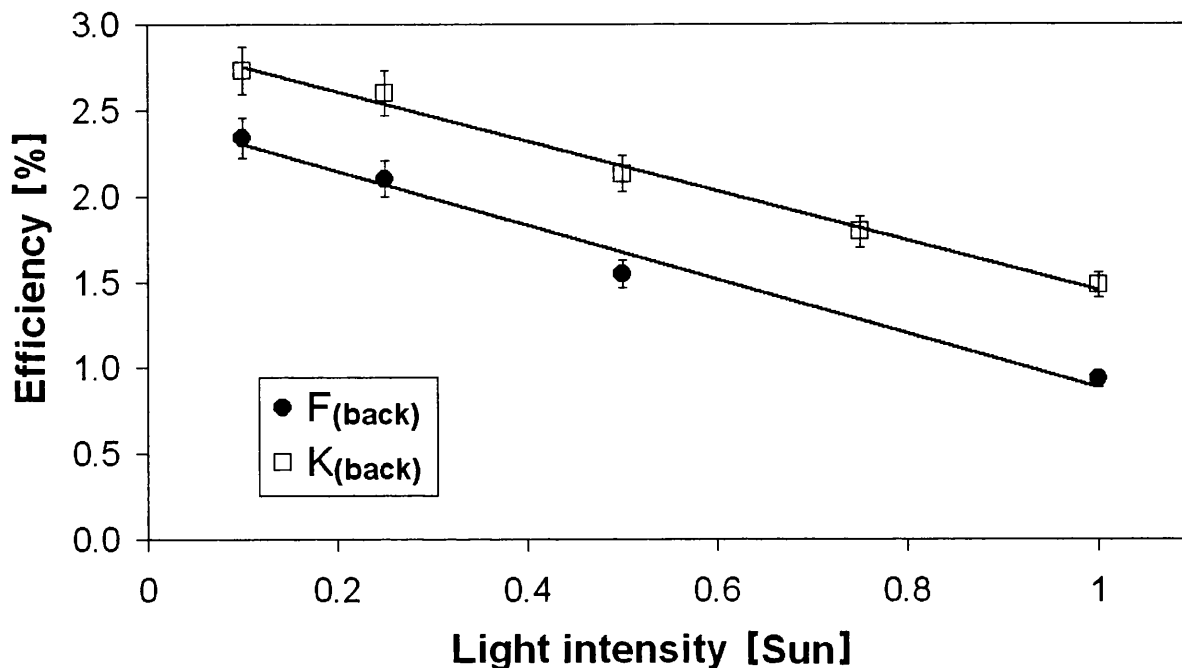


Figure 3-4 Comparison of the efficiency of cells built with FTO (KB) and ITO (FB) glass supports. Error bars at $\pm 5\%$ error.

3.2.2. Plastic vs glass (cell C cf B)

Plastic is more flexible than glass but this means at the same time that thinner semiconductor (TiO_2) films have to be applied in order to avoid detachment upon bending. Overall the performance of plastic cells is much poorer than that of glass cells. We believe that this is a consequence of the need for pressure sintering when using plastic and a higher sheet resistance for the ITO film on plastic.

The surface morphology of the titania changes due to the temperature treatment and depends on sintering temperature and time [2-5]. The semiconductor layer should be a homogeneous, mesoporous, sponge-like structure. If the titania is not heat sintered but pressure sintered then we believe that the charge transport channels

within the titania layer are not as homogenous as they are if they were fused together by heat. Pressure sintering may give a semiconductor film which consists of a lot of compacted particles with distinct grain boundaries which present an obstacle to the flow of electric current. This means that the semiconductor film consists of a lot of stacked particles whose grain boundaries also represent an obstacle for flow of electric current. High temperature annealing leads to fusing and to a recrystallisation from rutile to anatase [6, 7].

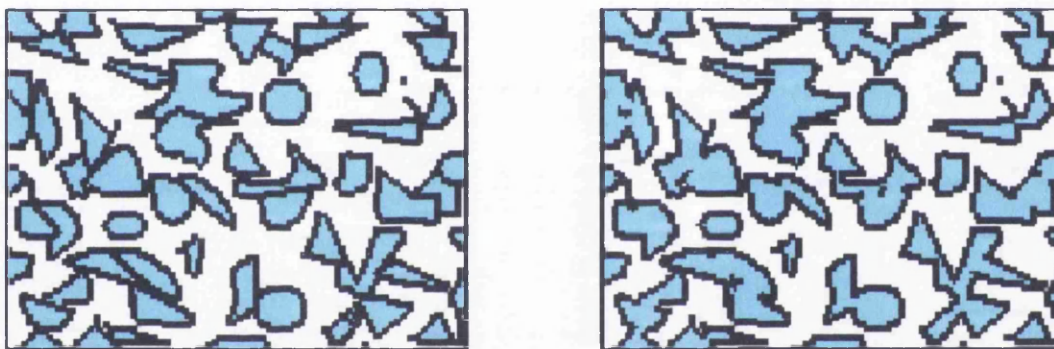


Figure 3-5 Idealised 2D demonstration of the heat sintering process, the connection between the particles in the 3D is not shown. The coloured elements are the TiO_2 particles. This fusing at grain boundaries improves the conducting properties of the semiconductor film between the TiO_2 particles and also the TCO surface.

It has already been shown, that the pore size of the mesoporous layer and, with this, cell performance can be controlled by sintering temperature [8]. It is very important to get the right pore size since it has to be big enough to accommodate the dye molecule and also allow transfer of the electrolyte redox couples in order to ensure reduction of the oxidised dye molecule formed by electron transfer into TiO_2 [4].

Circuit modelling shows us that the glass cell (B) has a shunt resistance ten times greater than that of the plastic cell (C) and a series resistance ten times less. They display almost equal fill factors but the glass cell is seven times more efficient at 0.1 Sun. (It should be noted that with those two cells the limits of the modelling software were reached. Another model, for example the two diode model, might have been preferable for this particular type of cell.)

3.3. The substrate

3.3.1. Nanoporous titania films using different binders

The aim was to investigate the effect, if any, of film surface morphology and homogeneity on cell performance. For this, different organic binders were used which, it was hoped, would control not only the degree of cracking of the film as it dried but also the porosity of the film as the binder was burnt out of the film during high temperature sintering. Different TiO₂ based aqueous sols were prepared according to a method described in the literature[1]. Conducting glass substrates were coated with films of these sols using different coating techniques (squeegee printing, spin coating) and at different film thicknesses. After sintering, dye was adsorbed onto the TiO₂ layers, and solar cells made with these working photoelectrodes as described in section 1, chapter 2. The choice of the different binders was based on the idea that the binder would distribute homogeneously within the sol mixture, that it would display good water solubility and that it would be completely burnt off under sintering conditions. In order to investigate this beforehand thermogravimetric tests were made using small amounts of the binder (mainly polysaccharides in amounts between 80 and 125 mg) on an 18 x 18 mm microscope cover slide with an average

weight of $0.1209 \text{ mg} \pm 0.5 \%$ and exposing them to the sintering conditions under normal atmosphere for 30 min. The fraction or initial weight remaining as ash after the heating process was calculated. The colour of the remains was considered too, in order to pick binders which leave a white to light grey ash rather than dark brown or black remains, since this would itself absorb light and therefore lead to less harvested light if incorporated in the semiconductor film.

During these preliminary investigations we tried substances like starch, various celluloses and derivatives, dextrose, shellac, a commercially available resin (N,N'-dibenzyl-N''(3,4-dihydro-2H-naphtalene-1-ylidene)-hydrazine), several polysaccharides, polyethylene glycol (PEG), and polyethylene oxide (PEO).

Substance and supplier	Average residue; % of total initial weight	Comments
Gum Arabic (Galactan) Sigma Aldrich	24	black residue
β -cyclodextrin (hydrate) Sigma Aldrich (85,608_8)	8	black
Cellulose from spruce Fluka (22182)	2.6	black
PE-oxide MW 300000 (BDH 29760)	1.3	white, almost transparent residue
PE-oxide MW 600000 (BDH 29762)	2.1	not as transparent as PEO 300000
PE Id (BDH 29780)	14.4	black glass
Ethyl-cellulose Aldrich 20067-0	0.5	was ground first (initial particle size ~ 400 μ m)
Methyl-cellulose Aldrich 27444-5	13.3	black residue
Cellulose acetate Polysciences 6203	11.9	deep black, fused together

Table 3-2 Gravimetric analysis of the pyrolysis of potential binders for TiO₂ (450 °C, 30 min, exposed to the atmosphere).

3.3.1.1. The reproducibility of the squeegee printing procedure

Out of a batch of 24 nominally identical TiO_2 -coated working electrodes 6 were randomly chosen and the TiO_2 absorption in the region below 400 nm was used for the determination of the reproducibility of the TiO_2 coating procedure. In particular, a comparison of the single wavelength absorption at 347 nm was made (see Figure 3-1). The reproducibility of the layer absorption and therefore of the layer thickness was 8 %.

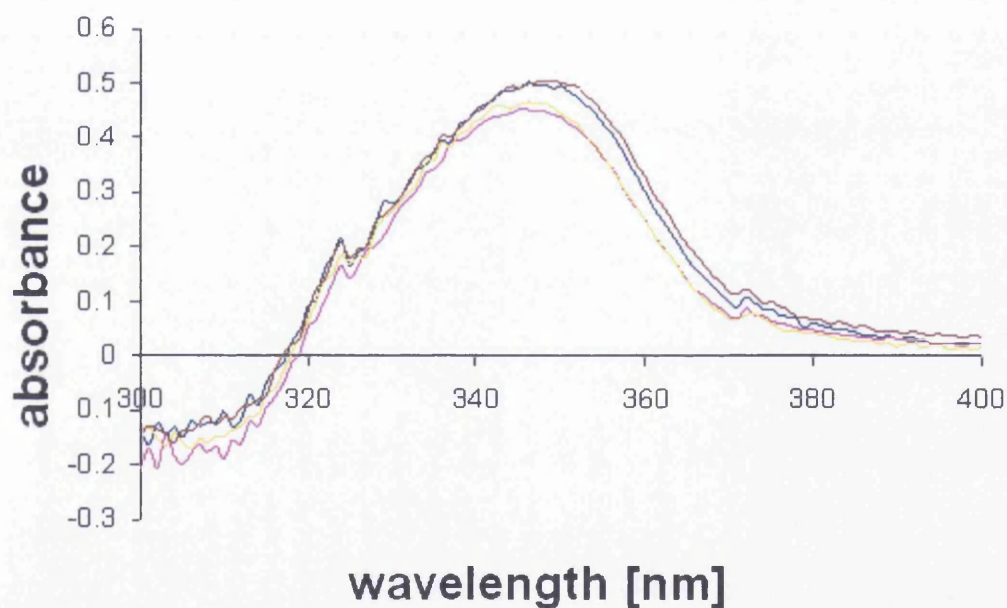


Figure 3-6 UV-VIS absorption spectra showing the TiO_2 absorption band of a series of glass slides covered with a TiO_2 film, compared to a glass slide without TiO_2 . (The decrease in absorbance below about 340 nm is an artifact due to absorption by the glass substrate present in both the sample and the reference).

3.3.1.2. Microscopy

3.3.1.2.1. Optical microscopy

All optical microscopy was carried out using an Olympus BH-2 optical microscope, and the photographs were taken with a Nikon Coolpix L4 digital camera and edited with Microsoft Photo Editor. Images were taken at optical magnifications of 120x, 300x, 600x, and in some cases 1200x.

Typical images of squeegee printed and spin coated TiO_2 surfaces made from different semiconductor sols are shown in Figures 7-10.

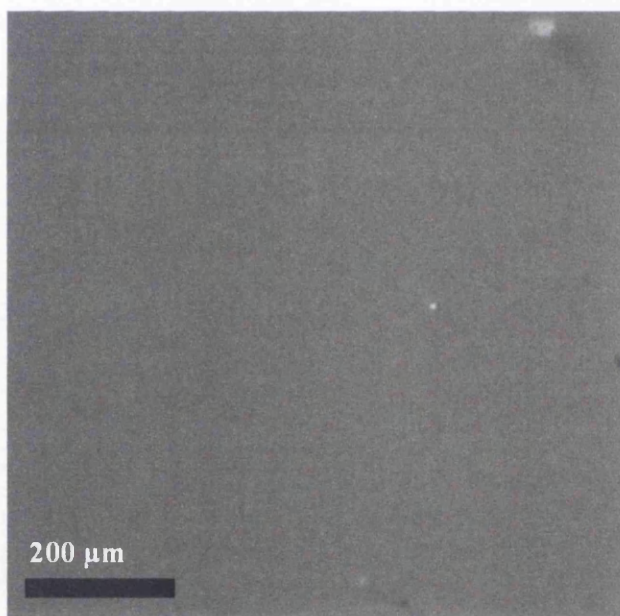


Figure 3-7 The surface of a titania film which was spin coated from sol P05 (for which the binder was PEO MW 600,000). The surface is very smooth and does not display any cracks. But the thickness is less than $1 \mu\text{m}$ (about 200 nm) as estimated from microscopic examination of the cross section.

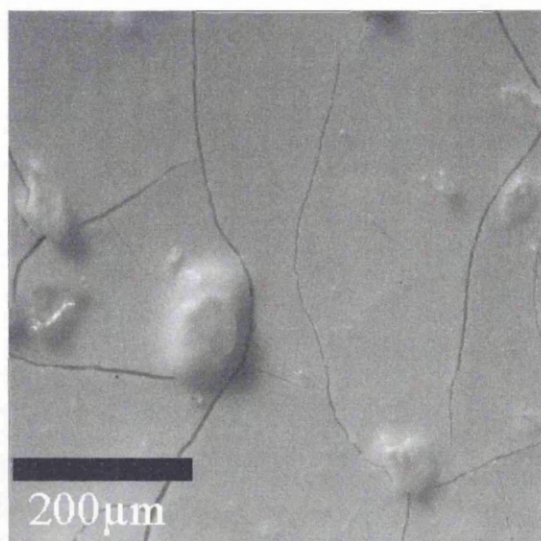


Figure 3-8 The surface of a titania film produced from sol P03 after sintering (for which the binder was ethyl cellulose) which was prepared by using 1 layer of Scotch Magic tape as a template. The film thickness is about 6 μm . The lumps seen on the film are probably larger ethyl cellulose particles which were insoluble in the sol.

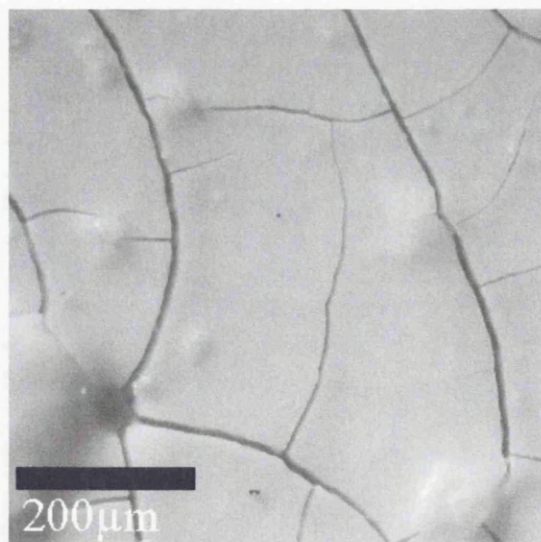


Figure 3-9 The surface of a titania film produced from sol P03 after sintering (for which the binder was ethyl cellulose) prepared using 2 layers of Scotch Magic tape. Film thickness about 10 μm . Again, the lumps are probably larger ethyl-cellulose particles.

The main difference in spin coated and squeegee printed films is the degree of cracking in the film. Squeegee printed films showed much greater cracking and this appears to be related to the much greater thickness of the films obtained by squeegee printing. The cracking occurs during the drying in air at room temperature. It seems that this causes stress within the thin films and leads to the generation of cracks if not prevented by a high concentration of binder. In Figures 3-8 and 3-9 it can be seen that the cracks in the thicker film are wider and greater in number than those in the thinner film. It may be possible that such stress cracking could be prevented by controlled drying of the samples prior to the sintering process. In the procedure used here samples were kept at room conditions for up to two hours before they were put into the 430 °C furnace, but an even slower drying process under controlled humidity and temperature might have helped reduce the amount of cracking.

3.3.1.2.2. SEM

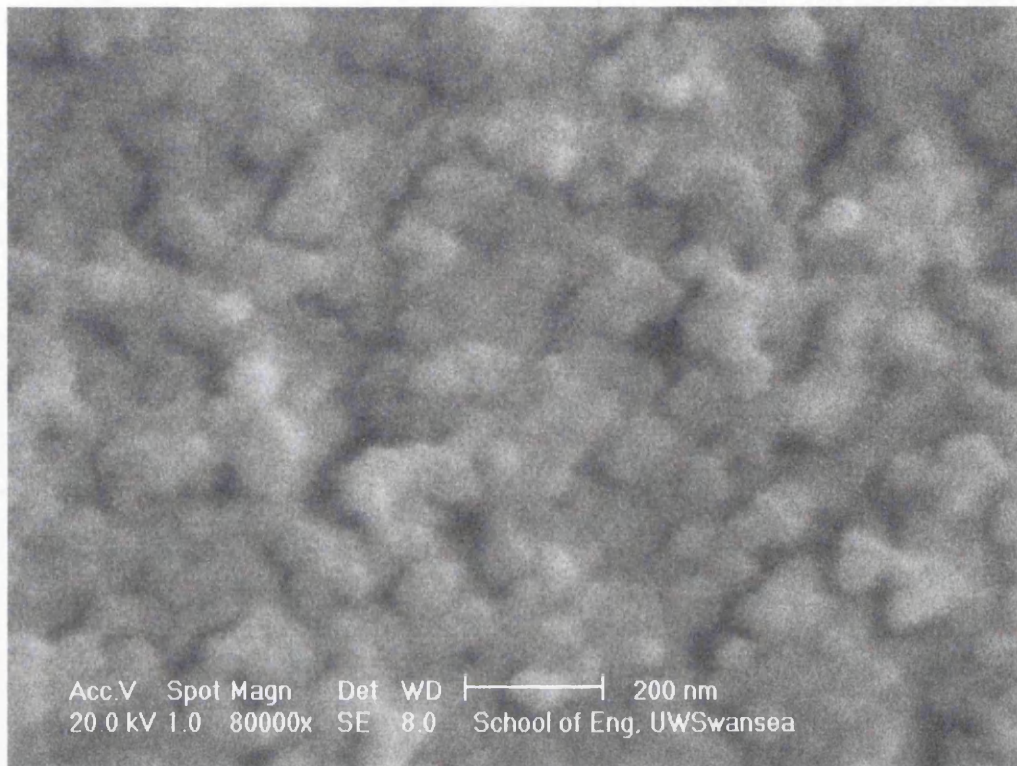


Figure 3-10 SEM image of a surface prepared with P04 (for which the binder is poly-ethyleneoxide, MW 300,000) under 80,000 fold magnification. The surface is made up of an agglomeration of particles of *ca.* 50 nm diameter.

The use of different additives did not lead to an obvious difference in surface morphology (see Figure 3-10), although additives did decrease the degree of cracking of the film. The amount of binder in the sol could have been increased and varied for a more thorough investigation of the influence of additives to the film morphology.

3.3.1.3. *Photoelectric measurements*

Cells from 6 different sols were prepared by either spin coating or squeegee printing and their photoelectric performance compared.

The layer thickness of the squeegee printed films was controlled by the number of tape layers used for the templates (one or two layers of Scotch Magic tape TM). The thickness of the spin coated films was controlled by the viscosity of the sol and the spin speed, but it was always below 1 μm . A general observation is that the thicker the semiconductor film the more cracks and the bigger cracks observed on the surface. The spin coated films are generally thinner than the squeegee printed ones. It is thought that cracks are a major source of back-reactions occurring as the conducting side of the glass substrate comes in contact with the electrolyte. This means, that the such sites provide a channel for potential back reactions from the TCO back to the electrolyte to reduce the oxidised dye species. This is not an electric short circuit in the conventional sense since no direct connection is made between the working and the counter electrode and we still have the electrolyte in between them which provides a substantial ohmic resistance. The effect is a deduction of the rate of electrons travelling into the desired direction and therefore the outcome is a lower overall efficiency of the device. However, even though the spin coated samples show less cracking the relatively low thickness may allow diffusion of the electrolyte through the semiconductor film leading to back-reactions as well. Table 3-3 collects photoelectrical data for these cells.

Cell	V _{oc} [V]	I _{sc} [mA]	V _{max}	I _{max}	FF	η %
SCP03	0.63	6.83	0.44	4.63	0.27	1.16
SCP04	0.588	3.54	0.43	2.70	0.56	1.16
SCP05	0.506	9.49	0.31	5.90	0.38	1.82
SCP06	0.489	2.98	0.33	2.08	0.47	0.68
SQP03	0.413	7.93	0.27	5.25	0.43	1.41
SQP04	0.45	8.16	0.25	4.37	0.31	1.14
SQP05	0.42	7.91	0.23	4.41	0.31	1.03
SQP06	0.538	3.77	0.40	2.82	0.55	1.16

Table 3-3 Photoelectrical data for cells prepared with TiO₂ sols containing different binders;. SC (spin coated) and SQ (squeegee printed) The photoelectrical characteristics (I-V) of these cells were measured using a 900 W Xenon arc lamp, a UV cut off filter (5% aqueous sodium nitrite) and an AM 1.0 filter. The measurements were taken at a light intensity of about 1000 Wm⁻² (1 Sun).

As can be seen above, the results for the different sols used were not conclusive. It seems as if P05 should be the sol of choice which gives the best performance. Whereas it was discovered later, that the sol P06 using ethyl cellulose as binder worked better after it had been stored for a few months. This is undermined, if one compared the efficiencies at this time with the results obtained months later with the same sol in the KODAK laboratories when the same type of cells was built as a reference. As reference, compare the efficiencies and currents of cell A with cell G or cell J with cell L. Especially the I_{sc} of the P06 cells increased a lot after storage. This

leads to the conclusion that different binders lead to changing performances dependent on the storage time of the sol. The reason for this seems to be slow dissolving processes which change the appearance of the binder in the sol.

3.3.1.4. *The influence of the semiconductor thickness*

The following graph shows a comparison of two cells built in the same way but with different thickness of the semiconductor thin film. As a template for the film thickness Scotch Magic tape was used in either one ($\sim 7 \mu\text{m}$) or two layers ($\sim 10 \mu\text{m}$). The samples were irradiated with one sun at 20°C and we can observe, that the voltages are similar, whereas the short circuit currents differ quite substantially.

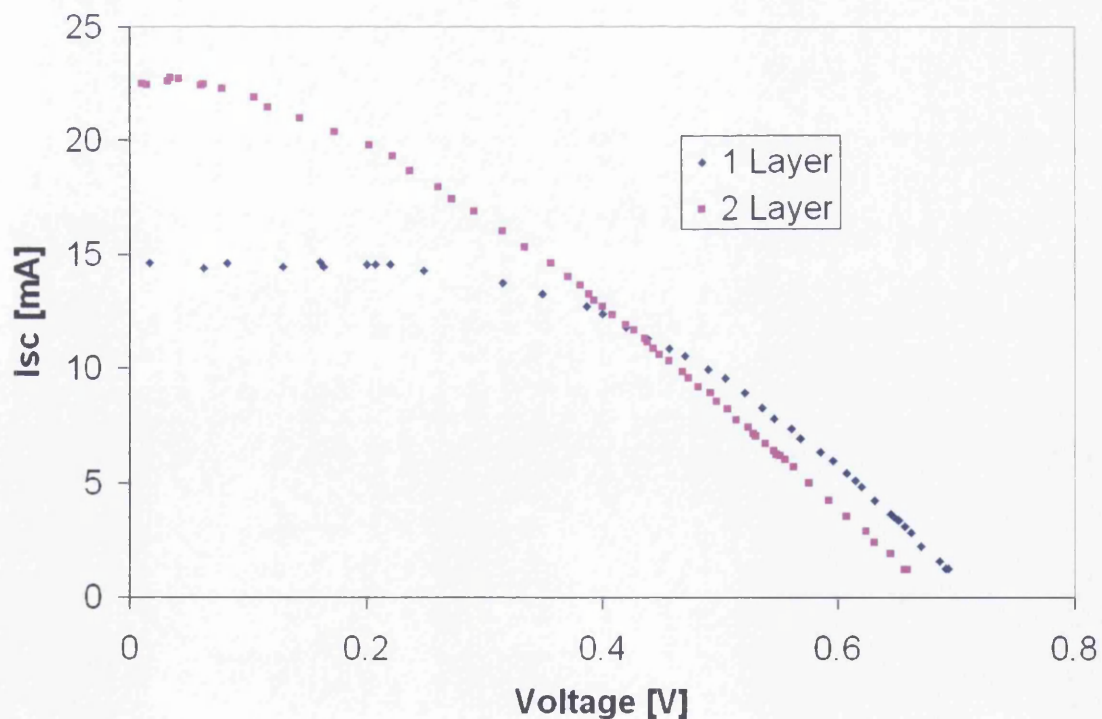


Figure 3-11 Gives the comparison of two cells built by using dye N3, electrolyte EL3, Solaronix HT sol and FTO glass supports. The cells were irradiated with 1 Sun (AM 1.0) at 20°C .

The higher current of the cell built with the thicker layer of TiO_2 can be explained by the higher amount of dye adsorbed per unit area onto the thicker semiconductor film. Actually, the values for the short circuit currents of the two cells correspond very well with the proportions of the layer thickness (7:10), see Figure 3-11. The difference in voltage seems to depend on the diffusion of the electrolyte through the semiporous layer. It has also been found, that a high number of excited dye molecules close to the electrolyte, with respect to the distance to the TCO opens a channel for possible back reactions (recombination reactions with the oxidised redox species in the electrolyte) [9]. In general, crack – free films are easier to produce, if the films are either thin or if thick films are built of sequences of thin films rather than one thick film which then dries too quick which causes stress – cracks on the surface. Those cracks can then lead to channels for back reactions.

3.4. The electrolyte

3.4.1. Introduction

A variety of different electrolytes were used, all based on the I/I_3^- couple. The major differences were between liquid and gel electrolytes but different concentrations of the electrolyte couple were also used, as well as those incorporating heterocyclic nitrogen compounds which are reported to improve the electron transfer characteristics of the electrolyte [10-12]. Gel electrolytes were chosen, because of the high loss of liquid through evaporation. Sealing has always been the major disadvantage of solvent based electrolyte systems in DSSCs [13-19], and gel electrolytes might help solve this problem. In general, it is expected that gel electrolyte cells last longer whilst having worse overall performance characteristics. Gel electrolytes were chosen for the cell experiments because gel might help to solve the problems with sealing and with it the loss of the electrolyte and cell function. There were expected to work for a longer time than solvent based DSSCs.

3.4.2. Liquid electrolyte

3.4.2.1. Effects of redox couple concentration on the cell performance (A cf L; G cf J)

The short circuit current of a cell with an acetonitrile based electrolyte increased with an increase in the concentration of the redox couple used (Figure 3-12). Further experiments with an even higher concentrated electrolyte at a later time confirmed this behaviour (see Figure 3-18). The open circuit voltage of the cells increased as well and so did the overall efficiency. Especially at higher illumination intensities it became evident that the higher redox couple concentration was

preferable since it resulted in higher voltage, current and as a consequence higher overall efficiency.

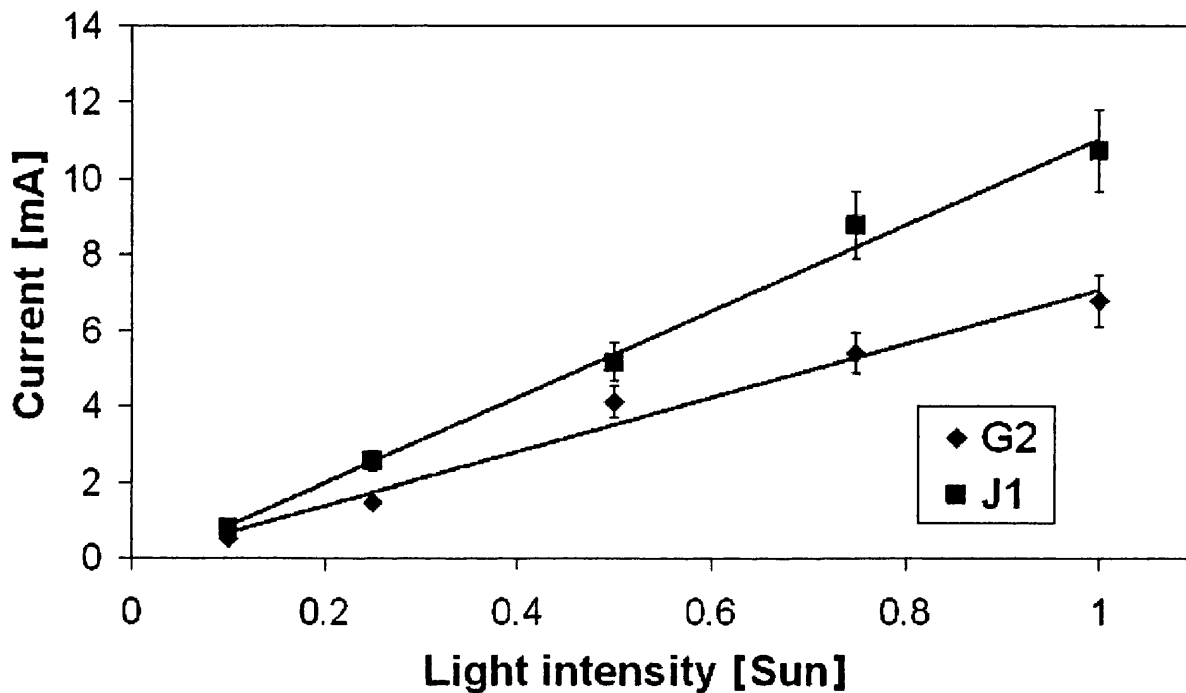


Figure 3-12 Short circuit current of two cells with different redox couple concentration in acetonitrile. Cell G2 corresponds to the lower redox couple concentration (0.03 M I₂/0.3 M LiI) and cell J1 to the higher one (0.05 M I₂/0.5 M LiI).

3.4.3. Gel electrolyte

3.4.3.1. Comparison of front and back illumination of gel cells (**H** and **K**)

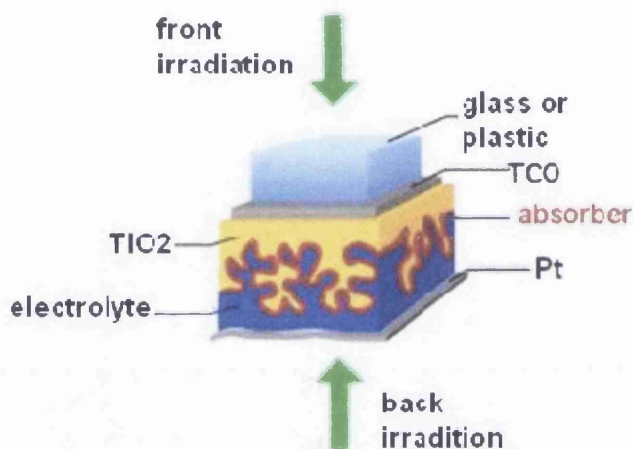


Figure 3-13 Scheme of a PV cell showing the direction of incident light for front and back irradiation

It was predicted that with decreasing mobility of the redox couple within the electrolyte it may become favourable to irradiate the DSSC from the back and by doing so, generate the majority of excited state dye molecules within the nanoporous semiconductor layer at the side closer to the counter electrode [20]. This shortens the effective pathlength the charge carrier (hole, electron) has to travel in order to lead to a charge recombination of the oxidised dye, which, in a cell using a redox couple which is embedded in a matrix of high viscosity (e.g. gel electrolytes or conducting polymers) has a relatively long lifetime because of hindered mobility of the reducing element in the redox couple. This means, the wanted reduction of the dye cation by the electrons coming from the counter electrode might happen at a higher rate due to

a closer proximity of this species to the counter electrode. Because of this there is expected to be a better fill factor and higher current for back illumination when irradiated at high intensity (relatively high steady-state concentration of oxidised dye) whereas front illumination is preferable for low intensities (relatively low steady-state concentration of oxidised dye), where mass transport limitations will not be so important. The degree of actual pore filling, which is a function of pore size and viscosity of the electrolyte plays a vital role too [21], since it determines what ratio of oxidised dye molecules can actually be reached by the redox couple in order to be reduced by it. Most gel and liquid electrolyte cells had a better performance on the day after preparation compared to freshly prepared cells. This has already been observed by many groups and was named dark effects by Nazeeruddin [1]. We believe this is due to the pore filling and related equilibrium processes which takes some time. Depending on the type of cell, the short circuit current and overall efficiency were very similar or significantly better when they were irradiated at 1.0 Sun. When cells made using a gel electrolyte are irradiated with 0.1 Sun there is a significant difference in current for front and back irradiation. At low irradiation intensities, front illumination gives a higher current but at high intensities the situation is reversed and back irradiation gives the higher current (see Figure 3-14). The idea is supported, that there is a hindered electron migration through the semiconductor layer. Reasons for the crossover could be the change in the charge transfer rate between the part of the cell which is just filled with electrolyte and the part of the cell in which the free charge transport is limited because of the porosity of the semiconductor layer.

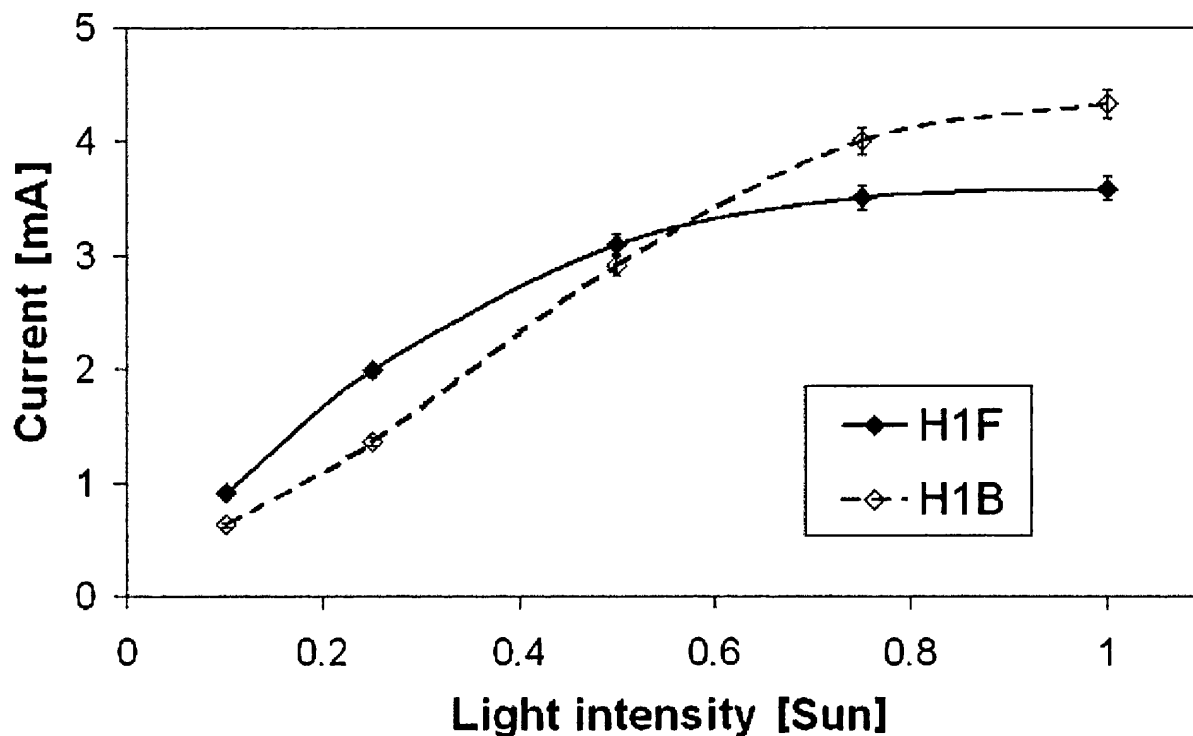


Figure 3-14 shows the short circuit current for front and back illumination of gel electrolytes cells with increasing light intensity. For better illustration only one cell, *H*, is shown. Error bars: $\pm 3\%$

Figure 3-15 shows an idealised graph of a sandwich type cell. If the cell is irradiated from the front, the majority of the charge carriers are bound to travel through the semiconductor layer because they are generated closer to the TCO|TiO₂ junction. On the other hand, if they are generated closer to or at the TiO₂|electrolyte junction (in the case of illumination from the back), they don't need to travel through the semiconductor layer and charge recombination of the oxidised dye species happens much quicker. The probability of the reduced electrolyte species travelling all the way through the semiconductor layer to the TCO|TiO₂ junction is much lower than charge

recombination occurring at the face of the semiconductor - where most oxidised dye species is formed in the case of back illumination.

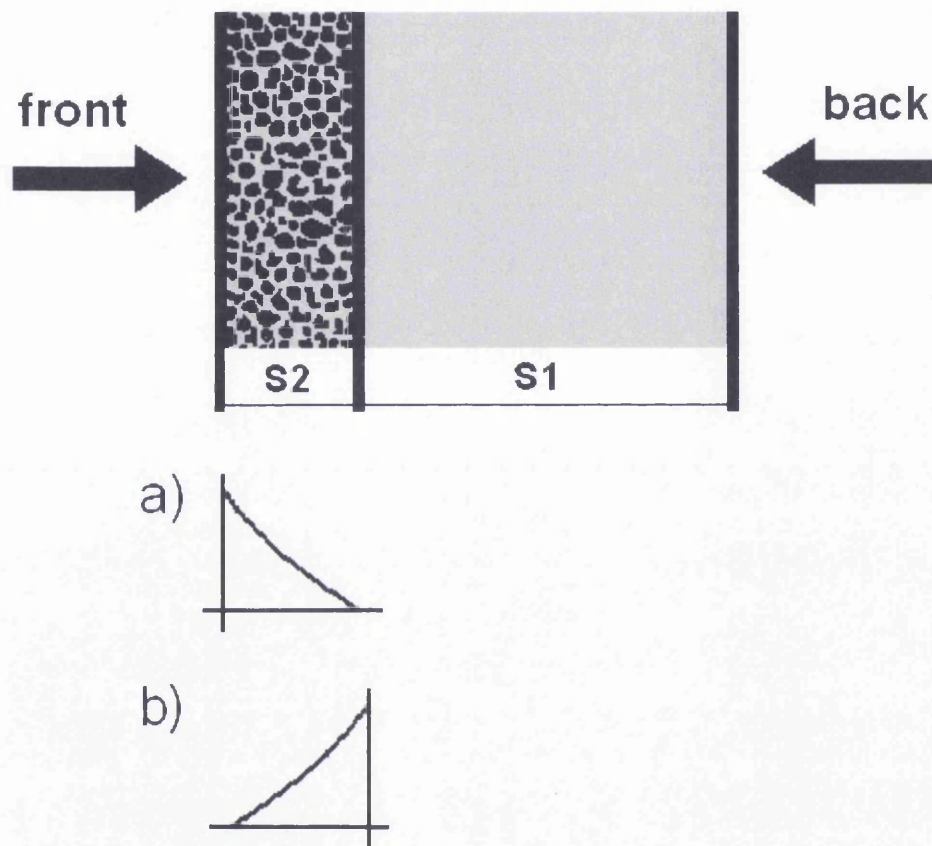


Figure 3-15, a graph of the sandwich type cell with the TiO₂ working electrode on the left and the Pt – counter electrode on the right. Front illumination is illumination from the left and back illumination from the right. It shows the pathway of the reduced form of the electrolyte (I⁻) from the platinum electrode (right) to the oxidised dye species in order to reduce the latter. The first part of the path (S1) is within the electrolyte matrix, whereas the second part of the charge carriers path leads through the semi-porous TiO₂ semiconductor film (S2).

a) Idealised distribution of excited dye molecules within the semiconductor layer when irradiated from the front. The exact shape of the distribution curve is unknown.

b) Idealised distribution of excited dye molecules when irradiated from the back.

The cell is operating most efficiently when the rate of charge recombination between oxidised dye and conduction band electrons is a minimum and reduction of oxidised dye by the redox couple is a maximum:

$$C_{D^+R^-} = \frac{n_{D^+R^-}}{t} \quad \text{(Equation 3-1)}$$

$n_{D^+R^-}$ number of dye cations reduced by the redox couple

t time

This value seems to be only dependent on the permeability of the semiconductor layer to the redox couple and thickness of the semiconductor, the photon flux and the site of excited dye generation.

3.5. Different dyes

3.5.1. Introduction

The dye everyone has been looking for during the past 16 years since the first publication of the Grätzel type sandwich cell [22] is one which gives maximum light absorption in the visible/near IR spectral region, with good anchoring groups to provide physical attachment to the semiconductor, as well as the right molecular structure for efficient electron injection into the semiconductor conduction band. A successful sensitizer dye used in Grätzel cells is one of our two reference dyes, N719 [22]. All sorts of light harvesting substances had been used as sensitizers in photovoltaic devices, with reported efficiencies ranging from a fraction of a percent to about 11 % for the black dye, a ruthenium terpyridine dye used and characterised by Grätzel's group [23] (see Chapter 2 for the structures of the dyes mentioned). In our studies, we have examined several organic dyes from the porphyrin and squaraine families, as well as the ruthenium bipyridines N719 and N3 which are commonly used by workers in the field as "standard" against which to compare new compounds.

3.5.2. Photoelectric Measurements

3.5.2.1. *Ruthenium bipyridines*

The ruthenium N3 dye (Solaronix SA Ruthenium 535) is probably the most widely studied sensitizer for DSSCs. The only difference between N3 and N719 is that the former is supplied as the carboxylic acid while the latter is supplied as di(tetra-butyl-ammonium) salt (see Chapter 2 for the structures).

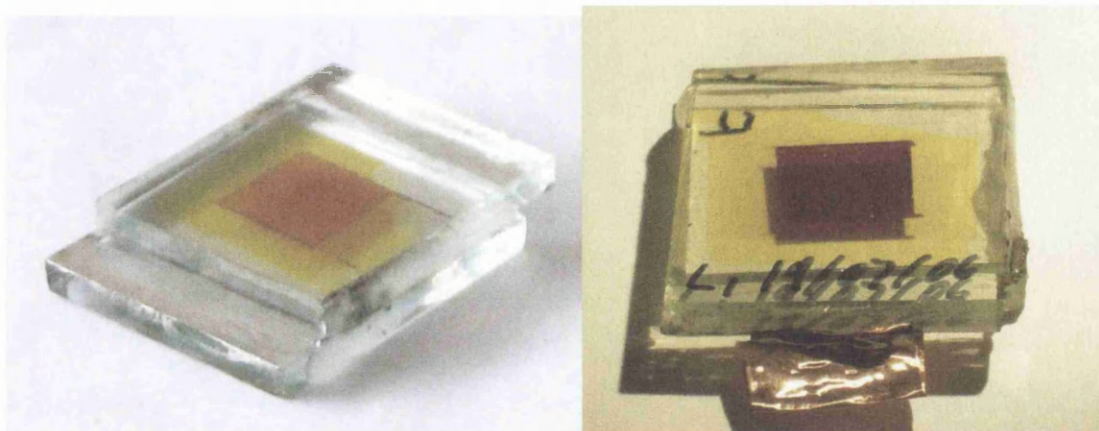


Figure 3-16 Pictures of cells built with N3 dye.

Figure 3-17 gives absorption spectra of five different samples of TiO₂ squeegee printed using the same thickness of Scotch Magic tape™ to which N719 has been adsorbed from a 3×10^{-4} M solution of N719 in EtOH.

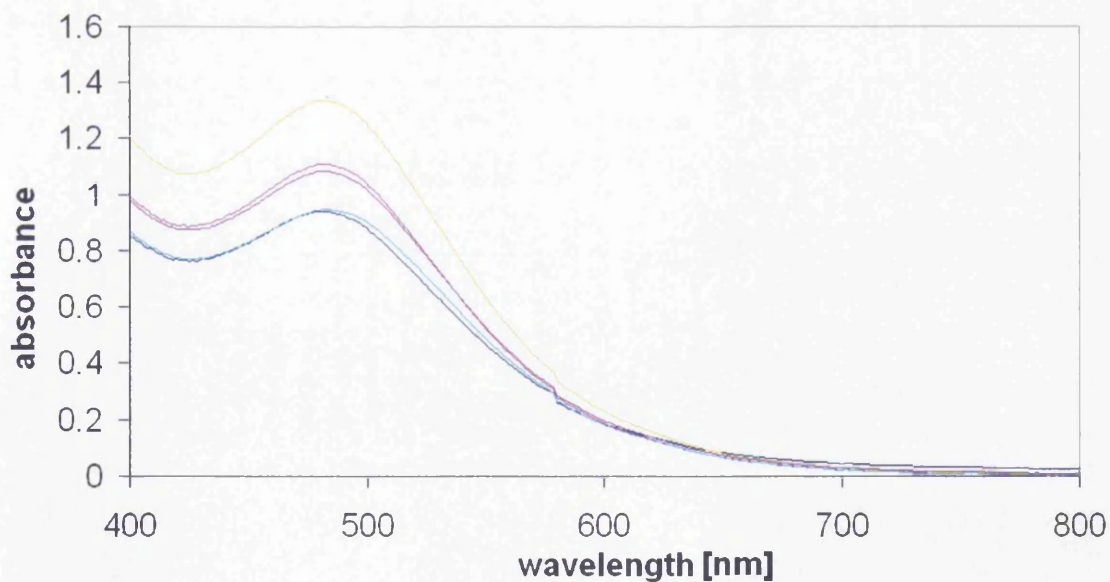


Figure 3-17 Absorption spectrum of N719 adsorbed onto of Solaronix nanopaste HT, squeegee print thickness 2 layers of Scotch Magic tape. Five different samples which were all made in the same way are shown to give some idea of the reproducibility of cell preparation.

Figure 3-18 shows the performance of the best cell built with N3, the redox couple concentration within the electrolyte was 0.1 M I₂/1.0 M LiI (EL 3) in a 20:80 mixture of 4-tert-butylpyridine and acetonitrile, this had already been used in different concentrations by Nazeeruddin in 1993 [1]. A finishing step in which pure anatase crystals were deposited onto the squeegee printed TiO₂ layer, by hydrolysis from aqueous TiCl₄, prior to dye adsorption was also carried out as part of the cell preparation [1]. As a comparison, Figure 3-19 gives a DSSC sensitised with N3 which is representative for those reported in the literature.

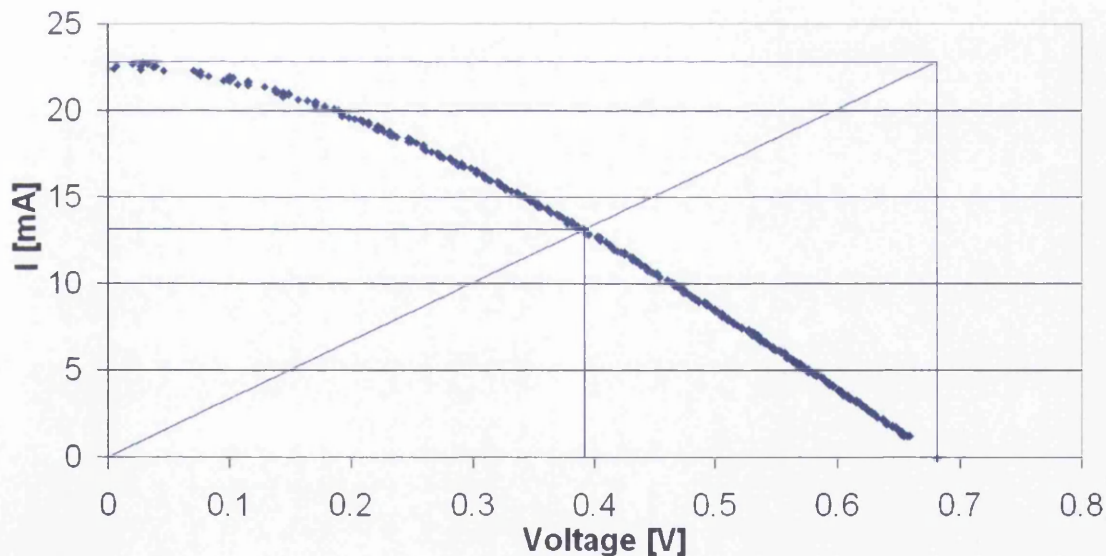


Figure 3-18, I-V curve for a cell built with N3, 2 layers of Scotch Magic tape squeegee print thickness, Solaronix HT sol and using electrolyte EL3, illumination 1000 Wm⁻², UV cut off \leq 400 nm

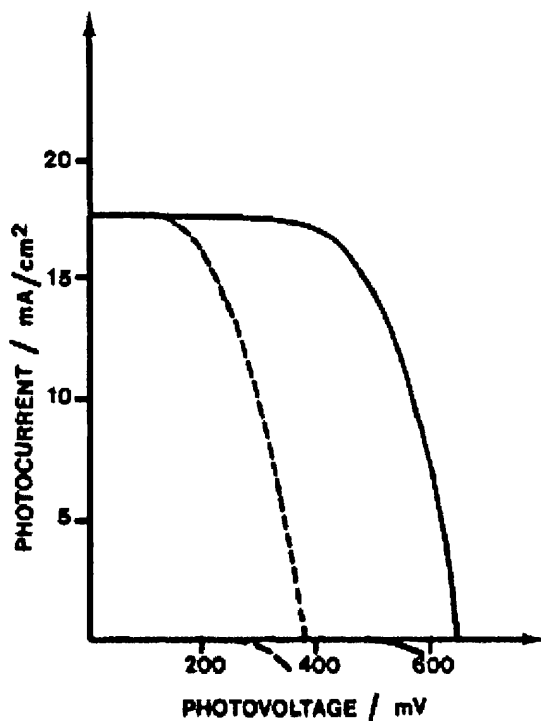


Figure 3-19 A diagram taken from the article published by Nazeeruddin in 1993 [1], the cell was built in a very similar way to the ones we built. In this case the used sol was made from Degussa P25 and put on a TCO glass substrate. The dashed line shows their cell before a 4-tert-butylpyridine dip and the full line shows the comparable system after a 15 min dip. The electrolyte was 0.3 :LiI + 0.03 M I₂ in acetonitrile, room temperature, light intensity 87 mW/cm², AM 1.5 spectral irradiance.

As shown above, our cell gives better photocurrent than the reference cell, which is probably down to the higher concentration of the redox couple in the electrolyte. The voltages are very similar which is probably down to the 4-tert-butylpyridine dip, or the 4-tert-butylpyridine used in the electrolyte, as it was done for our cell. The fill

factors are different because on the one hand, for our cells with an increase in current one has to accept a decrease in the fill factor. Another reason is, the size of the Nazeeruddin cells, they had an active area of 0.5 cm², whereas our cell were 1 cm². In the same paper, they are also reporting that the actual size of the cell influences it's characteristics with smaller cell displaying the better performance [1]. Due to the low fill factor of our cells, their overall light to current conversion efficiency is only 5.2 % compared to the 10 % reported by Nazeeruddin.

3.5.2.2. Squaraines

3.5.2.2.1. SQU1

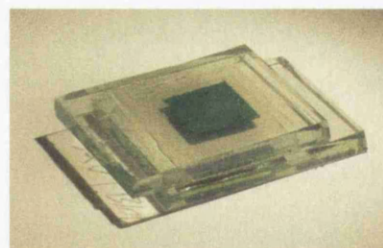
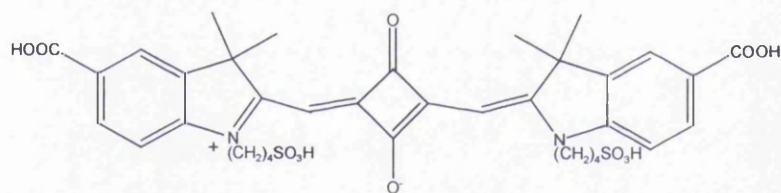


Figure 3-20 Structure of SQU1 and a PV cell built with it (without electrolyte).

Several cells were built using this greenish blue squaraine dye, with quite good results. This dye also seems to be remarkably stable for a dye of this type [24]. With its carboxylic acid binding groups it displayed very good binding capabilities to the semiconductor surface. The TiO₂ sol used was P06, which had ethyl cellulose as binder and the electrolyte used was EL 2 (0.5 M LiI/0.05 M I₂ in an 80:20 (v/v)

mixture of acetonitrile to 3-methyl-2-oxazolidinone (NMO)), without either of the two finishing steps (heterocyclic additives and anatase deposition) being used. Table 3-3 gives cell characteristics along with those of a comparable cell made using the N3 dye, and Fig. 21 gives the I-V curve.

	N3	SQU 1
V_{oc}	0.68 V	0.395 V
I_{sc}	22.8 mA	8.0 mA
V_{max}	0.39 V	0.24 V
I_{max}	13.33 mA	4.8 mA
P_{max}	5.21 mW	1.16 mW
FF	0.34	0.37
η	5.2 %	1.2 %

Table 3-1 Characteristics of cells built with N3 or SQU1 respectively at an incident radiation of 1000 Wm^{-2} , 1 Sun.

SQP06SQU1EL22_3

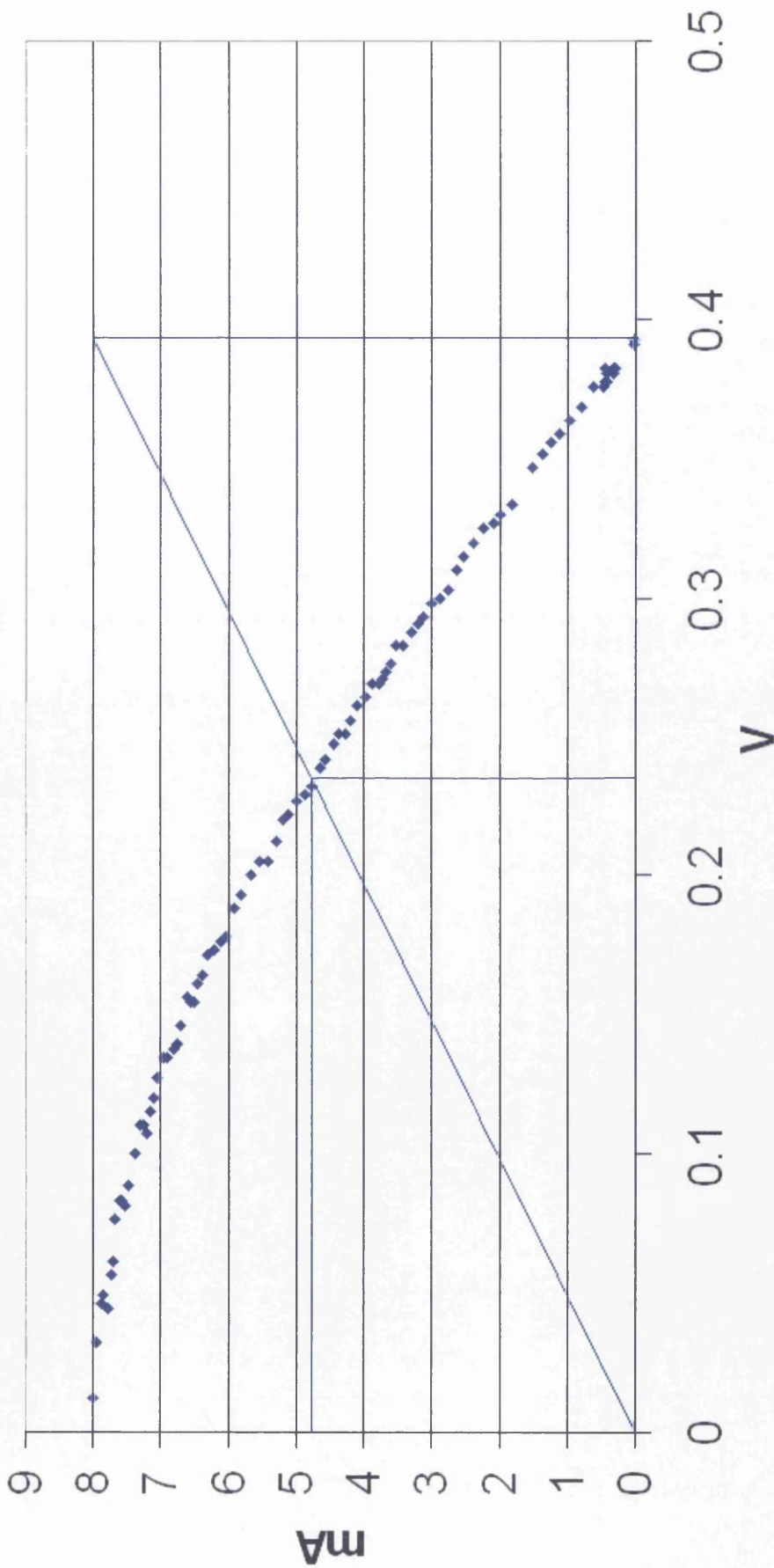


Figure 3-21, a cell built using P06 sol, the SQU1 dye and EL 2. The semiconductor was squeegee printed and the template thickness

was 1 layer of Scotch Magic tape. Irradiation: 1000 Wm^{-2}

3.5.2.2.2. SQU2

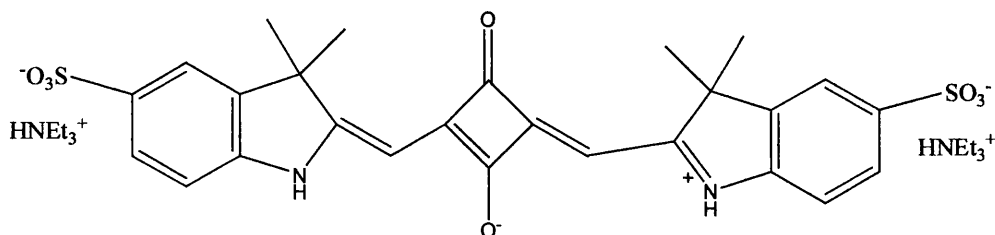


Figure 3-22 Structure of SQU2

In the case of this dye, no cell with any significant output could be made despite several efforts. Cells were built using the Solaronix nanosol HT plus anatase hydrolysis from TiCl_4 . The dye was dissolved in ethanol in which it probably did not fully dissociate and hence did not adsorb to the semiconductor in significant quantities. Electrolyte 2 (0.5 M LiI/0.05 M I_2 in an 80:20 (v/v) mixture of acetonitrile to 3-methyl-2-oxazolidinone (NMO)) was used to fill the cells and photoelectrical measurements showed an open circuit voltage of about 490 mV which is relatively close to the V_{OC} of SQU1. However, the current generated by the irradiation intensity of one sun onto the cell was beyond the lower detection limit of our apparatus.

3.5.3. Conclusion

Stable organic dyes are an interesting alternative to expensive and not always very environmentally friendly organo-metallic dyes. The squaraine dye SQU1 is easy and cheap to produce and gives a cell comparable in performance to those made using other organic dyes reported in the literature [25-29]. The anchoring group is a

carboxylic acid group and is also responsible for the comparatively good electron injection properties of this dye. The selection of organic dye mixtures which work together in harvesting most of the solar spectrum is one potentially useful way forward for solar cell manufacturers and researchers.

3.6. The counter electrode

For the counter electrodes the same glass and plastic FTO and ITO supports were used as for the working electrode. Two methods of depositing Pt were used; deposition *via* a paste or *via* sputtering. When using the paste the support was first cleaned with ethanol and then Pt-paste was spread over the electrode, leaving out the contact areas, using the same squeegee print method as for the working electrode, before first heating to 100 °C for 10 min and then 430 °C for another 30 min to decompose the paste and deposit metallic Pt. The paste was only used for glass cells, since it was not possible to heat the plastic substrate up to the temperature required. Sputtering onto TCO coated plastic was carried out by our collaborators in the Research laboratories, Kodak European Research, Cambridge. (Special thanks go to Nick Dartnell and Julie Baker, KODAK European Research, Cambridge, UK, for this.)

The aim of these experiments was to investigate whether a thick film of Pt applied onto the relatively high resistance TCO would lead to better cell efficiency, by a reduction in sheet resistance, than one in which a thin layer of Pt clusters were deposited on the TCO.

3.6.1. Counter-electrode comparisons

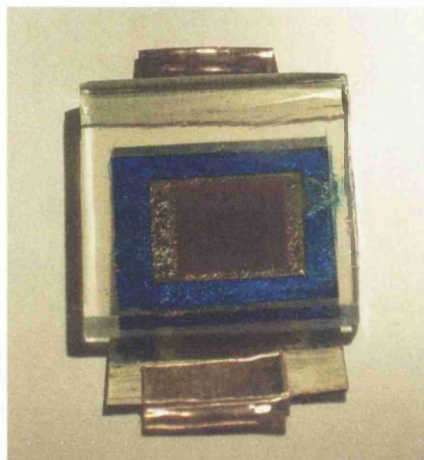


Figure 3-23 Cell built with plastic counter electrode and thick layer of Pt sputtered on it so that it turned out to be non-transparent (900 s sputtering). It is sealed by a blue self adhesive sealant frame. The working electrode is FTO coated glass, the counter electrode ITO coated plastic.

The experiment in which the thickness of the Pt – layer was varied lead to the conclusion that it does not matter how much Pt there is present (compare Table 3-1, cells H and I). On the contrary, it was better to have a thin but transparent Pt – layer, since with increasing light intensity back irradiation becomes favourable for cells made using high viscosity or solid electrolytes.

SEM images (Fig 3-24) support the suggestion that the role of Pt is as a catalyst for the charge carrier transfer between the TCO and the electrolyte [30-33] rather than as an additional conducting layer because it does not even have to form a homogenous layer covering the whole surface of the conducting oxide. SEM pictures of the surface of a counter electrode treated with the Pt paste show that, rather than forming a continuous layer on top of the TCO, the Pt is present as Pt islands or clusters on the oxide surface. Sputtered Pt is deposited as a much more coherent layer of Pt. However, even here, a thick mirror like layer of Pt did not show any advantage over a thin transparent layer over the whole light intensity range.

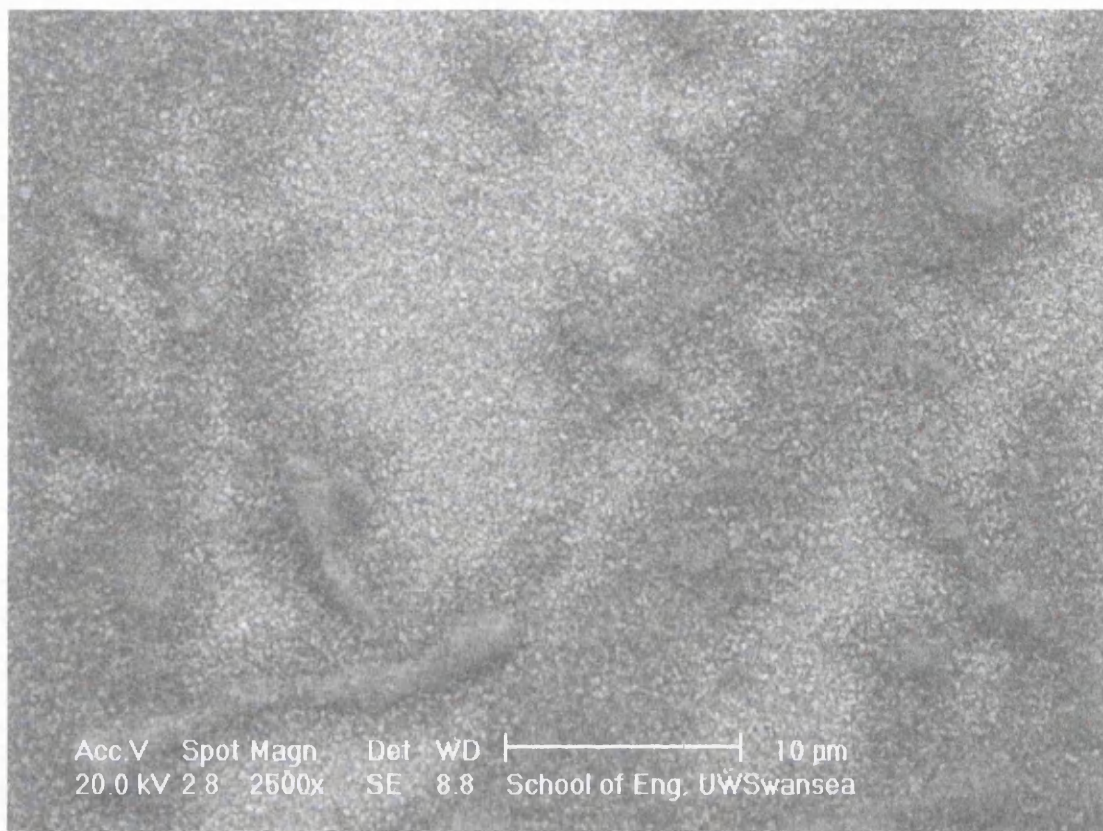


Figure 3-24, SEM image of the surface of FTO on conducting glass showing Pt clusters of a few μm in diameter which presumably act as a catalyst for the charge transfer from the FTO to the electrolyte.

3.6.2.1. The influence of the Pt-thickness at the counter electrode of plastic gel electrolyte cells (H cf I)

Both cells had an FTO semiconductor electrode and an ITO coated plastic counter electrode support onto which Pt was sputtered. Cell **H** was sputtered for about 10 s to give a very thin Pt-layer. It was not necessarily an interconnected conducting layer (see Figure 3-24) and the optical density differed only slightly from the optical density of the plastic substrate. This cell was irradiated from the front and from the back. On the other hand, cell **I** was sputtered for 900 s to give a very thick Pt film

which was optically opaque and mirror like. For this cell, it was only possible to irradiate it from the front. It has been suggested, that this mirror effect helps harvesting light which would otherwise go through the cell by reflecting it back onto the working electrode[1]. Our findings are that the mirror effect does not play a role for the cells we built. The comparison of the two cells showed that for light intensities of more than about 0.5 Sun the cell with a thin transmitting Pt-film irradiated from the back gave better performance than one with a thick Pt-layer irradiated from the front (Figure 3-25). Since Pt is also very expensive it is a noteworthy finding that a thick layer of it did not seem to have any advantage over a thin layer. It appears to make no difference whether the Pt is present in tiny amounts acting as a catalyst for the electron transfer into the TCO or as a thick conducting layer. The open circuit voltages are similar for the back irradiated cell (**HB**) and for the thick Pt-film cell (**I**) which could not be irradiated from the back, whereas the front irradiated cell **H** did show a higher voltage over the whole light intensity range, but it also had much worse fill factors and short circuit currents.

When irradiated from the back, less of the dye is excited, because less light hits the sensitiser dye layer due to the filter effect of the electrolyte. The kinetic limiting step is the transport of the hole through the electrolyte, not the electron transport within the semiconductor layer. Therefore, at higher light intensities where hole transport is limiting, it becomes favourable to use back illumination because this gives, on average a shorter excited-dye to electrolyte distance. It is interesting to note that the voltage is higher for the same cell if it is irradiated from the front rather than the back (cell **H**). This can be explained by a higher amount of excited dye species close to the TCO electrode and a hindered reduction of the dye cation through the electrolyte resulting in a higher electric potential.

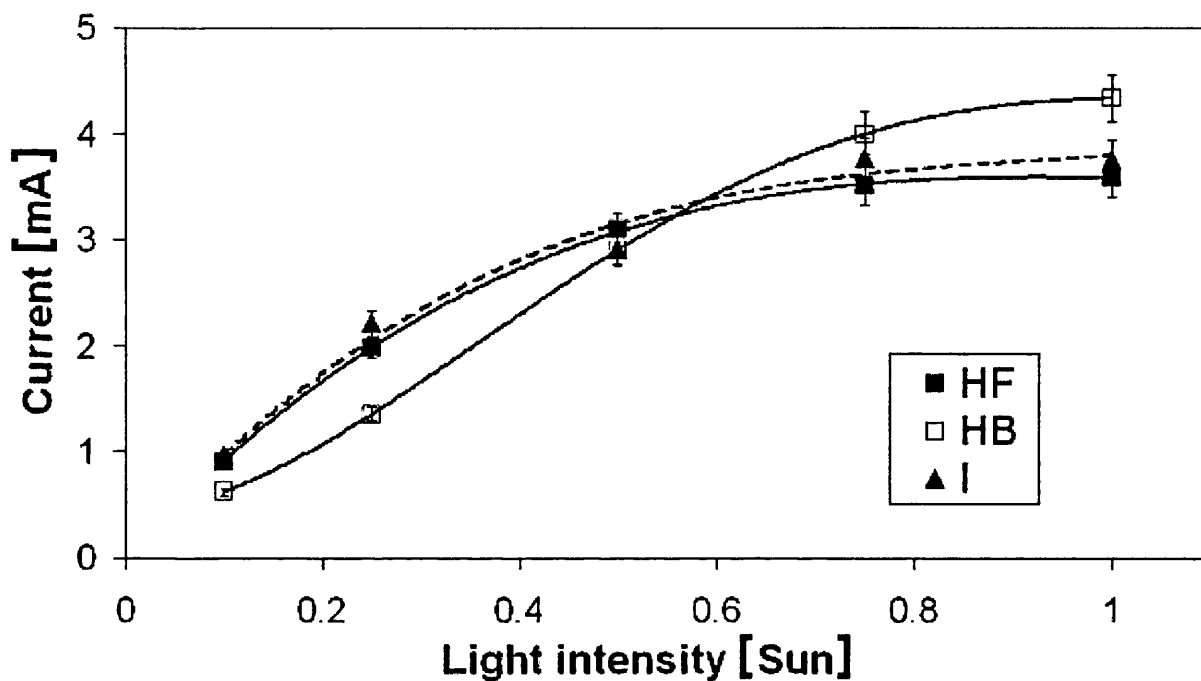


Figure 3-25 The short circuit currents of two cells with different Pt-thickness at the counter electrode (*H* & *I*). Cell *H*, which has a thin transparent layer of Pt, was irradiated from either front or back (HF & HB), whereas *I* was only irradiated from the front due to its mirror like, thick Pt layer. Error estimates are $\pm 5\%$.

3.6.2.2. Conclusion

It was shown that the Pt thickness did not influence the cell performance even though the series resistance of the cell with a thick Pt layer was one quarter of that for the cell with a thin Pt layer ($14.25\ \Omega$ and $53.8\ \Omega$, respectively). The role of Pt here is one of catalyst rather than conductor, and given the high costs of Pt there are major savings to be made by using as thin a Pt-layer as possible.

3.7. Conclusion

In terms of the different cell components examined we can make the following general comments.

Glass *versus* plastic

Since we built cells made of glass and plastic, one difference, which might become very important for industrial applications and large scale manufacturing of the cells is the weight difference between them. On the other hand, the use of plastic also means a big loss in stability of the cell. Flexible cells could also be something sought after though, especially for application in handheld or small devices. Plastic cells with a low sheet resistance in the region of the FTO glass cells could be much lighter, cheaper and more flexible than glass cells.

Liquid or gel electrolyte

If solvent and gel electrolytes are compared, then, at higher intensities, front illumination will be preferable for the solvent based electrolyte and back illumination for the gel. A low series resistance for the TCO is necessary alongside an electrolyte which carries enough of the redox active species in it to ensure efficient recombination of oxidised states with high enough rates to prevent back reactions from happening. The viscosity of the electrolyte and with it the mobility of the redox species in it are important as well as the pathlength the charge carrier has to travel within the cell. The working and counter electrode have to be separated enough to prevent short circuits or charge transfers between the semiconductor and the Pt covered counter electrode. With low mobility electrolytes back reaction can become favourable. At higher irradiation intensities, back illumination of the cell becomes

favorable, this depends on the speed of electron transfer through the electrolyte layer between the counter and the working electrode. The faster the electron transfer through the electrolyte media, the less difference occurs between front and back illumination. One major contributor to the speed the electrons can travel is, next to the viscosity of the electrolyte matrix, the morphology of the semiconductor surface. The easier accessible the dye docking places are for the redox species and the faster the redox species or the charge carrier can get in and out of the porous semiconductor, the better for cell performance.

Sensitiser dyes

The requirements of a good sensitiser dye are quite stringent. Ground and excited-state energy levels must straddle those of the redox couple and semiconductor for any photoelectrical activity at all, and, for maximum efficiency, the dye should absorb all the solar radiation with energy greater than the semiconductor absorption band. The sensitiser dye should be adsorbed in a monolayer and intermolecular charge transfer should be avoided. In terms of efficiency itself should harvest all the visible light with an efficiency close to unity and it should have an absorption band reaching into the near IR. Organic dyes, like the used squaraines are a cheap alternative with good photoelectric properties but often lack the stability that is needed for a long lasting cell. If this situation could be improved, then they could become strong competitors of the expensive organometallic sensitisers. It is probable that a combination of different dyes, which absorb in different wavelength regions, will give the best performance [34-36].

Finishing steps

The finishing steps: hydrolysis of TiO_2 from TiCl_4 on the semiconductor surface to form a thin layer of anatase crystals, and either dipping the sensitised working electrode in butylpyridine or the addition of butylpyridine to the electrolyte, definitely lead to an increased cell performance, especially much higher currents. It is very important, that the semiconductor layer covers the whole accessible area of the TCO so that no recombination reactions occur or so that they are hindered at least.

A very low and even distribution of Pt over all the counter electrode area touched by the electrolyte would lead to optimum results.

Perhaps the two most significant findings from this series of experiments in terms of understanding and modeling the nature of the series of electron reactions which occur in the cell are:

- a) the role of Pt on the counter electrode is that of a catalyst rather than conductor, and therefore a thicker Pt layer does not give a more efficient cell.
- b) for electrolytes in which diffusion of the redox couple is restricted, e.g. gel and solid electrolytes, back illumination will become favourable over front irradiation of the cell at high irradiation intensities.

The first of these findings immediately suggests the determination of the minimum amount of Pt necessary as an important follow-on experiment from those presented here. It would also be useful to explore any effect of Pt distribution geometry. For example, is a small patch of Pt as effective as a thin layer across the

whole electrode area. Such factors may be important in the design and production of DSSCs.

The second point, along with the observation of high currents at high light intensities with high electrolyte concentrations, suggests that at high illumination intensities mass transport of the redox couple through the semiconductor layer can limit cell efficiency. In addition to matrix viscosity another major contributor to the rate of oxidised dye reduction by the redox couple is the morphology of the semiconductor surface. The semiconductor pore size needs to be tuned to the sensitizer dye to allow adsorption from solution, and also to the viscosity of the redox couple to allow rapid electron transfer, whilst having maximum surface area in terms of available sites for the adsorption of the sensitizer dye. Ideally, no active potential anchor sites should be left after sensitisation because those could provide channels for back reactions between semiconductor and electrolyte and lower the efficiency of the cell. Hole blocking layers or protection groups such as small acid molecules could lead to satisfying solutions [37, 38].

As we have seen, many parameters contribute to an efficient solar cell. The different parts of a cell influence each other in a way that not for all aspects direct trends can be found. It is rather, that there is an optimum constellation with respect to the interactions at the different interfaces. Hence it can prove to be difficult to find the recipe to build the perfect cell but some general predictions could be made.

References:

1. Nazeeruddin, M.K., A. Kay, I. Rodicio, R. Humphrybaker, E. Muller, P. Liska, N. Vlachopoulos, M. Gratzel, *Journal Of The American Chemical Society*, 1993. **115**(14): p. 6382-6390.
2. Nakade, S., M. Matsuda, S. Kambe, Y. Saito, T. Kitamura, T. Sakata, Y. Wada, H. Mori, S. Yanagida, *Journal Of Physical Chemistry B*, 2002. **106**(39): p. 10004-10010.
3. Nguyen, T.-V., H.-C. Lee, O.B. Yang, *Solar Energy Materials and Solar Cells*, 2006. **90**(7-8): p. 967-981.
4. Saito, Y., S. Kambe, T. Kitamura, Y. Wada, S. Yanagida, *Solar Energy Materials and Solar Cells*, 2004. **83**(1): p. 1-13.
5. Roberson, L.B., M.A. Poggi, J. Kowalik, G.P. Smestad, L.A. Bottomley, L.M. Tolbert, *Coordination Chemistry Reviews*, 2004. **248**(13-14): p. 1491-1499.
6. Hart, J.N., R. Cervini, Y.B. Cheng, G.P. Simon, L. Spiccia, *Solar Energy Materials and Solar Cells*, 2004. **84**(1-4): p. 135-143.
7. Barbe, C.J., F. Arendse, P. Comte, M. Jirousek, F. Lenzmann, V. Shklover, M. Gratzel, *Journal of the American Ceramic Society*, 1997. **80**(12): p. 3157-3171.
8. Huang, C.-Y., Y.-C. Hsu, J.-G. Chen, V. Suryanarayanan, K.-M. Lee, K.-C. Ho, *Solar Energy Materials and Solar Cells*, 2006. **90**(15): p. 2391-2397.
9. Waita, S.M., B.O. Aduda, J.M. Mwabora, C.G. Granqvist, S.E. Lindquist, G.A. Niklasson, A. Hafeldt, G. Boschloo, *Journal of Electroanalytical Chemistry*, 2007. **605**(2): p. 151-156.
10. Kusama, H. and H. Sugihara, *Journal of Photochemistry and Photobiology A: Chemistry*, 2006. **181**(2-3): p. 268-273.
11. Kusama, H. and H. Arakawa, *Solar Energy Materials And Solar Cells*, 2004. **82**(3): p. 457-465.
12. Kusama, H. and H. Arakawa, *Solar Energy Materials And Solar Cells*, 2005. **85**(3): p. 333-344.
13. Nogueira, A.F., J.R. Durrant, M.A. De Paoli, *Advanced Materials*, 2001. **13**(11): p. 826-830.
14. Li, W., J. Kang, X. Li, S. Fang, Y. Lin, G. Wang, X. Xiao, 2005. **170**(1): p. 1.
15. Bandara, J. and H. Weerasinghe, *Solar Energy Materials and Solar Cells*, 2005. **85**(3): p. 385-390.
16. Ileperuma, O.A., M.A.K.L. Dissanayake, S. Somasunderam, L.R.A.K. Bandara, *Solar Energy Materials and Solar Cells*, 2004. **84**(1-4): p. 117-124.
17. Nogueira, A.F. and M.A. De Paoli, *Solar Energy Materials And Solar Cells*, 2000. **61**: p. 135-141.
18. An, H., B.F. Xue, D. Li, H. Li, Q.B. Meng, L. Guo, L. Chen, *Electrochemistry Communications*, 2006. **8**: p. 170-172.
19. Kaneko, M., T. Hoshi, Y. Kaburagi, H. Ueno, *Journal of Electroanalytical Chemistry*, 2004. **572**(1): p. 21-27.
20. Ferber, J., R. Stangl, J. Luther, *Solar Energy Materials and Solar Cells*, 1998. **53**(1-2): p. 29-54.

21. Schmidt-Mende, L. and M. Gratzel, *Thin Solid Films*, 2006. **500**(1-2): p. 296-301.
22. O'Regan, B. and M. Graetzel, *Letters to Nature*, 1991. **353**: p. 737-740.
23. Nazeeruddin, M.K., P. Pechy, M. Gratzel, *Chemical Communications*, 1997(18): p. 1705-1706.
24. Alex, S., U. Santhosh, S. Das, *Journal of Photochemistry and Photobiology A: Chemistry*, 2005. **172**(1): p. 63-71.
25. Yanagida, S., G.K.R. Senadeera, K. Nakamura, T. Kitamura, Y. Wada, *Journal of Photochemistry and Photobiology A: Chemistry*, 2004. **166**(1-3): p. 75.
26. Senadeera, G.K.R., T. Kitamura, Y. Wada, S. Yanagida, *Solar Energy Materials And Solar Cells*, 2005. **88**(3): p. 315-322.
27. Sayama, K., M. Sugino, H. Sugihara, Y. Abe, H. Arakawa, *Chemistry Letters*, 1998(8): p. 753-754.
28. Hara, K., Y. Tachibana, Y. Ohga, A. Shinpo, S. Suga, K. Sayama, H. Sugihara, H. Arakawa, *Solar Energy Materials And Solar Cells*, 2003. **77**(1): p. 89-103.
29. Ma, T.L., K. Inoue, K. Yao, H. Noma, T. Shuji, E. Abe, J.H. Yu, X.S. Wang, B.W. Zhang, *Journal Of Electroanalytical Chemistry*, 2002. **537**(1-2): p. 31-38.
30. Polo, A.S., M.K. Itokazu, N.Y. Murakami Iha, *Coordination Chemistry Reviews*, 2004. **248**(13-14): p. 1343-1361.
31. Liao, J.-Y. and K.-C. Ho, *Solar Energy Materials and Solar Cells*, 2005. **86**(2): p. 229-241.
32. Mills, A. and S. Le Hunte, *Journal of Photochemistry and Photobiology A: Chemistry*, 1997. **108**(1): p. 1-35.
33. Dai, S., J. Weng, Y. Sui, C. Shi, Y. Huang, S. Chen, X. Pan, X. Fang, L. Hu, F. Kong, K. Wang, *Solar Energy Materials and Solar Cells*, 2004. **84**(1-4): p. 125-133.
34. Bandara, J. and H. Weerasinghe, *Solar Energy Materials and Solar Cells*, 2006. **90**(7-8): p. 864-871.
35. Zhang, D., W. Wang, Y. Liu, X. Xiao, W. Zhao, B. Zhang, Y. Cao, *Journal of Photochemistry and Photobiology A: Chemistry*, 2000(135): p. 235-240.
36. Perera, V.P.S., P.K.D.D.P. Pitigala, M.K.I. Senevirathne, K. Tennakone, *Solar Energy Materials And Solar Cells*, 2005. **85**(1): p. 91-98.
37. Jang, S.-R., M.-J. Choi, R. Vittal, K.-J. Kim, *Solar Energy Materials and Solar Cells*, 2007. **91**(13): p. 1209-1214.
38. Lee, K.-M., V. Suryanarayanan, K.-C. Ho, K.R. Justin Thomas, J.T. Lin, *Solar Energy Materials and Solar Cells*, 2007. **91**(15-16): p. 1426-1431.

CHAPTER 4

**CHANGES IN CELL PERFORMANCE WITH
TEMPERATURE; FOR CELLS MADE USING THE
N3 DYE; NOVEL SQUARAIN DYES; AND
DIFFERENT BINDERS**

4.1. Introduction

The variation of cell performance with temperature is an important parameter, since we might expect large-scale solar cell applications to be outdoors, in areas of high solar flux and perhaps wide variations in temperature, such as the deserts of America, Australia and Africa. In these sites we can expect the cell to be exposed to regular diurnal and seasonal temperature changes. Furthermore in these sites the solar cell would normally be operating at relatively high temperatures (air temperatures of more than 40 °C). Therefore knowledge of the specific cells optimum working temperature is crucial. In addition, a study of the temperature variation in cell parameters may be useful in developing an understanding of the chemistry and thermodynamics of cell performance together with insight into those factor which limit cell performance.

There have been few reports on the temperature dependence of DSSCs, although Nazeeruddin *et al.* reported for their N3 cells an increasing current with temperature alongside a decrease in voltage. They also reported a power output maximum at an operating temperature of about 40 °C [1]. In this chapter, the changes in cell efficiency and performance for a variety of cells over a temperature range from 1°C to 60°C are reported and discussed. Temperature control was achieved by pumping water of a controlled temperature from the temperature control unit (a water bath of about 5 L volume and a pump with an inlet and an outlet nipple for silicone hoses) through the brass cell holder (see Figure 4-1). The temperature in the water bath was changed in 5 °C or 10 °C increments and the cell was left to equilibrate at each temperature for about 5 min before characterisation. After that time it was assumed, that the temperature in the water bath and the sample temperature were the same.

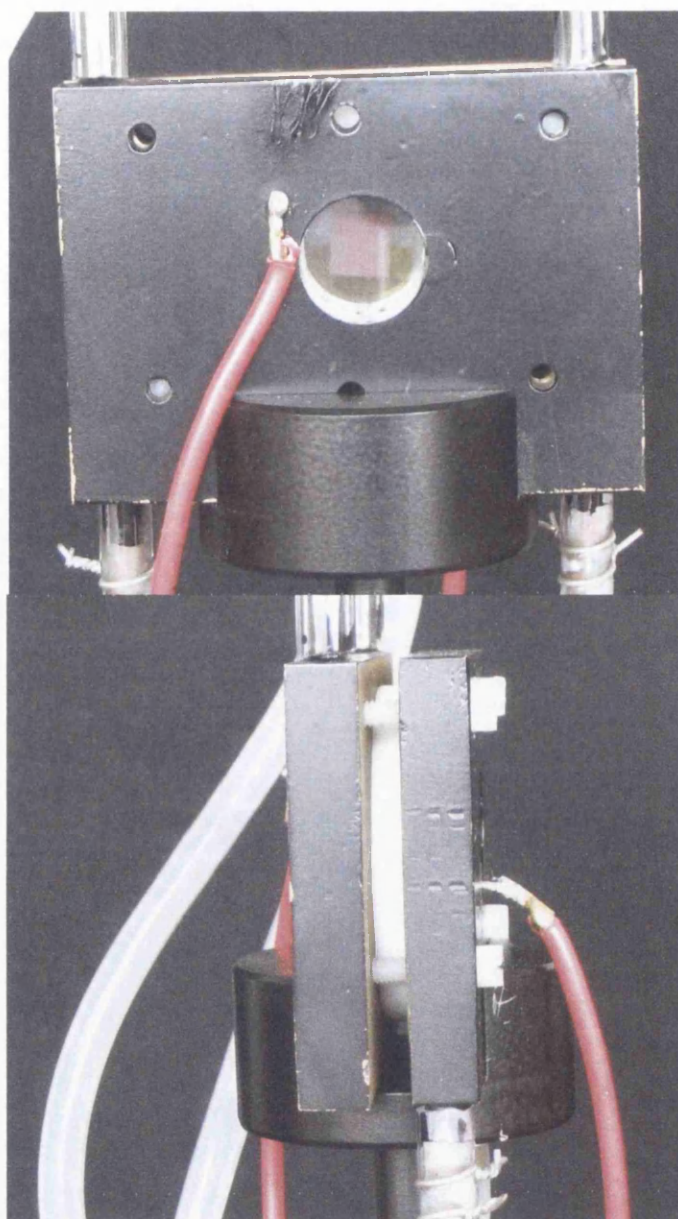


Figure 4-1 The brass sample holder from the front and the side. Each half had an inlet and an outlet which were connected to silicone tubing which supplied the sample holder with water from the temperature control unit. The two brass parts were separated by a Teflon® ring which acted as an insulator to protect the cell from air circulations and maintain temperature which were very close to the ones measured in the water-bath. The two plates were held together by plastic screws in order to prevent short circuiting the cell.

4.2. Results and Discussion

4.2.1. Variation in I-V curves with temperature for cells using different dyes and Solaronix HT paste

For this experiment, the well known N3 dye was employed alongside two novel squaraine dyes which had been synthesised in our laboratories in Swansea by Victoria Hughes, the structures of which have been given earlier (see section 2.1.8). The semiconductor substrate for these cells was Solaronix TiO₂ HT-Paste with a particle size of 9 nm. Either one or two layers of Scotch Magic tape[®] were used as a template to control the thickness of the TiO₂ layer, and the additional TiCl₄ treatment, described in [1], was applied. The electrolytes used were either EL2 (0.5 M LiI/0.05 M I₂ in an 80:20 (v/v) mixture of acetonitrile and 3-methyl-2-oxazolidinone (NMO)) or EL3 (1.0 M LiI/0.1 M I₂ in 60 % acetonitrile, 20 % 3-methyl-2-oxazolidinone and 20 % t-butyl-pyridine).

4.2.1.1 . N3

Solar cells with N3 adsorbed on of two thicknesses of Solaronix[®] HT TiO₂ sol were prepared as described in Chapter 2.

Figures 4-1 and 4-2 show the temperature dependent I-V curves for the cells made using electrolytes EL2 and EL3 respectively, and Figures 4-3, 4-4 and 4-5 give plots of the temperature variation of key parameters for three cells. The first two cells shown (Figures 4-2 and 4-3), were prepared with one layer of tape as template for the semiconductor thickness and the third was made using two layers of tape. Hence, the current of the third one is almost twice as high as the current of the two others. An even thicker semiconductor layer will lead to a worse performance curve though;

since it will lead to a worse fill factor of the cell, probably caused by a limited charge carrier transport of the redox couple within the semiconductor layer (see section 3.3.1.4).

Table 4-1 gives the cell characteristics of a cell built using N3, EL 2, 1 layer of Scotch Magic tape as a template for Solaronix HT paste and the TiCl_4 hydrolysis finishing step (see section 2.1). Electrolyte EL 2 does not contain any t-butylpyridine, and the working electrodes were not dipped in t-butylpyridine either after the dye adsorption. Therefore these cells have been built by only applying one of the two possible finishing steps (4-tert-butylpyridine dip and TiCl_4 hydrolysis). The role of the 4-tert-butylpyridine according to Nazeeruddin is to decrease the rate of triiodide reduction at the working electrode and with it to increase the cell voltage [1]. That means, the cells varied in the thickness of the semiconductor film, the type of sensitizer adsorbed on it, the type of electrolyte used, and whether or not finishing steps (one or two) were applied to improve the cell performance.

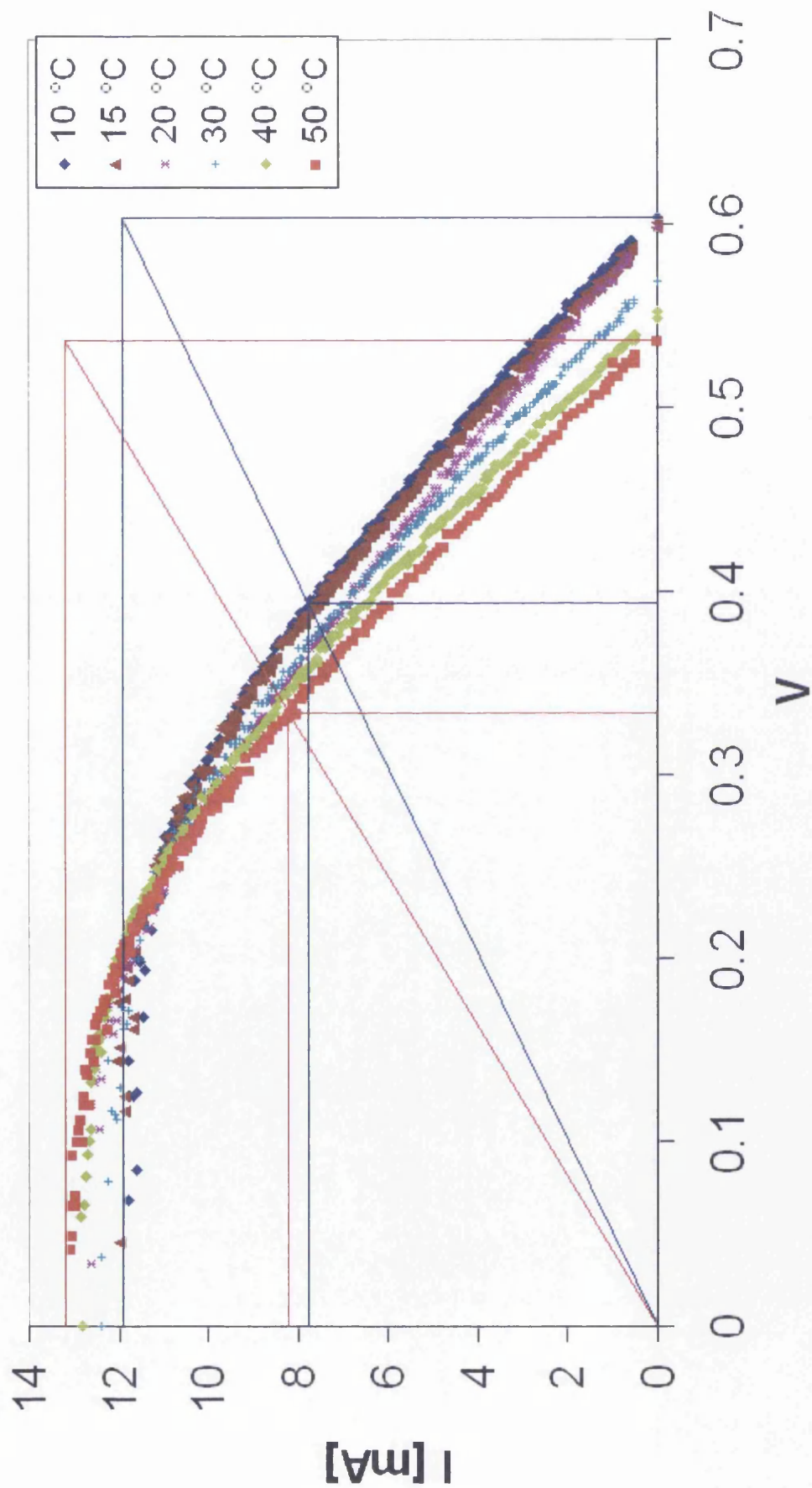


Figure 4-2 I-V curves of cells built with N3 dye, EL2, one layer of Solaronix Sol HT with further $TiCl_4$ treatment with changing temperature and 1 Sun irradiation intensity.

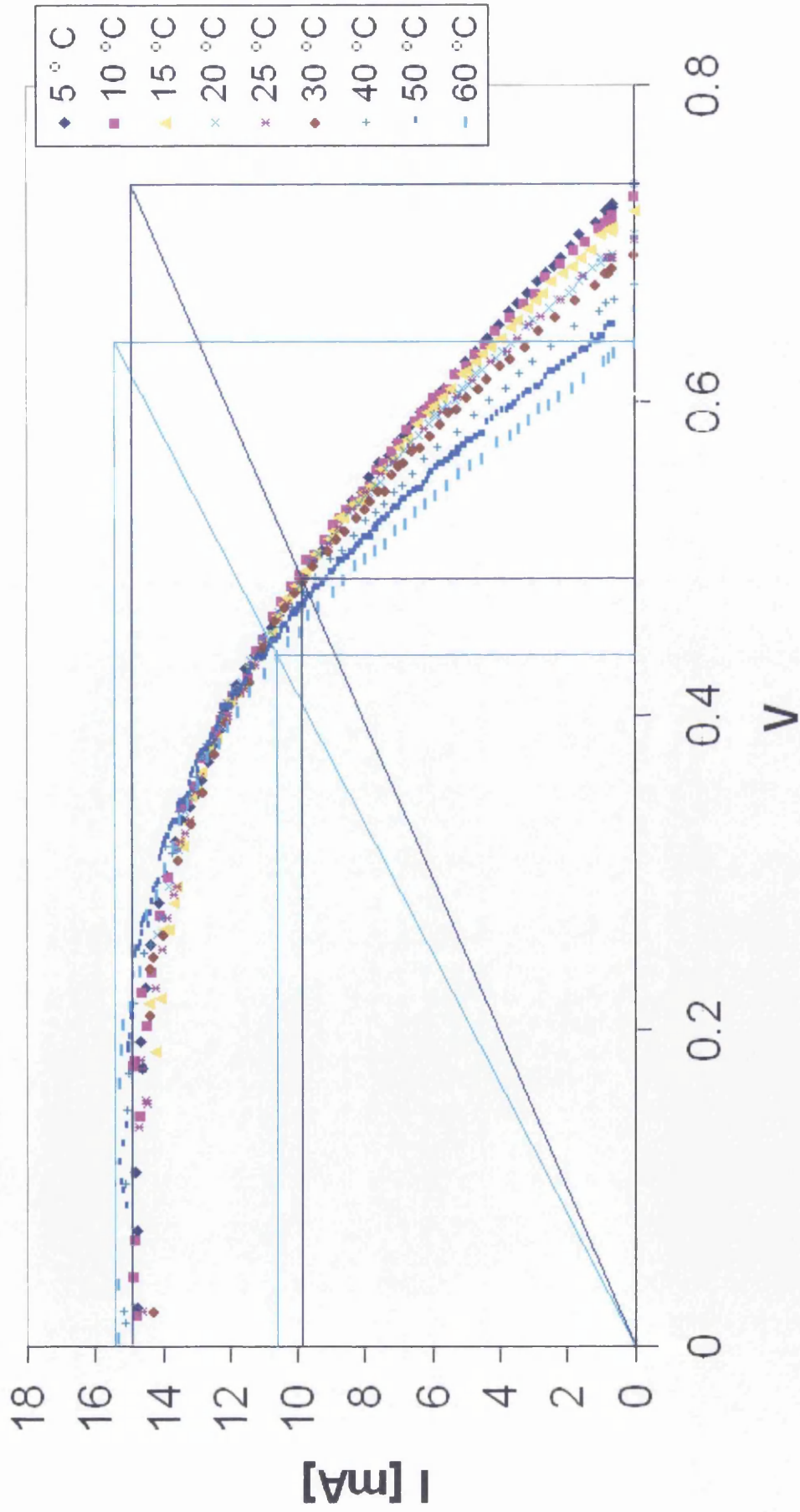


Figure 4-3 I-V curves of cells built with N3 dye, EL3, one layer of Solaronix Sol HT with further TiCl₄ treatment with changing temperature and 1 Sun irradiation intensity.

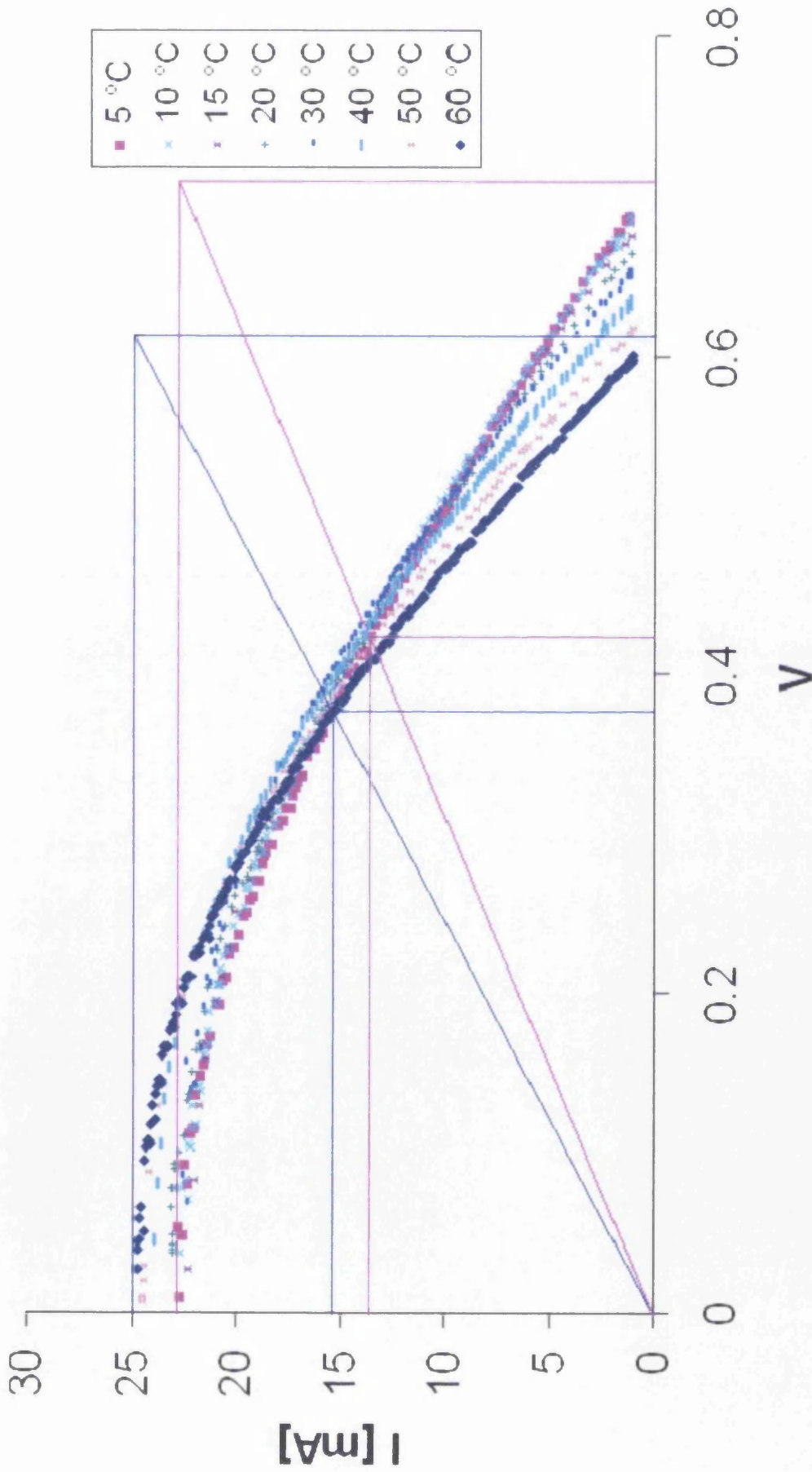


Figure 4-4 I-V curves of cells built with N3 dye, EL3, two layers of Solaronix Sol HT with further TiCl_4 treatment with changing temperature and irradiation intensity 1 Sun.

Cell N3 EL2 1L Sol HT TiCl ₄						
T [°C]	Voc [V]	Isc [mA]	Pmax [mW]	Vmax [V]	Imax [mA]	ff
10	0.602	11.81	3.03	0.393	7.70	0.43
15	0.600	11.96	3.00	0.387	7.74	0.42
20	0.596	12.41	2.83	0.367	7.70	0.38
30	0.567	12.22	2.87	0.364	7.89	0.41
40	0.558	12.78	2.79	0.346	8.07	0.39
50	0.535	13.07	2.71	0.333	8.15	0.39
±0.5	±0.002	±0.01	±0.02	±0.002	±0.01	±0.01

Table 4-1 Photoelectric characteristics of cells built with N3 dye, EL2, one layer of Solaronix Sol HT and TiCl₄ finishing step, with changing temperature at 1 Sun irradiation intensity.

The following 3 diagrams graphs display the open circuit voltage, the short circuit current and the maximum power output shown in Table 4-1.

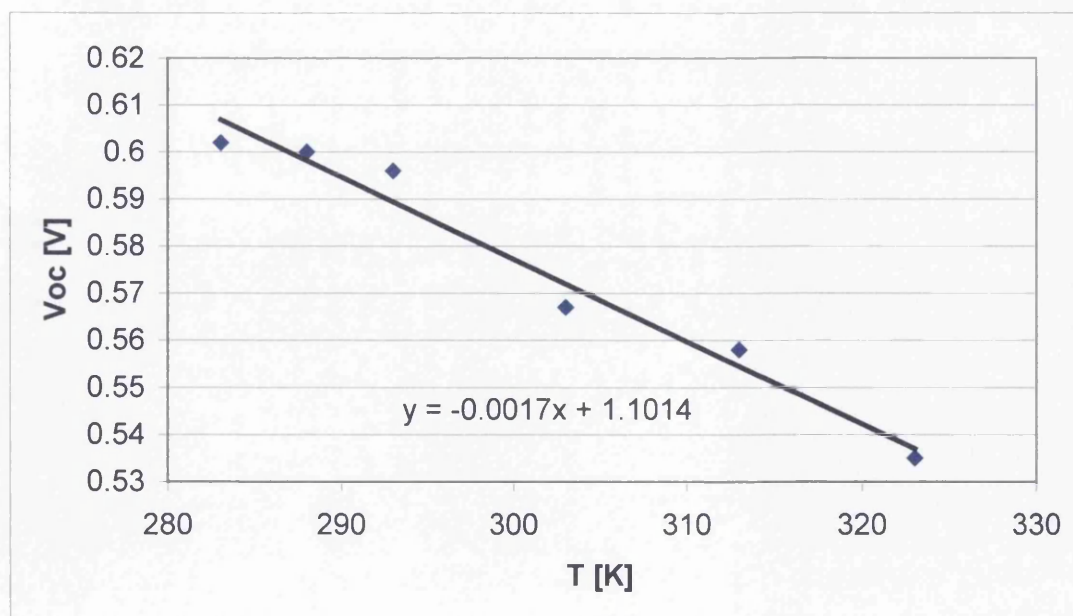


Figure 4-5 Cell voltage against temperature. Cell built with N3 dye, EL2, one layer of Solaronix Sol HT and TiCl₄ finishing step, measured at 1 Sun.

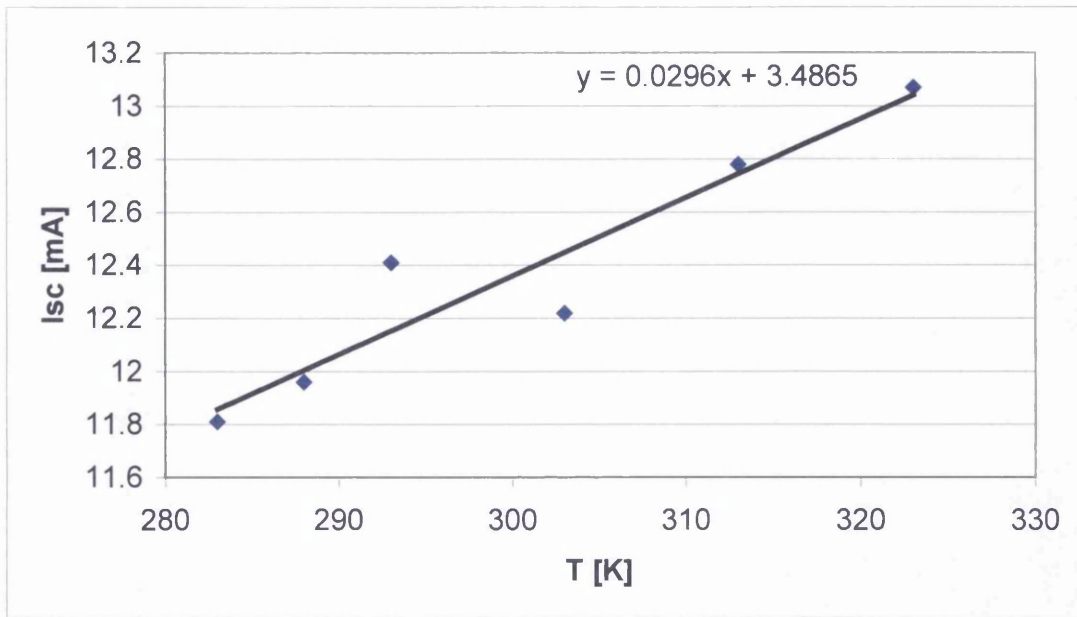


Figure 4-6 Cell current against temperature. Cell built with N3 dye, EL2, one layer of Solaronix Sol HT and $TiCl_4$ finishing step, measured at 1 Sun.

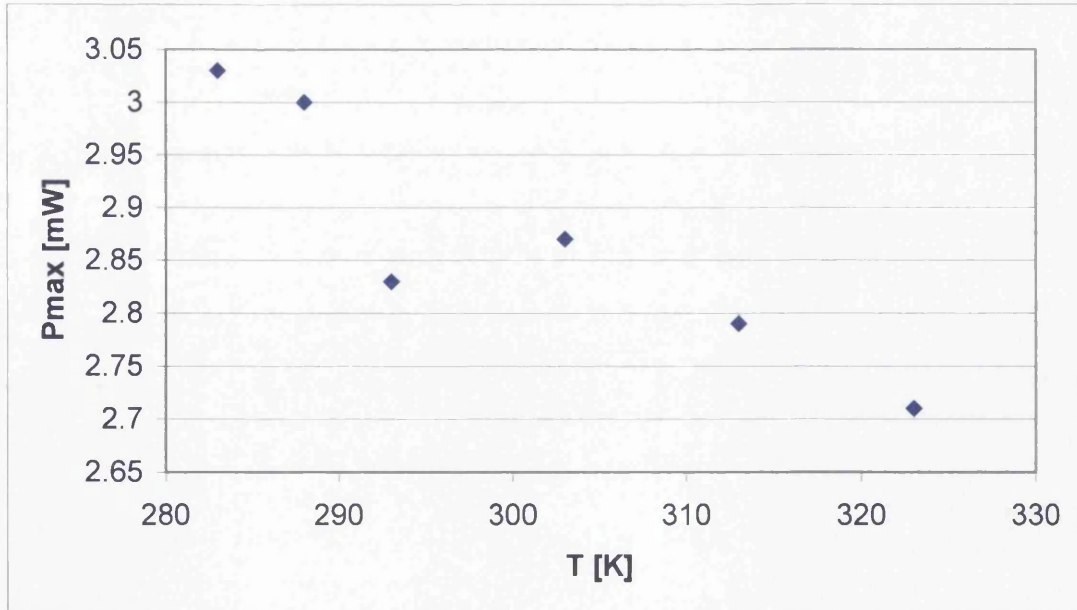


Figure 4-7 Cell power against temperature. Cell built with N3 dye, EL2, one layer of Solaronix Sol HT and $TiCl_4$ finishing step, measured at 1 Sun.

As can be observed from the Figures above, there is the general trend that the performance decreases with increasing temperature despite an increase in cell current. The form of the curve does not imply that this trend would stop soon below 0 °C (i.e. there is no flattening of the curve towards the lower end of the measurement range). The cell voltage has a maximum dependent on the semiconductor, electrolyte, dye coupling, but the cell current seems to increase still. The maximum current which can be drawn could be dependent on the amount of dye available for excitation and is limited by the charge transport rate through the electrical circuit (including all interfacial charge exchanges and the transport through the electrolyte). It suggests that with the right cooling agent, the cell performance would still increase below 0 °C. The changes for voltage as well as current are between 5 and 15 % over the temperature range of 60 K depending on the system.

The data shown in Table 4-2 was derived from a series of measurements using the same cell built using a different electrolyte, EL 3. Because this electrolyte contains a higher concentration of the redox couple, higher currents were achieved than with EL2.

Cell N3 EL3 1L Sol HT TiCl ₄ with T						
T [°C]	Voc [V]	Isc [mA]	Pmax [mW]	Vmax [V]	I _{max} [mW]	ff
5	0.733	14.68	4.68	0.482	9.71	0.43
10	0.725	14.63	4.77	0.487	9.80	0.45
15	0.717	14.44	4.72	0.484	9.75	0.46
20	0.7	14.78	4.75	0.475	10.00	0.46
25	0.698	14.59	4.74	0.476	9.95	0.47
30	0.687	14.24	4.72	0.477	9.90	0.48
40	0.671	14.93	4.71	0.46	10.24	0.47
50	0.654	15.08	4.66	0.455	10.24	0.47
60	0.634	15.17	4.55	0.436	10.44	0.47
±0.5	±0.002	±0.01	±0.02	±0.002	±0.01	±0.01

Table 4-2 Photoelectric characteristics of a cell built with N3 dye, EL3, one layer of Solaronix Sol HT, TiCl₄ after treatment, with changing temperature at 1 Sun.

The following 3 diagrams graphically display the open circuit voltage; the short circuit current and the maximum power output for a cell built with N3, EL3 and 1 layer of Scotch magic tape (see Table 4-2).

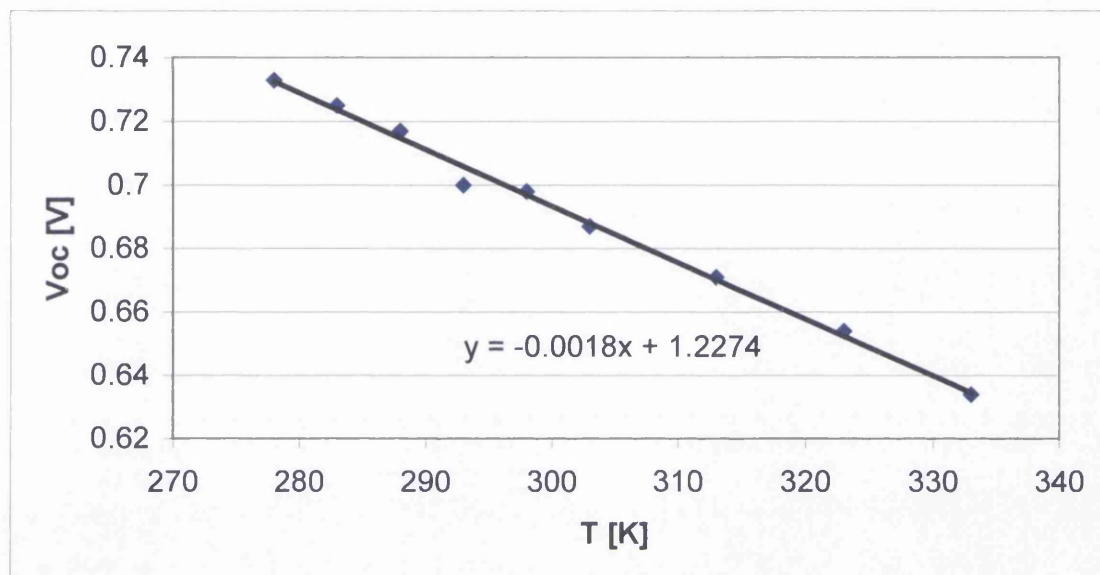


Figure 4-8 Cell voltage against temperature. Cell built with N3 dye, EL3, one layer of Solaronix Sol HT, TiCl_4 after treatment, measured at 1 Sun.

The graphs displayed for this system using the EL3 electrolyte show a similar behaviour as seen before. The system seemed to change dramatically if the thickness of the semiconductor was changed to two layers of Scotch Magic tape as a template (Figure 4-4). Then, the voltage (V_{OC}) and current (I_{SC}) changes behave very similarly to the cells built using 1 layer with changing temperature. The overall cell performance (at maximum power point) clearly showed a maximum in the same area as was predicted by Nazeeruddin [1]. This can be explained by a worse fill factor caused by the “hindered” exchange of redox species within the thicker semiconductor layer.

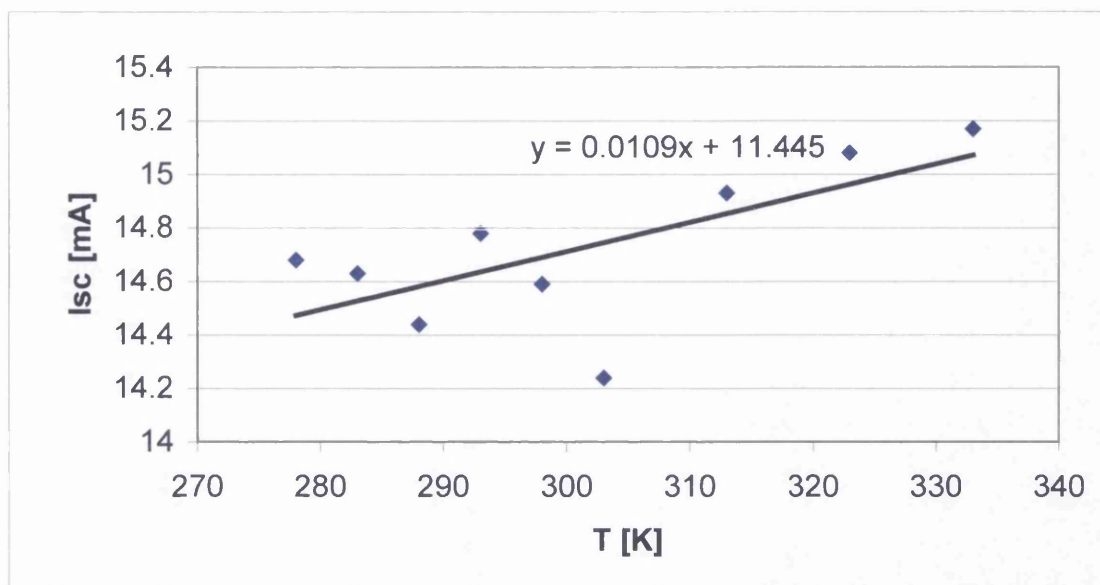


Figure 4-9 Cell current against temperature. Cell built with N3 dye, EL3, one layer of Solaronix Sol HT, $TiCl_4$ after treatment, measured at 1 Sun.

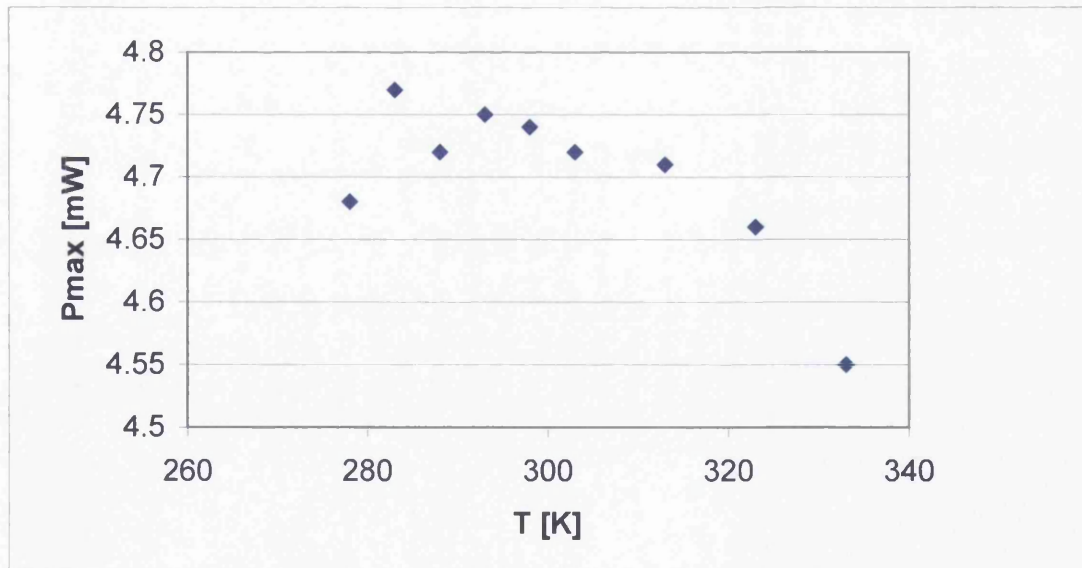


Figure 4-10 Cell power against temperature. Cell built with N3 dye, EL3, one layer of Solaronix Sol HT, $TiCl_4$ after treatment, measured at 1 Sun.

The next set of data displays the results gained from a cell with a thicker semiconductor film (2 layers of Scotch Magic tape as template for the squeegee printing procedure).

Cell N3 EL3 2L Sol HT TiCl ₄ parameters with T						
T [K]	Voc [V]	Isc [mA]	Pmax [mW]	Vmax [V]	Imax [mA]	ff
5	0.71	22.9	5.71	0.42	13.6	0.35
10	0.7	22.8	5.89	0.43	13.7	0.37
15	0.69	22.65	5.98	0.43	13.9	0.38
20	0.68	23.28	5.86	0.41	14.3	0.37
30	0.67	22.81	6.21	0.43	14.45	0.41
40	0.65	24.2	6.18	0.41	15.08	0.39
50	0.63	24.5	5.94	0.39	15.23	0.38
60	0.61	24.7	5.85	0.37	15.8	0.39
±0.5	±0.002	±0.01	±0.02	±0.002	±0.01	±0.01

Table 4-3 Photoelectric characteristics of cells built with N3 dye, EL3, two layers of Solaronix Sol HT with TiCl₄ treatment, with changing temperature at irradiation intensity 1 Sun.

The following 3 graphs display the open circuit voltage, the short circuit current and the maximum power output shown in Table 4-3.

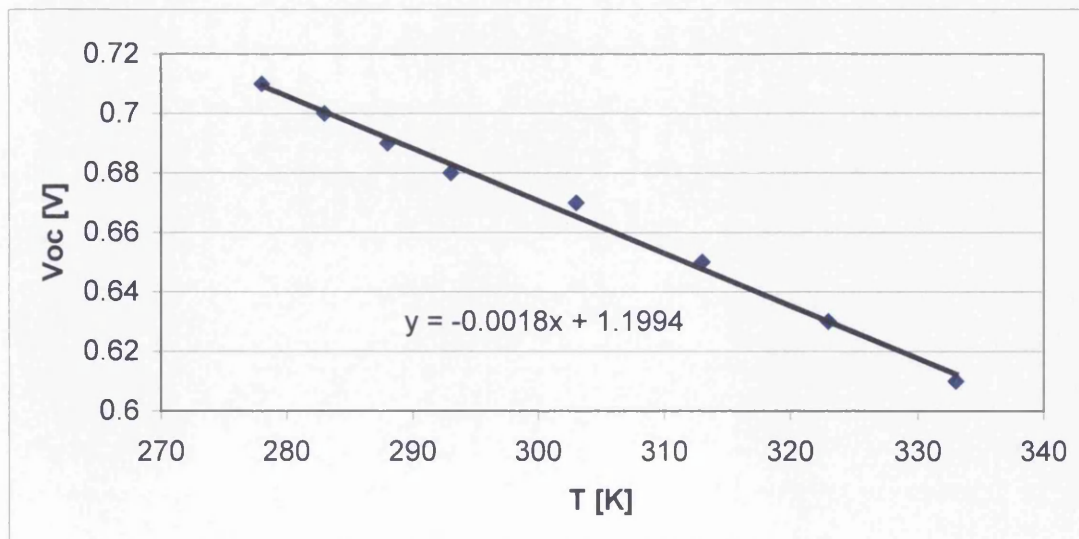


Figure 4-11 Cell voltage against temperature. Cells built with N3 dye, EL3, two layers of Solaronix Sol HT with TiCl₄ treatment, measured at 1 Sun.

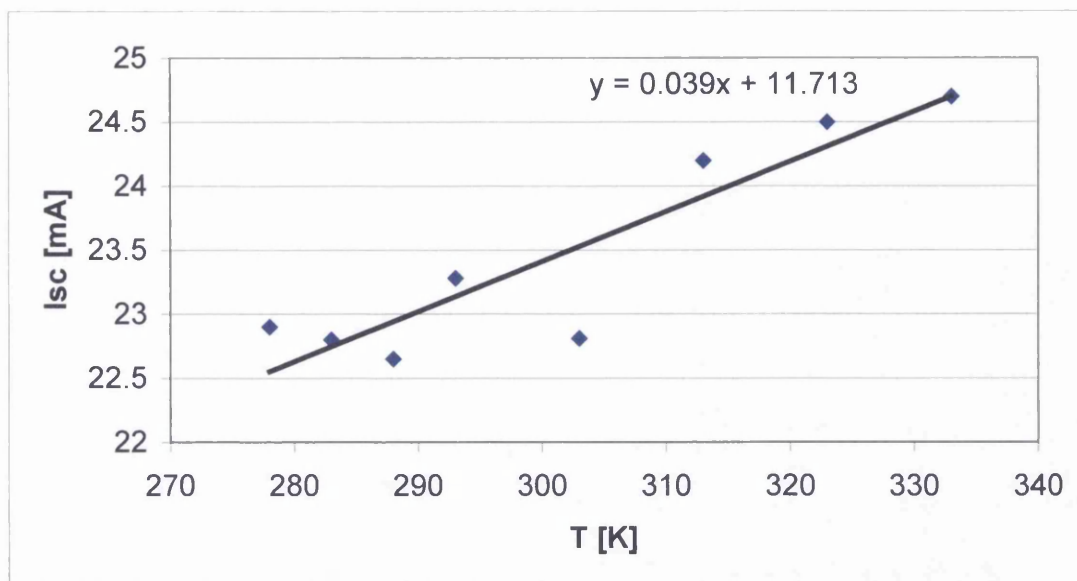


Figure 4-12 Cell current against temperature. Cells built with N3 dye, EL3, two layers of Solaronix Sol HT with TiCl_4 treatment, measured at 1 Sun.

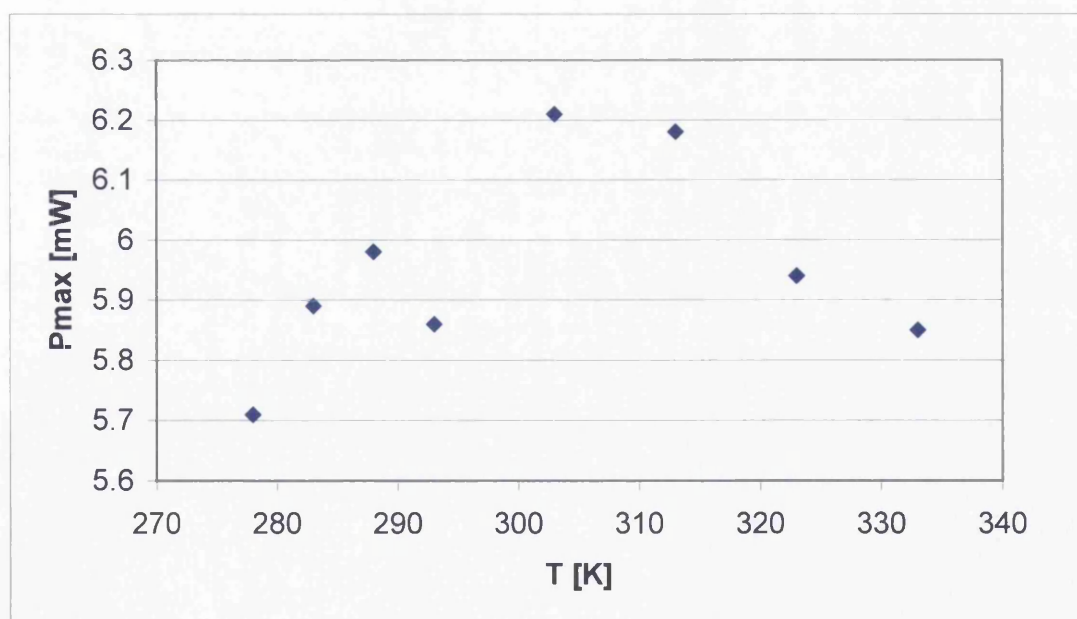


Figure 4-13 Cell power against temperature. Cells built with N3 dye, EL3, two layers of Solaronix Sol HT with TiCl_4 treatment, measured at 1 Sun.

As Figures 4-5 to 4-13 show there is, for all three cells, an increase in current and decrease in voltage as the temperature is increased. This is very much in concordance with the results reported by Nazeeruddin in 1993 [1]. Their paper also reports a linear behaviour for the cell voltages whereas they found cell currents to be much less predictable. The power output characteristics in [1] are very similar to the ones shown in Figures 4-10 and 4-13, with a maximum power output around 40 °C.

A general observation is the direct proportionality between temperature and I_{SC} whereas the V_{OC} decreased with temperature.

4.2.1.2. SQU1

The squaraine cells were built using the same methods as used for the N3 cells. The dye was adsorbed onto the TiO_2 from an ethanolic solution with a concentration of approximately 3×10^{-4} M under constant stirring for 24 hours. The dyed TiO_2 slides were green to blue in colour. The dyes are not very photostable when adsorbed on TiO_2 with the colour fading very quickly, especially for SQU2, if the slides are exposed to sunlight and air. The cells built with SQU1 were stable for several days once the cell was filled with electrolyte and sealed.

Cells measured at lower temperatures displayed better efficiencies than cells illuminated under high temperatures (this is valid for cells built with one layer of Scotch Magic tape). The fill factors stayed reasonably constant although the voltage decreased with temperature. The increase in cell current with higher temperatures partially makes up for that loss. This might be a characteristic of the whole cell rather than of the dye itself. In semiconductors, the position of the Fermi level lies within the band gap. This means that at 0 K there are no free conduction electrons and the

resistance is infinite. The resistance of a non doped semiconductor will decrease exponentially with increasing temperature, as the charge carrier density in the conduction band increases. Another observation which can be made when comparing the N3 and SQU1 data is that the fill factors for the squaraine dye are much better than for the N3 and for the cells built with squaraine dye the voltage as well as the current had their maxima at lower temperatures (1 °C) in contrast to the N3 dye cells which had reduced currents, and increased voltages at low temperatures. The squaraine cells did not reach the power output of the ruthenium dye but showed potential. Especially since some of the characteristics looked promising to lead to a competitive light harvester for photovoltaic applications if the efficiency could be increased. During this project, squaraine cells were built which had power outputs comparable (approximately half) that of cells built with N3 but the squaraine dyes are much less stable than N3. If they could be made stable then it is possible they could become effective competitors for the expensive ruthenium based dyes, especially in combination with other dyes which absorb in a different part of the spectrum.

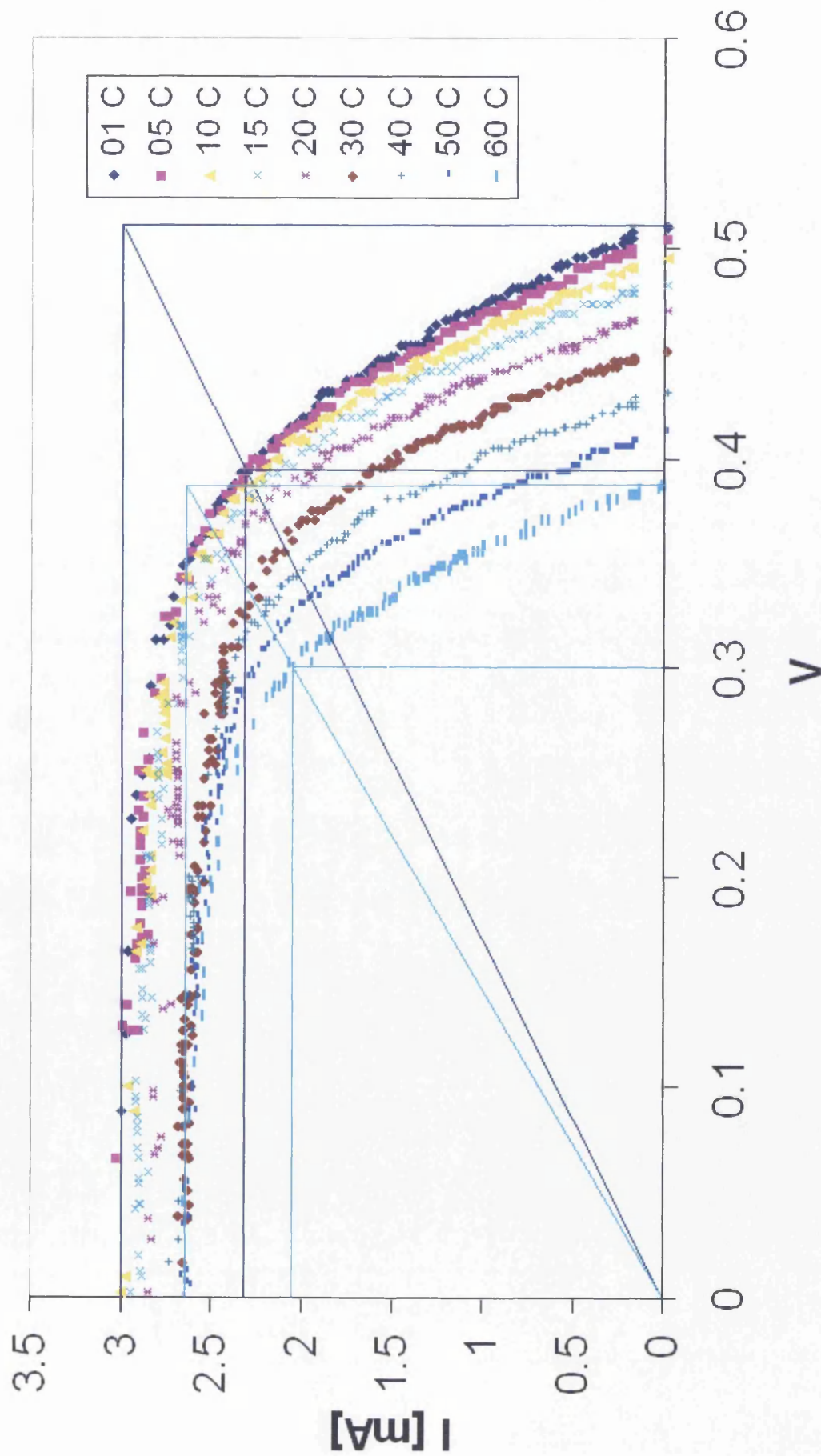


Figure 4-14 I-V curves of cells built with SQU1 dye, EL2, one layer of Solaronix Sol HT with further TiCl₄ treatment with changing temperature and irradiation intensity 1 Sun.

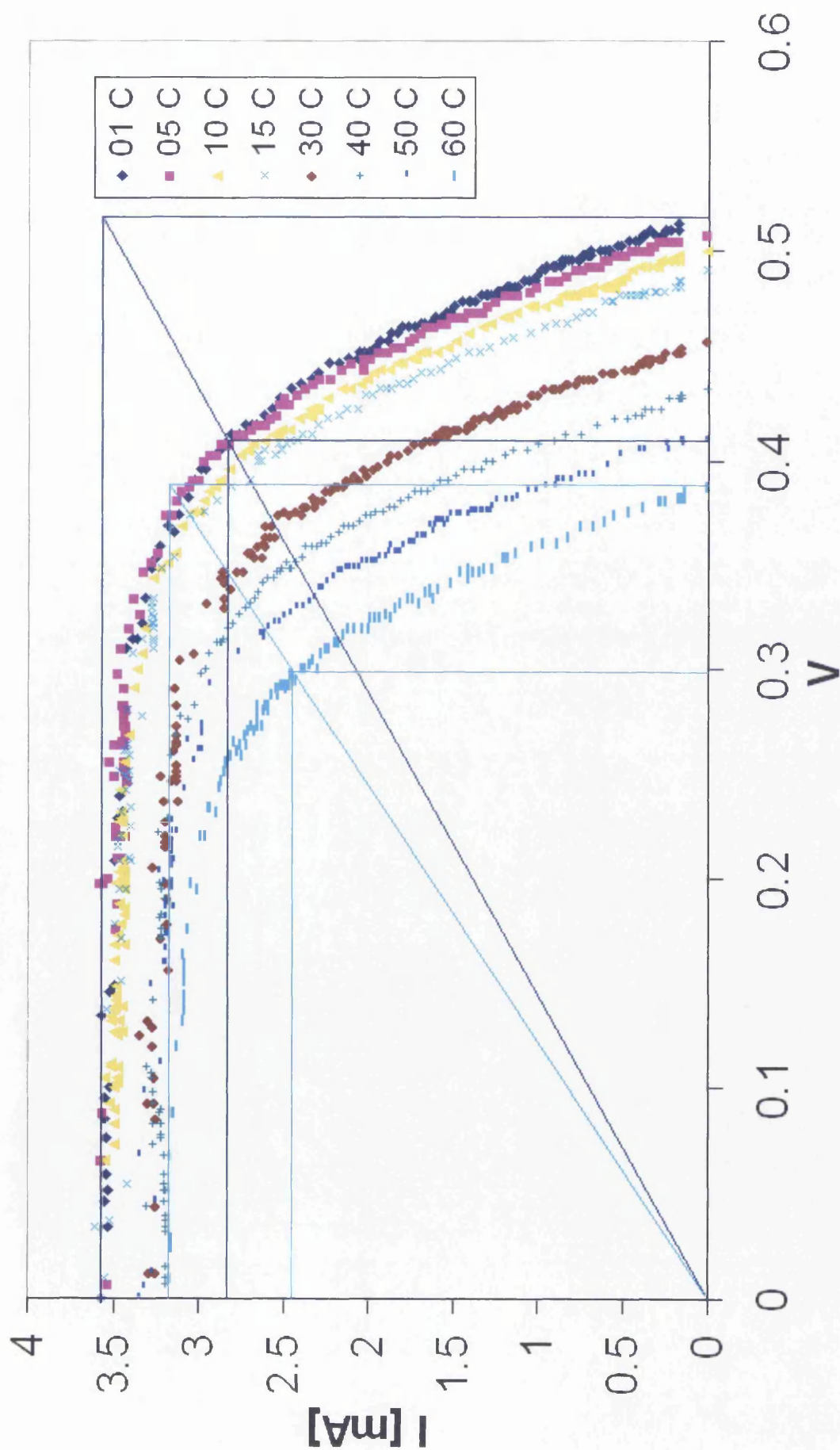


Figure 4-15 I-V curves of cells built with SQU1 dye, EL2, two layers of Solaronix Sol HT with further TiCl_4 treatment with changing temperature and irradiation intensity 1 Sun.

Characteristics SQU1 2L EL2 with T						
T	Voc	Isc	Pmax	Vmax	I_{max}	ff
1	0.509	3.00	0.91	0.393	2.32	0.60
5	0.503	2.97	0.91	0.394	2.32	0.61
10	0.488	2.95	0.89	0.387	2.29	0.62
15	0.481	2.92	0.88	0.380	2.30	0.62
20	0.469	2.84	0.84	0.373	2.27	0.63
30	0.449	2.70	0.76	0.355	2.13	0.62
40	0.429	2.69	0.72	0.338	2.12	0.62
50	0.413	2.67	0.68	0.322	2.10	0.61
60	0.386	2.65	0.61	0.299	2.05	0.60

Table 4-4 I-V curves of cells built with SQU1 dye, EL2, two layers of Solaronix Sol HT, and with TiCl₄ treatment, with changing temperature, at irradiation intensity 1 Sun.

Characteristics SQU1 1L EL2 with T						
T	Voc	Isc	Pmax	Vmax	I_{max}	ff
1	0.514	3.57	1.16	0.408	2.83	0.63
5	0.506	3.57	1.17	0.407	2.87	0.65
10	0.498	3.51	1.12	0.398	2.81	0.64
15	0.489	3.53	1.09	0.389	2.81	0.63
30	0.456	3.32	0.96	0.362	2.64	0.63
40	0.433	3.25	0.89	0.344	2.59	0.63
50	0.411	3.30	0.84	0.323	2.59	0.62
60	0.387	3.18	0.73	0.298	2.44	0.59

Table 4-5 I-V curves of cells built with SQU1 dye, EL2, two layers of Solaronix Sol HT with TiCl₄ treatment with changing temperature, at irradiation intensity 1 Sun.

A combination of two or more organic dyes which cover the whole visible spectrum on the semiconductor might not only harvest the light better but also present a cheaper solution for PV applications compared to ruthenium or other organometallic dyes.

4.2.2. Temperature behaviour of cells built with different binders in the substrate

Additives have already been used by others as binders, and to improve the surface characteristics of TiO₂. Many groups reported the use of PEG (polyethylene glycol) as a binder, and template for their semiconductor substrates [2-4]. Others claim that PEG helps to facilitate the dye adsorption onto the semiconductor substrate [5] or that the high molecular weight of the PEG together with the grain size of the TiO₂ influences the incident photon to current conversion efficiency (IPCE) [6]. However, up until now, the primary determining factors for TiO₂ morphology has been the grain size of the semiconductor nanoparticles and the sintering temperature [4, 7, 8], although some workers have used surfactants (laurylamine hydrochloride) as a templates for the morphology of the semiconductor substrate [9].

In the work presented here dye-sensitised solar cells were made using variations of a standard procedure, including the introduction of new binder materials into the TiO₂ semiconductor films. The effect of these additives, and film thickness, on the degree of cracking of the films was examined and photoelectric measurements of working solar cells were carried out.

The cells were built using the different binders (P03 to P06) as described earlier in the experimental section (Chapter 2). The semiconductor substrate was squeegee printed using 1 and 2 layers of Scotch Magic[®] tape as template for the film thickness.

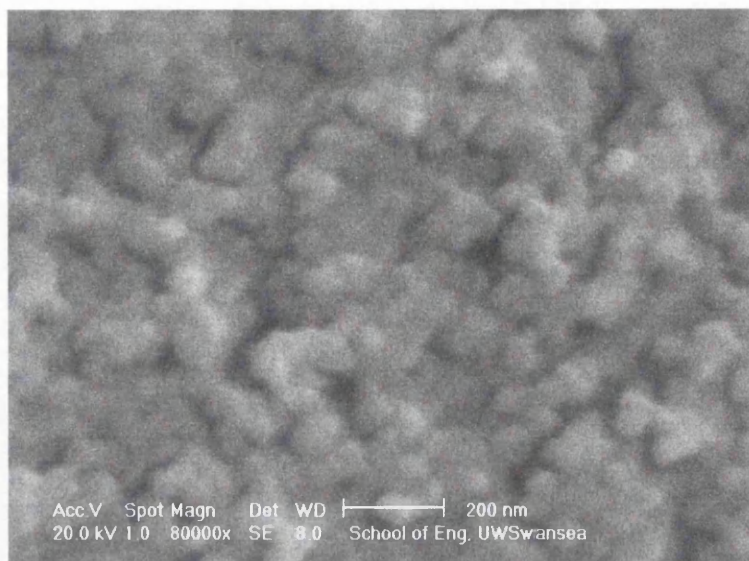


Figure 4-16 SEM image of a surface prepared with P04 (PEO, MW 300,000) under 80,000 fold magnification. Particle sizes below 50 nm can be seen on the surface of the TiO₂ substrate.

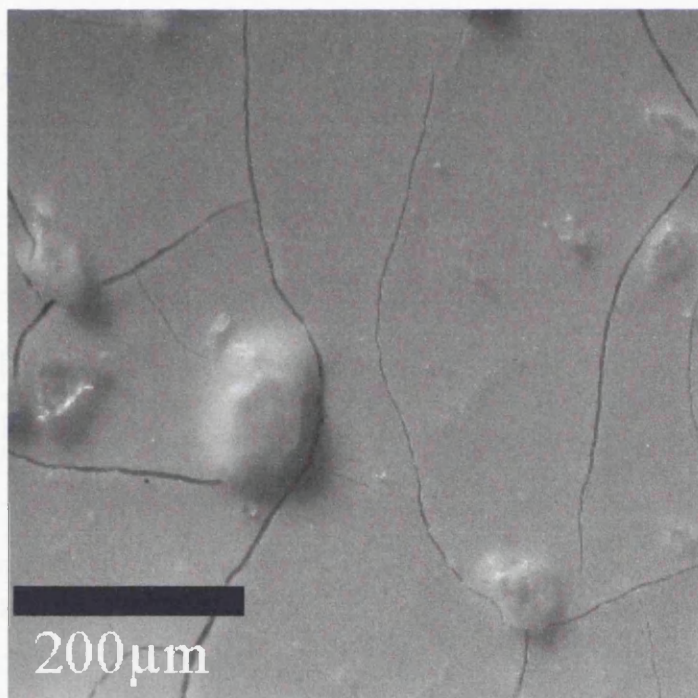


Figure 4-17 The surface of a titania film (binder: ethyl cellulose) which was prepared by using 1 layer of Scotch Magic tape as a template for the film thickness (about 6 μm) after sintering.

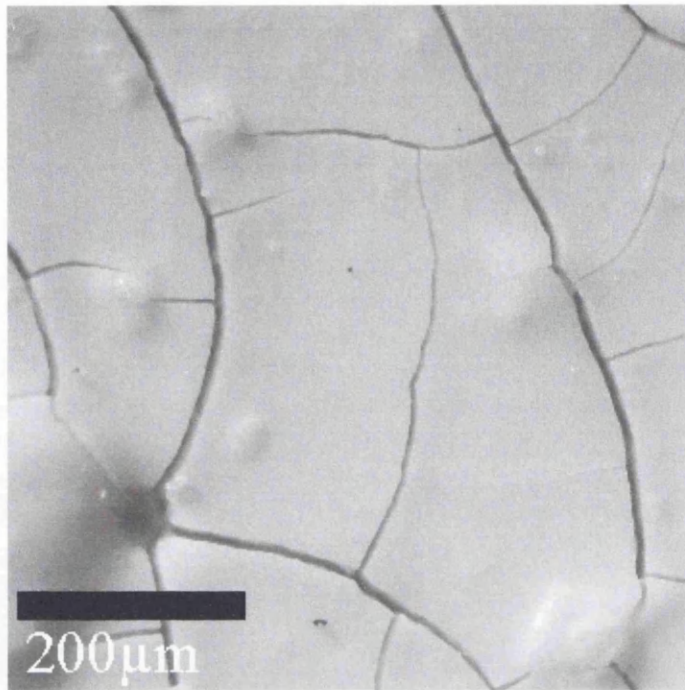


Figure 4-18 The surface of a titania film (binder: ethyl cellulose) prepared using 2 layers of Scotch Magic tape (thickness about 10 μm) after sintering.

4.2.3. Effect of binder on surface structure

The use of different additives did not lead to an observable difference in surface morphology on the nanostructure scale at the concentrations used (see Figure 4-16), however, as Figures 4-17 and 4-18 show, additives did lower the degree of cracking of the film. The main parameters which influenced the cracks in the film were the film thickness and the speed of the drying process. The cracking occurs during drying in air at room temperature which seems to cause stress within the thin films and leads to the generation of cracks if not prevented by a high concentration of binder (up to 50 %) [10]. In Figures 4-17 and 4-18 it can be seen that the cracks in the thicker film are wider and greater in number than in the thinner film. The degree of cracking was also dependent on the time taken for drying. The substrates were dried in air for about 2 hours but this may still be too fast. Although not examined here, the effect of drying under controlled humidity and temperature conditions may be worth studying. During the time of these PhD studies it was reported that higher concentrations of binder can both improve the cracking and also make it possible to control the pore size of the substrate [11].

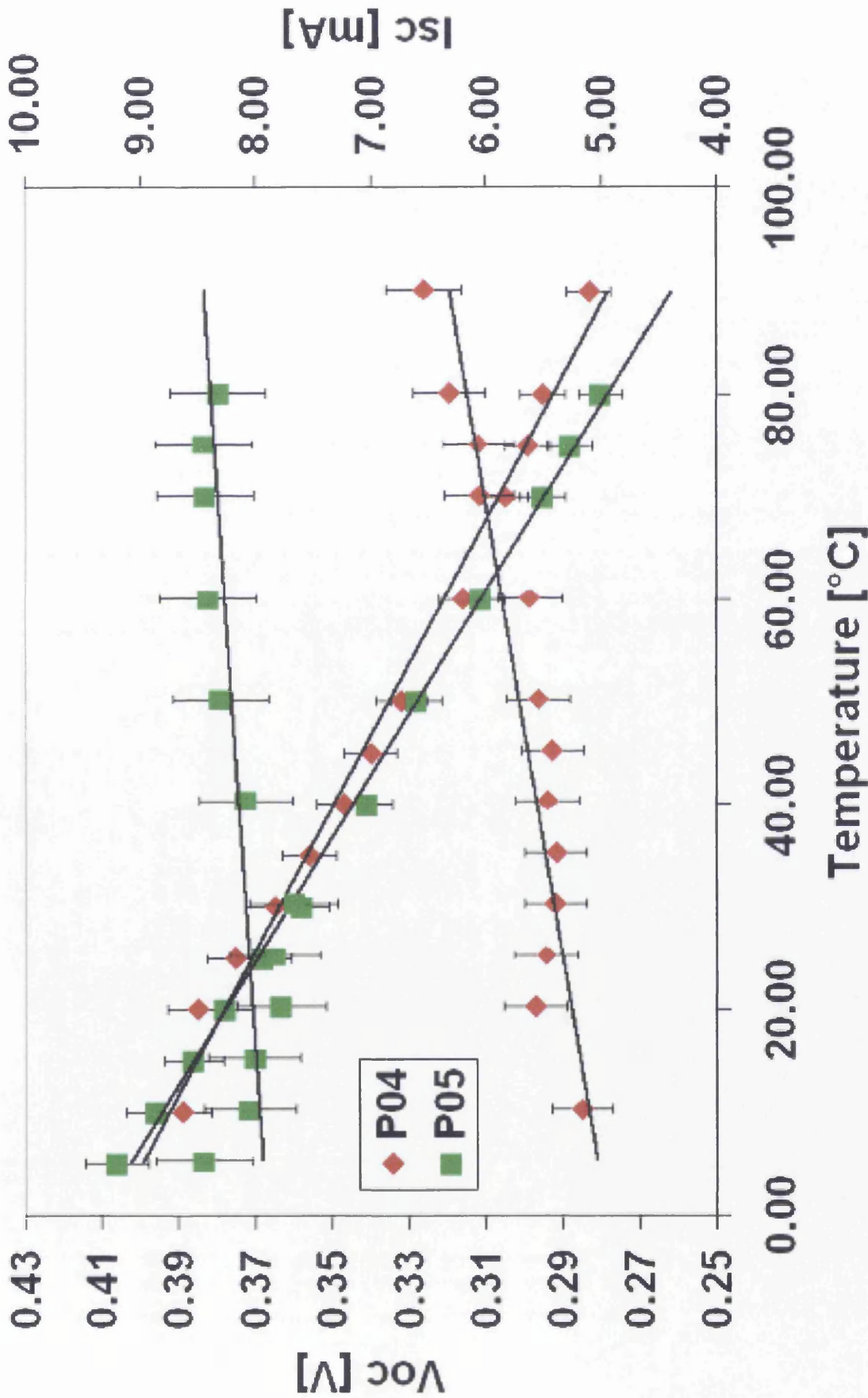


Figure 4-19 Effect of temperature I_{sc} and V_{oc} . Current increases with rising temperature, whereas the voltage decreases. Voltage $\pm 2\%$ error (voltage scale left); Current $\pm 5\%$ error (current scale right).

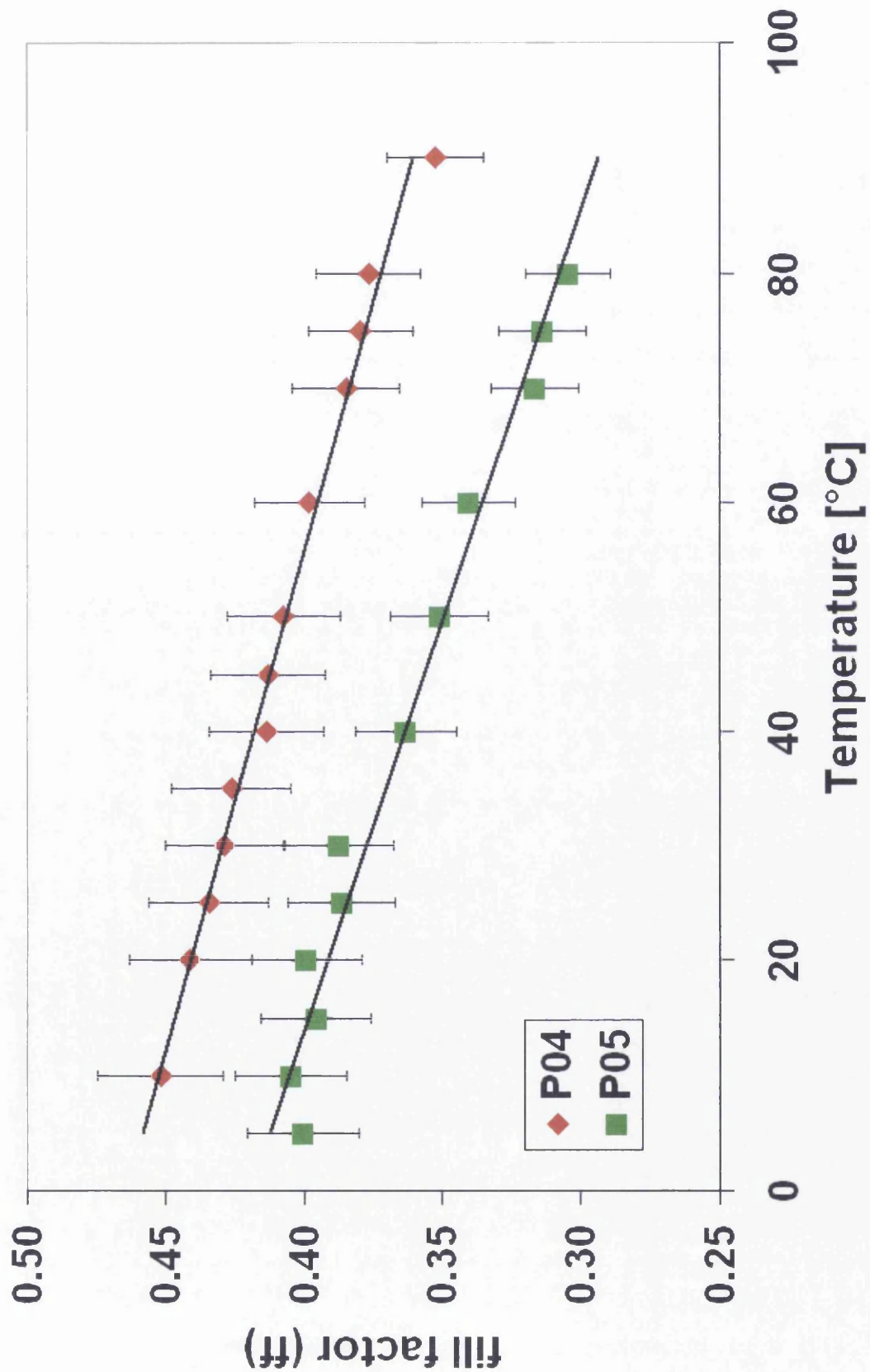


Figure 4-20 Influence of temperature on fill factor, showing the linear decrease in the fill factor of cells made up with both sols P04 and P05 with increasing temperature. The error bars represent $\pm 5\%$ error.

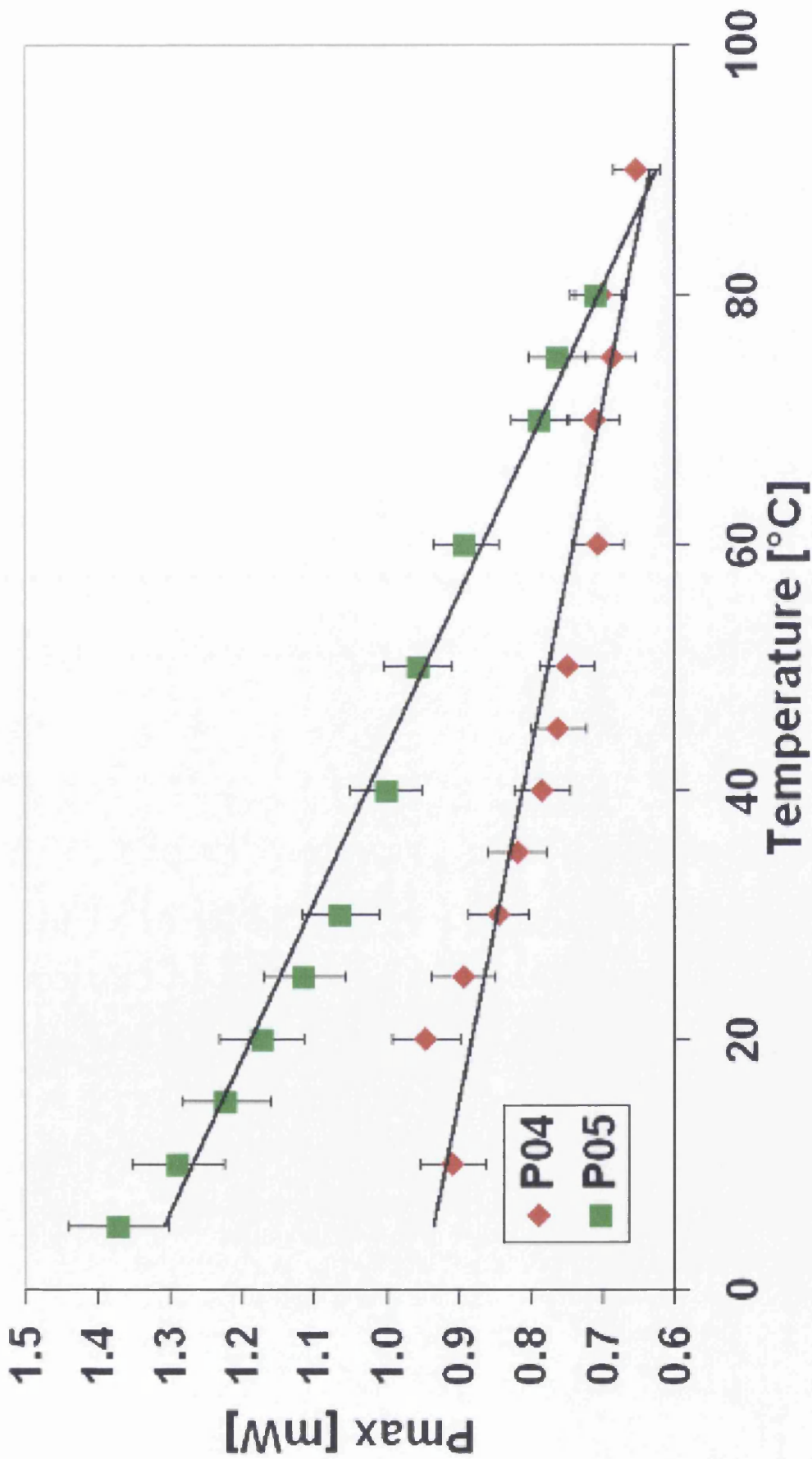


Figure 4-21 Maximum power of two cells made with different sols over temperature. The error bars represent $\pm 5\%$ error.

4.2.4. Temperature dependence of cell performance

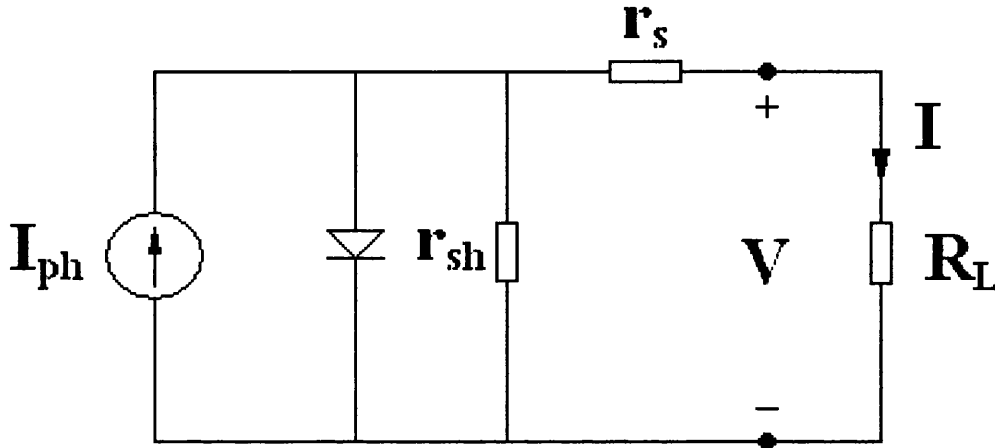


Figure 4-22 The equivalent circuit of a solar cell.

Figure 4-22 shows the simplest electronic model for the circuit of these solar cells

The general equation for the current in a solar cell is given in Equation 4-1 [12].

$$I = I_{ph} - I_0 \left[\exp\left(\frac{q(V + Ir_s)}{nkT}\right) - 1 \right] - \frac{V + Ir_s}{r_{sh}} \quad \text{(Equation 4-1)}$$

I is the measured cell voltage, I_{ph} the photogenerated current within the cell, I_0 the diode dark current, V relates to the measured voltage, r_s is the series resistance and r_{sh} the shunt resistance, k the Boltzmann constant and T the temperature. From this equation, it can be shown that with increasing temperature the current will show a slight increase which is balanced by the increase of the Ir_s term in the exponential part of the equation and therefore is not significant. The current flowing through the semiconductor series resistance will increase as the resistance decreases with

temperature, a characteristic of semiconductors. A much bigger influence of temperature is the effect on the voltage under the assumption that the series and shunt resistances stay constant throughout the temperature change. This equation does not take into account that both, I_0 , the saturation current, and n , the diode ideality factor, are not constant over the whole I-V range (constant I_0 and n would lead to a straight I-V plot). All but one of these terms in the equation are only influenced by the dye, redox couple and semiconductor coupling. The exception is the series resistance which is the sum of the semiconductor resistances, the resistance arising at the contacts and all the resistances from the interfaces within the cell as well as mass and charge transport properties of the whole system. These are the key points which would have to be improved in order to improve the efficiency of a specific cell system since a better dye-electrolyte-semiconductor coupling has not been found for the Grätzel cell up to this date.

When the temperature was raised, the short circuit current (I_{SC}) increased and the open circuit voltage decreased. This led to an overall decrease in cell output (P_{max}) and with it, efficiency. This is underlined further by the fact that the vertical slope of the I-V curve stays very much the same over a wide range of temperature (Figure 4-2). The absolute power of the cell decreased with increasing temperature in contrast to the reported maximum cell efficiency at 40 °C. According to Nazeeruddin *et al.*, V_{OC} decreases due to an increase in charge recombination rate (rate of triiodide reduction) at the working electrode with higher temperature and an increased dark current in the cell [1]. It seems as if changes in I_{SC} and V_{OC} with temperature are very much determined by the nature of the electrolyte, the I/I_3^- concentration and its viscosity (see Equation 4-2). For our system, the trends are the same as observed

previously [1], but we found less of an increase in the current which could be due to charge carrier transport limitations at the counter electrode. Equation 4-2 below gives the open circuit voltage whereas n_{cb} stands for the number of charge carriers in the conduction band and k_{et} is the rate for triiodide reduction by electrons from the conduction band [12].

$$V_{OC} = \left(\frac{kT}{q} \right) \ln \left(\frac{I_{ph}}{n_{cb} k_{et} [I_3^-]} \right) \quad \text{(Equation 4-2)}$$

This equation was derived from

$$V_{OC} = \left(\frac{kT}{q} \right) \ln \left(\frac{I_{ph}}{I_0} \right) \quad \text{(Equation 4-3)}$$

where

$$I_0 = n_{cb} k_{et} [I_3^-] \quad \text{(Equation 4-4)}$$

There is no current flowing in an open electric circuit, so the I_{ph} would have to be determined experimentally first, but those equations are a good approximation when determining solar cell parameters.

In the case of our cells, the fill factor decreased with increasing temperature (see Figure 4-9) which probably can be related to the relatively low concentration of the redox couple and the low viscosity of the electrolyte medium. For electrolyte media with a high viscosity, the fill factor has been shown to increase with temperature,

possibly due to a decrease in viscosity of the electrolyte and enhanced charge carrier mobility with increasing temperature.

4.3. Conclusion

Although ruthenium bipyridine dyes are still the best reported sensitiser dyes for photovoltaic applications [13], our squaraine cells may be able to compete with them if their stability can be improved.

All the cells whether they were built using N3 or SQU dyes showed an increase in performance with decreasing temperature. For our N3 systems this does not always agree with an already reported performance maximum at 40 °C. The reason for this could be found in the use of different electrolytes or in very special characteristics of each system.

It has been shown that varying layer thicknesses influence the surface morphology of the semiconductor film in a dye-sensitised solar cell. The use of different binders for the sols influences the surface homogeneity rather than the surface morphology itself. In consequence there are only slight variations in the performance of the cells with different binders, compared to variations caused by the electrolyte, or the semiconductor thickness. A higher concentration of binder would probably also lead to them acting as templates for pore size rather than just as binding additives. The change in cell parameters with increasing temperature is influenced by the type and concentration of the electrolyte, and can probably be explained by charge transport limitations [14].

References

1. Nazeeruddin, M.K., A. Kay, I. Rodicio, R. Humphrybaker, E. Muller, P. Liska, N. Vlachopoulos, M. Gratzel, *Journal Of The American Chemical Society*, 1993. **115**(14): p. 6382-6390.
2. Miki, T., K. Nishizawa, K. Suzuki, K. Kato, *Materials Letters*, 2004. **58**: p. 2751-2753.
3. Lee, K.-M., V. Suryanarayanan, K.-C. Ho, *Solar Energy Materials And Solar Cells*, 2006. **90**: p. 2398-2404.
4. Huang, C.-Y., Y.-C. Hsu, J.-G. Chen, V. Suryanarayanan, K.-M. Lee, K.-C. Ho, *Solar Energy Materials and Solar Cells*, 2006. **90**(15): p. 2391-2397.
5. Tai, W.-P., *Solar Energy Materials And Solar Cells*, 2003. **76**(1): p. 65.
6. Shen, Q., D. Arae, T. Toyoda, *Journal Of Photochemistry And Photobiology A-Chemistry*, 2004. **164**(1-3): p. 75-80.
7. Saito, Y., S. Kambe, T. Kitamura, Y. Wada, S. Yanagida, *Solar Energy Materials and Solar Cells*, 2004. **83**(1): p. 1-13.
8. Diebold, U., *Surface Science Reports*, 2003. **48**(5-8): p. 53-229.
9. Ngamsinlapasathian, S., T. Sreethawong, Y. Suzuki, S. Yoshikawa, *Solar Energy Materials and Solar Cells*, 2005. **86**(2): p. 269-282.
10. Barbe, C.J., F. Arendse, P. Comte, M. Jirousek, F. Lenzmann, V. Shklover, M. Gratzel, *Journal of the American Ceramic Society*, 1997. **80**(12): p. 3157-3171.
11. Schmidt-Mende, L. and M. Gratzel, *Thin Solid Films*, 2006. **500**(1-2): p. 296-301.
12. Schroder, D.K., *Semiconductor Material and Device Characterization 2nd Ed.*, John Wiley & Sons: New York, 1998.
13. Nazeeruddin, M.K., P. Pechy, M. Gratzel, *Chemical Communications*, 1997(18): p. 1705-1706.
14. Schabauer, J., C.P. Morley, J. Baker, N. Dartnell, P. Douglas, C. Winscom, *Synthesis and Reactivity in Inorganic Metal-Organic and Nano-Metal Chemistry*, 2007. **37**(5): p. 347-351.

CHAPTER 5

CHANGES IN CELL PERFORMANCE WITH LIGHT INTENSITY

5.1. Introduction

In the same way as variation of cell performance with changing temperature was examined, we also investigated the changes of cell parameters with changing light intensity for cells made using the N3 dye. The same test apparatus which was used for the temperature studies was used for these investigations. The temperature was kept constant at 20 °C and the light intensity was changed by either changing the energy input into the Xenon arc lamp *via* a transformer or, in the lower light intensity range, with neutral density filters. The electron transfer characteristics with changing laser light intensity for example have been investigated before [1-3]. It had been found before, that cell efficiencies and fill factors decrease with increasing light intensity and increasing cell area [4, 5]. To keep the fill factors as high as possible, probably very small cells (cell area smaller than 1 cm²) will have to be built although it is unsure why smaller cell areas lead to better fill factors [4].

5.2. I-V of N3 cells with changing light intensity

The cells compared here are two N3 cells built using a very concentrated electrolyte (EL3) with either 1 or 2 layers of Scotch Magic tape as a template for the semiconductor thickness. We chose those two cells, as they represented the cells with the highest efficiencies investigated throughout this project (around 5 % at 1 Sun). They were prepared using exactly the same methods described earlier in Chapter 2 and involved both finishing steps i.e. TiO₂ crystal growth on the finished surface and 4-tert-butylpyridine added to the electrolyte. Figures 5-1. and 5-2 show I-V curves for these cells at different irradiation intensities, while Tables 5-1 and 5-2 give their photoelectric parameters.

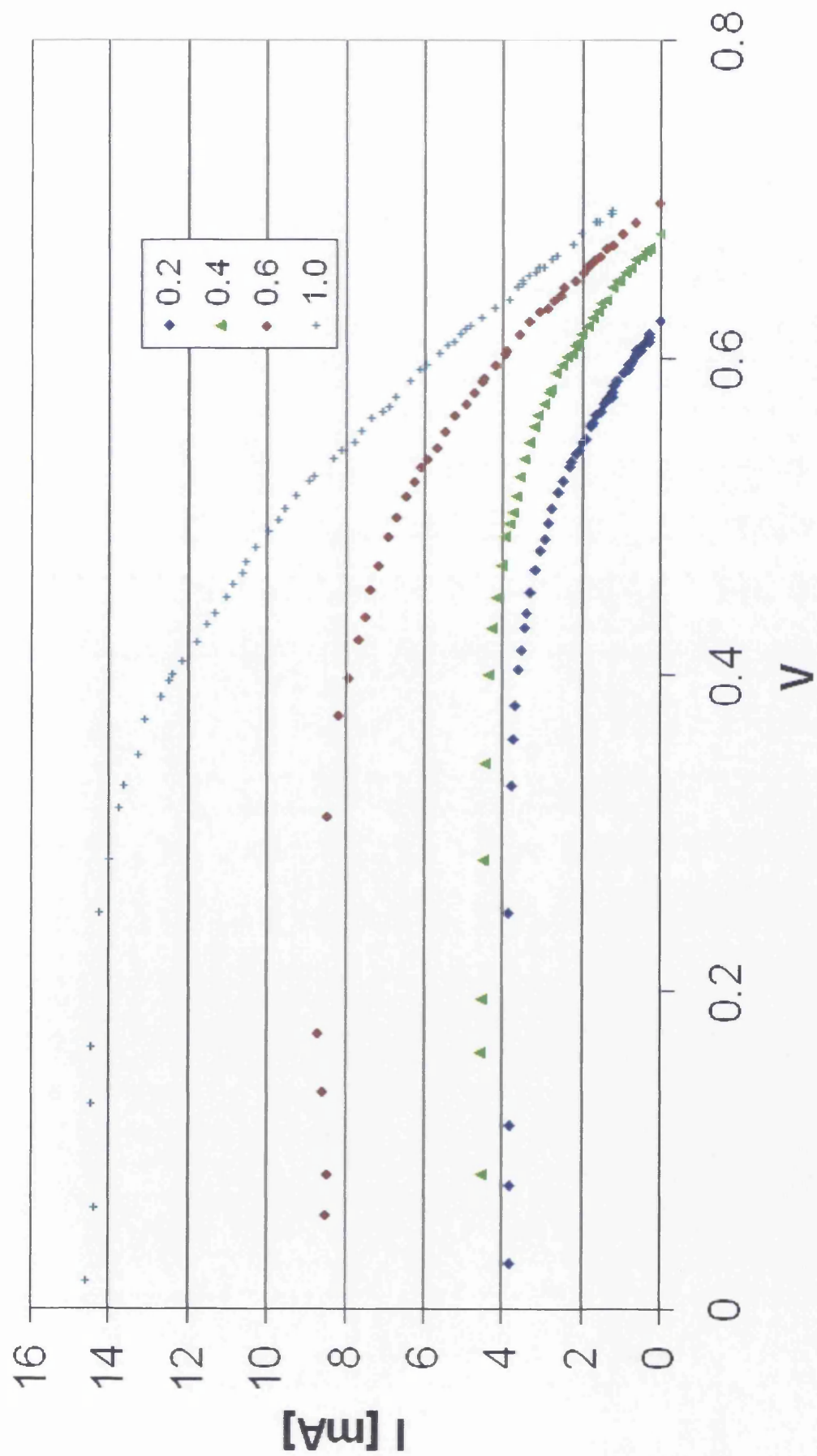


Figure 5-1 Variation in I-V curves of a cell built using N3 dye and electrolyte EL3 at different irradiation intensities (shown as sun levels): 1 layer of Scotch Magic tape as a template for the thickness of the semiconductor layer; cell area 1 cm²

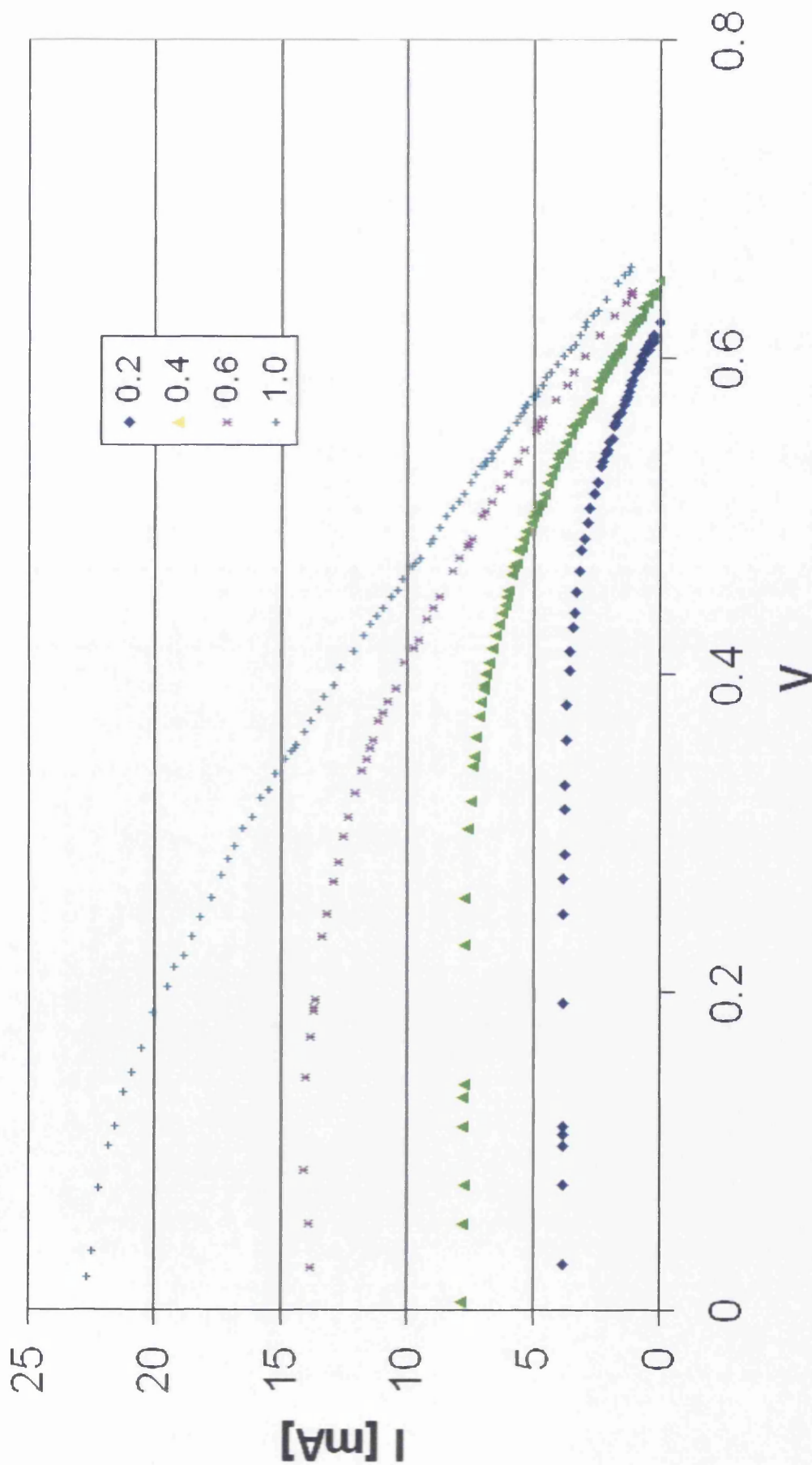


Figure 5-2 Variation in I-V curves for a cell built using N3 dye, with EL3 electrolyte, at different irradiation intensities: 2 layers of Scotch Magic tape as a template for the thickness of the semiconductor layer; cell area 1 cm²

Sun	Voc [V]	Isc [mA]	Vmax [V]	Imax [mA]	ff	Pmax [mW]
0.2	0.63	3.83	0.49	3.00	0.61	1.47
0.4	0.68	4.50	0.54	3.50	0.61	1.88
0.6	0.70	8.50	0.53	6.17	0.55	3.25
1	0.71	14.50	0.49	10.00	0.48	4.95

Table 5-1 Photoelectric characteristics of a cell prepared with N3 dye, electrolyte EL3: 1 layer Scotch Magic tape, Solaronix HT; cell area 1 cm²

Sun	Voc [V]	Isc [mA]	Vmax [V]	Imax [mA]	ff	Pmax [mW]
0.2	0.62	3.90	0.49	2.93	0.59	1.44
0.4	0.65	7.80	0.47	5.61	0.52	2.63
0.6	0.66	13.90	0.43	9.27	0.44	4.03
1	0.67	22.44	0.39	13.17	0.34	5.13

Table 5-2 Photoelectric characteristics of a cell prepared with N3 dye, EL3 electrolyte: 2 layers Scotch Magic tape, Solaronix HT; cell area 1 cm²

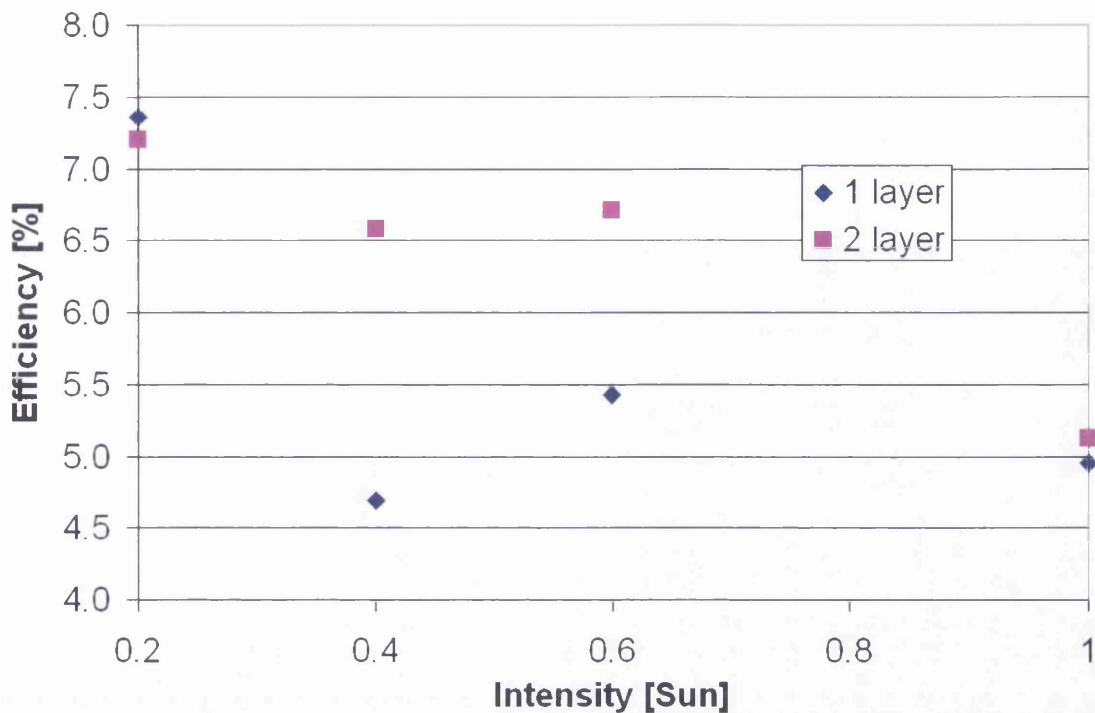


Figure 5-3 Overall efficiencies of the two cells described above (made with either 1 or 2 layers of Scotch Magic tape to control the thickness of the TiO₂ layer) at different light intensities.

5.3. Discussion

Here we observed the same trends as already discussed in earlier chapters. Most prominently, a declining fill factor with increasing short circuit current which is linked to an increased semiconductor resistance together with limited charge carrier transport (redox couple) within the electrolyte especially inside the mesoporous semiconductor.

If Figures 5-1 and 5-2 are compared, one can observe a proportionality of the short circuit current with incident sunlight in the thicker semiconductor layer (Figure 5-2) which is not so apparent in the cells built with a thin layer of semiconductor

(Figure 5-1). As expected, the overall efficiencies of the cells decreased with increasing illumination intensity. This is again caused by the difference in fill factor, most likely arising from a difference in the series resistance of the cell with increasing current. This change of fill factor appears to be a characteristic of our specific cell and dependent on the short circuit current.

5.4. Conclusion

We have again confirmed, that the fill factor and with it the efficiency of a cell decrease with increasing light intensity and increasing currents which are a consequence of the increasing light intensity. The decline of the fill factor seems to be a characteristic of each specific type of cell and is closely linked to the resistances occurring at every single interface within the cell and the nature of the semiconductor film.

References

1. Kuciauskas, D., M.S. Freund, H.B. Gray, J.R. Winkler, N.S. Lewis, *Journal Of Physical Chemistry B*, 2001. **105**(2): p. 392-403.
2. Schwarzburg, K., R. Ernstorfer, S. Felber, F. Willig, *Coordination Chemistry Reviews*, 2004. **248**(13-14): p. 1259.
3. Hagfeldt, A. and M. Gratzel, *Accounts Of Chemical Research*, 2000. **33**(5): p. 269-277.
4. Nazeeruddin, M.K., A. Kay, I. Rodicio, R. Humphrybaker, E. Muller, P. Liska, N. Vlachopoulos, M. Gratzel, *Journal Of The American Chemical Society*, 1993. **115**(14): p. 6382-6390.
5. van de Lagemaat, J., N.G. Park, A.J. Frank, *Journal Of Physical Chemistry B*, 2000. **104**(9): p. 2044-2052.

CHAPTER 6

**TIME RESOLVED PHOTOACOUSTIC STUDIES OF
DYES ADSORBED TO TiO₂ FILMS, AND IN THIN
POLYMER FILMS**

6.1. Introduction

Following light absorption by the dye, the first chemical step in dye sensitised solar cells is the injection of an electron from an excited state of the dye into the conduction band of the TiO₂. The efficiency of this electron injection is of primary importance for the overall efficiency of dye-sensitised solar cells. The overall efficiency for solar cells consisting of a dye adsorbed on a nanocrystalline TiO₂ electrode, is *ca.* 10 % at maximum [1]. However, the direct measurement of the electron-injection efficiency remains uncertain. The quantum yield of the electron injection is often estimated indirectly from the rate constant for electron injection and the excited-state lifetime in the absence of injection, which cannot be determined under the same experimental conditions, or from transient absorption spectroscopy, which is complicated by the overlap between ground-state and transient absorption spectra and by the short lifetimes of the transients.

The work described in this chapter presents a new approach for measuring charge injection efficiencies in solar cells. It is based on the detection of the pressure wave generated in the conversion of the radiative energy into heat, as the electronic excitation of the dye evolves to a charge-separated (CS) state with the electron located in the conduction band of the semiconductor. This method, known as time resolved photoacoustic calorimetry (PAC) gives a direct measure of the quantum yield of the CS state when its energy is known [2] and the energy of the CS state when the quantum yield is known. The principle of the method is illustrated in Figure 6-1 below.

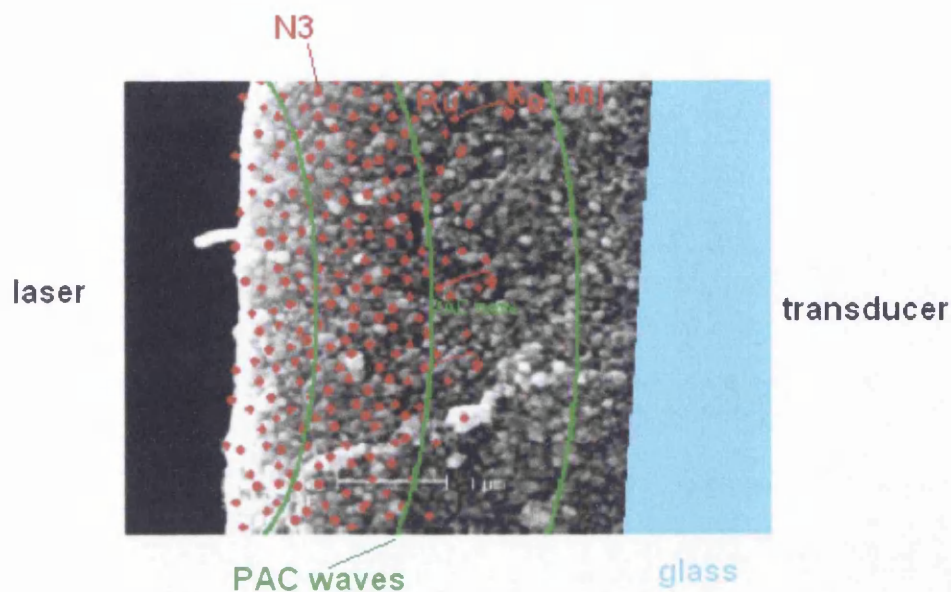


Figure 6-1 Principles of time resolved PAC as applied to the N3 dye adsorbed on TiO₂. The formation of the photoacoustic wave after the sample was pulsed by a laser beam incoming from left. The non-radiative decay of the dye molecules involved (red dots) generates the wave.

6.2. Design of instrumentation

Up until our experiments, no instrumentation for solid state photoacoustic measurement of time-resolved non-radiative decays has been reported. It was our goal to design an instrumental set up based on existing methods of photoacoustic calorimetry. The previously available methods for solid state photoacoustic calorimetry give the steady-state spectrum of non-radiative processes as a function of irradiation wavelengths. For this steady-state method, the detector is usually situated perpendicular to the window and the light beam.

The arrangement for time resolved solution phase PAC has the pulsed laser excitation source, window, sample, a mirror for reflection of the laser pulse, and the detector all inline, as shown in Figure 6-4.

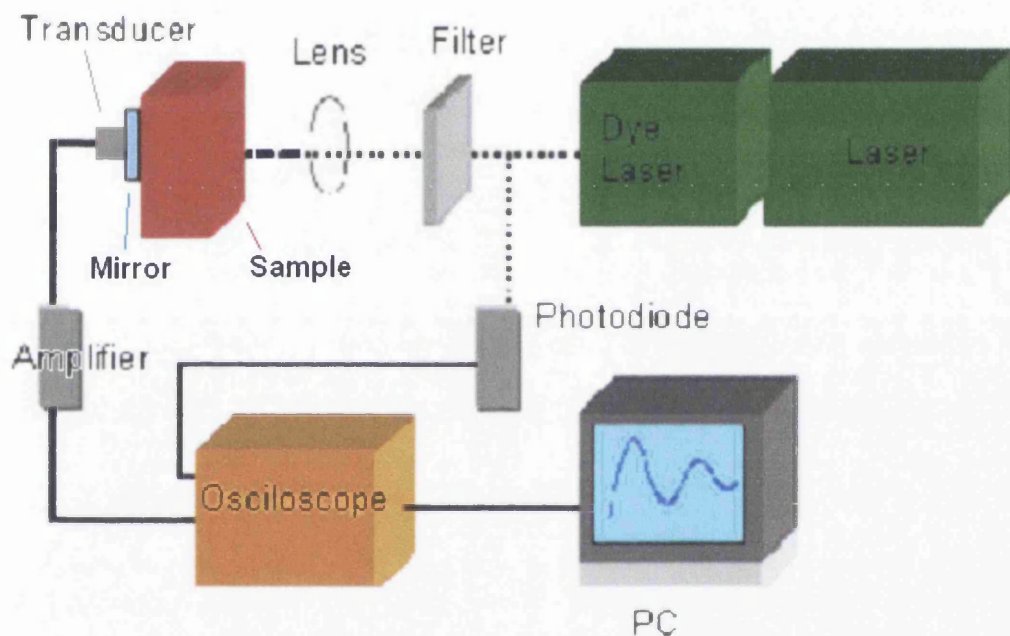


Figure 6-2 Scheme of a typical set up for photoacoustic calorimetry as it would be used for liquid samples. The sample is situated between the lens and the transducer.

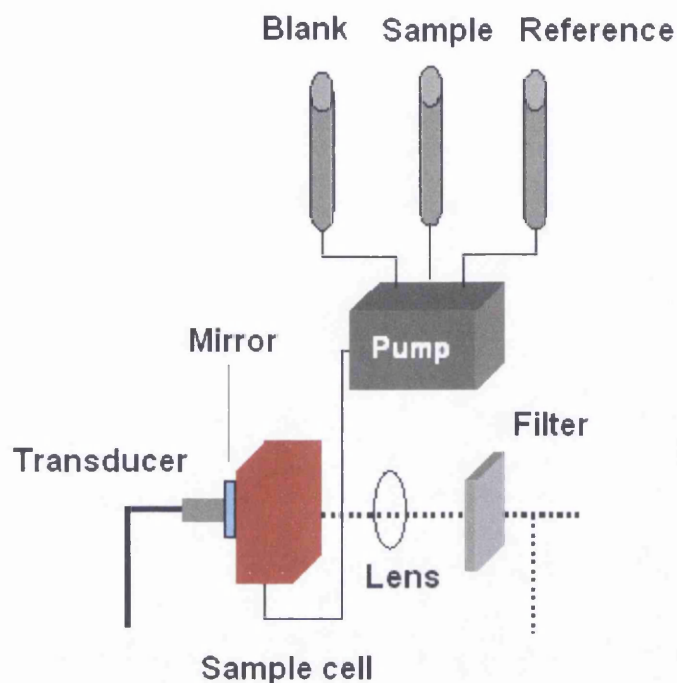


Figure 6-3 In the liquid PAC apparatus, the liquid samples (blank, reference and sample), are continuously pumped through a chamber in front of the transducer.

The most important parts in this PAC arrangements, are a good optical window, which transmits the laser wavelength close to unity whilst blocking out the rest of the spectra, and the mirror, which totally reflects the exciting wavelength in order to prevent direct heating of the transducer. Then, perfect acoustic coupling has to be ensured so that none of the generated signal is lost. For liquid PAC, the sample and a reference are pumped into the “cell” between the window and the mirror, and acoustical contact is made directly by the liquid. The contact between the window and the transducer has to be very high. It can be improved by the use of silicon grease for better acoustic coupling.

In the case of the solid state PAC, as shown in this thesis, acoustic coupling proved to be the key to obtaining reproducible results, because in this case we need to couple a solid sample to the transducer. (Details of the preparation and characterisation of the samples is given in the following section 6.2.1; but at this stage it is useful to know that they are essentially a dye adsorbed onto a very thin layer of TiO_2 coated onto a glass slide.) We encountered several problems trying to get the first usable results. The first experiments took place on the bench, temporarily aligning the different parts of the photoacoustic cell in different orientations and using several contact fluids and greases for acoustic coupling. The reproducibility of the experiment was our main objective. In order to achieve highest reproducibility we considered the following factors of high importance: alignment of the laser, the sample, the window and the mirror, and the best possible contact between transducer, mirror and sample. We also found out that the contact to the window on the upper side of the sample, in contact with the optical window, was important for the quality of the signal. Therefore we used the contact medium on both sides of the sample. First, we applied pressure by hand, and realised that different pressures gave different results. Increasing the pressure onto the sample increased the signal amplitude up to maximum signal strength. When the pressure was released, the signal strength decreased but only to a point where the tension within the material relaxed and then the signal was very reproducible. It was discovered that there were two ways to get a reproducible result; either to always apply the same pressure or to once press the mirror and the window with the sandwiched sample together very tight and then only keep it in place with a constant weight on top. We decided to press the sample hard together to gain maximum signal strength and then leave a steel ring with the window inside, on top of the sample before we started our measurements.

During these preliminary tests, we tried several types of greases and lubricants to ensure maximum signal strength and reproducibility. Amongst these substances were hexadecane, silicone grease, and glycerol.

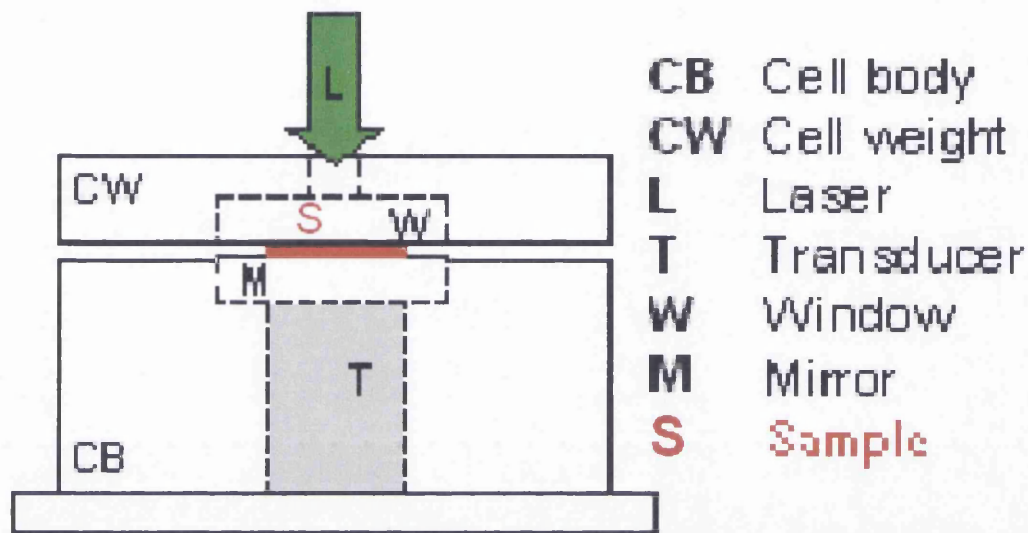


Figure 6-4 Scheme of the front-face PAC cell for solid and solid/liquid samples.

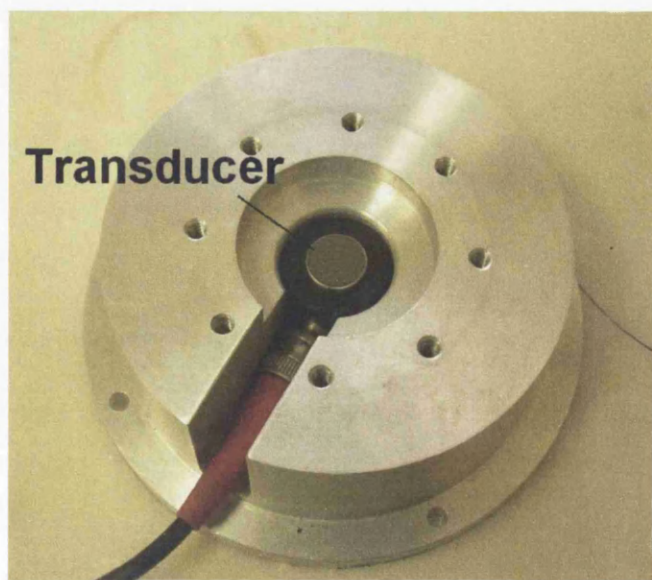


Figure 6-5 The lower part of the PAC sample holder with the transducer.

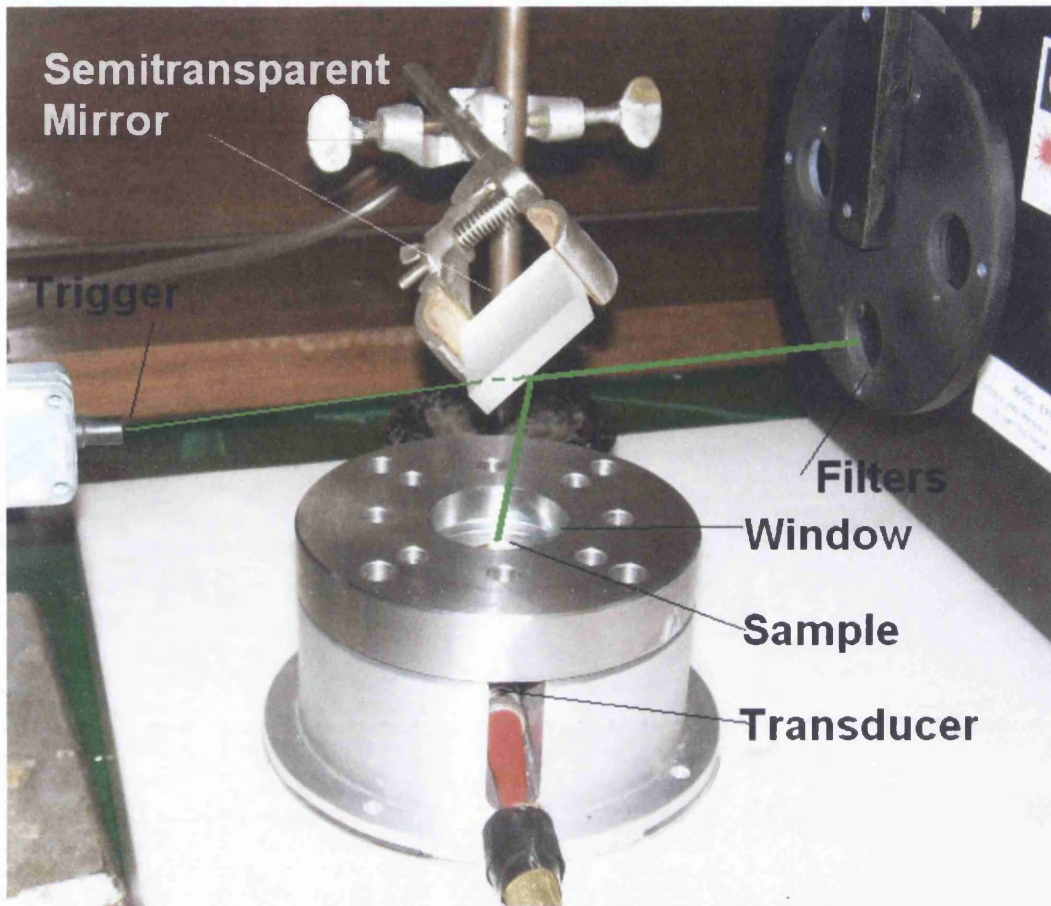


Figure 6-6 Picture of the sample holder.

6.3. The PAC signal

Whether or not time resolved information can be obtained is determined by the response range of the transducer in relation to the timescale of the observed process. If the process is too fast, the signal cannot be resolved to get time resolved data but integration will still give useful data on the amount of energy degraded thermally. In the other case if the processes is too slow, the signal can neither be resolved nor integrated. With the piezoelectric transducer used in our case we were able to resolve signals between 10 ns up to a few hundreds of μs .

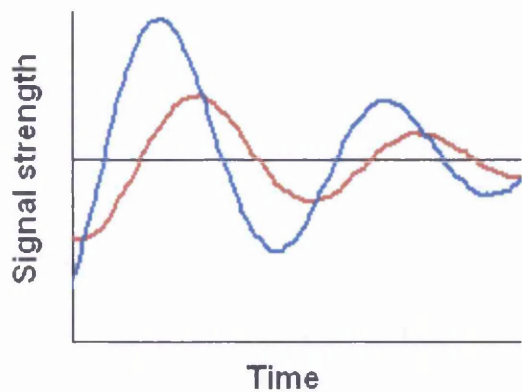


Figure 6-7 Typical signal derived from a PAC measurement: blue reference; red sample.

Figure 6-7 shows a typical PAC signal which compares the response from a sample, in red, to that of a reference, in blue. The reference is a material which degrades all of the incident energy to heat within a timescale much shorter than the time resolution of the transducer. As will be discussed later, obtaining a good reference is a very important part of experimental design in PAC. As shown, the signals differ in amplitude and also in phase. The difference in amplitude is related to the difference in energy degraded to heat for sample and reference, while the difference in phase is related to the timescale over which this thermal degradation occurs in the sample. The reference is specifically chosen so that the degradation timescale is faster than the instrument response time. In order to give a signal which resolves both differences, the process has to happen in the right timescale. Depending on the process to be observed, it can become necessary to use different transducers. Figure 6-8 shows the time range of the transducer used here; while Table 6-1 summarises the information which can be obtained for processes occurring on different timescales.

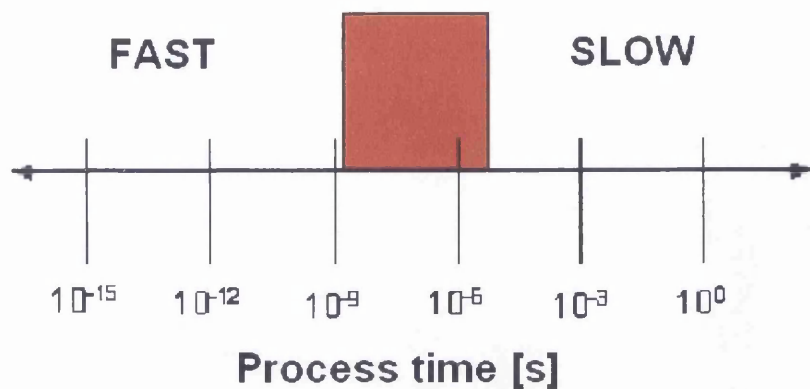


Figure 6-8 Time range of the transducer used in our system.

Processes	Signal	
fast	integrated, not resolved	AMPLITUDE changes
	integrated and resolved	AMPLITUDE and PHASE changes
slow	neither integrated, nor resolved	no changes

Table 6-1 Time resolved measurements can only be done if the time scale of the process matches the measurement range of the transducer.

6.5. Sample preparation

TiO₂ film

A standard procedure was used to make the TiO₂ films (see, for example, reference [1]). Nanoporous titania films were prepared by applying, with a micropipette, TiO₂ sol (HT/SP from Solaronix) to one edge of a square glass slide previously covered on the two other parallel edges with Scotch Magic adhesive tape (3M) of *ca.* 20 μm thickness. The colloid was distributed over the slide with a glass rod pulled over the tape-covered edges. This is similar to the squeegee printing

process described in the experimental section of this thesis (see Chapter 2). After air drying the film was sintered in an oven at 430-450 °C for about 20 minutes. The resulting films were optically transparent and had a thickness in the order of 4 µm (*vide infra* SEM analysis).

Choice of dyes and reference materials

The outstanding performance of the Ru(II)(dcbpy)₂(NCS)₂ (RuN3, dcbpy = 4,4'-dicarboxy-2,2'-bipyridine) dye (N3) adsorbed on nanocrystalline TiO₂ and the detailed studies available for this system [3], motivated the choice of this dye for the first measurements of time-resolved PAC on solution/solid interfaces. Such measurements can only be accomplished with the measurement of PAC signals from samples and photoacoustic references under the same experimental conditions. Mn-tetraphenylporphyrin (MnTPP) was shown to behave as a good photoacoustic reference in solution before by the group in Coimbra [4]. However, it does not adsorb onto TiO₂ films. Therefore the porphyrin synthesis group in Coimbra prepared a sulphonated, 5,10,15,20-tetrakis(4-sulphophenyl)porphyrinate manganese (III) chloride (MnTPPS), as a reference. They also provided 5,10,15,20-tetrakis(4-sulphophenyl)porphyrinate copper (II) (CuTPPS) for comparison. Neither of these porphyrins showed emission in aqueous solution or when absorbed onto TiO₂ films, and did not exhibit transient absorption spectra in the timescale of nanoseconds or longer.

Dye adsorption

The nanoporous titania layer prepared for PAC experiments was not saturated with the dye, as it would be for use in photovoltaics. Low absorbances were

employed, to avoid multilayer and multiphotonic effects and facilitate the matching of the absorption between sample and reference films at the excitation wavelength. Each dye was adsorbed by immersing the glass slides coated with TiO_2 in an ethanoic solution of the dye for the period of time required for the desired absorbance. Typical absorbances at the excitation wavelength, 532 nm, were 0.2, before subtraction of the TiO_2 background signal. The adsorption time varied between 5 min for the lower N3 dye absorbances to a few hours for the MnTPPS samples of higher absorbance. The dyes with sulfonyl anchoring groups took longer time to adsorb to the titania surface than the N3 ruthenium dye, which has carboxylic anchoring groups. As shown below, this method produces a uniform titania layer with a homogenous layer of dye adsorbed onto it. However, it should be noted that when the CuTPPS adsorbed to TiO_2 remains in contact with glycerol for a sufficiently long period of time, CuTPPS is released from the surface and colors the solvent. The absorption spectra of MnTPPS, CuTPPS and N3 adsorbed on TiO_2 film and in alcohol are shown in Figure 6-9. There is a good correspondence between the porphyrin bands in solution and the corresponding one of the compounds adsorbed on the material, with the latter shifted by 4 nm (Q-bands) to 8 nm (Soret band) relative to the solution spectra.

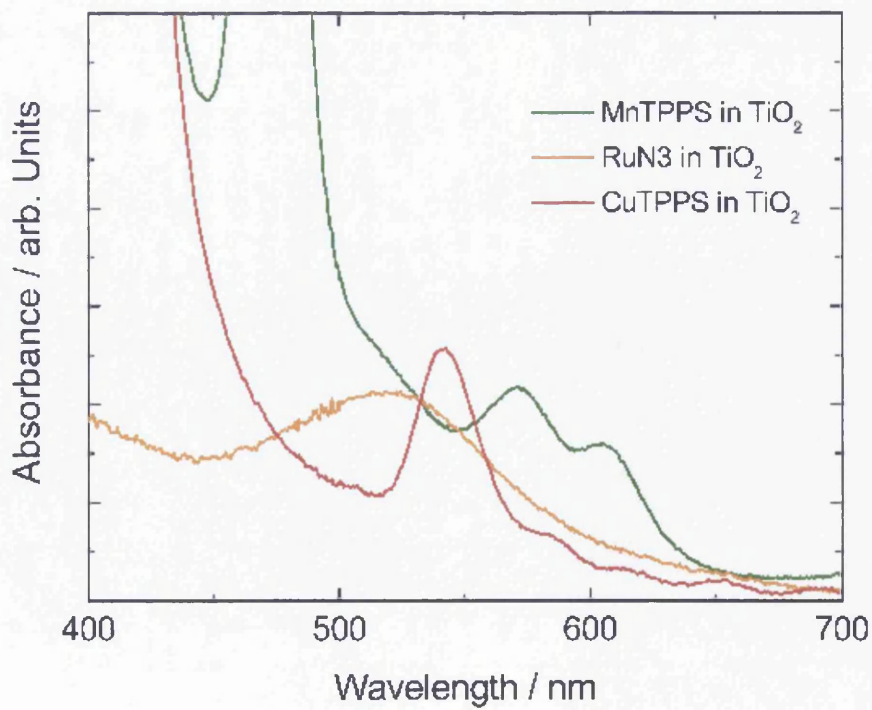
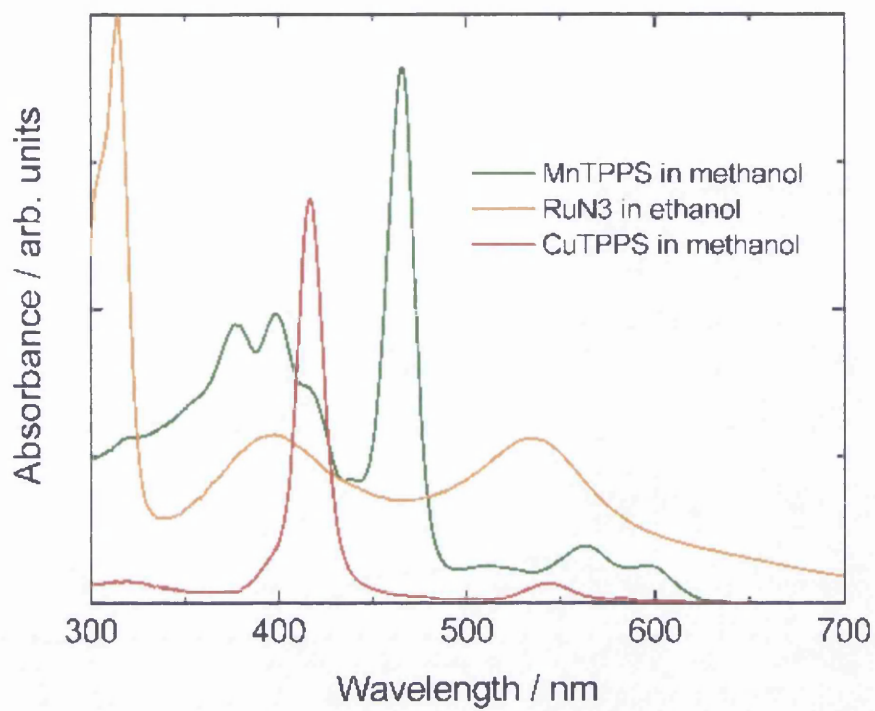


Figure 6-9 Absorption spectra of the dyes in solution (top) and on TiO₂ (bottom).

6.5.1. Surface characterisation of the TiO₂ films

The surface characterisation of the TiO₂ layers was carried out in the laboratories of the ICEMS-Mechanical Engineering Department, University of Coimbra by Ana P. Piedade. The morphology of the TiO₂ films, with and without dyes, was analysed by Scanning Electron Microscopy (SEM). Prior to the observation, the samples were sputter coated with 30 nm of gold to obtain a conductive surface. The surface and cross section morphologies were observed on a Philips XL30 instrument with an accelerating voltage of 15 keV. Electron Probe Micro Analysis (EPMA) was used to evaluate the uniformity of distribution of N3 and CuTPPS dyes in the TiO₂ thin films. After sputter-coating with 30 nm of gold, the samples were analysed using a Camebax SX50 instrument. Qualitative spectra were performed in both samples aiming at establishing the correct wavelength of the electronic transitions of the chemical elements: Ru L α (Figure 6-10) and Cu K α (Figure 6-11).

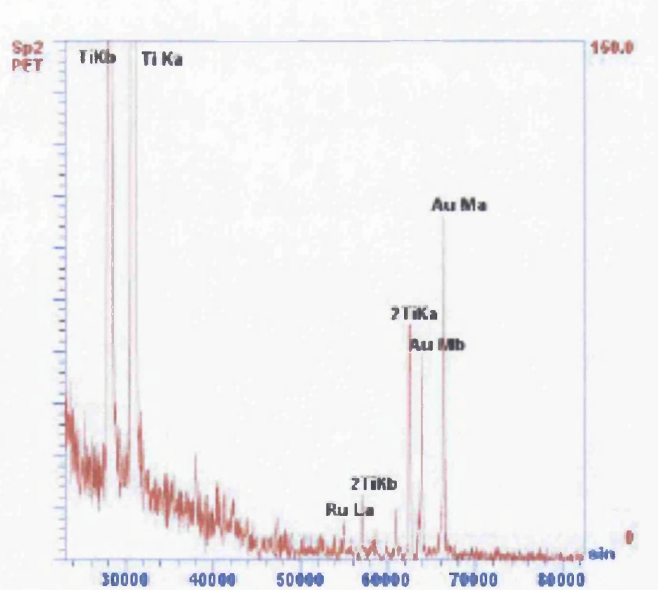


Figure 6-10 Wavelength spectra (PET crystal) of the sample N3 adsorbed on TiO₂ indicating the value of $\sin\theta$ for the Ru L α transition used in the elemental map distribution of ruthenium.

The elemental map distribution of each element was obtained by scanning an area of 1000 x 1000 μm (Figure 6-12).

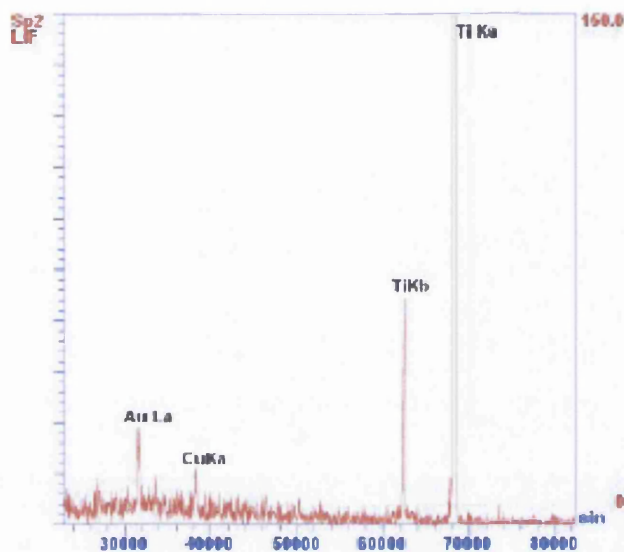


Figure 6-11 Wavelength spectra (LiF crystal) of the sample CuTPPS adsorbed in TiO_2 indicating the value of $\sin\theta$ for the Cu $K\alpha$ transition used in the elemental map distribution of copper.

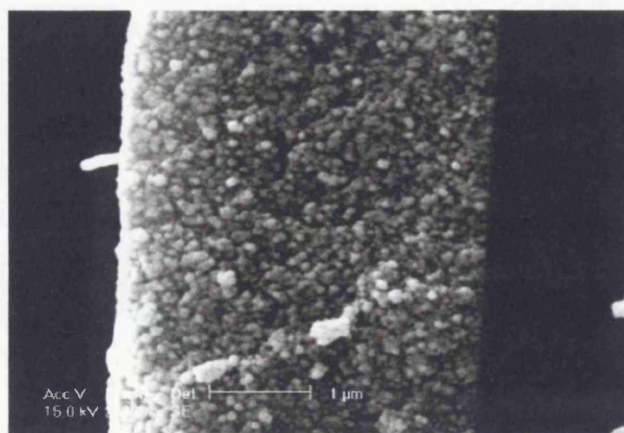


Figure 6-12 Morphology of a transversal section of TiO_2 nanoporous transparent film

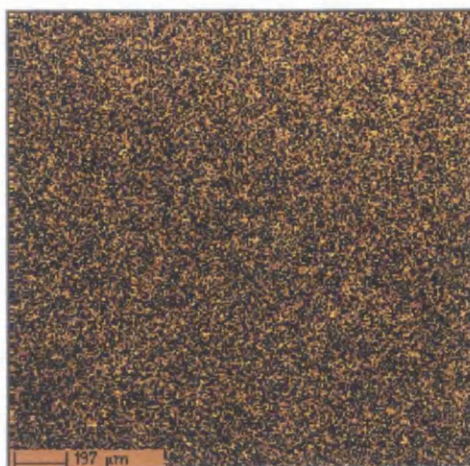


Figure 6-13 EDX-SEM image, showing the homogeneous CuTPPS dye distribution on the TiO₂ surface (top view).

6.5.2. Calibration, reproducibility and preliminary measurements

Figure 6-14 shows PAC waves for the N3 dye adsorbed on TiO₂, as a function of laser intensity. The different signals were obtained by using neutral density filters with transmissions between 25 % and 75 %. The same linear behaviour as illustrated for the N3 dye was found for MnTPPS and CuTPPS films on TiO₂.

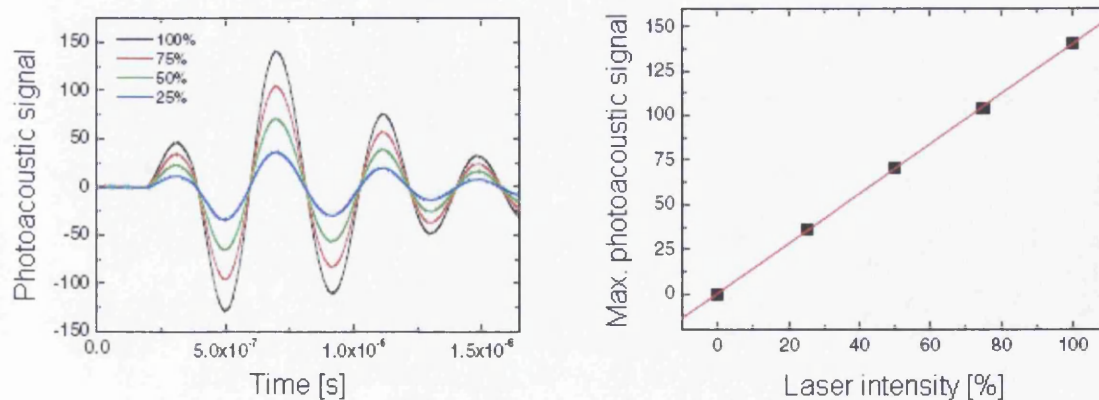


Figure 6-14 The photoacoustic signal in relation to the laser intensity. The signal was proportional to the intensity of the laser.

Figure 6-15 shows PAC waves for MnTPPS, and N3 adsorbed on TiO₂ along with the zero signal from TiO₂ alone. Studies showed that the photoacoustic waves of MnTPPS and CuTPPS adsorbed on TiO₂ were indistinguishable.

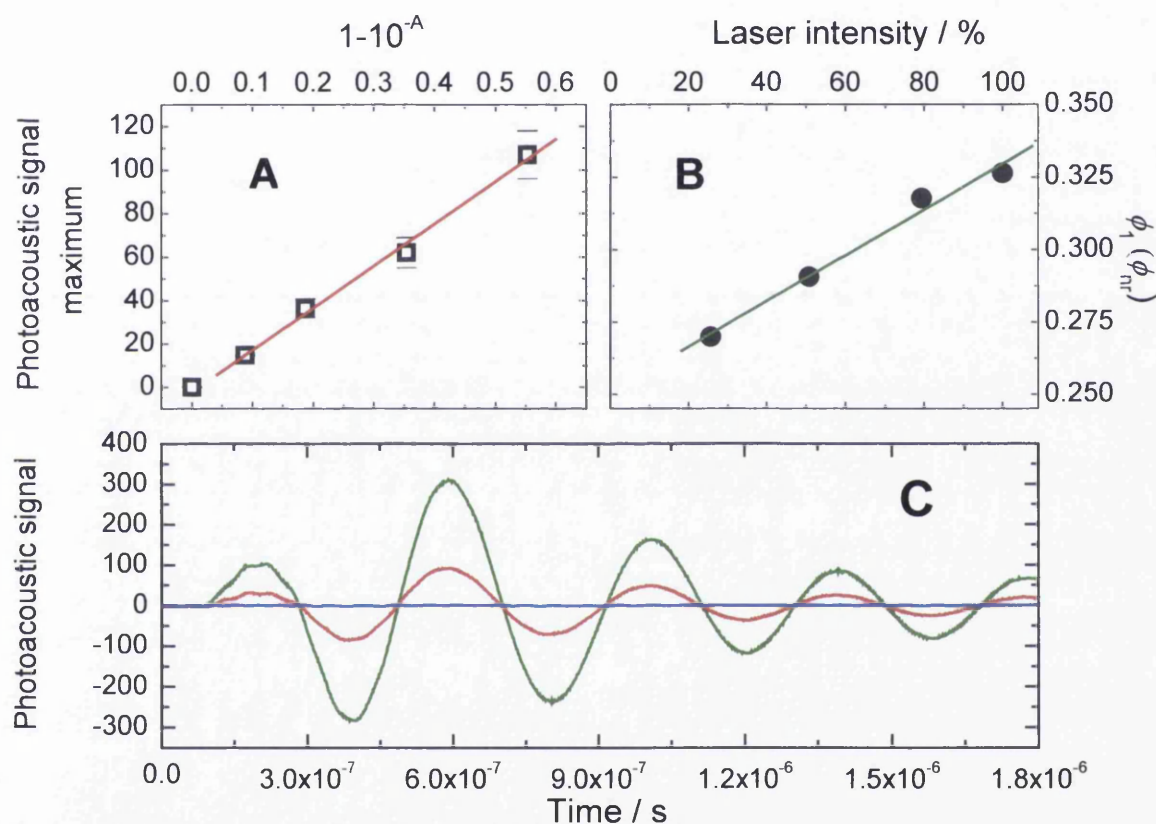


Figure 6-15 (A) Intensity dependence of PAC waves on the fraction of energy absorbed for MnTPPS adsorbed on TiO₂; five independent measurements were made for each absorbance. (B) Fraction of the fast non-radiative decay of N3 at various laser intensities. (C) PAC waves of MnTPPS (green) or N3 (red) adsorbed on TiO₂, normalized for the absorbance of 0.18 at 532 nm; the blue line is the signal from TiO₂ with no dye; all data was taken with glycerol as the acoustic coupling medium.

Deconvolution

We observed no phase shift in the signal from N3 compared to MnTPPS. Therefore we could not determine the rate of formation of the N3-TiO₂ CS state. However there was an obvious difference in the signal amplitudes

When the rate of formation of the CS state is much faster than the response time of the transducer and the decay rate of the CS state much slower, then the ratio of amplitudes between sample and reference wave gives the fraction of the total input energy released as heat in the “fast” time region of the transducer i.e. in the formation of the CS state. The remaining fraction corresponds to the energy trapped in the CS state. As this state is relatively long lived, subsequent processes are not detected in the time window of the experiment. Hence we only detect the heat deposition corresponding to the formation of the CS species, and Φ_1 gives this heat as a fraction of all the absorbed energy.

The deconvolution employs a kinetic model consistent with a fast exponential decay and is based on an implementation of the Marquardt algorithm. This gives the fraction of heat deposited within less than 1 ns. Figure 6-15 gives an example of deconvolution of photoacoustic waves. The calculated wave is superimposed on the sample wave.

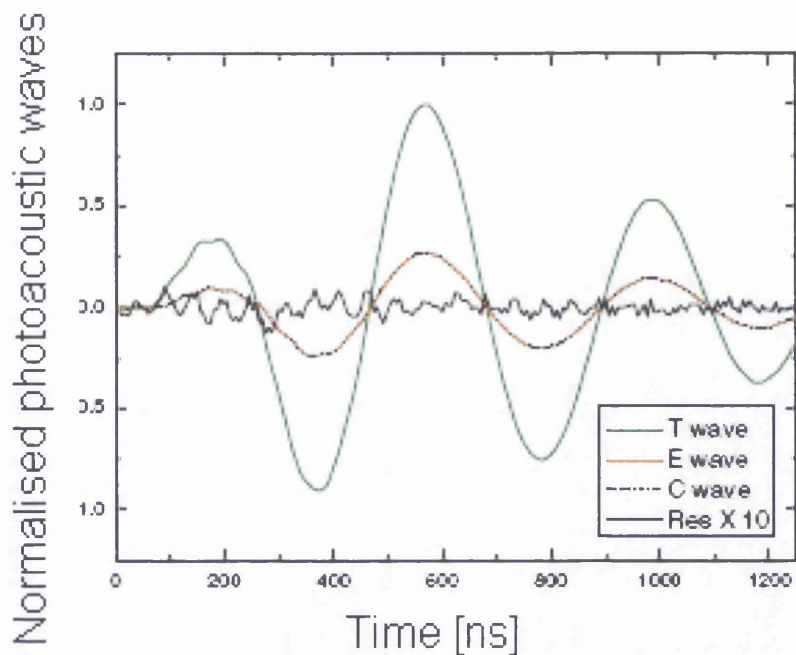


Figure 6-16 Deconvolution of the photoacoustic waves. Normalised reference wave (MnTPPS, T-wave, green line), sample wave (N3, E-wave, orange line), the calculated wave was obtained from fitting with a single fast exponential decay (C-wave, dotted line that overlaps with the sample wave line) and residuals x 10, i.e. (sample wave – calculated wave) x 10.

6.5.3. A comment on entropy and volume changes

Entropy and volume changes associated with solvent electrostriction were neglected because our Coimbra collaborators have evaluated their roles in TR-PAC signals measured in solution and concluded that they are small and tend to compensate each other [2]. Electrostriction in interfacial ET must be even smaller because the bulky ligands insulating the redox centres from the solvent and the nanocrystalline structure offer additional shielding from the solvent. Structural volume changes are also negligible in these systems [5].

The free-energy of the charge-separated state is given by Kuciauskas *et al.* [6]

$$\Delta G^{0'} = -RT \left(\frac{E_{CB}}{q} - E^{0'} \right) \quad \text{(Equation 4-1)}$$

where $E^{0'}$ is the redox potential of the ground state of the sensitiser, E_{CB} is the energy of the edge of the conduction band of the semiconductor and q is the fundamental charge. This is not the same quantity as the enthalpy of the charge separated state measured by PAC. The photoacoustic waves contain, in addition to enthalpy of formation of the CS state, the volume changes associated with electrostriction (ΔV_{es}) and structural volume changes. While the latter are negligible for the dyes employed in this work, the PAC signals must be corrected for ΔV_{es} . Furthermore, the comparison between PAC data and free-energies also requires a correction for the electrostriction entropy of the solvent (ΔS_{es}) and translational entropy of the electron (ΔS_t). When the charge separation is 100 % efficient and structural volume changes are neglected, we can write

$$\Delta G_{CS} = -(1 - \phi_1)E_{hv} + K_{VE} \Delta V_{es} - T\Delta S_{es} - T\Delta S_t \quad \text{(Equation 4-2)}$$

where $K_{VE} = \rho C_p / (MW \alpha)$ is the conversion between molar volumes and energies, which involves the solvent density, heat capacity at constant pressure, molecular weight and thermal expansion coefficient [4]. We have shown that for incompressible free ions in a dielectric continuum, $K_{VE} \Delta V_{es}$ and $-T\Delta S_{es}$ have opposite signs and nearly cancel each other out at room temperature [2]. An upper estimate of the translational entropy of the electron injected in the conduction band of the anatase TiO_2 nanocrystallite (ΔS_t) can be obtained with the Sackur-Tetrode equation for the molar entropy of one particle of a mono atomic gas of mass m in a volume V ,

$$S = R \ln \left(\frac{e^{5/2} V}{\Lambda} \right) \quad \text{(Equation 4-3)}$$

where the thermal wavelength is

$$\lambda = \frac{h}{\sqrt{2\pi m k_B T}} \quad \text{(Equation 4-4)}$$

The analogy between the two systems assumes that the electron injected in the conduction band of the nanocrystallite can be regarded as a free particle with the mass of one electron. The average size of the nanocrystallites employed in TiO_2 films is 15 nm, which, for a cubic shape corresponds to $T\Delta S_t = 0.16$ eV at 298 K. This is an upper limit because the dominant effect for electron movement in a bulk crystal or in a nanocrystallite is wave diffraction, and the effective mass of that movement is a

small fraction of the electron mass m_e . For a more realistic value of $m = 0.1m_e$ [7], we obtain $T\Delta S_t = 0.07$ eV at 298 K, which does not change the conclusion that structural volume changes are negligible.

The author wants to thank Carlos Serpa and Luis Arnaut for the analysis of the importance of these effects to PAC studies of dyes adsorbed on TiO_2 thin films [5].

6.6. Final experimental arrangement and results

6.6.1. The determination of charge injection efficiency for N3 dye adsorbed on TiO_2

The sample (i.e. dye adsorbed to nanocrystalline TiO_2 deposited on a glass slide) was placed over a dielectric mirror previously covered with a thin layer of an acoustic coupling medium (hexadecane or glycerol) and a quartz window, with the same pre-treatment, was placed in the top of the sample. A 2.25 MHz Panametrics transducer (model 5676) was coupled to the back of the mirror, and the sample holder ensures that laser beam, transducer, mirror, sample and window were always in the same relative position. The cell also included a weight of 1.5 kg exerting a constant pressure on top of the window. This was critical to achieve the desired reproducibility. The irradiation of the sample was made through the quartz window, following the front-face PAC cell design previously proved to achieve maximum sensitivity [8, 9]. We employed the 532 nm second harmonic of a Nd:YAG laser (either a Spectra Physics Quanta Ray GCR-130 or a EKSPLA PL 2143A) for sample excitation. These lasers had pulse widths of 8 ns and 30 ps, respectively, but this did not influence the results of this study. Laser frequencies from 2 Hz to 10 Hz were tested and shown not to influence the PAC signals.

The procedures for data collection and analysis were the same as for time-resolved PAC in solution [2, 4, 8, 10]. Energy balance requires that the energy of the laser pulse (E_{hv}) minus the energy released in the formation of the charge-separated state ($\phi_1 E_{hv}$) and the energy lost radiatively ($\Phi_F E_{vmax}$), must equal the energy stored in the charge-separated state:

$$\Phi_{CS} E_{CS} = (1-\phi_1) E_{hv} - \Phi_F E_{vmax} \quad \text{(Equation 4-5)}$$

where E_{vmax} is taken as the energy at the maximum emission intensity of the laser, and $E_{hv} = 2.33$ eV at 532 nm. The value of ϕ_1 is obtained from the deconvolution between the reference and sample signals.

When the rate of formation of the CS state is orders of magnitude faster than its decay, high-frequency transducers do not respond to the slow decay and the ratio of amplitudes between reference and sample waves gives essentially the same results as the numerical deconvolution of slow and fast events. Under such conditions, the only assumption implicit in this method is that the pressure wave is exclusively due to thermal processes, that is, volume changes are negligible. The validity of this assumption depends on the chemistry of the system.

The acoustic coupling between all parts of the cell influenced significantly the amplitude and the onset of the acoustic wave. We covered the back and the front of the slide with a thin layer of glycerol to optimise the acoustic coupling with the dielectric mirror and with the quartz window, respectively. The layer of glycerol on the top of the slide also played an additional function: it had a dielectric constant

comparable to that of ethanol and stabilized the charge-separated state to the same extent ($\Delta G^0 = 1.75$ eV) [3]. The quartz window and the constant weight exerted on it improved and stabilised the acoustic coupling.

The fraction of heat released promptly by RuN3, measured by the ratio of the PAC waves of MnTPPS and RuN3, was $\phi_1 = 0.25 \pm 0.2$. Eq (1) with $E_{CS} = 1.75$ eV, gives $\Phi_{CS} = 0.99 \pm 0.02$. The value obtained by transient spectroscopy measurements is 0.8 ± 0.15 [11], possibly too low in view of the rates involved.

Eq (1) can also be used to obtain reaction energies when the CS efficiencies are known. Using hexadecane in the place of glycerol, we produced a CS state in partially apolar environment. The fact that there is hardly any medium dependence on this interfacial ET rate and that the ET barrier is dominated by high-frequency modes [3], implies that the efficiency of electron injection in the semiconductor is not appreciably dependent on the polarity of the medium. Using $\Phi_{CS} = 0.99$ with $\phi_1 = 0.45 \pm 0.02$ measured with hexadecane, we obtain $E_{CS} = 1.3$ eV. This implies that the energy of oxidised N3 relative to the TiO₂ conduction band appears to increase by 0.45 eV when the solvent is changed from an alcohol to a hydrocarbon, Figure 6-17, meaning that the energy of the hole located in the dye is more sensitive to solvent effects. Time resolved PAC is unique for the determination of the energy of such charge-separated states and, when the oxidation potential of the dye is known, it also gives the energy of the conduction band of the semiconductor.

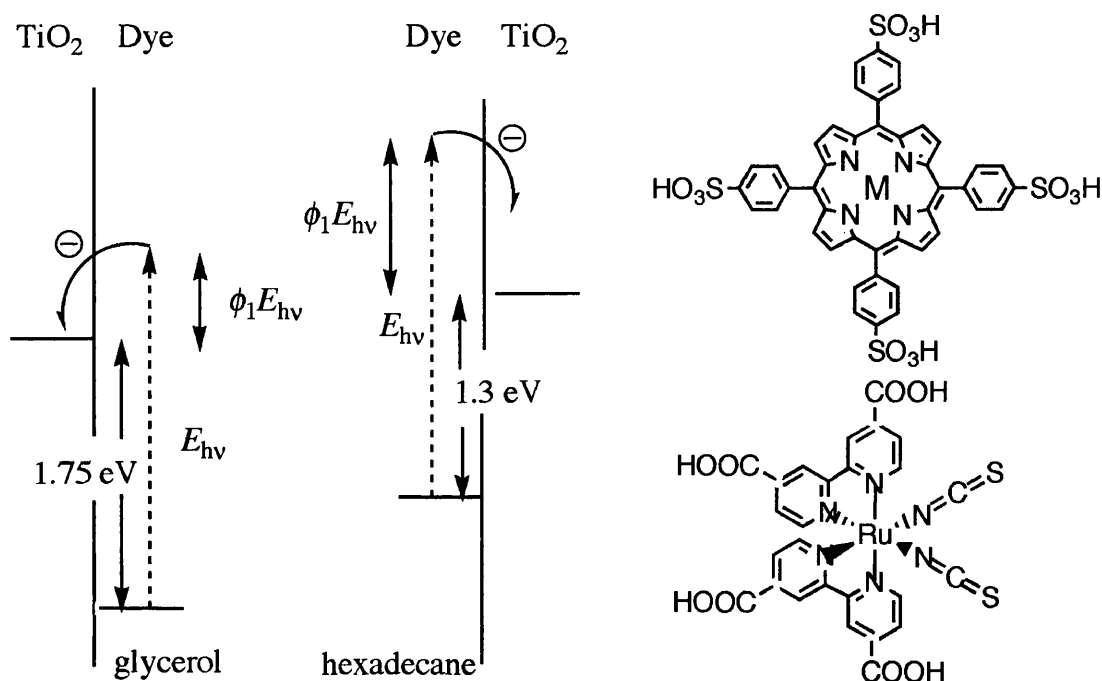


Figure 6-17 Schematic diagram showing the relative energies of the transients involved in the electron injection from dyes in TiO₂. The absolute energies in hexadecane are not known. The dye on the top right is the MnTPPS dye, which was used as a reference and the dye on the bottom right is the N3 dye, our sample dye.

6.6.2. Time resolved PAC on dyes incorporated in polymer matrices

Similar experiments to those with TiO₂ thin films have been done with porphyrins incorporated in a polymer matrix. The polymer films were spin coated from a solution of polymer and porphyrin following a previously published technique [12].

Figure 6-18 shows the PAC signal for CuTPP incorporated in a cellulose acetate matrix. In this case the PAC signals show a phase difference for the sample and reference from which a lifetime of 98 ns can be obtained for the transient CuTPP triplet state.

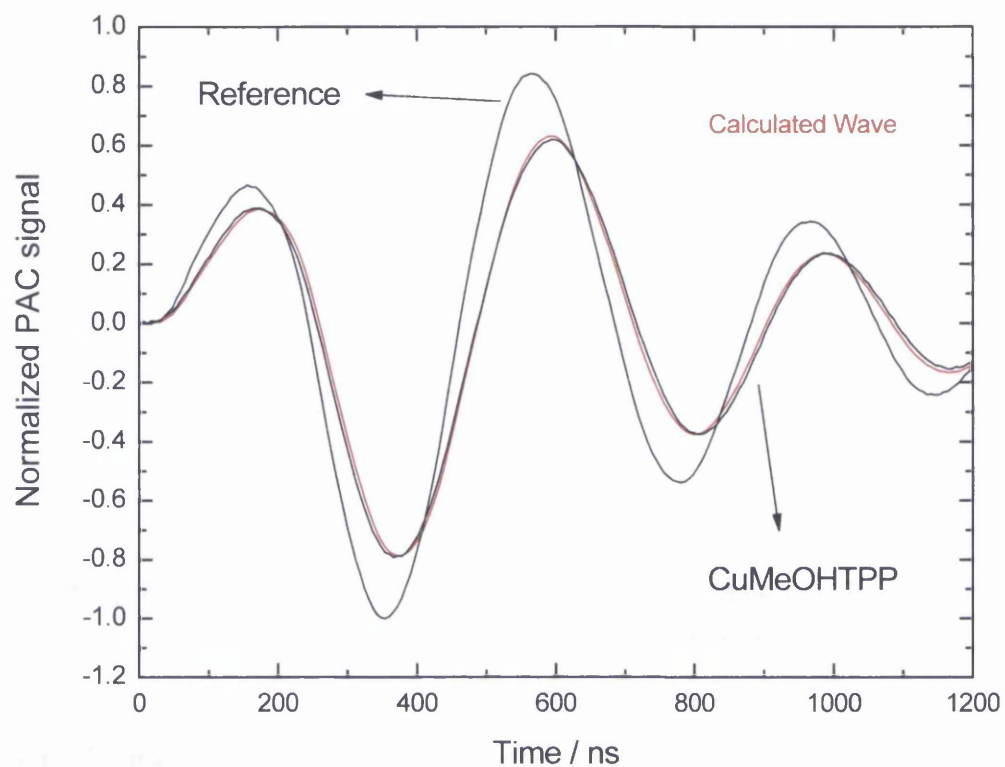


Figure 6-18 PAC signal for CuTPP in a cellulose acetate matrix. Reference is MnTPP in cellulose acetate.

Figure 6-19 shows the corresponding laser flash photolysis transient absorption decay for the CuTPP triplet state in a cellulose acetate matrix; kinetic analysis gives lifetime of 90 ns in good agreement with that obtained by time resolved PAC.

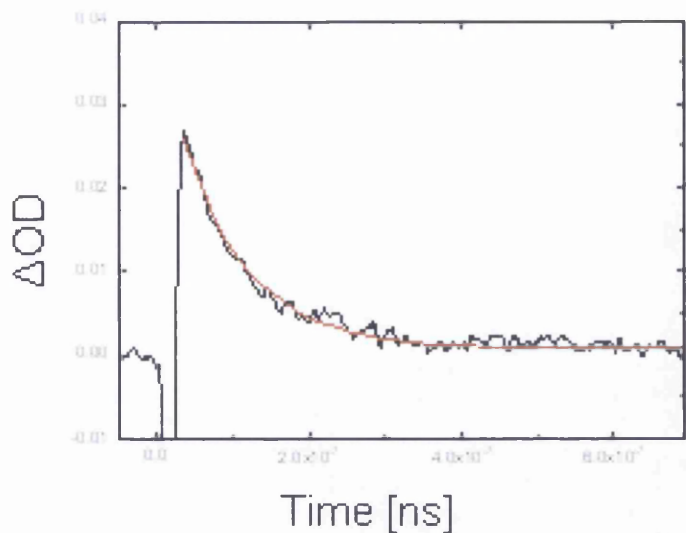


Figure 6-19 Laser flash photolysis of CuTPP in a cellulose acetate.

6.7. Conclusion

In this chapter, we presented the successful development of time resolved PAC for thin films, a completely new technique for interfacial studies in the solid state. It was possible to detect the non-radiative emissions of lumophores in the solid state either incorporated in a polymer matrix or adsorbed onto a semiporous oxide. The charge transfer efficiencies derived using this set up matched the ones derived *via* conventional methods.

We observed, that when the surroundings of the N3 dye adsorbed on TiO_2 are changed, the energy of the hole generated on the dye is susceptible to solvent effects and increases from alcohol as a solvent to an alkane.

With the use of polymers many dyes can be photochemically characterised in their solid state in very low concentrations with this very sensitive method.

6.8. Outlook

At this point, I want to especially thank Carlos Serpa, Luis G. Arnaut and Hugh D. Burrows, all from the University of Coimbra, for their great help and the warm welcome during my visits to Portugal whilst working on the TR-PAC.

It is worth mentioning that the extension of time-resolved PAC to operational solar cells and to the study of other solid:liquid interfaces is straightforward, after small changes to the cell, and that its adaptation to biological systems can be envisaged. Preliminary studies have already been done during our initial development of solid state time resolved PAC and will be reported soon.

References

1. Nazeeruddin, M.K., A. Kay, I. Rodicio, R. Humphrybaker, E. Muller, P. Liska, N. Vlachopoulos, M. Gratzel, *Journal Of The American Chemical Society*, 1993. **115**(14): p. 6382-6390.
2. Serpa, C. and L.G. Arnaut, *J. Phys. Chem. A*, 2000. **104**: p. 11075-11086.
3. Gratzel, M. and J.-E. Moser, *Solar Energy Conversion*, in *Electron Transfer in Chemistry*, I. Gould, Editor. 2001. p. 587.
4. Serpa, C., P.J.S. Gomes, L.G. Arnaut, S.J. Formosinho, J. Pina, J.S.d. Melo, *Chem. Eur. J.*, 2006. **12**: p. 5014-5023.
5. Serpa, C., J. Schabauer, A.P. Piedade, C.J.P. Monteiro, M.M. Pereira, P. Douglas, H.D. Burrows, L.G. Arnaut, *Journal of the American Chemical Society*, 2008. **130**(28): p. 8876-8877.
6. Kuciauskas, D., M.S. Freund, H.B. Gray, J.R. Winkler, N.S. Lewis, *Journal Of Physical Chemistry B*, 2001. **105**(2): p. 392-403.
7. Brus, L., *Journal of Physical Chemistry*, 1986. **90**(12): p. 2555-2560.
8. Pineiro, M., A.L. Carvalho, M.M. Pereira, A.M.d.A.R. Gonsalves, L.G. Arnaut, S.J. Formosinho, *Chem. Eur. J.*, 1998. **4**: p. 2299-2307.
9. Katalnikiv, I.V., M.v.d. Auweraer, F.C.d. Schryver, *J. Photochem. Photobiol. A:Chem.*, 1994. **77**: p. 103-107.
10. Melo, J.S.S.d., H.D. Burrows, C. Serpa, L.G. Arnaut, *Angew. Chem. Int. Ed.*, 2007. **46**: p. 2094-2096.
11. Katoh, R., A. Furube, T. Yoshihara, K. Hara, G. Fujihashi, S. Takano, S. Murata, H. Arakawa, M. Tachiya, *J. Phys. Chem. B*, 2004. **108**: p. 4818-4822.
12. Douglas, P., Eaton, K., *Sensors and Actuators B* 2002. **82**: p. 200-208.

CHAPTER 7

FUTURE WORK AND CONCLUSIONS

7.1 Future Work

In addition to the studies reported in previous chapters in this thesis, there were many more experiments carried out during this research for which, unfortunately, the looming deadline for submission of this thesis has meant a detailed analysis and presentation has not been made here. But they will hopefully provide an interesting base for future work, and for this reason we include a brief account of these experiments.

The time resolved response of a cell to rapid switching of irradiation between “on” and “off” has been studied over temperature and light intensity. The data derived this way may lead us to a better understanding of the chemical processes at the different interfaces of the cell, and the lifetime and possible diffusion characteristics of the active species involved.

Experimentally the first step was to measure the response time of our electric circuit without a cell to prove that the signal obtained was not a characteristic of the instrumentation used for measurement. We then placed a working cell in the sample holder and measured the current and voltage response of the cell when the light was rapidly switched on or off as a function of time, using a photodiode as triggering source for data capture.

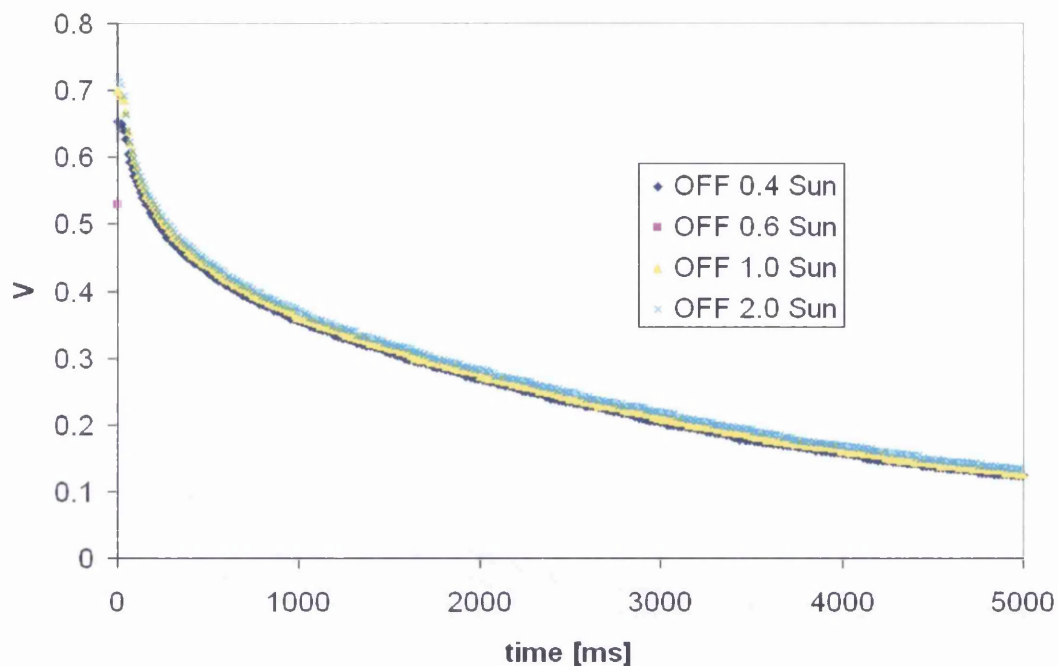


Figure 7-1 The voltage response of a solar cell, when the light source as switched off. Measured at different initial light intensities at 20 °C. The cell was built using N3, EL3 and 2 layers of Scotch Magic tape to control the film thickness of the Solaronix HT sol.

In Figure 7-1 we can see the response of the cell voltage if the light source is switched off. The cell was irradiated with different light intensities but the rate of the decay seems to be very similar. When looking at the off response of a similar cell with changing temperature (Figure 7-2), we can observe a change in the rate of the decay of the potential as one would expect from any chemical reaction. The decay curve, as can be observed, especially for low temperatures seems to be a combination of several mechanisms, perhaps arising from a number of different diffusion or interfacial processes. Our hope is that analysing this data may provide some insight into these processes and help identify those which are rate limiting and thus influence cell performance.

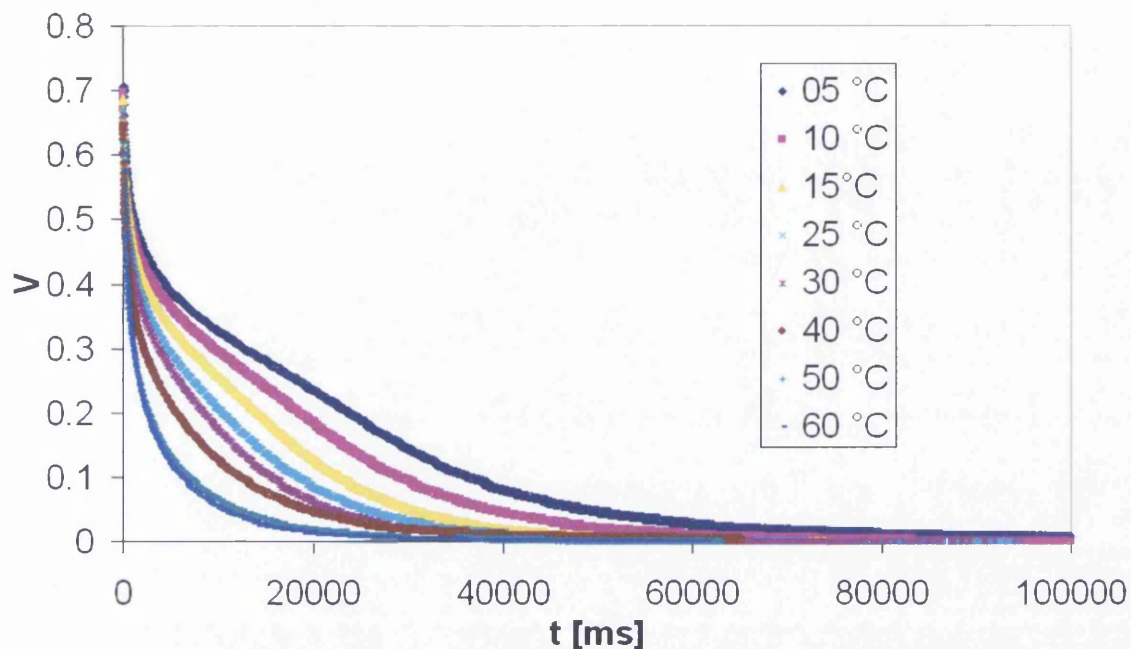


Figure 7-2 The voltage response of a cell built using N3, EL3, and 2 layers of Scotch Magic tape as a template to control the film thickness of the Solaronix HT TiO₂ sol.

In terms of future work with the PAC system, the challenge this faces in the near future will be to characterise charge injection efficiencies of many more dyes using our system and compare the data with that in the literature obtained from more indirect methods. We would also like to directly measure the non-radiative processes in whole assembled photoelectric devices like OLEDs and solar cells, indeed such work is currently taking place in Coimbra. In the case of the solar cells, we have already done some preliminary measurements and found that the adsorption of the light through the electrolyte strongly affected the signal. Building a cell with a non absorbing electrolyte at the laser wavelength, even if it was not as efficient as the current ones, could lead to a better insight into the photochemistry of these cells.

7.2 Conclusion

The study of the different parts of the Grätzel cell system has shown us that at present it appears that solar cells using either the N3 dye, the “black” dye, or other related organometallic polypyridine complexes as a sensitiser dye in TiO₂ systems are still at the forefront in terms of efficiency and long term stability. Some organic compounds (e.g. coumarins) are able to rival them today at least in terms of cost effectiveness and are closing in on them in terms of overall efficiency as shown in this work using squaraine dyes. The cells built during this project displayed comparatively very good cell efficiencies of around 5 %. This could be increased by building smaller cells. We only investigated the TiO₂ system as semiconductor, and with respect to this, it can be said that it is important to maintain a morphology of the semiconductor film which ensures the maximum number of binding sites for dye molecules whilst having pores and channels large enough to guarantee an effective exchange of charge carriers to and from the dye molecules. This leads to another major criterion, the charge mobility in the electrolyte system. The important parameters are the concentration of the redox species, the viscosity and nature of the solvent or matrix in which the redox species is incorporated, and the size of the mobile charge carriers.

It has to be ensured that electric resistances at the interfaces and the rates of back reactions are kept at a minimum, for example by ensuring complete coverage of the transparent conducting oxide by the semiconductor. Similarly it is important that all possible docking sites on the semiconductor are either blocked by sensitiser molecules or made inaccessible to the charge carriers in the electrolyte.

One major finding was that the amount of Pt on the counter electrode is only necessary in minute amounts since the series resistance of the interface is not lowered

by a thicker layer of Pt on the counter electrode and the role of Pt is as a catalyst for charge transfer at the interface rather than as a conducting medium. That means, a minimum amount of Pt for the counter electrode could be determined.

All contacts and series resistance outside the cell have to be kept as low as possible. This did not need to be taken into account for our comparative studies of the cell systems but will become an important factor once the cells are manufactured industrially and are linked together to form photovoltaic panels. In short, a good dye sensitised solar cell consists of a doped transparent conducting oxide with minimum series resistance, all channels for back reactions either through the conducting oxide or exposed areas of the semiconductor are blocked. The electrolyte species has a high mobility in an otherwise stable matrix. The counter electrode is a conducting oxide with catalytic amounts of Pt on it and all electric resistances at the interfaces are kept as low as possible to ensure a high fill factor.

With the development of the set up for time resolved photoacoustic calorimetry in the solid state, photochemistry has gained a very useful technique for the direct determination of photochemical phenomena which until now have not been investigated in this way, or which have not even been accessible for investigation at all.

We showed, that even solvent effects on compounds in the solid state can be derived using this method. We were able to determine triplet lifetimes and quantum yields of charge separation and successfully compared them with values from the literature (triplet lifetimes, charge injection efficiencies). The direct quantitative and time-resolved measurement of non-radiative processes in the solid state, quantitatively will become a valuable tool for photochemists in the future. During our

studies we have already come up with many possible further applications such as photocalorimetric studies of whole electric devices (OLEDS, DSSCs) and we are confident that there is plenty more to follow.